



HAL
open science

Mimicking C-C bond forming reactions of core metabolism

Sreejith Jayasree Varma

► **To cite this version:**

Sreejith Jayasree Varma. Mimicking C-C bond forming reactions of core metabolism. Organic chemistry. Université de Strasbourg, 2018. English. NNT : 2018STRAF038 . tel-02317724

HAL Id: tel-02317724

<https://theses.hal.science/tel-02317724>

Submitted on 16 Oct 2019

HAL is a multi-disciplinary open access archive for the deposit and dissemination of scientific research documents, whether they are published or not. The documents may come from teaching and research institutions in France or abroad, or from public or private research centers.

L'archive ouverte pluridisciplinaire **HAL**, est destinée au dépôt et à la diffusion de documents scientifiques de niveau recherche, publiés ou non, émanant des établissements d'enseignement et de recherche français ou étrangers, des laboratoires publics ou privés.



**UNIVERSITÉ DE
STRASBOURG**

EDSC
École Doctorale des
Sciences Chimiques

ÉCOLE DOCTORALE 222
Laboratoire de Catalyse Chimique
Institut de Science et d'Ingénierie Supramoléculaires (ISIS)

THÈSE de DOCTORAT

Présentée par :

Sreejith Jayasree VARMA

Soutenue le : **05 Octobre 2018**

Pour obtenir le grade de : **Docteur de l'université de Strasbourg**

Discipline/ Spécialité : Chimie organique

Mimicking C-C bond forming reactions of core metabolism

THÈSE dirigée par :

Prof. Joseph MORAN

Directeur de thèse, Université de Strasbourg

RAPPORTEURS :

Prof. Marie-Christine MAUREL

Rapporteur, Sorbonne Université, Paris

Dr. Cornelia MEINERT

Rapporteur, Université de Nice Sophia Antipolis

AUTRES MEMBRES DU JURY :

Prof. Peter FALLER

Examineur, Université de Strasbourg

ॐ सह नावतु ।
सह नौ भुनक्तु ।
सह वीर्यं करवावहै ।
तेजस्विनावधीतमस्तु मा विद्विषावहै ॥
ॐ शान्तिः शान्तिः शान्तिः ॥

Om saha nāv avatu
saha nau bhunaktu
saha vīryaṃ karavāvahai
tejasvi nāv adhītam astu
mā vidviṣāvahai |
Om śāntiḥ śāntiḥ śāntiḥ ||

Literal meaning

Om! Let us be together.
Let us eat together.
Let us be vital together.
Radiating Truth; radiating the light of life
Never shall we denounce anyone; never
entertain negativity.
Om Peace, Peace, Peace!

Inner meaning

Om! May God protect us both together.
May God nourish us both together.
May we work conjointly with great energy.
May our study be vigorous and effective.
May we not mutually dispute (or may we
not hate any).
Om! Let there be peace in me!
Let there be peace in my environment!
Let there be peace in the forces that act on
me.

-Shanti mantra (hymn of peace) from Upanishads-

Dedication

To my ever-loving mother

Acknowledgements

My sincerest gratitude to my supervisor Prof. Joseph MORAN who despite getting numerous emails from my fellow countrymen everyday asking for a research position, considered my application and offered me this doctoral position. Although in the beginning I was lost in the area of prebiotic chemistry, his constant guidance and encouragement allowed me to find my way and develop my own way of thinking. Myself being a person with difficulty in communicating science, thanks to the numerous opportunities he provided me, I was able to improve it which shall be a great asset to my career. Most importantly, in an era where you consider yourself lucky if your supervisor knows your name, I consider myself privileged to have had a supervisor whom I could approach anytime for his guidance. Through Joseph, I also consider lucky to have been introduced to many researchers in origin of life (OoL) field like Prof. Will Martin, Prof. Eric Smith and many others at the Earth Life Science Institute. Their ideas have also influenced my thinking and helped in conceiving this thesis.

Subject like the OoL research is challenging especially if it is a new area of research in a laboratory and even more challenging if you were on your own, without any peers to discuss with. I am thankful to Dr. Kamila MUCHOWSKA who changed that situation. Her joining added momentum to our investigations in prebiotic chemistry. I particularly acknowledge Kamila's contributions and help in my research projects without which this thesis wouldn't have been complete. Together we have tackled many peaks in our analytical spectra as well the Vosges. I shall really miss them both. Thank you, Kamila, for being an awesome colleague, a good friend and the best partner in crime :D.

Elodie CHEVALLOT-BEROUX and Lucas LETHUILLIER, whose joining in our quest for OoL brought us newer perspectives into our investigations especially during our initial investigations on the rTCA cycle. I am particularly indebted to them for the French resume of this thesis without whose help it wouldn't have been possible. Above all, the lab wouldn't have been so lively without you guys!

I thank Paul CHATELAIN for his contributions to the acetyl CoA pathway chemistry and Guang LI for his contributions to the rTCA cycle experiments. I acknowledge Jing YI for her attempts and assistance with the citric acid retro aldol chemistry. Learning with you had been a great experience for me. Finally, it had been a pleasant experience to do chemistry with Dr. Leandro COTOS-MUÑOS, Martina PREINER and Dr. Jan GORGES with whom I had only a brief period of overlap.

About three and a half years back, when I first arrived at Strasbourg, the first person of MoranlabUdS I was introduced to, was Dr. Edward RICHMOND. He helped me getting started in the lab and over the years offered invaluable suggestions in research. I acknowledge his help with numerous issues inside and outside the laboratory during these three years.

Experiences in scientific research are not always pleasant. I was lucky to have had a company across my table during those unpleasant times (and of course during the good times as well! :)). Me and Vuk VUKOVIC, colonized salle 422 in the same time 3 years back and since then our friendship had only grown stronger. I'll miss you buddy..

From the interactions during the limited time I had, I strongly feel the legacy of MoranLabUdS is within the safe hands of the newer generation of post-docs and PhD students, Abijit, Jan, Paul, Florent, Shaofei and Jing. Of particular mention, I had the pleasure to work, although briefly, with Marian, Eléna, Ismat, Junya, Stefania, Pavle, Samuel, Anton and Subradip. Their presence has added to the diversity of our laboratory. Outside our laboratory my research career and life has been enriched by other members of ISIS- Vladimir, Valentin, Aromal, Elise, Regis (Torbeev group); Pawel, Yang, Imane, Dawid, Karolina (Dydio Group); Muthu Kumar, Artem, Meixia, Jan, Yousef (Lehn Group); Mithun, Nina (Hermans Group); Jino, Anoop, Kalaiivanan (Ebbesen Group).

I am very much indebted to Nathalie MONNIN, who from my very 1st day of (and even before) my arrival in France took care of all the volumes of paper and bureaucratic work. While it was tricky in the beginning when we didn't understand each other, we learned each other's language to arrive on the same page over these three years. I also extend my sincerest gratitude to Muriel, Fabien, Fabienne, Jean-Louis, Thierry, Philippe and Caroline whose efforts have ensured the smooth progression of my research at ISIS.

I also take this opportunity to thank Prof. Maurel, Dr. Meinert and Prof. Faller who kindly agreed to review this manuscript and agreed to be the members of my jury.

Being about 7500 km from my home would have made me homesick in Strasbourg if it wasn't for my friends from India, Anoop, Jinsi, Mithun, Aromal, Kalaiivanan, Jino and his family and the rest of the StrasMA. I thank you all for making Strasbourg a home away from home for me during these 3 years.

Above all, I thank my mother Jayasree K R, for sending away her only son to a place far, far away, to pursue his dreams. ഒടുവിൽ ഞാനത് നേടി അമ്മേ...

Table of Contents

List of Abbreviations.....	10
Résumé.....	11

PART I

1. Literature Review.....	22
1.1 Abiogenesis	22
1.1.1 Timeline	22
1.2 Metabolic origins of life	26
1.2.1 Perspective of nutrition	26
1.2.2 Perspective of phylogenetics.....	27
1.2.3 Ancient CO ₂ fixation pathways.....	30
2 The Wood-Ljungdahl pathway	31
2.1 Topology.....	31
2.2 Enzymes and mechanism.....	31
3 Tricarboxylic acid cycles	34
3.1 Introduction	34
3.2 Enzymes, mechanisms of the rTCA and TCA cycles.....	34
3.2.1 Reductive tricarboxylic acid (rTCA) cycle biochemistry	35
3.2.2 Oxidative TCA cycle biochemistry	41
4 Amino acids	44
4.1 Introduction	44
4.2 Biosynthesis.....	44
4.2.1 Transamination.....	45

PART II

Central aim of this thesis	47
1 The reverse Tricarboxylic Acid Cycle.....	48
1.1 Introduction	48
1.2 Could the (r)TCA cycle have its origins in prebiotic chemistry? - state of the art....	48
1.2.1 Non-enzymatic reactions of reductive TCA cycle	49
1.2.2 Non-enzymatic reactions of oxidative TCA cycle	51
1.3 Aim of this chapter	51
1.4 ATP Independent reactions: reduction and (de)hydration.....	52
1.4.1 Reduction reactions	52
1.4.2 Dehydration reactions	53

1.4.3	Effect of compartmentalization	55
1.4.4	Hydration.....	55
1.4.5	Sequential reactions.....	57
1.4.6	Selectivity issues	57
1.5	Conclusion and perspectives	58
2	The Wood-Ljungdahl pathway	60
2.1	Introduction	60
2.2	State of the art in the investigations on abiotic origins of the W-L pathway	60
2.3	Aim of this Chapter	61
2.4	Can native metals promote reactions of W-L pathway?.....	62
2.4.1	Chemistries of different native metals.....	62
2.4.2	Effect of physical parameters	63
2.4.3	Change in the distribution of products over time	66
2.4.4	Mechanistic considerations	67
2.4.5	Link to other metabolic pathways	71
2.5	Conclusions	72
3	Reductive amination	74
3.1	Reported abiotic scenarios for reductive amination	74
3.2	Aim of this chapter	75
3.3	Reductive amination under acidic medium	75
3.3.1	Hydrazine (H ₂ N-NH ₂)	76
3.3.2	Hydroxylamine (H ₂ N-OH).....	77
3.4	Conclusions	78
4	General conclusions and outlooks	79

PART III

1	The reverse Tricarboxylic acid cycle	82
1.1	General information.....	82
1.2	Materials	82
1.3	Analytical methods	83
1.3.1	Derivatization procedure	83
1.3.2	Product identification	83
1.4	Experimental data	84
1.5	Gas chromatography traces	90
1.6	Synthetic procedures.....	103
1.6.1	General procedure: Fe ⁰ / Zn ²⁺ / Cr ³⁺ and Ni ⁰ /Zn ²⁺ /Cr ³⁺ –catalyzed reactions...	103

1.6.2	Metal screens.....	103
1.6.3	Reactions in micellar solutions.	104
1.6.4	Portion-wise reagent addition.....	104
1.6.5	Reactions with oxalosuccinic acid	104
1.6.6	Triethyl oxalosuccinate	105
1.6.7	<i>Cis</i> -aconitic acid.....	107
2	The Wood-Ljungdahl pathway	108
2.1	General information.....	108
2.1.1	Materials.....	108
2.2	Analytical methods	109
2.2.1	Product identification	109
2.2.2	Starting material control experiments	110
2.2.3	NMR sample preparation	111
2.2.4	Confirmation of formate, acetate and pyruvate by GC-MS.....	111
2.3	Synthetic procedures.....	117
2.4	Experimental data	117
2.4.1	Control reactions	117
2.4.2	Reaction parameter screens.....	119
2.4.3	Distribution of electrons among detected CO ₂ fixation products	123
2.4.4	Detection of ethanol in the reaction mixture after 85 h.....	124
2.4.5	Metal screens in CO ₂ fixation reactions	125
2.4.6	The effect of salt concentration on reaction yields.....	137
2.4.7	Miscellaneous experiments	138
2.4.8	Compatibility with 3-reaction sequences of the rTCA cycle	141
3	Reductive Amination	146
3.1	General information.....	146
3.1.1	Materials.....	146
3.2	Analytical methods	146
3.2.1	Derivatization procedure	146
3.2.2	Product identification	147
3.3	Experimental data	147
3.4	Gas chromatography traces	148
Appendix I.....		152
Yield determination and error analysis		166
Appendix II		175

Appendix III	177
Yield determination and error analysis	179
References	182

List of Abbreviations

ACS	acetyl CoA synthase	M	molar
AMP	adenosine monophosphate	MCF	methylchloroformate
ATP	adenosine triphosphate	MeOH	methanol
BC	before Christ	mg	milligram
cm	centimeter	MHz	mega hertz
CO	carbon monoxide	min	minute
CO ₂	carbon dioxide	mL	milliliter
CoA	Coenzyme A	mM	millimolar
CoFeSP	corrinoid iron sulfur protein	mmol	millimole
conc	concentrated	MPEA	N-methylphenyl- ethylamine
Da	dalton	N	normal
dd	doublet of doublet	NAD ⁺ /NADH	nicotinamide adenine dinucleotide
deriv.	derivatised	NADP ⁺ /NADPH	nicotinamide adenine dinucleotide phosphate
DSS-Na	sodium 3- (trimethylsilyl)-1- propanesulfonate	NMR	nuclear magnetic resonance
ECF	ethylchloroformate	°C	degree celsius
EDC	1-ethyl-3-(3-dimethyl- aminopropyl) carbodiimide	PEP	phosphoenolpyruvate
equiv.	equivalent	PNA	protein nucleic acid
EtOAc	ethyl acetate	ppm	part per million
EtOH	ethanol	PTFE	polytetrafluoro ethylene
FAD/FADH ₂	flavine adenine dinucleotide	q	quartet
FDH	formate dehydrogenase	R6P	ribose 6-phosphate
g	grams	RNA	RiboNucleic Acid
G3P	glycerol 3-phosphate	rpm	revolution per minute
GC-MS	gas chromatography mass spectrometry	rTCA	reverse/reductive tricarboxylic acid
h	hour	s	singlet
H ₂ S	hydrogen sulfide	t	triplet
HCl	hydrochloric acid	TCA	tricarboxylic acid
HCN	hydrogen cyanide	TPGS-750-M	DL- α -Tocopherol methoxypolyethylene glycol succinate
Hz	hertz	TPP	thymine pyrophosphate
kJ	kilo joule	V	volt
KOH	potassium hydroxide	w/w	weight by weight
LUCA	Last Universal Common Ancestor	W-L	Wood-Ljungdahl
		μ L	microliter

Résumé

Reproduction des réactions de formation de liaisons C-C s'opérant au cœur du métabolisme

Contexte

L'abiogenèse est définie comme "le développement ou l'évolution de la vie à partir de substances inorganiques ou inanimées. L'abiogenèse est pensée comme étant un processus évolutif plutôt qu'un événement ponctuel."

Les premières théories sur les origines de la vie remontent au 3ème siècle av. J.-C, avec la théorie de génération spontanée proposée par Aristote. Notre compréhension du vivant a changée à travers les siècles qui ont suivi, certaines idées et découvertes majeures ayant permis cette évolution sont récapitulées dans la Figure 1.

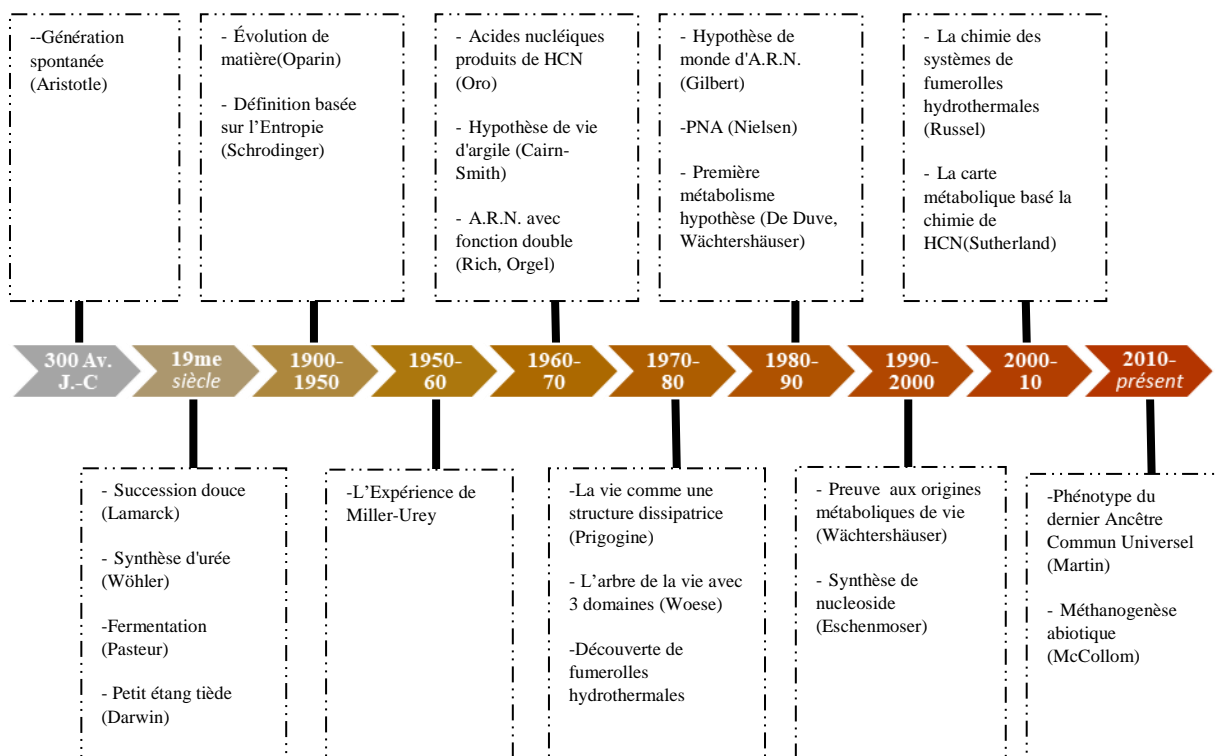


Figure 1 Chronologie de l'évolution de la recherche sur l'origine de la vie

Ces découvertes ont ouvert la voie à deux hypothèses majeures ayant trait à l'abiogenèse ou l'origine de la vie – une origine génétique ou métabolique. La première hypothèse affirme que l'émergence d'un système basée sur la génétique capable de catalyser sa propre répllication serait à l'origine de la vie. Cette idée commence à être largement acceptée après la découverte des ribozymes, mais la complexité de la nature de ces composants (ARN) suscite quelques

doutes quant à la plausibilité de son apparition sous des conditions prébiotiques. Au contraire, l'hypothèse selon laquelle le métabolisme serait apparu en premier repose sur une rétrodiction de la biochimie, dans laquelle l'ordre d'apparence de la biochimie primitive peut être comprise à partir de l'organisation des réseaux biochimiques dans les organismes autotrophes. Dans les sections suivantes, je présente des arguments en faveur d'une origine métabolique de la vie.

Introduction

Toutes les formes de vie assemblent et désassemblent continuellement des composés chimiques via un processus de consommation d'énergie appelé métabolisme. Ce dernier est comparable à un ouragan à l'échelle moléculaire. Tout comme la structure interne d'un ouragan est aussi importante que les deux éléments qui le constitue (l'air et l'eau); l'organisation des voies métaboliques est aussi importante que les briques chimiques qui le constitue (métabolites). Traditionnellement, la recherche chimique sur les origines de la vie est concentrée principalement sur la synthèse de composés chimiques sans suffisamment apprécier leur place dans la plus grande organisation biochimique de la vie. La vie construit toutes ses molécules à partir du dioxyde de carbone, pourtant elle manque étonnamment d'innovation à cet égard. Malgré presque 4 milliards d'années d'évolution, les organismes autotrophes utilisent seulement six voies différentes pour construire leurs molécules à partir du CO₂. Parmi elles, deux voies – la voie de l'acétyl CoA (aussi appelée voie Wood-Ljungdahl) et le cycle du rTCA (également appelé le cycle de Krebs inverse) - sont considérées comme primitives, et contiennent les cinq molécules servant de précurseurs chimiques universels pour toute la biochimie (Figure 1).

Comment et pourquoi les voies de l'acétyl CoA et du rTCA sont elles apparues? Pour répondre à cette question, une recherche systématique a été effectuée afin de trouver des catalyseurs chimiques non-enzymatiques ou des minéraux simples, ainsi que des réactifs pouvant promouvoir les réactions d'anabolisme principal, particulièrement la voie de l'Acétyl CoA et le cycle du rTCA. A l'origine, pour créer les molécules organiques complexes comme les enzymes il a fallu que des molécules plus simples avec un moins grand nombre de carbone se forment sur terre et cela à partir du CO₂. On peut donc supposer que les premiers produits chimiques à plusieurs atomes de carbones sont issus de voies de synthèses totalement inorganique comme celles développées dans notre laboratoire. Une évolution chimique et organométallique simultanée permettrait alors une interaction efficace entre une molécule organique et un ou plusieurs métaux, à l'instar de certaines métalloenzymes. Après avoir trouvé différents moyens de promouvoir individuellement chaque étape des cycles catalytiques étudiés, seules les conditions réactionnelles mutuellement compatibles (à savoir un ensemble

de conditions permettant de reproduire les séquences des voies métaboliques étudiées) ont été retenu.

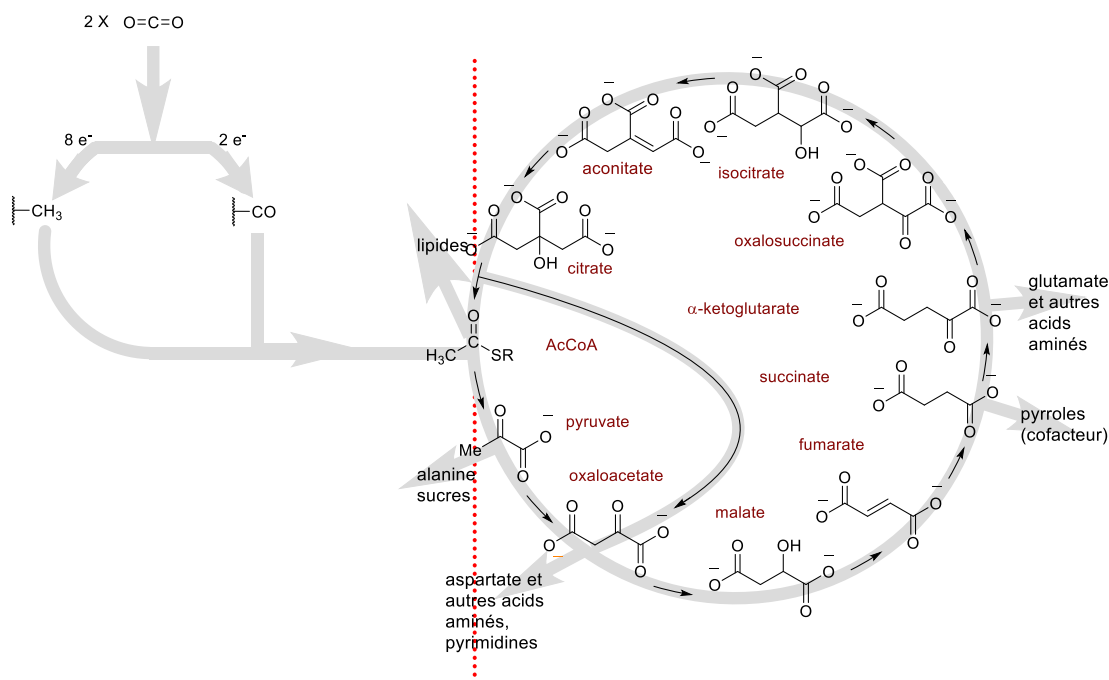


Figure 2 Le voie de Wood-Ljungdahl et le sentier de Krebs inverse

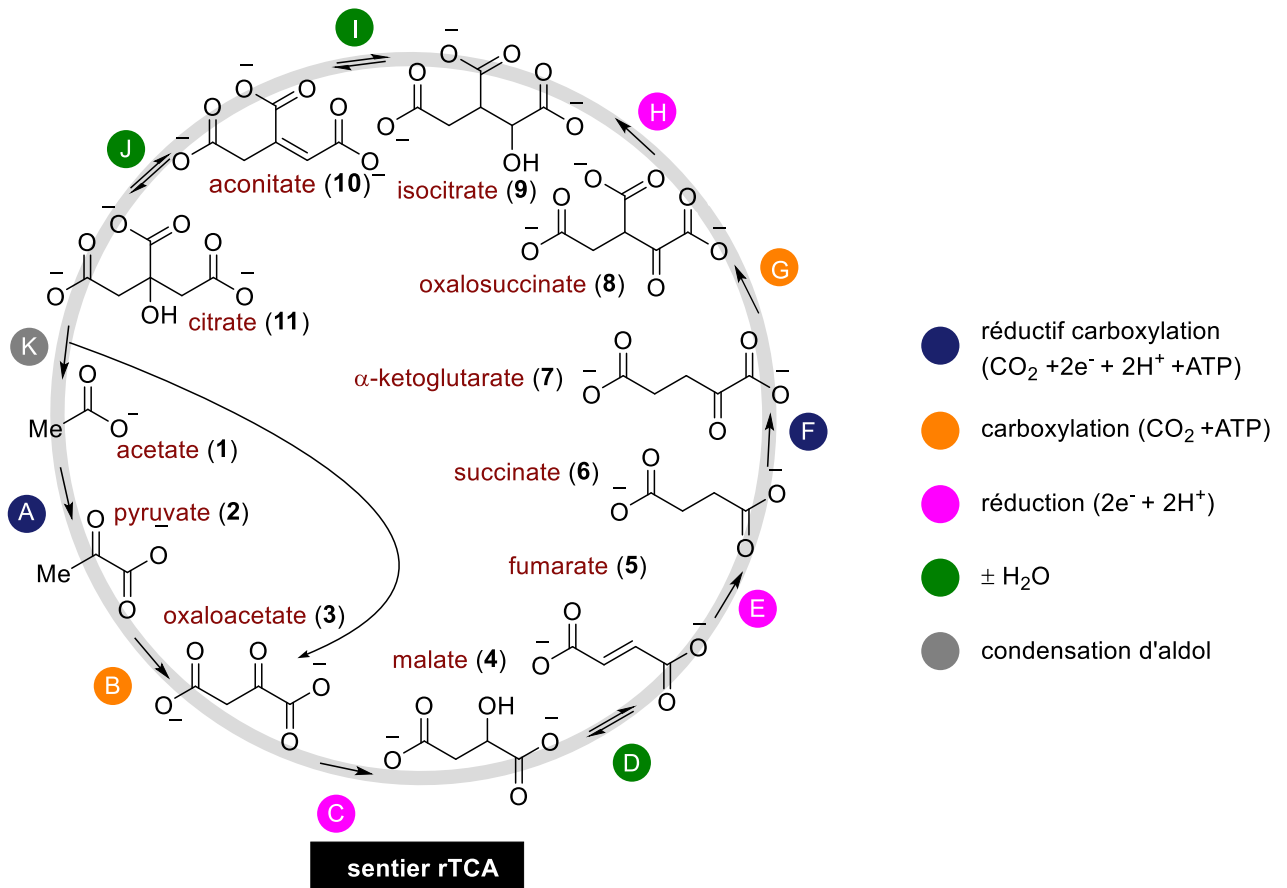
Résultats et discussions

I. Le cycle du rTCA

Le but principal de cette étude est de trouver des catalyseurs simples et des réactifs qui pourraient promouvoir la réduction, la déshydratation et les réactions d'hydratation (Scheme 1 ; étapes C, D, E, H, I et J) du cycle Krebs inverse. Quelques travaux sur les réactions de réduction non-enzymatiques de ce dernier ont déjà été publiés avant le début de cette étude par des équipes de recherche comme le laboratoire de Scot Martin et bien d'autres encore.. Afin de reproduire le cycle du rTCA les travaux effectués dans le cadre de cette thèse sont basés sur l'utilisation adéquate d'une méthode analytique haute débit. Des expériences d'exploration systématiques (screening) ont été effectuées pour trouver toutes les manières de reproduire chaque étapes du cycle du rTCA. Le nombre colossal d'expériences possibles a été réduit en limitant les paramètres examinés à l'utilisation : d'ions métalliques simples comme catalyseurs, de températures différentes, de pH différents et d'agents réducteurs différents (Table 1).

Il a été découvert que le fer métallique (un agent de réduction) en présence des ions Zn^{2+} et Cr^{3+} , peut promouvoir toutes les six réactions de réduction, déshydratation et hydratation du

cycle du rTCA, ainsi que la synthèse d'acide aminé, sous un unique ensemble de conditions. Ceci révèle qu'au moins la moitié de la chimie du cycle du rTCA est si simple qu'il pourrait être à l'origine de la chimie prébiotique. Cette étude n'a pas pour objectif de démontrer que Zn^{2+} et Cr^{3+} étaient nécessairement les catalyseurs du rTCA à l'origine de la vie mais plutôt de prouver conceptuellement que ce cycle peut procéder par des ions métalliques simples. Nous avons seulement examinés des ions métalliques, mais il existe des centaines de minéraux et argiles dont certains pourraient avoir une aussi bonne, voire une meilleure réactivité.



Scheme 1 Les réactions de la sentier rTCA

Table 1 Les réactions de la sentier rTCA qui sont promues par des métaux/ions

Rubrique	Substrat (0.1 mmol)	Conditions ^a				L'espèce détecté après la réaction dans le mélange (%) [‡]													
		Fe ⁰ (equiv.)	Zn ²⁺ (equiv.)	Cr ³⁺ (equiv.)	Micelles	Cycle de marche										Hors cycle			
						2	4	5	6	7	9	10	11	12	13	14			
<i>Réduction</i>																			
1	3	10	-	-	-		90	10											
2 ^b	5	10	-	-	-		15	20	65										
3 ^c	8	10	-	-	-				2		98								
<i>Hydratation/Déshydratation</i>																			
4 ^d	5	-	-	-	-		77	23											
5 ^d	4	10	10	-	-		94	4	2										
6 ^e	4	10	10	-	oui		82	7	11										
7 ^{d,f}	9	-	1	-	-						51	49							
8 ^{d,f}	10	-	1	-	-						12	88							
9 ^g	10	-	-	6	-							67	33						
10 ^g	11	-	-	6	-							23	77						
<i>Séquence en trois étapes</i>																			
11 ^e	3	10	15	4	oui		52	3	41						4				
12 ^h	8	5	10	6	-						65	30	2		3				
13 ^h	8	5	10	6	oui				5		72	21	2						
<i>Réduction compétitive</i>																			
14 ^c	2+3+5 7+10	10	15	6	oui		20	6	18	4	20		28		2	2	<1		

[‡] Les valeurs rapportées ont été déterminées par GC-MS après une procédure derivatization et représenter la moyenne d'au moins deux courses. Les composés 3 et 8 n'ont pas été détecté par cette méthode et sont ainsi omis.

^aSauf indication contraire: 1 M HCl en H₂O, 16 h, 140 °C. ^b3 h, 140 °C. ^c3 h, 40 °C. ^d48 h, 140 °C. ^e20 °C, 24 h.

^fRéaction dans 1 M H₂SO₄ en H₂O, 16 h, 140 °C. ^g1 h, 20 °C, 24 h, 140 °C. ^hCyclage thermique: 16 h, 140 °C; 10 h, 20 °C; 16 h, 140 °C.

II. La voie de Wood-Ljungdahl

Parmi les six voies chimiques connues comme étant utilisées par des organismes autotrophes pour fixer le CO₂, la voie Acétyle CoA (aussi connu comme la voie de Wood-Ljungdahl), est la seule qui est non cyclique mais linéaire. Avec l'aide d'enzymes contenant des métaux de transition et des cofacteurs, elle donne lieu à la réduction d'une première molécule de CO₂ en monoxyde de carbone (CO), puis d'une deuxième molécule de CO₂ en groupe méthyle (-CH₃) et finalement, à la combinaison des deux molécules résultantes pour former un groupe acétyle

($\text{CH}_3\text{CO}-$). Les groupes acétyles peuvent réagir encore une fois avec le CO_2 et deux électrons pour former du pyruvate, le précurseur commun à tous les sucres. Certains biochimistes considèrent que cette étape fait partie de la voie de l'acétyl CoA, tandis que d'autres non. Découvrir une méthode chimique simple permettant de faire la même chose pourrait nous permettre d'établir un lien entre cette chimie et la biochimie ayant lieu sur la Terre primitive. La biochimie de la voie de l'acétyl CoA utilise des enzymes et des cofacteurs pour diviser le gaz H_2 en deux protons et deux électrons, qui sont alors utilisés pour réduire le CO_2 . Si la fixation du CO_2 est apparue avant l'évolution de ces enzymes, alors elle a été obtenue : soit grâce à H_2 par certains mécanismes encore non découverts, soit la vie est parvenue à réaliser la fixation de CO_2 grâce à une source d'électrons plus réductrice que H_2 . Notre prochain objectif a donc consisté à essayer de trouver des réactifs ou des catalyseurs pour réaliser les étapes de fixation du CO_2 de la voie de l'acétyl CoA et du cycle du rTCA, qui sont sans doute les réactions chimiques les plus complexes à mettre en œuvre dans un métabolisme primitif.

Nous avons identifié le fer métallique comme réducteur du CO_2 aqueux en acétate et pyruvate sous un large éventail de températures et de pressions, même en conditions ambiantes. La chimie se produit sur la surface du métal et produit des espèces carboniques comme l'acide formique et le méthanol, en plus de l'acétate et du pyruvate (Figure 3). La distribution des produits observés, l'évolution de la réaction au fil du temps (Figure 4) et la façon dont la réaction répond aux expériences de contrôle diverses, est compatible avec un mécanisme relativement proche de la voie biologique étudiée. La grande simplicité des réactifs engagés dans cette réaction chimique (du fer, du CO_2 et de l'eau salée), montre que la fixation de CO_2 n'est pas seulement un mécanisme prébiotique valable pour construire des biomolécules, mais aussi qu'elle suit un chemin qui ressemble à celui employé par la biochimie. Bien qu'il soit impossible d'affirmer avec certitude que cette réaction est la voie biologique employée à l'origine pour la synthèse de l'acétyl CoA, la méthode développée par notre laboratoire est cependant en adéquation avec les études phylogénétiques réalisées sur le sujet. Et elle fournit au moins un aperçu sur la façon dont les premières voies de fixation de CO_2 pourraient avoir vu le jour.

Table 2 Amination réductive des α -cétoacides avec hydrazine et hydroxylamine

Rubrique ^a	cétoacide	Les équivalents de source d'azote	Température (°C)	Produits (% of mixture)							
				12	14	18	19	4	15	13	16
<i>Hydrazine</i>											
1		1	80	13	87	-	-	-	-	-	-
2		2	80	3	97	-	-	-	-	-	-
3	2	4	80	1	99	-	-	-	-	-	-
4		8	80	0	100	-	-	-	-	-	-
5		2	140	17	83	-	-	-	-	-	-
6		2	25	6	94	-	-	-	-	-	-
7	17	2	80	-	-	8	92	-	-	-	-
<i>Hydroxylamine</i>											
8		1	80	17	83	-	-	-	-	-	-
9		2	80	9	91	-	-	-	-	-	-
10	2	4	80	3	97	-	-	-	-	-	-
11		8	80	2	98	-	-	-	-	-	-
12		1	100	19	81	-	-	-	-	-	-
13		2	140	100	-	-	-	-	-	-	-
14		2	25	-	100						
15	17	1	100	-	-	29	71	-	-	-	-
16	3	1	100	-	-	-	-	46	54	-	-
17	7	1	100	-	-	-	-	-	-	61	38
18	2+3+7+ 17	1	100	-	1	37	40	12	-	10	-

^a 0.1 mmol de α -cétoacides avec 10 mmol de Fe⁰ en 1 M HCl.

L'exposition de plusieurs alpha-cétoacides à l'hydrazine ou l'hydroxylamine dans les conditions réactionnelles décrites dans la section précédente (Fe⁰ en milieu acide et à température élevée) aboutit à la formation des aminoacides correspondants. L'utilisation de deux équivalents de sources d'azotes à 80°C constitue les conditions optimales pour les réactions d'aminations réductrices. Seul l'hydroxylamine a permis de former les acides aminés

correspondant à partir de l'ensemble des cétoacides utilisées, tandis que l'hydrazine fonctionne qu'à partir de l'acide glyoxylique et de l'acide pyruvique.

Conclusion générale

Ces dernières années, il a été prouvé que la glycolyse, la gluconéogenèse, le cycle de Krebs, le cycle de Krebs inverse et maintenant la voie de l'Acétyle CoA peuvent être effectuées sans enzymes et uniquement avec des catalyseurs inorganiques. Des cycles non-biologiques incorporant quelques intermédiaires du cycle de Krebs ont récemment été démontrés. Des processus anaboliques comme l'amination réductrice d' α -cétoacides pour produire des acides aminés ont aussi été démontrés dans des conditions similaires. Les origines du métabolisme ne devraient plus être considérés comme purement enzymatique, mais plutôt comme une conséquence de réactions abiotiques diverses qui se seraient développées sur Terre depuis sa formation.

PART I

1. Literature Review

1.1 Abiogenesis

Abiogenesis is defined as “the development or evolution of life from inorganic or inanimate substances. It is believed to have been a gradual process of increasing complexity rather than a single event”.¹

1.1.1 Timeline

Inquiries into the origins of life trace back several millennia. In the 3rd century BC, Aristotle promoted the theory of spontaneous generation, that life regularly arose from non-life. Although in 17th century Francesco Redi disproved the theory of spontaneous generation through his works on maggots and parasites, it was not popularized due to its controversial nature to the existing theological traditions of the church. Starting from the early days of chemistry in the early 1800's, Berzelius' concept of vitalism, that organic compounds could only be produced by life and Lamarck's theory of inheritance of acquired characteristics were also widely believed. These theories remained unrefuted until Friedrich Wöhler's urea synthesis in 1828 showed that biological molecules were not unique to life but could also be produced abiotically, and when Louis Pasteur's fermentation experiments in 1860 proved that bacteria arose only from other bacteria.^{2,3} Based on his observations, Charles Darwin speculated that life initially could have originated in a warm little pond that was nutrient-rich.⁴

The earliest attempt to define life using a framework of physical sciences was in the early 1920s by Aleksandr Oparin, who postulated that life would have emerged as a process of evolution of matter; for instance, through interaction of organic molecules in a solution.⁵ This was further improved by a definition based on entropy, “Life is something that resists decaying to disorder and equilibrium” by physicist Erwin Schrödinger in 1944.⁶

The first attempt to model the chemical environment present on the early Earth was done by Stanley Miller, who together with Harold Urey reported their results under the title “A production of amino acids under possible primitive earth conditions”.⁷ These results inspired the development of proteinoid world theory by Sidney Fox in 1958, asserting that life initially emerged as a self-replicating collection of small peptides having life-like properties.⁸ Although this theory was soon abandoned, it was the first to identify the origin of life as a deterministic process.

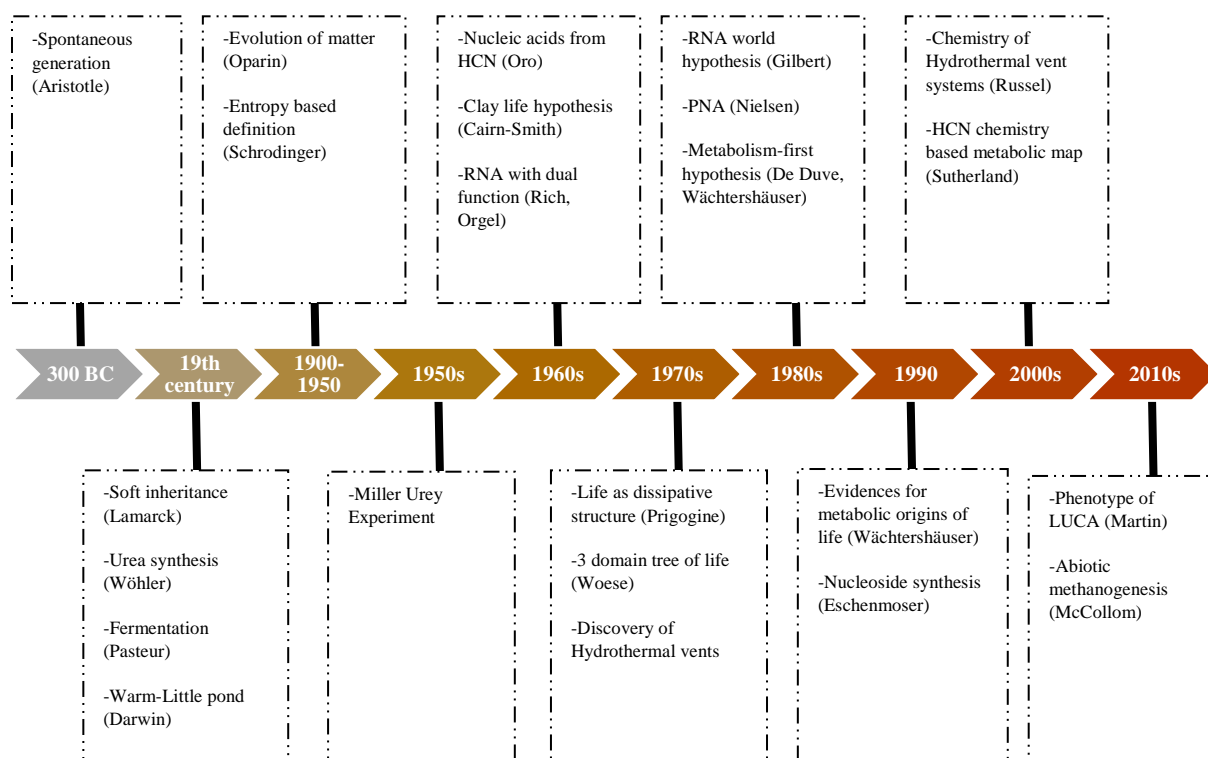


Figure 6 Time line of Origin of Life research

In 1960, a report from John Oró demonstrated that simple molecules like HCN could condense to give adenine, one of the nucleobases.⁹ This was followed by Cairns-Smith's clay life hypothesis, that suggested evolving clay minerals could have predated the life we see today.¹⁰ Later in 1982, the dual function of RNA (as a genetic material and a catalyst) was also identified by Cech and Altman.¹¹ In light of these evidences, Alex Rich and Leslie Orgel suggested the Genetics-first origins of life, with a biochemistry that was catalyzed by RNA-like polymers.¹² This idea soon gained the support of Nobel laureate Walter Gilbert who coined the term "RNA world" for origins in 1986.¹³ In the following years, the works of James Ferris's clay catalyzed RNA polymerizations (1988), Eschenmoser's nucleoside synthesis (1991) and Peter Nielsen's Peptide nucleic acid synthesis (1991) gave compelling evidence to the genetics-first RNA world hypothesis.^{14,15,16}

Meanwhile in the 1970s, the works of Ilya Prigogine on dissipative structures and complex systems demonstrated that complex patterns emerge when energy flows through a system containing interacting particles.¹⁷ It suggested that life is an emergent property of complex chemical systems under a specific energetic stress. At the same time advancements in genetics and taxonomy allowed Carl Woese to revise the tree of life with three domains: Bacteria, Archaea and Eukarya.¹⁸ One consequence of this was the emergence of the concept of a Last

Universal Common Ancestor (LUCA), an entity that is imagined to be at the base of the phylogenetic tree and that was the progenitor of all life forms that we see on Earth today.

Deep-sea explorations in the late 1970s revealed submarine hydrothermal vents such as the “Lost City”, that inspired a new competitor to the prevailing theories on surface origins of life. The underwater chimneys were identified as large reactors where water, gases and minerals interact to generate a myriad of organic molecules. Russell and co-workers, through laboratory experimentations, predicted that such alkaline hydrothermal vents could provide the culture chambers and flow reactors for life to originate.¹⁹ Further investigations of the hydrothermal vent systems revealed a metal-rich reducing environment containing H₂S, CO₂, and CO, among others.²⁰ Around this time, Christian de Duve proposed the thioester world scenario for the origin of life, in which abiotically formed thioesters play a key role as activated intermediates for early biochemistry.²¹ Building on the chemistry of recently discovered hydrothermal vents, Günter Wächtershäuser proposed the iron-sulfur world scenario for origins in 1988.²² The critical innovation of this proposal was the concept of biochemical retrodiction, in which the order of appearance of primitive biochemistry can be inferred from the organization of biochemical networks in autotrophic organisms. In the following years, this idea was expanded, and more experimental evidences were put forth.^{23,24} The relatively simple chemistry compared to proposed RNA-focused prebiotic chemistry allowed this theory to become a strong competitor to the RNA world hypothesis.

The following years saw arguments and battles between the genetics-first RNA-based hypotheses and the metabolism-first based approach. A few of the features of both the hypotheses are summarized in Table 3.

Table 3 Main features of genetics-first and metabolism-first hypotheses

Feature	Genetics First	Metabolism First
Continuity in chemistry	No	Yes
Darwinian evolution	Yes	No
Selective chemistry	Yes	No
Robust chemistry	No	Unclear
Need for Chirality	Required early	Required later

A primary argument from the metabolism-first camp is the necessity for continuity in chemistry from prebiotic chemistry on the early Earth to primitive life.²⁵ In other words, the developments that led to the origin of life should be able to explain at least some of the overall organization of biochemistry and the types of reactions that it uses. Many prebiotic chemistries for nucleotide synthesis that are reported within the context of a genetics-first proposal have no parallel to any biosynthetic pathways in metabolism and therefore little explanatory power.²⁶ In contrast, the chemistry of the metabolism-first hypothesis is built within the framework of current biochemistry, with a chemistry driven by Earth-abundant minerals. It therefore can help account for why metabolism relies on certain metabolites as crucial branching points and uses the pathways that it does.

A second argument against many experimental reports rooted in genetics-first theory is that they require numerous mutually incompatible steps and are thus intrinsically unlikely to have occurred. Robert Shapiro has likened this to “*a golfer, having played an 18-hole course, claiming that he had shown that the golf ball could have, through some combination of wind, rain, heating, cooling, dehydration, and ultraviolet irradiation played itself around the course without the golfer’s presence.*”²⁷ Furthermore, the geochemical viability of the proposals, often requiring continuous delivery in substantial quantities of compounds such as cyanoacetylene, remain highly geochemically doubtful.²⁸

In genetics-first proposals, RNA molecules act as both carriers of genetic information and as catalysts. This explains how early life could have evolved and also have carried out specific reactions which otherwise would have been completely random. Although metabolism-first theory does not immediately create a role for replication and evolution, recent computational studies on the inevitability of autocatalytic replicators in a catalytic reaction network provide an argument in its favor.²⁹ The topology of a reaction network can also have important consequences for the ability of a reaction network to persist. For example, an autocatalytic network stabilized by a constant input of one of its intermediates could sustain a metabolic cycle which otherwise would attenuate due to parasitic reactions.³⁰ Also, highly specific catalytic machinery associated with a polymeric catalyst reduces the likelihood of promiscuous catalysis, which would have been critical for early metabolic networks.

In the following discussions, I would like to discuss metabolic origins of life scenario in more detail in order to elaborate the context of this thesis.

1.2 Metabolic origins of life

1.2.1 Perspective of nutrition

Metabolism functions to provide an organism with necessary elements (carbon, hydrogen, etc.) and energy for its survival. Present day organisms have a myriad of interconnected reactions that make this possible and the process by which an organism acquires them is called nutrition. There exist two forms of nutrition: autotrophic and heterotrophic (Figure 7). If an organism can synthesize all the necessary biomolecules for its survival by itself, using simple substances and energy found in its surroundings, it is defined as an autotroph. In this case, a complete metabolism occurs within a single individual. On the other hand, if an organism is incapable of this process and therefore relies on another organism for the necessary biomolecules, then it is called a heterotroph. The metabolism in this case is shared between multiple individuals. It is often surmised that the first living systems would have been autotrophic.³¹

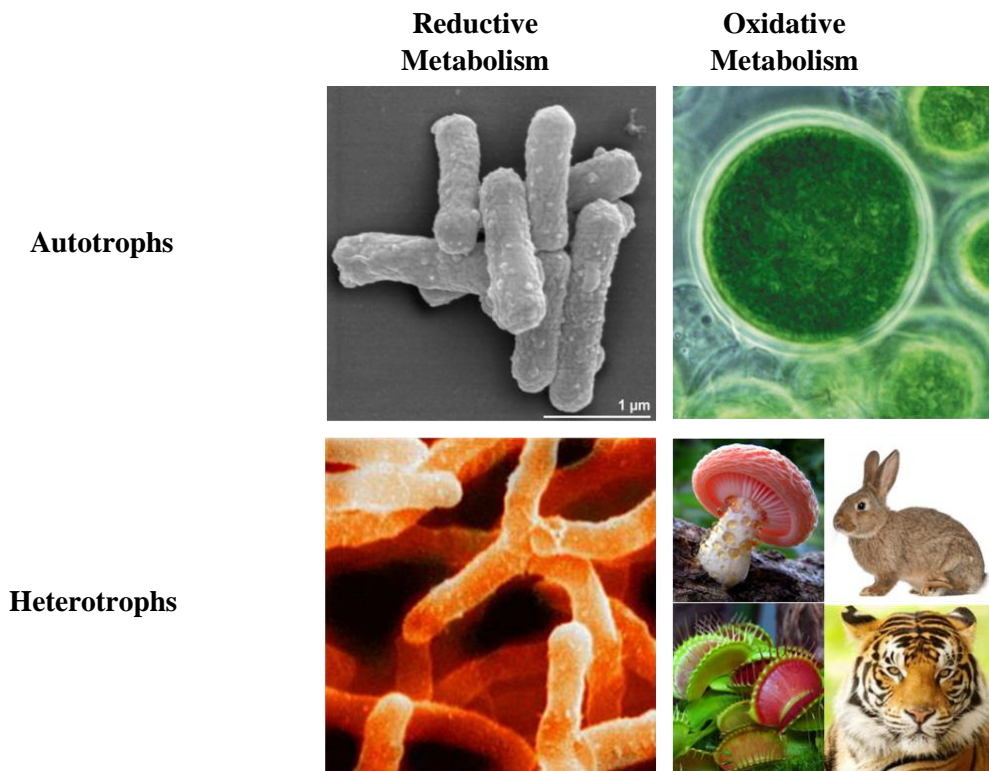


Figure 7 Metabolism from the perspective of nutrition: based on energy it can be classified as reductive and oxidative (vertical axis) and based on carbon acquisition as autotroph and heterotroph (horizontal axis).

Another important distinction within metabolism is the redox-directionality in the way an organism obtain energy. Certain organisms (mammals and other extant terrestrial organisms for instance) release energy from the food synthesized/consumed through oxidation of C-C bonds, in what is known as oxidative metabolism. This process requires an electron acceptor or an oxidant such as O_2 , SO_4^{2-} , NO_3^- etc. There are also other classes of organisms which obtain

energy by reducing or reductively forming C-C bonds, using dihydrogen, H₂S or another source of electrons. Such processes fall under the category of reductive metabolism. Again, it is believed that in the origins scenario, the first lifeforms would have relied on reductive metabolism due to the highly reducing environments found on the early Earth, as devised from the geological evidence.³²

Given these considerations, it has been proposed that the Last Universal Common Ancestor (LUCA), a hypothetical organism from which all extant organisms were derived, was a reductive autotroph.³¹

1.2.2 Perspective of phylogenetics

The previous discussion allowed us to infer the nature of metabolic reactions of ancient life forms. However, the type of reactions that occurred within them could be deduced only through extrapolation of extant metabolic reactions. Through phylometabolic analyses of biochemical pathways, it has been concluded that among the myriad of metabolic reactions that one finds in the biosphere, the reactions that occur in the tricarboxylic acid cycle (also known as the TCA cycle, the Krebs cycle or the citric acid cycle) are highly conserved and therefore probably the oldest.³¹ In a great percentage of extant organisms this cycle operates in the clockwise direction, generating energy through C-C bond cleavage to release CO₂, and is therefore oxidative. Notably, it is possible for the cycle to operate in the reverse direction, by incorporating electrons and carbon in the form of CO₂. In some deep-branching organisms, the reverse TCA cycle, also known as the reductive tricarboxylic acid (rTCA) cycle or the Arnon-Buchanan cycle, is the key player in metabolism.³³

The (r)TCA cycle could be imagined as a gear box of the metabolic reaction network as it embodies five universal precursors to all anabolic (the synthesis of complex molecules from simple molecules for the development or energy storage in an organism) reactions in biochemistry. Intermediates such as acetate, pyruvate, oxaloacetate, succinate and α -ketoglutarate form the precursors to fatty acids, sugars, amino acids and cofactors (Figure 8). This cycle and the associated biochemical mechanisms will be discussed in detail in Chapter 3.

In addition to its key role in biosynthesis, the chemistry of the (r)TCA cycle is unique as it confers autocatalysis to the network formed by its intermediates.³⁴ In the rTCA cycle, starting from acetate, a complete turn of the cycle would generate a molecule of oxaloacetate and acetate, regenerating the molecule that began the cycle. It has been pointed out that in the absence of highly specific enzymes to maintain the cycle, which would have been the case when

life was being formed on the early Earth, the cycle with yields less than 50% would have failed to survive due to other parasitic reactions.³⁰

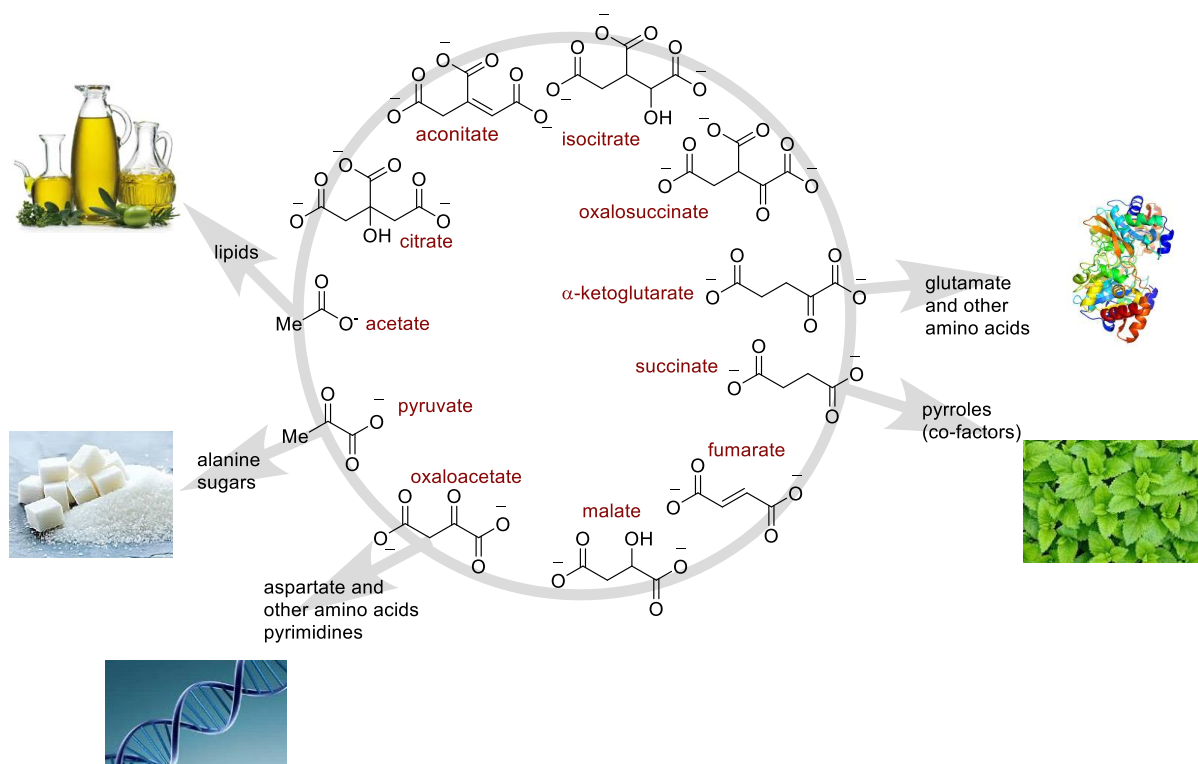


Figure 8 The (reverse)Tricarboxylic acid cycle and its metabolites

Nonetheless, it has been proposed that in the presence of a feeder pathway that could constantly supply one of the rTCA cycle intermediates, yields below 50% would be enough to sustain the chemistry of the rTCA cycle (Figure 9). Supporting this idea, a combined acetate feeder pathway and rTCA cycle has been proposed to constitute an ancient metabolic network.³¹

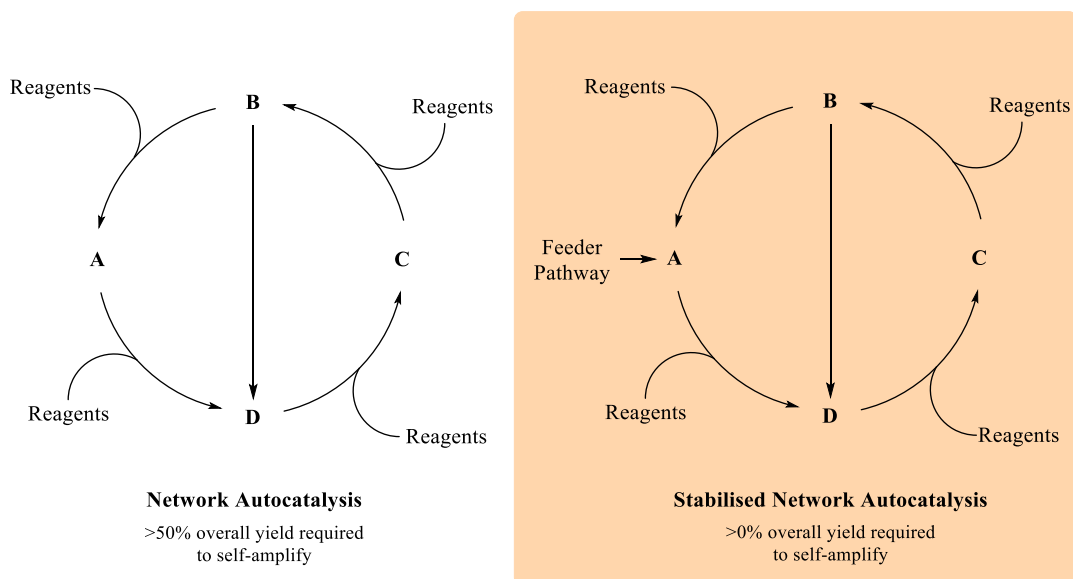


Figure 9 Autocatalytic reaction networks

Additional evidence comes from a phylogenetic analysis of evolutionarily conserved genes across all domains of life, which reveals that a small number of genes are common to all kingdoms without having been introduced through horizontal gene transfer, and therefore could have been the features of LUCA.³⁵ Amongst its features are Fe-Ni-S clusters, the second most abundant cofactor/prosthetic group in biochemistry after ATP. The identified clusters are involved in the autotrophic generation of acetate using CO_2 and an electron source, through a linear carbon fixation pathway known as the Wood-Ljungdahl (W-L) pathway. In addition to the generation of acetate, the W-L chemistry in extant organisms is exergonic, which would allow an organism to extract energy through the process.³⁶ Thus, a combined W-L pathway and the rTCA cycle could allow an organism to obtain both energy and the carbon for it to flourish. While the W-L pathway provides a constant supply of acetate from geochemical inputs, the reverse citric acid cycle chemistry subsequently builds up the biochemical reaction network, resulting in stabilized network autocatalysis (Figure 10), which could now address many of the shortcomings of the metabolism-first hypothesis.³⁴

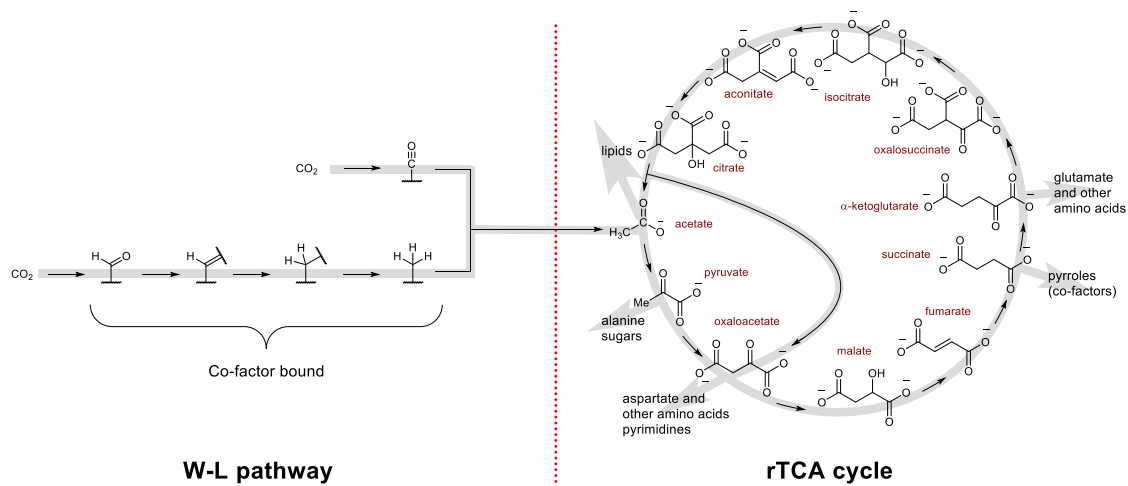


Figure 10 A stabilized network autocatalysis exhibited by W-L pathway and rTCA cycle

An alternative, chemically simpler version of the network above has also been proposed, where the “horseshoe” part of the rTCA cycle, comprising of all the five metabolic precursors, would have predated the complete rTCA cycle (Figure 11).²⁰ It remains to be experimentally evaluated which among these two proposals was more likely under a geological setting of the early Earth.

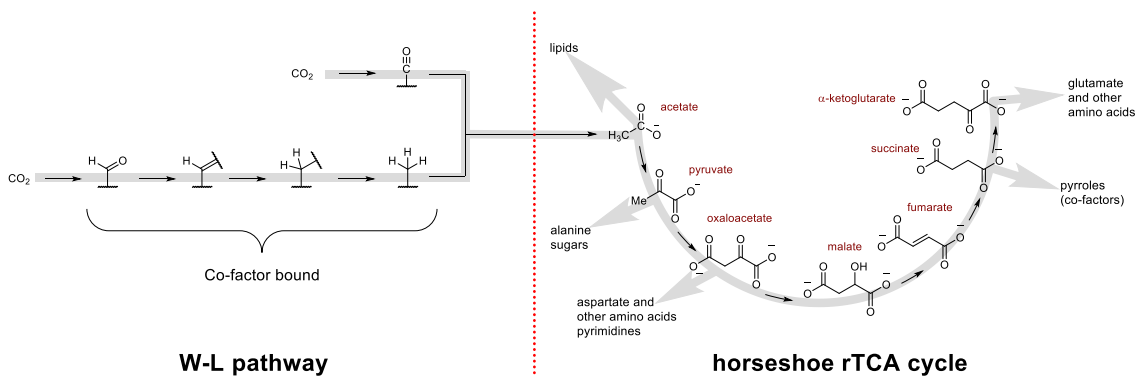


Figure 11 A W-L pathway and horseshoe rTCA hybrid

1.2.3 Ancient CO₂ fixation pathways

The following two chapters will discuss the carbon fixation pathways most commonly associated with metabolic theories for the origin of life with focus on the biochemistry of these pathways and evaluate their prospects in prebiotic chemistry.

2 The Wood-Ljungdahl pathway

2.1 Topology

Among the six known carbon fixation pathways in biochemistry, the Wood-Ljungdahl (W-L) pathway is believed to be the most ancient (others being the reverse tricarboxylic acid cycle, reductive pentose phosphate cycle, 3-hydroxypropionate cycle, 3-hydroxypropionate/4-hydroxybutyrate cycle and dicarboxylate/4-hydroxybutyrate cycle), as it is the starting point for carbon and energy metabolism in both acetogens and methanogens.³⁷ Unlike the other five autocatalytic carbon fixation pathways,^{38,39} the W-L is short and linear. Like the other carbon fixation pathways, it reduces carbon dioxide using electron sources found in the environment, usually dihydrogen (Figure 12). Utilising a process that couples exergonic and endergonic redox reactions to simultaneously generate (or utilize) low- and high-potential electrons, called electron bifurcation, electrons that have sufficiently negative reduction potentials (< -0.5 V) for certain key steps are generated.^{40,42} The assembly of acetate from carbon dioxide comprises two sets of reactions: reduction of one CO₂ molecule to a methyl group, and simultaneously, reduction of another CO₂ to carbon monoxide.⁴¹ In methanogens, the methyl group is channeled to methane formation (termed as methanogenesis, see Figure 12, grey arrows) which is coupled to energy metabolism. In acetogens, the methyl moiety is combined with a carbonyl to generate acetate (termed as acetogenesis, see Figure 12, black arrows) which could then take part either in energy metabolism or carbon metabolism. This series of reactions generates a proton gradient across the mitochondrial membrane (eukaryotes), plasma membrane (bacteria) and thylakoid membrane (photosynthetic organisms), which is then exploited by these organisms to generate the energy-rich ATP molecule via coupling an ADP and an inorganic phosphate molecule using a molecular rotor-stator.⁴²

2.2 Enzymes and mechanism

The first step in acetogenesis comprises of a reversible two-electron reduction of carbon dioxide to formate (Figure 12, step I) and is carried out by an enzyme called *formate dehydrogenase* (FDH) when a suitable reductant such as H₂ is available.⁴³ In anaerobic organisms, this enzyme may consist of oxygen-sensitive metal centers based on tungsten (W), molybdenum (Mo), non-heme iron (Fe) or molybdopterin cofactors. Most often the tungsten-containing FDHs are highly homologous to the molybdenum-containing FDHs. Subsequently this formate moiety is condensed with a tetrahydrofolate to form a 10-formyl-H₄ folate, which in turn is reduced to a (6S)-5-CH₃-H₄ folate through a series of intermediates known as 5,10-methenyl-H₄ folate and 5,10-methylene-H₄ folate (Figure 12, step II).⁴⁴

Simultaneously, a Ni-containing metalloenzyme called *carbon monoxide dehydrogenase* (CODH) catalyzes the reversible reduction of CO₂ to CO (Figure 12, step III). The next enzyme one encounters in the W-L pathway is the cobalamin-containing corrinoid iron sulfur protein (CoFeSP), which acts as a mediator for two processes. In the first process, the methyl moiety is transferred from methyl tetrahydrofolate to the Co(I) center of CoFeSP. The newly generated methyl-Co(III) species then transfers the methyl group to the reduced active site of an enzyme called *acetyl CoA synthase* (ACS) (Figure 12, step IV).

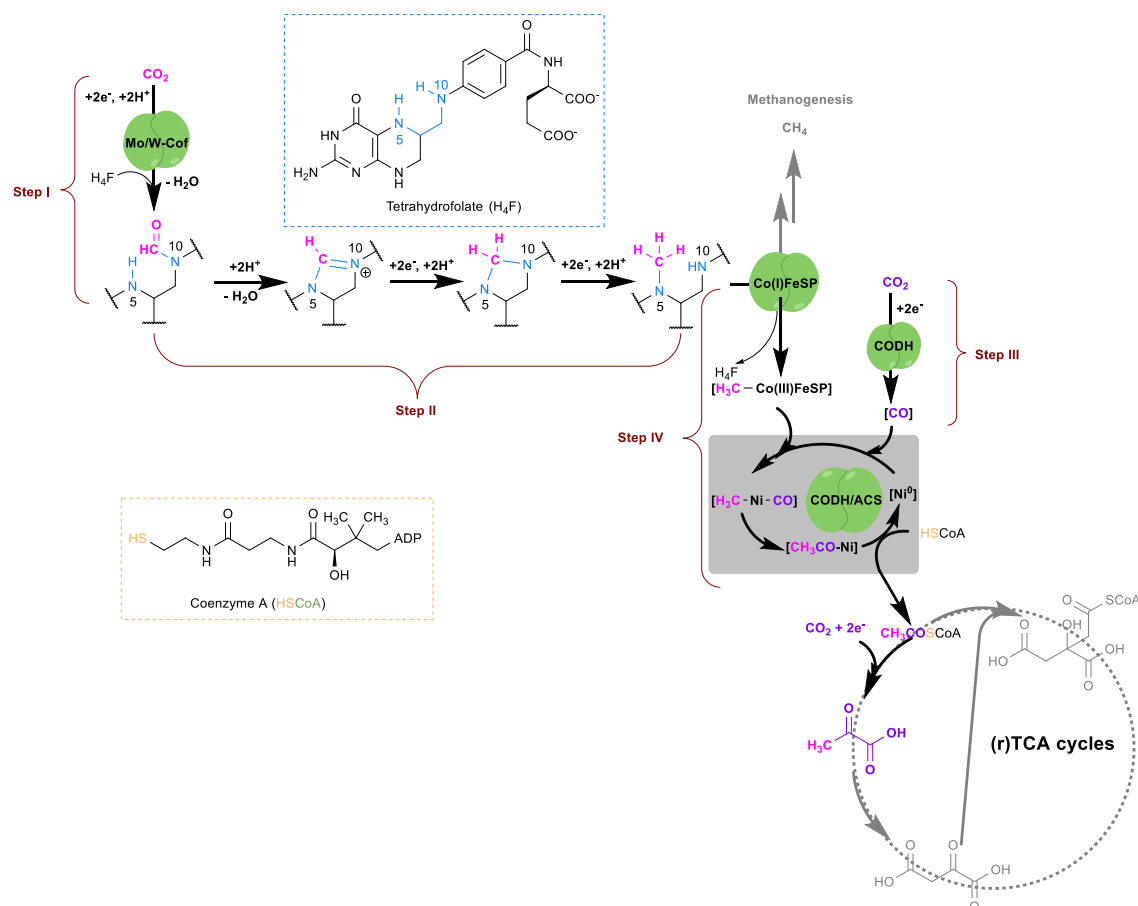


Figure 12 The metalloenzymes and cofactors of the W-L pathway

Ultimately, the CO that is generated in step III is combined with the methyl-group-bearing CoFeSP from step IV in the presence of coenzyme A to produce acetyl CoA by yet another Ni-metalloenzyme, ACS. These two equations portray a reaction that is typically organometallic in nature, with the nickel of the ACS enzyme acting as the transition metal catalyst (Figure 12, grey field).⁴¹ There are two types of ACS in anaerobic microbes: a monofunctional variant that is capable of only generating acetyl CoA (Figure 12, grey field) and a bi-functional variant can additionally perform the reduction of CO₂ to CO. But both have been known to contain Ni as the catalytic metal. Studies have shown that Cu, Ni and Zn can occupy the neighboring sites,

but only Ni is the catalytically active metal.⁴⁵ In the case of methanogens, the methyl-Co(III)FeSP is intercepted and channeled to methane generation.

3 Tricarboxylic acid cycles

3.1 Introduction

Regardless of the redox-direction of their metabolisms, living organisms always build their biochemistry from a small collection of carboxylic acids that can be interconverted to generate the five precursors to all other metabolic pathways: acetate, pyruvate, oxaloacetate, succinate and α -ketoglutarate, which universally act as the starting point for various anabolic processes like synthesis of fatty acid, sugars, amino acids, and cofactors. Due to its relevance to human biochemistry, the best-known pathway for interconversion of central carboxylic acid metabolites is the Krebs cycle, also known as the citric acid cycle or the Tricarboxylic Acid (TCA) cycle.³⁸ The TCA cycle, in part or in whole, typically operates in organisms that derive energy and carbon from complex molecules such as sugars and fats, usually obtained from other organisms (heterotrophy). It serves to break down complex molecules into simpler building blocks while conserving energy in the form of ATP and electrons in the form of reduced co-factors. The energy harnessed from this breakdown (catabolism) can then be used to build up complex molecules for its survival (anabolism). Being a player in both metabolic processes, the TCA cycle acts as a gear box or a hub of biochemistry. However, to the astonishment of many in the biochemistry community, in 1966 Arnon and co-workers discovered that some organisms living in reducing environments such as *Chlorobium thiosulfatophilum*, run the cycle in the reductive (anti-clockwise) direction.³⁹ This cycle is known as the reverse Krebs cycle, also known as the reverse citric acid cycle, the Arnon cycle or the reverse Tricarboxylic Acid (rTCA) cycle (Figure 13). Organisms running the rTCA cycle use a source of electrons in their environment to build up their biochemistry completely from CO₂ as the sole carbon source.

3.2 Enzymes, mechanisms of the rTCA and TCA cycles

The rTCA and TCA cycle comprises of the same 11 intermediates (or 13, if one considers thioester intermediates) that are connected by 6 different reaction types. Although the TCA and rTCA cycles run in opposite redox directions, the catalytic machineries that mediate them share many similarities. In the following sections, we will briefly describe the enzymes and

mechanisms of the reactions making up both cycles, starting first with the rTCA cycle due to its greater relevance to the work in this thesis.

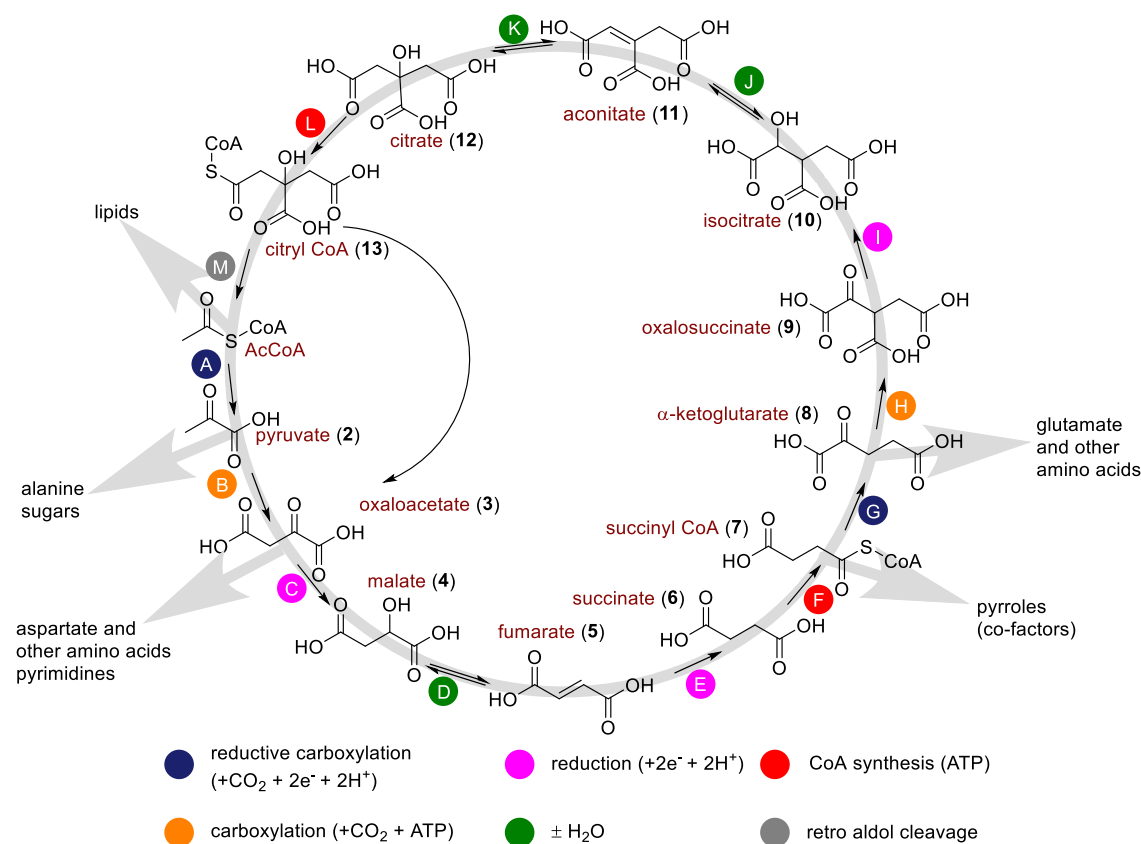


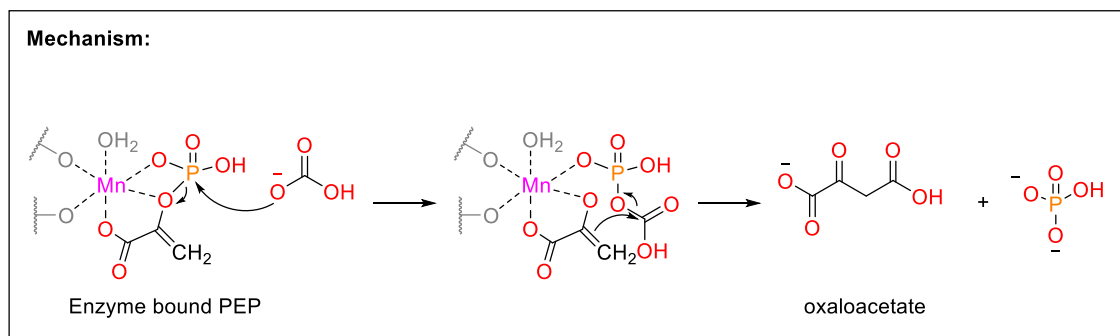
Figure 13 The reverse Tricarboxylic acid (rTCA) cycle

3.2.1 Reductive tricarboxylic acid (rTCA) cycle biochemistry

I. Reductive Carboxylations (Steps A, G)

This step of the rTCA cycle is catalyzed by a ferredoxin dependent enzyme and thus contains a Fe-S cluster (Figure 14, D). The enzyme catalytic site also harbors a thymine pyrophosphate (TPP), which attacks the coenzyme A bound acyl group.⁴⁶ Instead of forming an aldehyde, the TPP bound intermediate is maintained as an acetyl radical bound to a non-aromatic thiazole molecule. This typically makes these enzymatic reactions oxygen sensitive but certain enzyme variants can nevertheless operate in the presence of oxygen.⁴⁷ In certain species, a promiscuous enzyme (i.e. an enzyme that could catalyze multiple chemistries) is capable of carbonylating both acetyl-CoA and succinyl-CoA.⁴⁸ Although the mechanism is not well understood yet, it is believed to operate in a similar fashion to the oxidative TCA cycle, shown later in Scheme 5.

II. Carboxylation (Steps B, H)



Scheme 2 Mechanism of pyruvate carboxylation⁴⁹

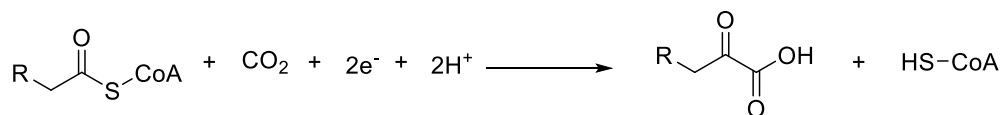
Pyruvate is converted into oxaloacetate in a two-step process, via an intermediate phosphoenolpyruvate (PEP) (Figure 14, II). The first step comprises an ATP-dependent phosphorylation of pyruvate by an enzyme *pyruvate dikinase* to generate PEP. This enzyme is also active in the gluconeogenesis pathway, where PEP is the starting C₃ compound for sugar biosynthesis. In the next step, PEP is combined with a bicarbonate ion to generate oxaloacetate by a biotin-dependent enzyme *PEP carboxylase*. The second step requires the presence of divalent metals such as Mg²⁺ or Mn²⁺ for stabilizing the intermediate while, on the other hand, other divalent metals like Ni²⁺ could be detrimental for the reaction. The mechanism of the carboxylation reaction is shown in **Scheme 2**. Certain organisms use a single enzyme *pyruvate carboxylase* to catalyze both the ATP-dependent and biotin-dependent steps.⁴⁹

In the case of α -ketoglutarate, the reaction proceeds like with pyruvate: α -ketoglutarate is converted into oxalosuccinate in the presence of Mg²⁺ through ATP hydrolysis. The oxalosuccinate thus generated is immediately converted into isocitrate, discussed in the next section.^{50,51}

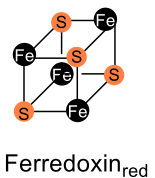
III. α -Ketoacid reduction

These *dehydrogenase* enzymes catalyze the reversible reduction of oxaloacetate (R=H) or oxalosuccinate (R=CH₂COOH) to the corresponding 2-hydroxy acids malate and isocitrate respectively, using NADPH as the two-electron donor (Figure 14, III). In the case of *isocitrate dehydrogenase*, the enzyme activity is not limited to the reduction of the ketoacid but also the carboxylation of α -ketoglutarate that occurs prior to the reduction.⁵²

I. Reductive carboxylation : Steps A G



2e⁻ from



Step

A

R

-H

Enzyme

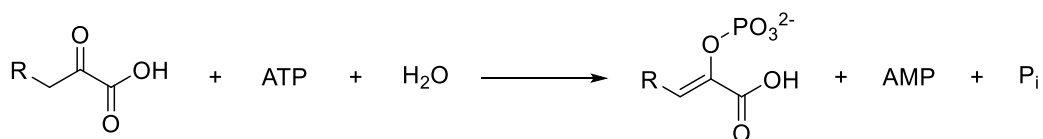
Pyruvate
synthase

G

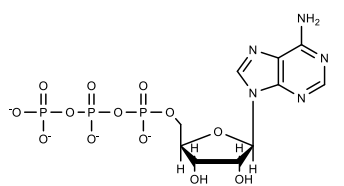
-CH₂COOH

α-ketoglutarate
synthase

II. Carboxylation : Steps B H



for R=H, Phosphoenolpyruvate (PEP)



Adenosine Triphosphate (ATP)

Step

B

R

-H

Enzyme

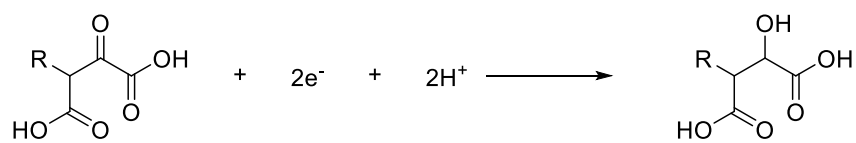
Phosphoenol
pyruvate
carboxylase

H

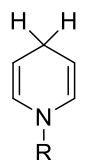
-CH₂COOH

Isocitrate
dehydrogenase

III. Carbonyl reduction: Steps C I



2e⁻ from



Step

C

R

-H

Enzyme

Malate
dehydrogenase

I

-CH₂COOH

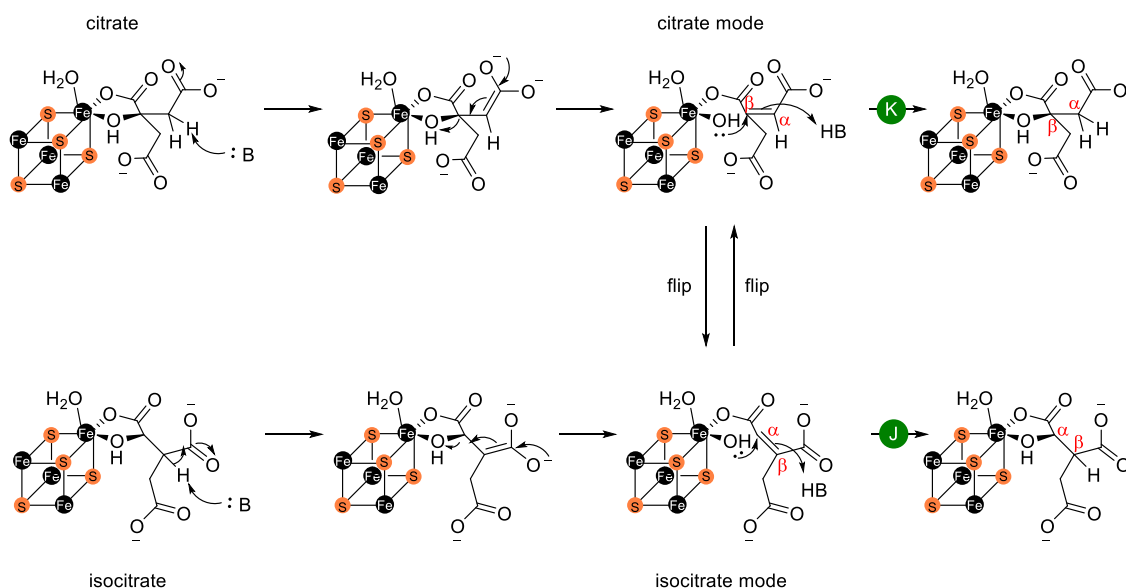
Isocitrate
dehydrogenase

Figure 14 Enzymatic reactions of rTCA cycle

IV. Dehydration-Hydration

The dehydration chemistry is reversible and is carried out by an iron-sulfur cluster-containing enzyme and is therefore oxygen sensitive (Figure 15, IV). This enzyme, *aconitase*, can be found in mitochondria carrying out the rTCA reactions while *fumarase* is found in the cytosol and is also a part of the amino acid salvage pathway and the urea cycle.⁵³

The function of *aconitase* is not limited to the dehydration of isocitrate to aconitate. Neilson observed that *aconitase* enzyme of certain organisms could be separated into two components with one catalyzing isocitrate dehydration to aconitate and other hydrating the aconitate to citrate.⁵⁴ The Fe-S cluster promoted hydration is believed to proceed according to the following mechanism (Scheme 3). Upon binding the of isocitrate, a base residue abstracts the proton from the most acidic C-H bond. This in turn favors the removal of a water molecule from the isocitrate in a conjugate-type elimination. At this point the molecule undergoes a rotation of 180° called a flip, from isocitrate mode to citrate mode, followed by hydration on the opposite face to yield a citrate molecule. The overall process is reversible, implying the enzyme is also capable of catalyzing the reverse reaction of citrate to isocitrate.



Scheme 3 Mechanism of citrate-isocitrate isomerization⁵⁵

V. Alkene reduction

This reaction is catalyzed by *fumarate reductase* using a reductant with a low reduction potential (Figure 15, V). This is due to the low reduction potential of fumarate/succinate couple (- 0.03 V). While many organisms use quinone (menaquinone, a vitamin K₂ analogue) as reductant, certain autotrophs that operate rTCA use NADH as an electron donor.^{56,57}

VI. Thioester synthesis

The ATP-consuming conversion of a carboxylic acid to a thioester by *succinyl CoA ligase* is a critical step that, besides its important role in the rTCA cycle, controls other metabolic pathways like propanoate acid metabolism, porphyrin and heme biosynthesis (Figure 15, VI).⁵⁸ Analogously, *citryl CoA synthase* produces activated citrate thioester that undergoes retro-aldol cleavage to generate acetyl CoA, the precursor to lipid synthesis (Figure 15, VI).⁵⁹

VII. Retro-aldol cleavage

The redox neutral cleavage of citryl CoA to oxaloacetate and acetyl CoA completes the rTCA cycle (Figure 15, VII). The enzyme *ATP citrate lyase* can perform both the thioester synthesis and retro-aldol cleavage steps, although in many organisms a two-enzyme citryl-CoA synthetase / citryl-CoA lyase tandem is used.⁶⁰ This reaction is critical because it imparts the rTCA cycle with an autocatalytic topology.

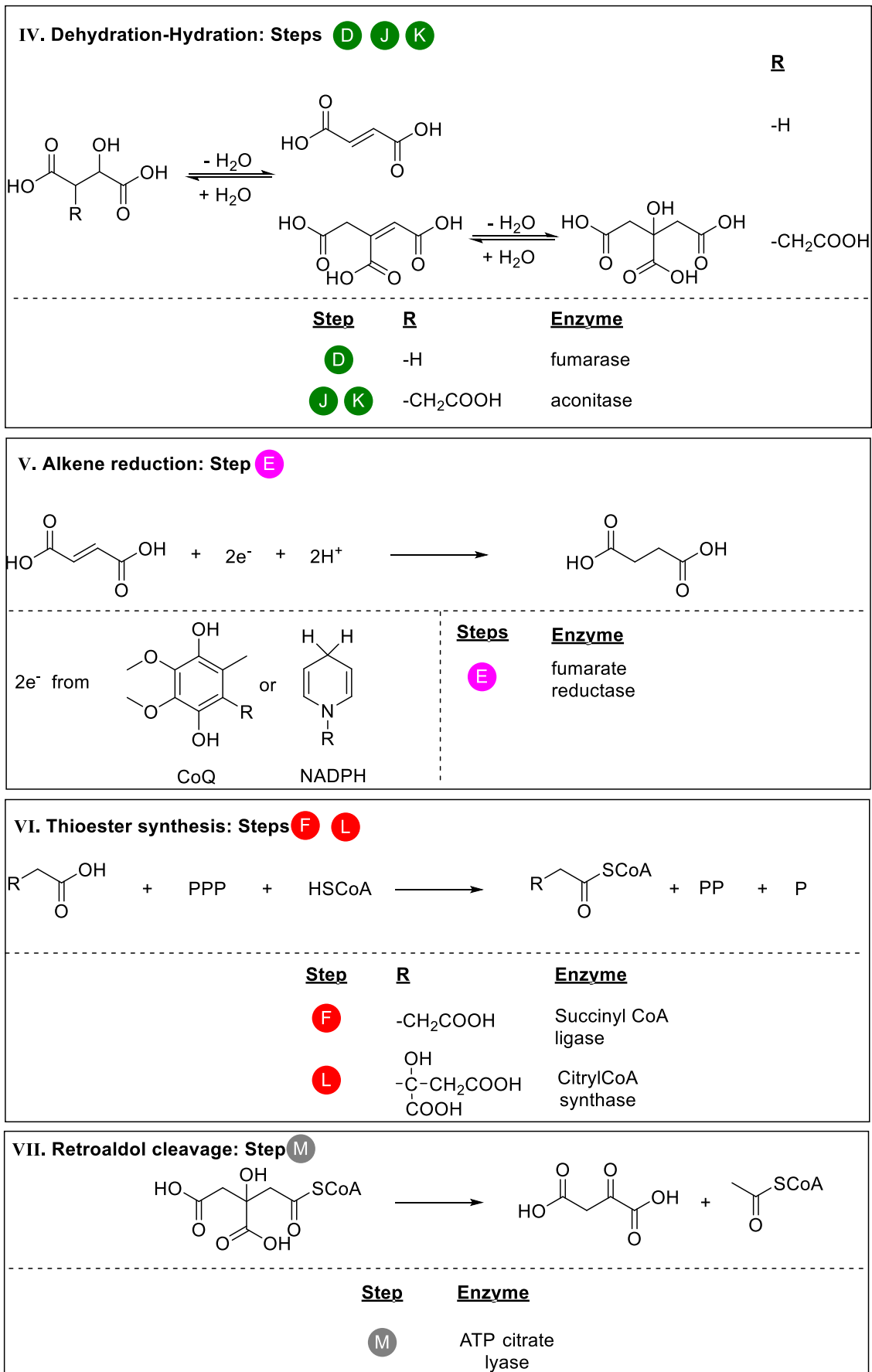


Figure 15 Enzymatic reactions of rTCA cycle (continuation...)

3.2.2 Oxidative TCA cycle biochemistry

The oxidative TCA cycle, in part or in whole, is of central important to oxidative biochemistries, including in humans. Due to phylogenetic analysis and the generally accepted low amount of oxygen on the early Earth, the purely oxidative TCA cycle is nowadays thought to have been a late development in the origin of life compared to parts of the rTCA cycle. However, it remains a core hub of biochemistry that, like its reductive variant, contains the five universal precursors to biological metabolism and has been the object of experimental studies in prebiotic chemistry. Furthermore, recent discoveries suggest that the precursor to both TCA and rTCA cycles may not have been unidirectional, but one that can run in either direction. For this reason, the reactions of the pathway may still have some relevance to prebiotic chemistry and we therefore review the reactions of the TCA cycle.

I. Decarboxylation

This is the reverse reaction of the carboxylation reaction discussed earlier. It is used by certain organisms to pump sodium ions across membranes (Scheme 4, eq. I). Although a spontaneous process, the *oxaloacetate decarboxylase* uses a Zn^{2+} ion to stabilize the pyruvate that is formed.⁶¹ In the case of oxalosuccinate, the decarboxylation is concomitant to the dehydrogenation catalyzed by *isocitrate dehydrogenase* in a one-step process to generate α -ketoglutarate. While the *isocitrate dehydrogenase* operating in mitochondria (involved with the TCA cycle) are NAD^+ dependent, those found in cytosol (involved with metabolic pathways not related to the TCA cycle) use $NADP^+$ as cofactor.

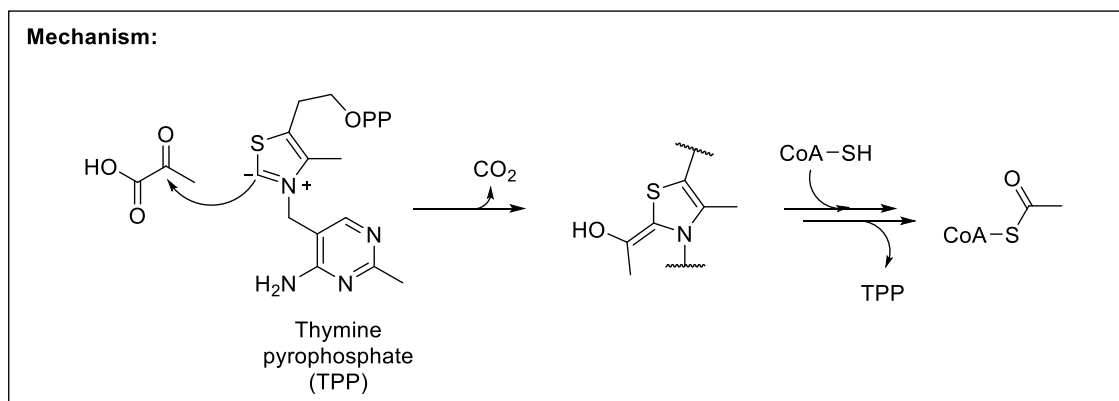
II. Aldol condensation

In this initial step of the TCA cycle, acetyl CoA is condensed with oxaloacetate by the enzyme *citrate synthase* to generate a molecule of citrate which then proceeds to the TCA cycle (Scheme 4, eq. II).⁶²

III. Alkane to alkene oxidation

Succinate dehydrogenase, which catalyzes this oxidative transformation, forms a part of the respiratory complex (II) located in the inner mitochondrial membrane (Scheme 4, eq. III). In addition to the FAD, the enzyme complex also possesses a heme group, ubiquinone and a network of iron-sulfur clusters for efficiently transporting electrons abstracted from succinate.⁶³

V. Decarboxylative oxidation



Scheme 5 Mechanism of pyruvate decarboxylation

Pyruvate dehydrogenase is part of an enzyme complex “pyruvate dehydrogenase complex” and is related to other 2-oxoacid dehydrogenases structurally and functionally (Scheme 4, eq. V). The enzyme produces a molecule each of acetyl CoA and NADH through the decarboxylation of pyruvate catalyzed by thymine pyrophosphate (mechanism shown in Scheme 5).⁶⁶ *α-Ketoglutarate dehydrogenase* functions in a similar fashion to pyruvate dehydrogenase and is structurally related.⁶⁷

4 Amino acids

4.1 Introduction

Amino acids, in the form of peptides, form a significant share (45 %, w/w) of the cellular biomass.⁶⁸ Making up the enzyme structures that catalyze the formation of the very amino acids they are built from, these biomolecules present the prototypical chicken-egg problem of prebiotic chemistry. A closer examination of different amino acids with a focus on the source of their carbon skeleton reveals that 17 out of the 20 amino acids used by life are synthesized in biochemistry from three TCA cycle intermediates: pyruvate, oxaloacetate and α -ketoglutarate (Figure 16).

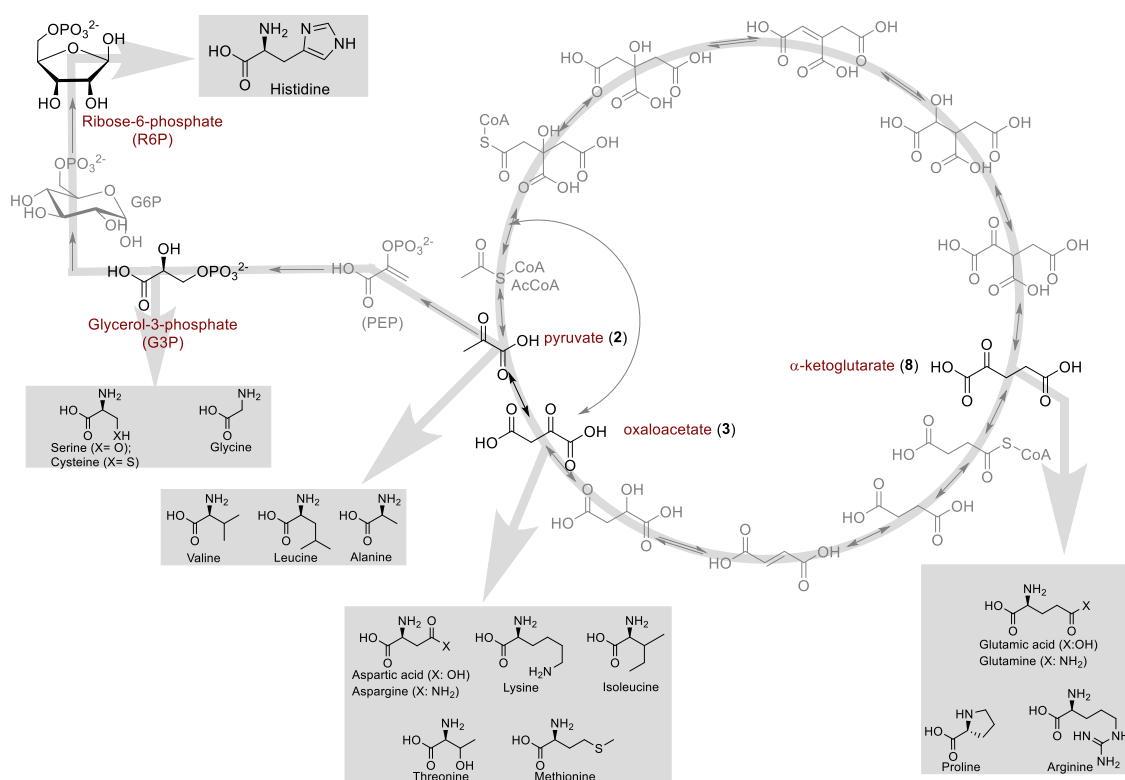


Figure 16 Biosynthesis of amino acids.

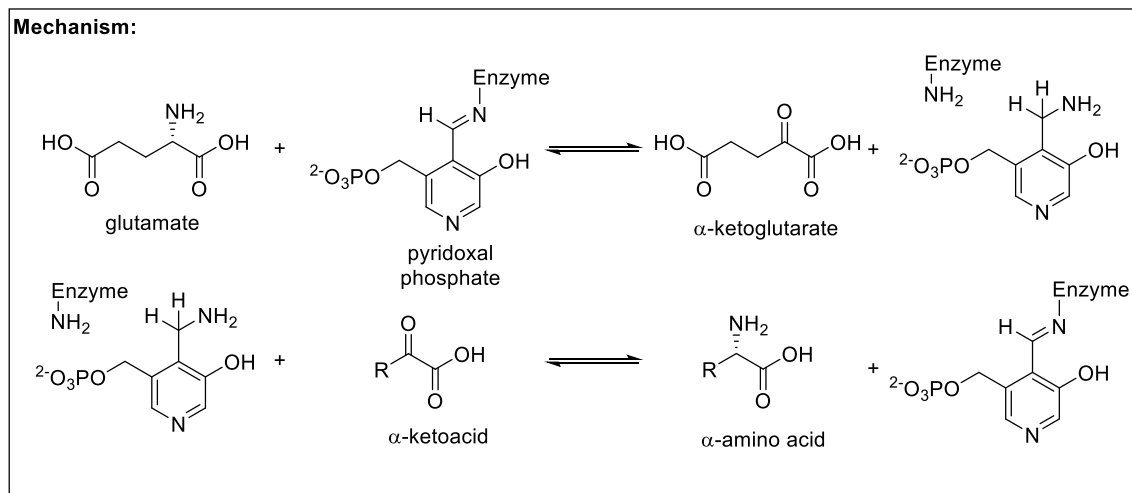
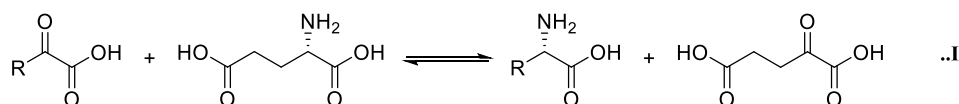
4.2 Biosynthesis

Biosynthesis of amino acids comprises of two parts:⁶⁹

1. Synthesis of the α -keto acid carbon skeleton.
2. Introduction of nitrogen atom to the carbon skeleton via transamination or reductive amination.

4.2.1 Transamination

Transamination consists of an amino group transfer from glutamate to an α -keto acid (Scheme 6, eq. I) by a class of enzymes called *aminotransferases* or *transaminases* that require a cofactor called pyridoxal phosphate. The mechanism proceeds in two steps, first being the transfer of the amine group from glutamate to the pyridoxal phosphate (Scheme 6). The second step involves the transfer of the amino group from the pyridoxal phosphate to the target α -keto acid to generate the corresponding amino acid.⁶⁹



Scheme 6 Mechanism of transamination

Interestingly, the biosynthetic entry of nitrogen into metabolism always occurs first via the glutamine/glutamate couple.⁷⁰

PART II

Central aim of this thesis

While the hypotheses for a metabolism-first origin of life are highly intellectually appealing and have several advantages compared to genetics-first theories, surprisingly little experimental work has been done in this regard. I suspect it is because most synthetic organic chemists with the skills to experimentally evaluate such hypotheses are unaware of them due to minimal overlap of this field and evolutionary biochemistry. The door of opportunity is thus open for our laboratory.

This thesis describes my efforts to experimentally evaluate some key ideas regarding the origins of metabolism: **“Could the W-L pathway and rTCA cycle be catalyzed by simple inorganic catalysts? Could amino acids also be synthesized starting from intermediates of these pathways under a mutually compatible set of conditions?”**

1 The reverse Tricarboxylic Acid Cycle¹²

1.1 Introduction

Due to its autocatalytic, and therefore potentially self-amplifying topology and its central place in biochemistry, the rTCA cycle has been suggested to be a metabolic pathway that likely arose very early in the emergence of life, possibly at the stage of prebiotic chemistry. In 1988, Wächtershäuser proposed a prebiotic sulfur-based analog of the rTCA cycle catalyzed by FeS minerals.²² In 2004, Smith and Morowitz proposed that a more biology-resembling rTCA cycle may have operated before enzymes, possibly catalyzed by metal ions.³⁴ However, the full rTCA cycle is only found in one major branch of the tree of life (bacteria) and not the other (archaea), and thus it has been argued that it is unlikely to have been operating in its full form in a hypothetical common ancestor.⁴⁰ Rather, the first six steps of the rTCA cycle, known as the horseshoe rTCA, are widely found across both major branches and thus are more likely to be the most ancient.⁷¹

1.2 Could the (r)TCA cycle have its origins in prebiotic chemistry? - State of the art

Today, the biological rTCA cycle is regulated by no fewer than ten distinct enzymes, but evidence exists that mechanistically similar steps were once catalyzed by a smaller, more promiscuous set of enzymes.⁷² If some form of the rTCA cycle was indeed prebiotic, it would obviously need to be enabled by much simpler inorganic catalysts. Many of the enzymes of the rTCA cycle rely on metal-based co-factors in their active sites, which may provide a clue as to how a prebiotic precursor to the cycle could have operated on early Earth. In fact, some hydration/dehydration reactions closely related to the rTCA cycle had already been demonstrated under acid, base or metal ion catalysis even before the enzymology of the cycle was elucidated.^{73,74} A Lewis acid mediated process was postulated to promote the isocitrate-aconitate dehydration.⁷⁵

¹ Parts of this chapter have been published as: Muchowska, K.B., Varma, S.J., Chevallot-Beroux, E., Lethuillier-Karl, L., Li, G., and Moran, J. (2017). Metals promote sequences of the reverse Krebs cycle. *Nat. Ecol. Evol.* 1, 1716–1721.

² For detailed experimental description please see: Part III, section 1

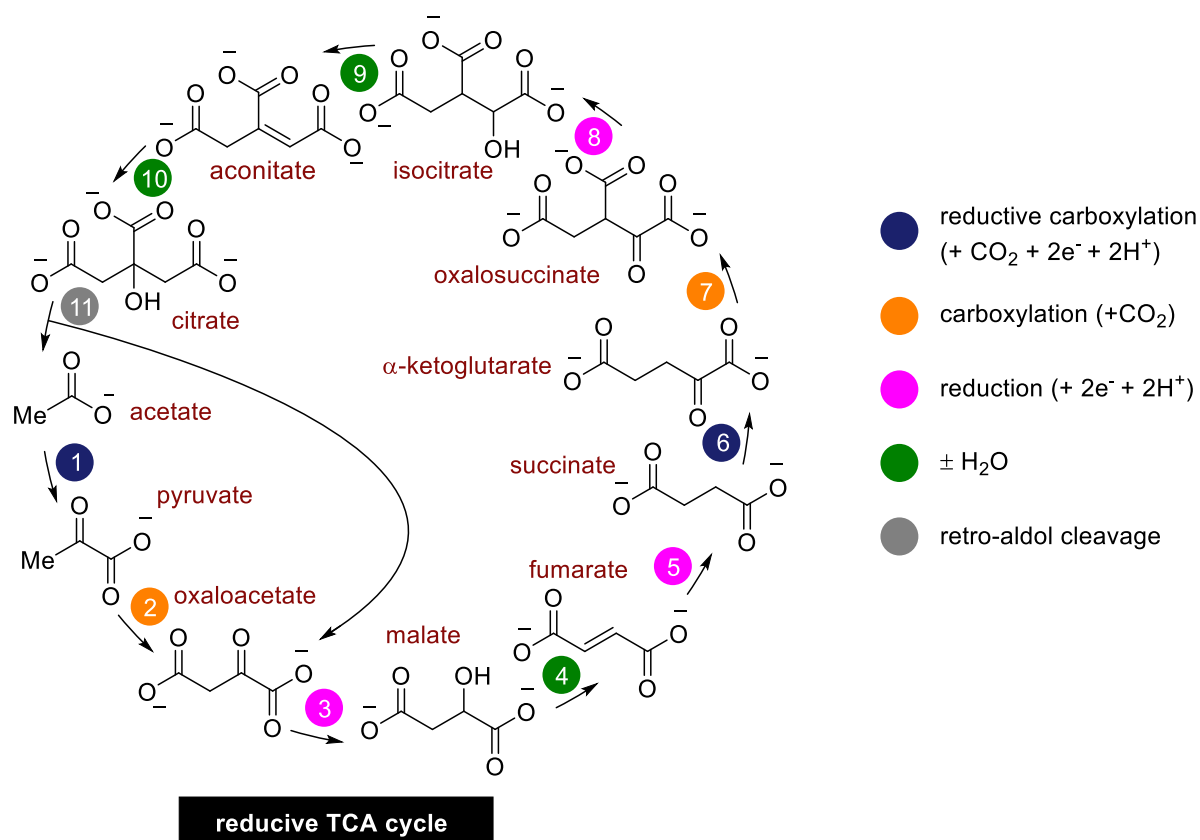
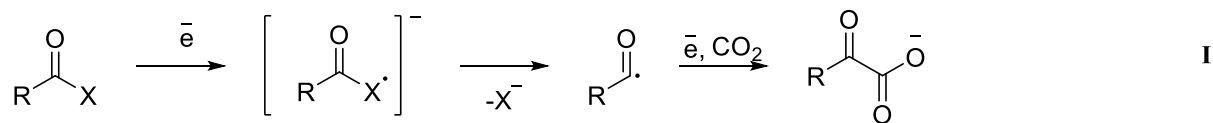


Figure 17 Reactions of the reductive TCA cycle

1.2.1 Non-enzymatic reactions of reductive TCA cycle

Net reductive reactions are observed when the citric acid cycle operates in the counter-clockwise direction (Figure 17). The chemistry involves a reducing agent donating two electrons to a carboxylic acid/ester, ketone or an alkene, converting them to a ketone, alcohol or alkane, respectively. The first reductive step in the rTCA cycle is the reductive carboxylation of acetyl to pyruvate. Like the enzymatic reaction discussed earlier, this reaction would require an activated acid in the form of a (thio)ester. The earliest attempts of this type of transformation were reported by Tabushi and coworkers using Schrauzer's complex ($(\text{FeS}_4\text{C}_4\text{Ph}_4)_2$) to reductively carboxylate an acetyl thioester in a manner reminiscent of the biochemical mechanism.⁷⁶ In spite of very low yields with respect to the thioester, they were able to show that the pyruvate that was generated could subsequently be reacted with ammonia to produce the corresponding amino acid, alanine. In a similar study, Cody and co-workers used FeS-NiS clusters instead of Schrauzer's complex to transform formic acid to acetate and pyruvate and established that the pyruvate is formed through an acetyl intermediate.⁷⁷ A more synthetic organic variant of this transformation was demonstrated by Lopushanskaja and co-workers,

who showed that acetyl chloride undergoes electrochemical reductive carboxylation to pyruvate in 60 % yield (Eq. I).⁷⁸



The widespread occurrence of FeS clusters in many rTCA enzymes and co-factors prompted investigations into their ability to promote redox transformations of the rTCA cycle in the absence of enzymes. Su and coworkers reported a bi-directional catalytic system, which could operate with FeS in the oxidative or reductive direction depending on the presence or absence of S⁰/H₂S respectively for the redox interconversion between pyruvate-lactate or oxaloacetate-malate.⁷⁹ The chemistry was further extended towards other steps of the cycle using ZnS photocatalysis, allowing multiple steps of the rTCA cycle (Figure 18, reactions 5, 6 and 7) to be carried out under a single set of reaction conditions.⁸⁰ The in-situ generated ZnS colloidal particles, upon irradiation by UV/visible light, give electrons to the reduceable rTCA cycle intermediates.

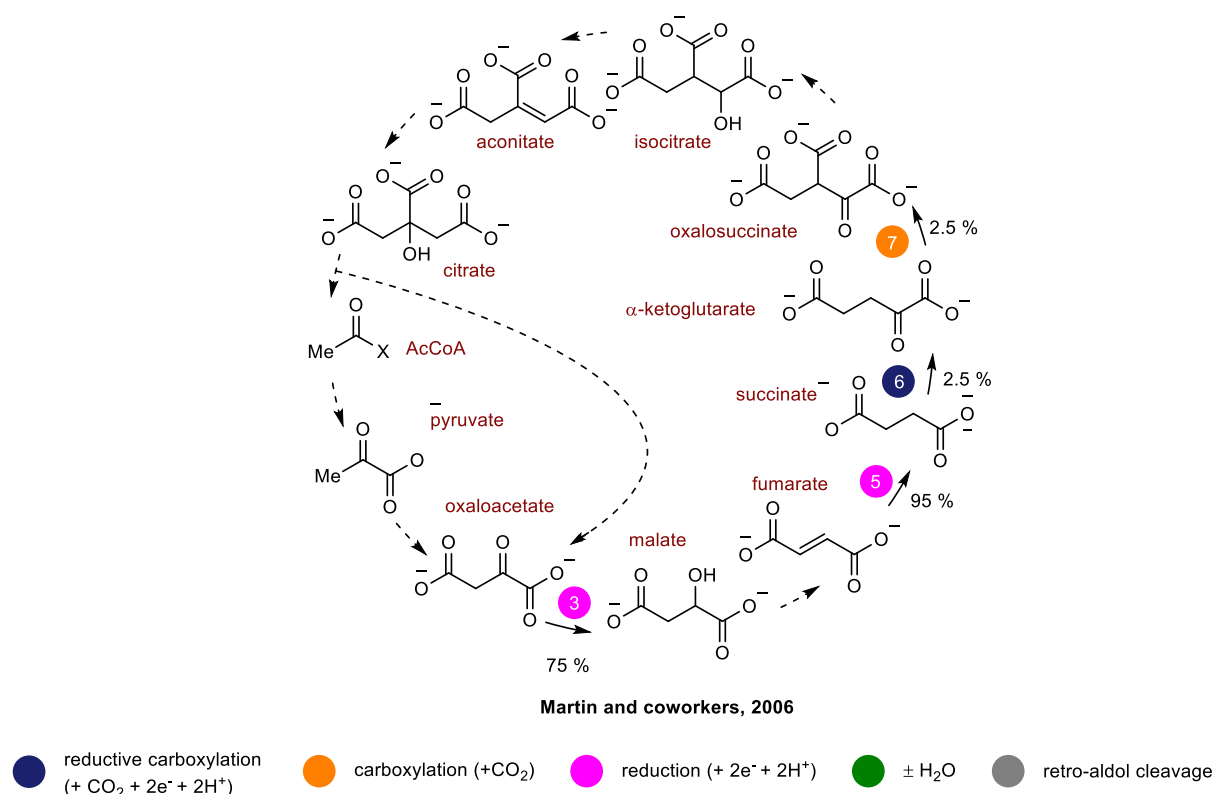


Figure 18 Driving multiple steps of rTCA cycle using ZnS photochemistry (solid arrows show transformations of rTCA that were successful in the study).⁸⁰

1.2.2 Non-enzymatic reactions of oxidative TCA cycle

Although Su and coworkers reported the oxidation of α -hydroxy acids to their corresponding α -keto acids using FeS/S⁰/H₂S system,⁷⁹ the scope of the transformations was further explored by Ralser and co-workers. Using a combination of FeS and S₂O₈²⁻ they were able to show that starting from almost any intermediate of the TCA cycle, the reactions of the TCA cycle could be triggered with a similar topology in up to 90% carbon efficiency through a sulfate radical mediated process.⁸¹ Although such a non-enzymatic variant of the TCA cycle lacks one of its critical biological features, the ability to conserve energy from its breakdown in the form of ATP, it nonetheless demonstrates that even oxidative biochemistry likely follows a pathway that resembles the abiotic chemistry and enzymes serve only to speed up and to guide selectively. Whether these fascinating observations have any direct relevance to the origin of life remains to be seen.

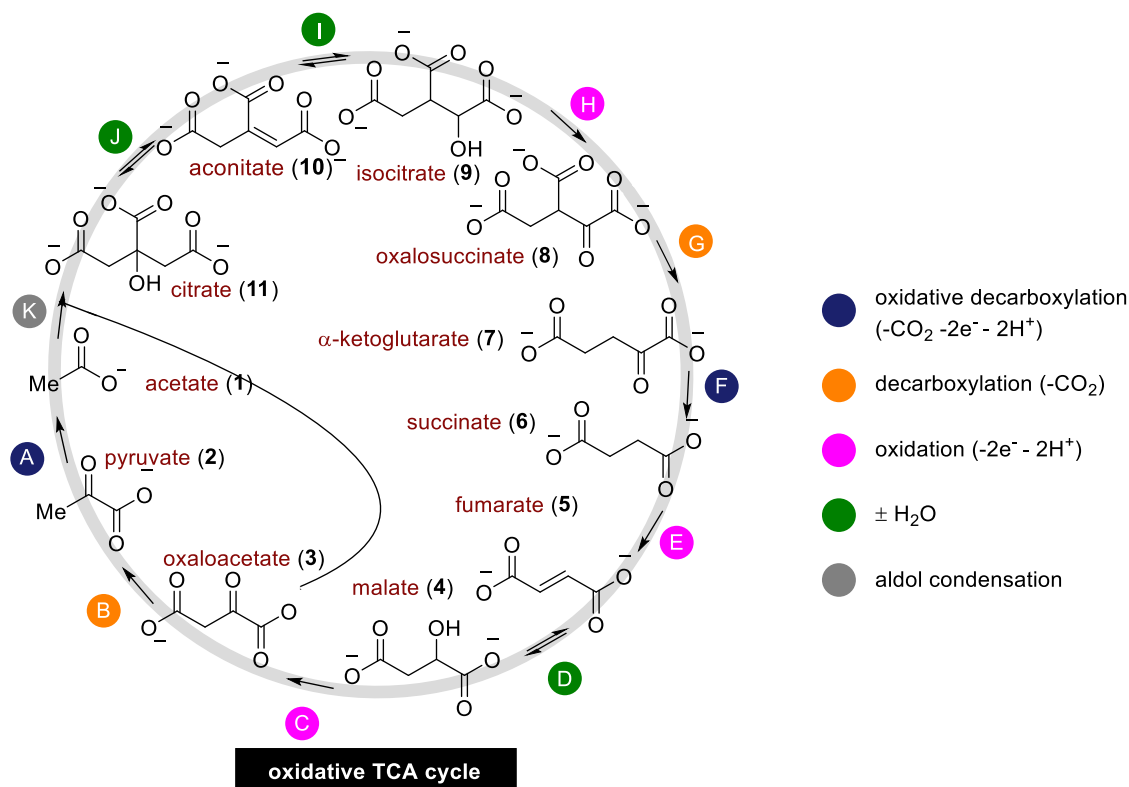


Figure 19 Reactions of the oxidative TCA cycle

1.3 Aim of this chapter

While there exist several studies demonstrating the viability of individual reactions of the rTCA/TCA cycles without enzymes, little is known regarding the plausibility of operating sequential reactions under a single set of conditions. In the following sections, I explore

chemical conditions that were plausible on early Earth that would allow the chemistry of ATP independent rTCA cycle sequences to occur.

1.4 ATP Independent reactions- reduction and (de)hydration

1.4.1 Reduction reactions

The reduction of oxaloacetate to malate has a reduction potential of -0.166 V and as seen earlier, is reduced in cells using the reductant NADPH, which has a reduction potential of -0.32 V.⁸² On the other hand, the reduction of fumarate to succinate has a reduction potential of -0.031 V and uses FADH₂ that has a reduction potential of -0.21 V.⁸² Translating this to abiotic environments would therefore require reducing agents with a lower reduction potential than -0.166 V. A preliminary screen of simple inorganic reducing agents (Fe⁰, Ni⁰, Zn⁰, Mn⁰, Mo⁰ and Na₂S₂O₄; all are strictly reducing under the conditions employed for the study) over a range of temperatures and pH on a mixture of various rTCA intermediates that could be reduced (pyruvate, oxaloacetate, fumarate, α -ketoglutarate and aconitate), identified several metals that were capable of reduction (Table 4). But, it was only Fe⁰ and Ni⁰ that could also promote the on-cycle reductions while minimizing other parasitic off-cycle reductions (Figure 20). These results together with the compelling evidence of Fe being the major component of Earth's core and being widely distributed in Earth's crust, prompted us to choose Fe for our subsequent investigations.⁸³

Table 4 Reduction selectivity screen on five rTCA intermediates. ^a

Entry	Substrates	Reductant	Species present in the mixture post-reaction (%)								
			<i>On-cycle</i>						<i>Off-cycle</i>		
			2	4 ^b	5 ^b	6	7	10	12	13	14
1		Fe	13	13	3	19	1	25	1	23	1
2		Ni	32	3	5	11	25	22	0	1	1
3		Zn	0	20	30	4	0	1	2	35	8
4	2+3+5+7+10	Mn	19	7	14	4	11	25	1	14	4
5		Na ₂ S ₂ O ₄	35	0	14	3	14	33	0	0	1
6		Mo	<i>No reaction (only starting materials present)</i>								
7		MoO ₂	<i>No reaction (only starting materials present)</i>								

^a Reaction conditions: 0.1 mmol of each: sodium pyruvate, oxaloacetic acid, fumaric acid, α -ketoglutaric acid, *cis*-aconitic acid; 10 equiv. of reductant, 3 mL 1M HCl in H₂O, 3 h, 40 °C. ^b Malate-fumarate equilibrium.

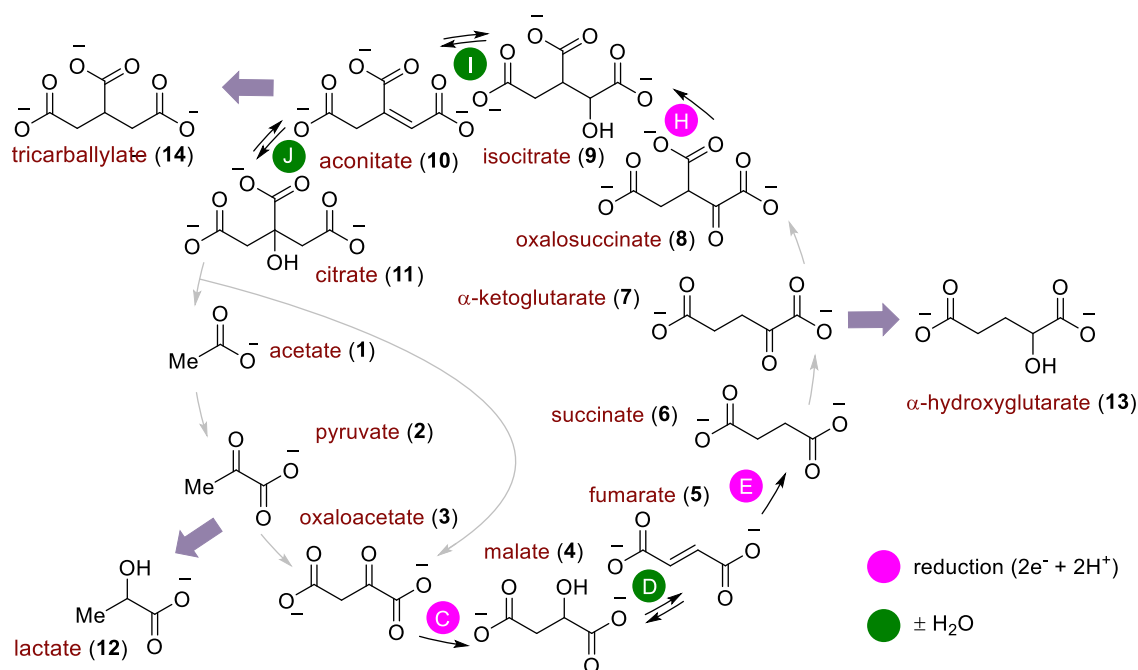


Figure 20 On-cycle (thin black or grey arrows) reactions of the rTCA cycle and off-cycle (mauve bold arrows) parasitic reactions.

1.4.2 Dehydration reactions

The dehydration reactions in biological systems are catalyzed by dehydratases to give a small amount of the unfavorable endergonic product ($+2.3 \text{ kJmol}^{-1}$, neutral pH) at equilibrium. After screening a variety of metal ions as promoters, only traces of the dehydration products fumarate and aconitate were observed even after treating the reaction mixture at $140 \text{ }^\circ\text{C}$. On the contrary, the reverse hydration reaction of fumarate and aconitate to malate and isocitrate occurred even in the absence of metal ions. I therefore decided to push the dehydration reaction forward by coupling the dehydration product to the subsequent reaction: reduction in the case of the malate-fumarate system and hydration in the case of the isocitrate-aconitate system. A screen of metal ions in the presence of Fe^0 revealed that Zn^{2+} in hot acidic conditions was able to dehydrate malate to fumarate and subsequently reduce to succinate, albeit in low yield (Table 5). Although Ni^{2+} offered the best conversion from malate to fumarate (entry 2), I chose Zn^{2+} due to its efficiency in promoting the malate to fumarate to succinate sequence (entry 10). A similar screen of metal ions revealed that Zn^{2+} under hot acidic conditions also promotes the dehydration of isocitrate to aconitate (Table 6).

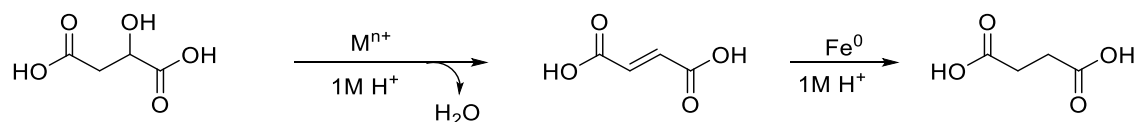


Table 5 Metal-promoted malate dehydration screen.^a

Entry	Metal salt (10 equiv.)	Malate (4) (% of mixture)	Fumarate (5) (% of mixture)	Succinate (6) (% of mixture)
1	Ni(acac) ₂	95	5	0
2	NiCl ₂ 5H ₂ O	88	12	<1
3	FeSO ₄ 7H ₂ O	94	6	0
4	CuSO ₄ 5H ₂ O	96	4	0
5	MnSO ₄ H ₂ O	94	6	0
6	CoCl ₂ 6H ₂ O	96	4	0
7	VCl ₂	92	8	<1
8	CrCl ₂	95	5	0
9	Cr ₂ (SO ₄) ₃ 12H ₂ O	98	2	<1
10	ZnCl ₂	94±1	4±1	2±1

^a Unless otherwise specified: 0.08 mmol malic acid, Fe⁰ powder (10 equiv.), 3 mL 1 M HCl in H₂O, 16 h, 140 °C.

Where applicable, errors correspond to ±mean absolute deviation.

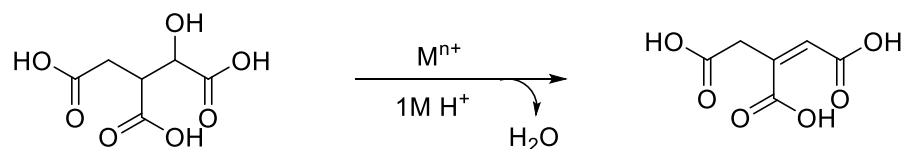


Table 6 Metal-promoted isocitrate dehydration screen.^a

Entry	Metal salt (1 equiv.)	Temp. (°C)	Isocitrate (9) (% of mixture)	Aconitate (10) (% of mixture)
1	Ni(acac) ₂	140 °C	91	9
2	FeSO ₄ 7H ₂ O	140 °C	95	5
3	CuSO ₄ 5H ₂ O	140 °C	94	6
4	MnSO ₄ H ₂ O	140 °C	94	6
5	CoCl ₂ 6H ₂ O	140 °C	94	6
6	Cd(OAc) 2H ₂ O	140 °C	95	5
7	VCl ₂	140 °C	95	5
8	Fe ₂ O ₃	140 °C	95	5
9	Mn ₂ O ₃	140 °C	97	3
10	Cr ₂ O ₃	140 °C	95	5

Continued in the next page

Continued from the previous page

11	As ₂ O ₃	140 °C	49	51
12	RuCl ₃	140 °C	58	42
13	IrCl ₃	140 °C	51	49
14	RhCl ₃	140 °C	54	46
15	TiCl ₃	140 °C	100	0
16	CrCl ₃	160 °C	100	0
17	Pd(acac) ₂	140 °C	47	53
18 ^b	CrCl ₂	140 °C	62	38
19	ZnCl ₂	140 °C	51±12	49±12
20 ^c	ZnCl ₂	140 °C	93±1	7±1

^a Unless otherwise specified: 0.08 mmol isocitrate (as trisodium isocitrate hydrate), 3 mL 1 M HCl in H₂O, 48 h, 140 °C. ^b TiCl₃ as 20% w/w solution in 2N HCl ^c 0.5 M H₂SO₄ in H₂O, 48 h. Where applicable, errors correspond to ±mean absolute deviation.

1.4.3 Effect of compartmentalization

To test whether compartmentalization might enhance the efficiency of the potential prebiotic process, I set out to incorporate a non-ionic surfactant α -tocopherol methoxypolyethylene glycol succinate (although non-prebiotic) into the reaction conditions developed.⁸⁴ These micelles form nano-sized reaction compartments and their application revealed that the dehydration reactions can occur even at ambient temperatures, in a proof-of-concept manner (Table 8, entries 6, 11, 13 and 14). While other surfactants such as anionic sodium dodecyl sulfate (SDS) and cationic cetrimonium bromide (CTAB) were explored, none of these proved to be effective.

1.4.4 Hydration

The only hydration reaction of aconitate to citrate in the rTCA cycle is carried out by the FeS cluster of aconitase enzyme. Attempts to observe this transformation using acid or base catalysis met with no success. An exhaustive screen of more than 20 metal ions revealed that an acidic solution of Cr³⁺ significantly promotes the hydration of aconitate to citrate at 140 °C. Citrate was observed in a much lesser quantity in the presence of other metals or at lower temperatures (Table 7).

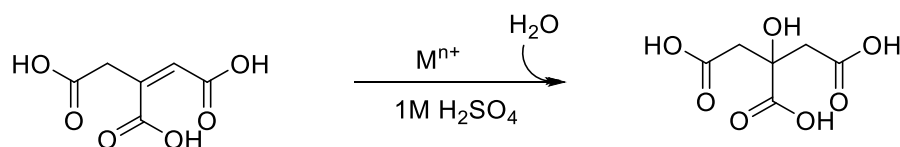


Table 7 Metal-promoted aconitate hydration screen.^{a,‡}

Entry	Metal salt (1 equiv.)	Species present in the mixture post-reaction (%)			
		Isocitrate (9)	Aconitate (10)	Citrate (11)	Tricarallylate (14)
1	FeCl ₃	-	99	1	-
2	Cr ₂ (SO ₄) ₃ 12H ₂ O	-	67	33	-
3	TiCl ₃ ^b	-	82	10	9
4	IrCl ₃	-	67	2	31
5	RuCl ₃	-	97	3	-
6	Co(OAc) ₂	-	98	2	-
7	BiBr ₃	-	>99	<1	-
8	TbCl ₃ 6H ₂ O	8	92	<1	-
9	-	-	100	-	-

^a Unless otherwise specified: 0.08 mmol aconitate, 3 mL 1 M H₂SO₄ in H₂O, 1 h at 20 °C, then 16 h at 140 °C. ^b

TiCl₃ as 20% w/w solution in 2N HCl

[‡] In the aconitate hydration screen the following salts/oxides did not yield any citrate: CuI, ZnSO₄, CuSO₄ 5H₂O, NiSO₄ 7H₂O, CoSO₄ 7H₂O, FeSO₄ 7H₂O, MnSO₄ H₂O, CrCl₂, Cd(OAc)₂ 2H₂O, HgCl₂, Co(NH₃)₆Cl₃, Mn(OAc)₃ 2H₂O, MoO₂, MoO₃, WO₂, WO₃

The efficacy of Zn²⁺ and Cr³⁺ to dehydrate and hydrate in acidic medium reflects the involvement of aquated metal species, potentially as polyoxometallates, which can in turn coordinate with the rTCA cycle intermediates. In contrast, under alkaline environments the metals tend to precipitate rendering them incapable of chelating the rTCA intermediates and allowing the observed catalysis. In analogy with a previous study on metal catalyzed hydration reactions of maleate by Olson and Taube,⁷³ I propose the following mechanism for the dehydration-hydration reactions. Upon chelation of the dicarboxylic acid to the aquated metal ion, dehydration (Figure 21, a) or hydration (Figure 21, b) proceeds with the aid of water molecules coordinated to the metal complex. This mechanism is also comparable to the well-studied enzymatic mechanism of aconitase-catalyzed hydration–dehydration, with Zn²⁺ playing the role of the Fe–S cluster’s ‘isocitrate mode’ and Cr³⁺ functioning in its ‘citrate mode’ (see Scheme 3, Part I).

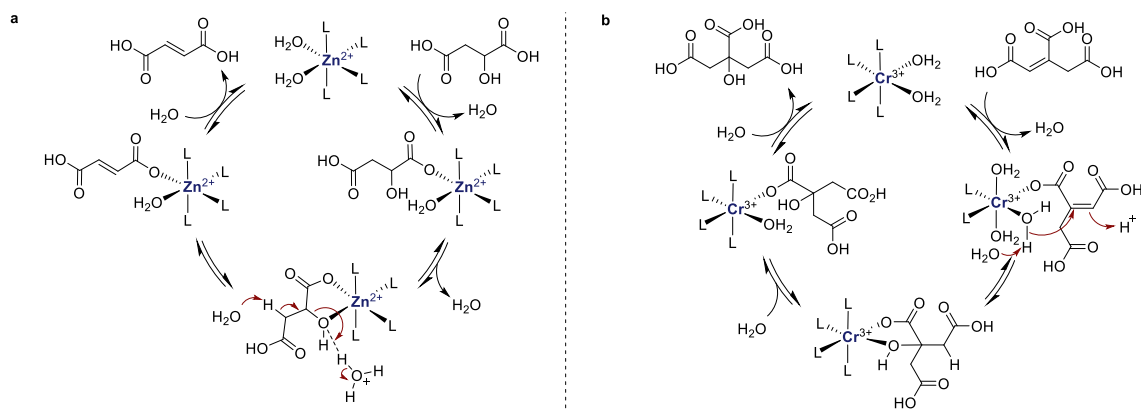


Figure 21 Mechanism of metal catalyzed dehydration and hydration reaction

1.4.5 Sequential reactions

The observation that Fe⁰, Zn²⁺, Cr³⁺ and micelles are able to promote individual reduction, dehydration and hydration reactions of the rTCA cycle prompted us to inquire whether sequential reactions of rTCA cycle could be carried out in one pot. Subjecting oxaloacetate to an acidic solution containing Fe⁰, Zn²⁺, Cr³⁺ and micelles showed that, the three-step reduction-dehydration-reduction sequence (3-6) proceeded even at ambient temperatures to give succinate (Table 8, entry 11). In a similar attempt, oxalosuccinate was subjected to the above-mentioned promoting components at 140 °C to observe the reduction-dehydration-hydration sequence (8-11) (Table 8, entries 12, 13). Citrate was observed as a product, but the presence of micelles did not afford a significant improvement in the product distribution. These results point out the fact that sequential reactions of the rTCA cycle could be carried out under simple and mutually compatible reaction conditions. It should be noted that despite Ni⁰'s capability of promoting the same reductions as Fe⁰ with better selectivity, it was unable to promote sequential reactions.

1.4.6 Selectivity issues

In addition to the reduction reactions that afford the on-cycle products malate, succinate and isocitrate, several parasitic reactions are possible: reduction of pyruvate (Figure 20, 2) to lactate (12), α -ketoglutarate (7) to α -hydroxyglutarate (13) and aconitate (10) to tricarballylate (14), all leading to potential dead-ends for the protometabolic cycle. This has been a major criticism against the plausibility of non-enzymatic metabolic cycles on the primitive Earth.³⁰ It has been pointed out that simple non-enzymatic reactions lack the sufficient selectivity to promote the on-cycle reactions over the off-cycle parasitic reactions, so as to afford efficiency over >50 %, a sustainability threshold for autocatalytic cycles. To evaluate the extent to which parasitic reactions might be a problem for a non-enzymatic rTCA cycle, a mixture of five intermediates

of the rTCA cycle that could undergo on-cycle and off-cycle reductions (Figure 20, intermediates **2**, **3**, **5**, **7** and **10**) were exposed to the conditions developed (10 equiv. Fe⁰, Zn²⁺, Cr³⁺ and micelles). The product distribution showed that less than 5% of the compounds observed in the mixture corresponded to off-cycle products after 3 h at 40 °C (Table 8, entry 14), compared to twice as much of the on-cycle reduction products were present along with ~85% of the starting materials. This experiment showed that about one third of the material flows off-cycle due to reduction by Fe, while about 2/3 moves forward within the cycle. While a significant amount goes off-cycle, it is not such a high amount that it is unlikely to be viable in a stabilized autocatalytic network with a significant flux of material from the stabilizing pathway.

1.5 Conclusion and perspectives

Identifying a single set of conditions under which multiple steps of the rTCA cycle could operate in sequences, without a significant loss of substrates towards parasitic reactions, provides a new insight into the types of prebiotic chemistry that might have operated on the early Earth leading to life. Metallic iron as a source of electrons is plausible under a prebiotic setting, due to the widespread occurrence of the element in Earth's interior as well as its continuous production as the mineral awaruite at hydrothermal vents in the crust.^{20,85} These results support the plausibility of a protometabolism promoted by geochemically accessible metals/metal ions. Additionally, the present study, using a generic micelle, further supports the idea that compartmentalization could have been advantageous for metabolic reactions. Further investigations are warranted to identify the missing links such as the carboxylation reactions, as well as using the rTCA intermediates as prebiotic feedstocks for the synthesis of other biomolecules.

Table 8 Summary of reactions of rTCA cycle under unified set of conditions (Fe⁰, Zn²⁺ and Cr³⁺ in 1 M HCl)

Entry	Substrate (0.1 mmol)	Conditions ^a				Species detected in the mixture post-reaction (%) [‡]											
						On-cycle					Off-cycle						
		Fe ⁰ (equiv.)	Zn ²⁺ (equiv.)	Cr ³⁺ (equiv.)	Micelles	2	4	5	6	7	9	10	11	12	13	14	
<i>Reduction</i>																	
1	3	10	-	-	-		90	10									
2 ^b	5	10	-	-	-		15	20	65								
3 ^c	8	10	-	-	-				2		98						
<i>Hydration/Dehydration</i>																	
4 ^d	5	-	-	-	-		77	23									
5 ^d	4	10	10	-	-		94	4	2								
6 ^e	4	10	10	-	yes		82	7	11								
7 ^{d,f}	9	-	1	-	-						51	49					
8 ^{d,f}	10	-	1	-	-						12	88					
9 ^g	10	-	-	6	-							67	33				
10 ^g	11	-	-	6	-							23	77				
<i>Three-step sequences</i>																	
11 ^e	3	10	15	4	yes		52	3	41					4			
12 ^h	8	5	10	6	-						65	30	2		3		
13 ^h	8	5	10	6	yes				5		72	21	2				
<i>Competitive reduction</i>																	
14 ^c	2+3+5 7+10	10	15	6	yes		20	6	18	4	20		28		2	2	<1

[‡]Reported values were determined by GC-MS after a derivatization procedure and represent the average of at least two runs. Compounds **3** and **8** were not detected by this method and are thus omitted. See the Supplementary Information for additional control experiments, mean absolute deviations, and crude ¹H NMR spectra of selected reactions. ^aUnless otherwise specified: 1 M HCl in H₂O, 16 h, 140 °C. ^b3 h, 140 °C. ^c3 h, 40 °C. ^d48 h, 140 °C. ^e20 °C, 24 h. ^fReaction in 1 M H₂SO₄ in H₂O, 16 h, 140 °C. ^g1 h, 20 °C, 24 h, 140 °C. ^hThermal cycling: 16 h, 140 °C; 10 h, 20 °C; 16 h, 140 °C.

2 The Wood-Ljungdahl pathway³⁴

2.1 Introduction

Years following the elucidation of the mechanism of the Wood-Ljungdahl (W-L) pathway, studies comparing ¹²C/¹³C isotopic fractionation patterns between sedimentary carbon records and anaerobic organisms that use the W-L pathway have indicated that these organisms would have been the first autotrophs on Earth. Arising as early as 3.8 billion years ago, soon after Earth became habitable, these organisms could utilize CO or H₂ as energy source and CO₂ as electron acceptor long before O₂ appeared on the planet.⁸⁶ Later years witnessed attempts to replicate this biochemical process abiotically, considering geological evidences available about the early Earth. In this chapter, I describe my efforts to identify links between the geochemistry and ancient biochemistry of W-L pathway.

2.2 State of the art in the investigations on abiotic origins of the W-L pathway

Given the ancient nature of the W-L pathway and its reliance on metalloenzymes for catalysis, several researchers in the origins of life field have tried to discover non-enzymatic variants starting from various C₁ sources (CO₂, CO, CO₃²⁻ and HCOOH) using a wide variety of approaches. Furthermore, researchers specializing in CO₂ fixation unrelated to origins of life research, have also reported some relevant chemistry. Both types of results are discussed in Table 9. Generally, reports using CO₂ as C₁ source require an external reducing agent, such as a reduced metal or a reducing electrode. However, some employ reduced C₁ sources such as formic acid or CO that can themselves act as reducing agents. **Erreur ! Source du renvoi introuvable.** Table 9, entry 1). Their work, showing that acetate could be produced from an alkyl(methyl) thiol and carbon monoxide, was the first abiotic approach to the biological W-L pathway.⁸⁷ The described chemistry was a non-enzymatic analogue to the enzyme ACS described earlier. This result sparked further chemical explorations, becoming one of the supporting pillars of the FeS world theory. Taking the chemistry a step further, Cody and co-workers were able to obtain acetate and pyruvate using neat HCOOH (as C₁ source), nonyl thiol and FeS under high temperatures and pressures (entry 2).⁸⁸ While the specific reaction products parallel those seen in the W-L pathway, the use of neat formic acid, which decomposes to a

³ Parts of this section has been published as: Varma, S.J., Muchowska, K.B., Chatelain, P., and Moran, J. (2018). Native iron reduces CO₂ to intermediates and end-products of the acetyl-CoA pathway. *Nat. Ecol. Evol.* 2, 1019–1024.

⁴ For detailed experimental description please see: Part III, section 2.

mixture of H₂O, H₂, CO₂ and CO under the extreme reaction conditions, is geologically unrealistic. Takahashi and co-workers in 2006 described the two electron reduction of CO₂ to formate using an alloy of Fe and Ni at elevated temperatures (entry 3).⁸⁹ This was later extended to abiotic acetogenesis by Feng and co-workers, who described the production of both acetate and formate from CO₂ using freshly prepared iron nanoparticles at elevated pressures and temperatures, indicating that abiotic acetogenesis is not only a property of metal sulfur clusters, but one that can also be accomplished by zero-valent metal (entry 4).⁹⁰ This idea was substantiated by investigations using *N*-doped nanodiamond electrodes,⁹¹ though outside a prebiotic context (entry 5). Another electrochemical report, this time carried out in a prebiotic context, used greigite (Fe₂S₄) electrodes at -1.1 V, a potential that is too reducing to be geochemically relevant to hydrothermal vents. In this case, acetate and pyruvate were produced in addition to formate and methanol (entry 6).⁹²

Table 9 Abiotic reactions of the W-L pathway, a review.

Entry	Reaction Conditions	Product Yields				Reference
		Formate	Methanol	Acetate	Pyruvate	
1	FeS-NiS (1:1), CO (1 bar), CH ₃ SH, pH 8, 100 °C, 7 d	-	-	3.28 mM	-	87
2	HCOOH, FeS, RSH, 500-2000 bar, 250 °C, 6h	-	-	5.5 x 10 ⁻⁵ mmol	7.7 x 10 ⁻⁵ mmol	77
3	FeNi (98.75:1.25), CO ₂ (22.5 mmol), 300 °C, 6h	1.4 mM	-	-	-	89
4	CO ₂ (14 bar), Fe(0) (5 mmol), H ₂ O, 200 °C, 72 h	8.5 mM	-	3.5 mM	-	90
5	NaHCO ₃ (aq), <i>N</i> -doped diamond (3.68%) electrode, rt, 1 h	1.2 mM	-	16.1 mM	-	91
6	Greigite electrode (-1 < ε ₀ < 0 V, 1 mVs ⁻¹), pH 6.5, sat. CO ₂ 120 h, rt	1.3 μmol	0.35 μmol	0.57 μmol	0.48 μmol	92

2.3 Aim of this Chapter

The above-mentioned studies report generating C₁, C₂ or C₃ products using either metal sulfides, metal nanoparticles or electrochemistry – conditions that are harsh and/or unlikely to be prebiotic. Herein, I report our explorations to achieve reductive CO₂ fixation to C₂ and C₃ products, using native metals under mild conditions that are also prebiotically plausible.

2.4 Can native metals promote reactions of W-L pathway?

2.4.1 Chemistries of different native metals

Widespread occurrence of metals in the W-L pathway (See Part I, Section 2.2) inspired me to investigate whether the metals found in biochemistry, in their native state, could exhibit the chemistry that one observes in the W-L pathway. Our initial efforts comprised of screening metals Mn, Fe, Co, Ni, Cu, Zn, Mo and W under hydrothermal settings of 1 M KCl and 35 bar CO₂ at 100 °C for 16 h using a high-pressure autoclave (For detailed experimental procedures, see Part III, Section 2.3.1). Following a treatment with KOH (the significance of KOH treatment is described in section 2.4.4) and analysis by NMR, it was found that all metals except Cu afforded acetate up to 0.28 ± 0.01 mM, and in the case of Fe, Co and Ni, considerable quantities of pyruvate up to 0.03 ± 0.01 mM (Fe) were also observed (Figure 22). Additionally, substantial quantities of formate (2.3 ± 0.2 mM, for Co) and methanol (0.39 ± 0.00 mM, for Mo) were found. As a control, the metal samples were analyzed without exposing them to CO₂, in which case no significant quantities of CO₂ fixation products were observed (see Part III, Section 2.2.2).

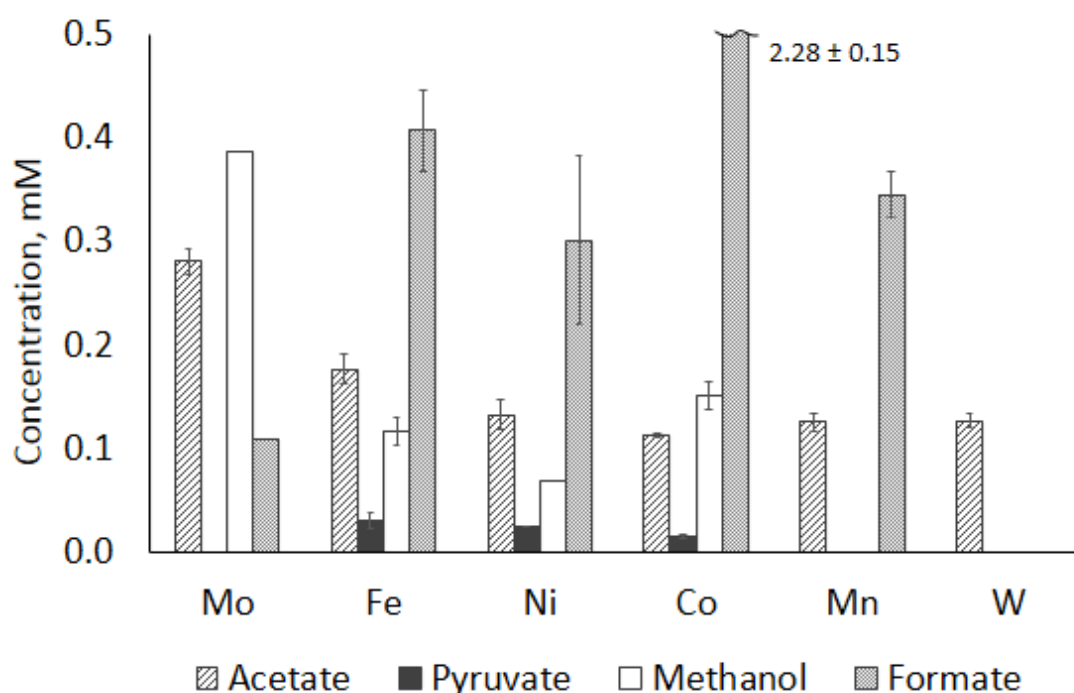


Figure 22 Metal screen for W-L pathway chemistry consisting 1 mmol of native metal in 1 M aqueous KCl pressurized to 35 bar CO₂ at 100 °C during a time span of 16h.

2.4.2 Effect of physical parameters

Due to iron being the most abundant metal on Earth, present as Fe^0 in the core and $\text{Fe}^{2+}/\text{Fe}^{3+}$ in the crust, I selected Fe^0 as the metal of choice for the subsequent detailed investigations, focusing on the effect of temperature, pressure, pH and salinity (ionic strength) on the CO_2 fixation chemistry.

2.4.2.1 Temperature

First, I looked at the effect of temperature over a range of 30-150 °C for Fe^0 under 35 bar CO_2 (final pressure) and 1 M KCl in deionized water during a time period of 16 h. At lower values of temperature, acetate is the predominant species, with significant quantities of pyruvate and formate (Figure 23). As the temperature is increased to 100 °C, methanol begins to appear amongst the products. A further increase to 150 °C results in the disappearance of pyruvate, possibly due to thermal decomposition.

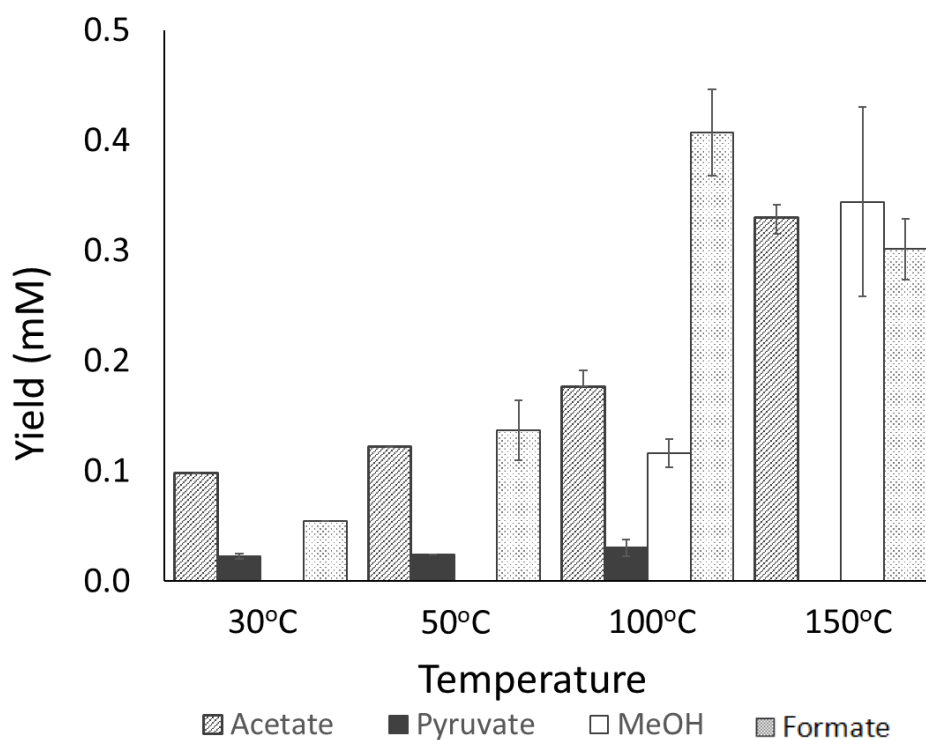


Figure 23 Temperature screen for W-L pathway chemistry consisting 1 mmol of Fe^0 in 1 M aqueous KCl pressurized to 35 bar CO_2 for 16 h.

2.4.2.2 Pressure

Upon subjecting Fe^0 in 1 M KCl at 30 °C (the temperature was chosen so as to limit the effects of temperature on pressure) to a range of pressures, it was found that the reaction was

considerably immune to pressure effects with acetate and pyruvate being the major products at lower pressures (Figure 24). A similar robustness trend was observed with respect to pressure variations. While C₂ and C₃ species were the only products at lower pressures, higher pressures resulted in the observation of formate. As higher pressures imply higher molecular collisions, this observation may be due to the higher intermolecular collisions with the metal species causing the decomposition of metal bound intermediates before they could react further.

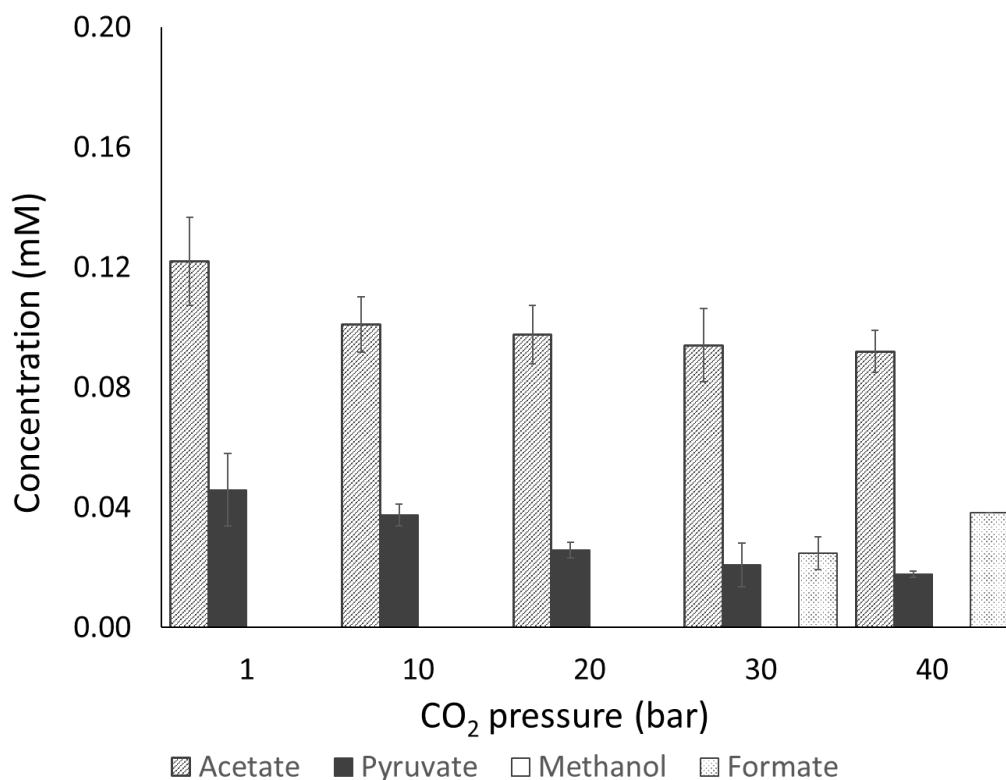


Figure 24 CO₂ pressure screen for W-L pathway chemistry consisting 1 mmol of Fe⁰ in 1 M aqueous KCl at 100 °C for 16 h.

2.4.2.3 pH and salinity

Varying either the initial unbuffered pH (pH 2, 7 and 10 were chosen to cover the plausible pH ranges that are found on present day earth's surface) without any electrolytes (Figure 25) at temperatures (a) 100 °C and (b) 30 °C at 35 bar CO₂ had little effect on the reaction outcome. Likewise, varying the nature of the electrolyte by replacing K⁺ with other biologically relevant cations like Na⁺, Mg²⁺ or Ca²⁺ also had little effect (Figure 26). However, the concentration of the salt used (KCl was used for this study due to abundance of K⁺ within cell membrane compared to exterior) had a minor but noticeable effect on the product distribution, with a decrease by about 20% in case of acetate and pyruvate concentrations in the absence of salt (Figure 27). The effect of anions was not studied.

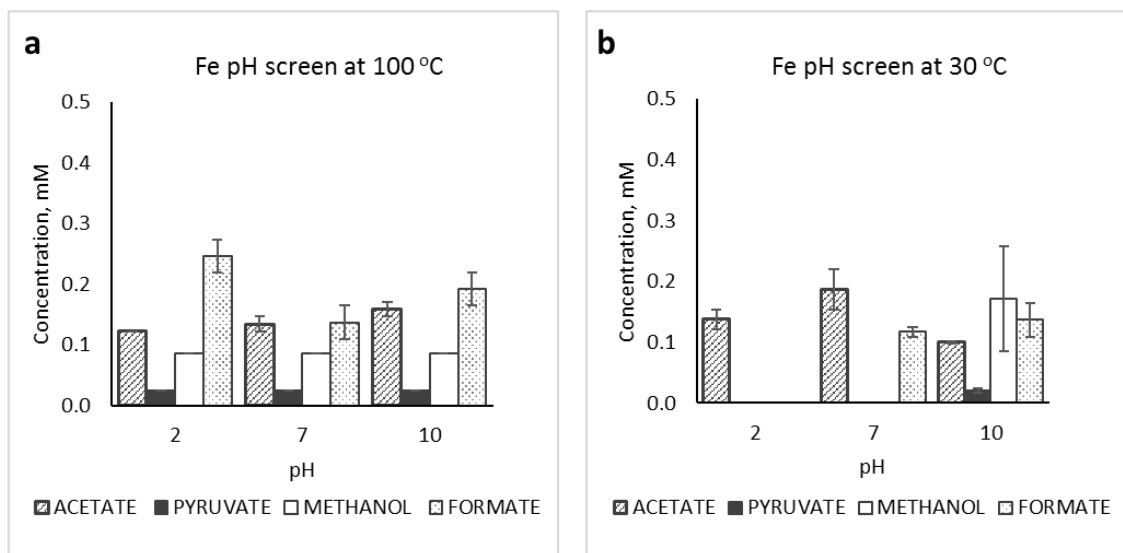


Figure 25 Screen of initial pH for W-L pathway chemistry consisting 1 mmol of Fe⁰ in 1 M aqueous KCl pressurized to 35 bar CO₂ for 16 h at (a) 100 °C (b) 30 °C.

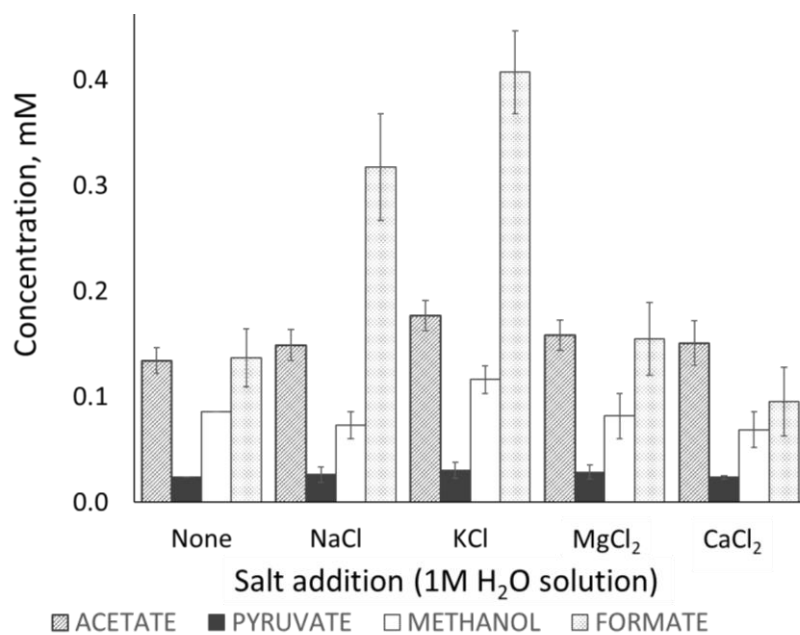


Figure 26 Screen of various physiologically relevant salt for W-L pathway chemistry consisting 1 mmol of Fe⁰ in 1 M aqueous salt solution pressurized to 35 bar CO₂ for 16 h at 100 °C.

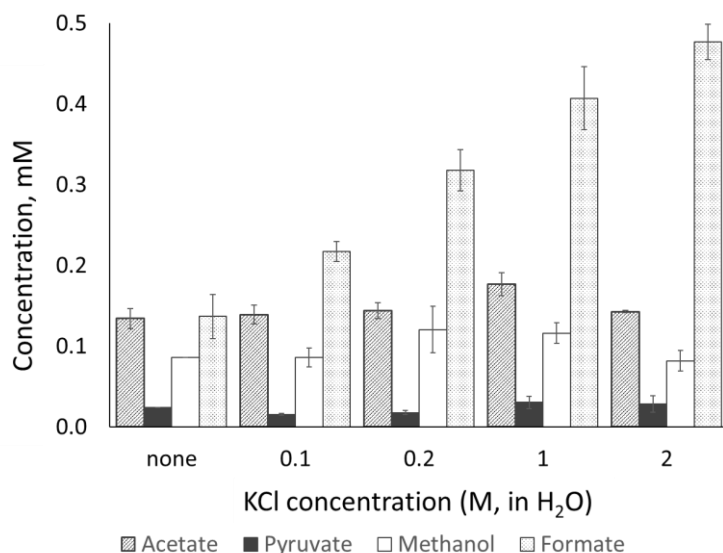


Figure 27 Salt (KCl) concentration screen for W-L pathway chemistry consisting 1 mmol of Fe⁰ in various concentrations of aqueous KCl pressurized to 35 bar CO₂ for 16 h at 100 °C.

2.4.3 Change in the distribution of products over time

The reaction progress was studied under two representative sets of conditions: 1 bar CO₂ at 30 °C (Figure 28, a) and 35 bar CO₂ at 100 °C (Figure 28, b). At 30 °C under 1 bar CO₂, acetate and pyruvate were the major products between the time frames 6 h and 60 h with acetate reaching almost 0.7 mM at 40 h before decreasing. In the case of 35 bar CO₂ at 100 °C, there was an initial quick buildup of formate reaching 7.2 ± 0.4 mM after 6 h, which then gave way to acetate and pyruvate. A part of the electrons from metallic iron could have been channeled to gaseous products like CO which was not analyzed in the present study. By 60 h, the maximal concentrations of acetate and pyruvate (1.09 ± 0.00 mM and 0.11 ± 0.01 mM respectively) were achieved. Examination of the reaction mixture at this point revealed no visible quantity of Fe⁰ remaining although only ~1% electrons from the metallic iron was channeled to CO₂ reduction products (See Part III, Section 2.4.3). The disappearance of Fe⁰ implied the “fuel” to maintain the steady state of the reaction is exhausted. This was reflected in the disappearance of all components in the reaction mixture by 85 h and ethanol was observed for the first time presumably through thermal decomposition of pyruvate (See Part III, Section 2.4.4).

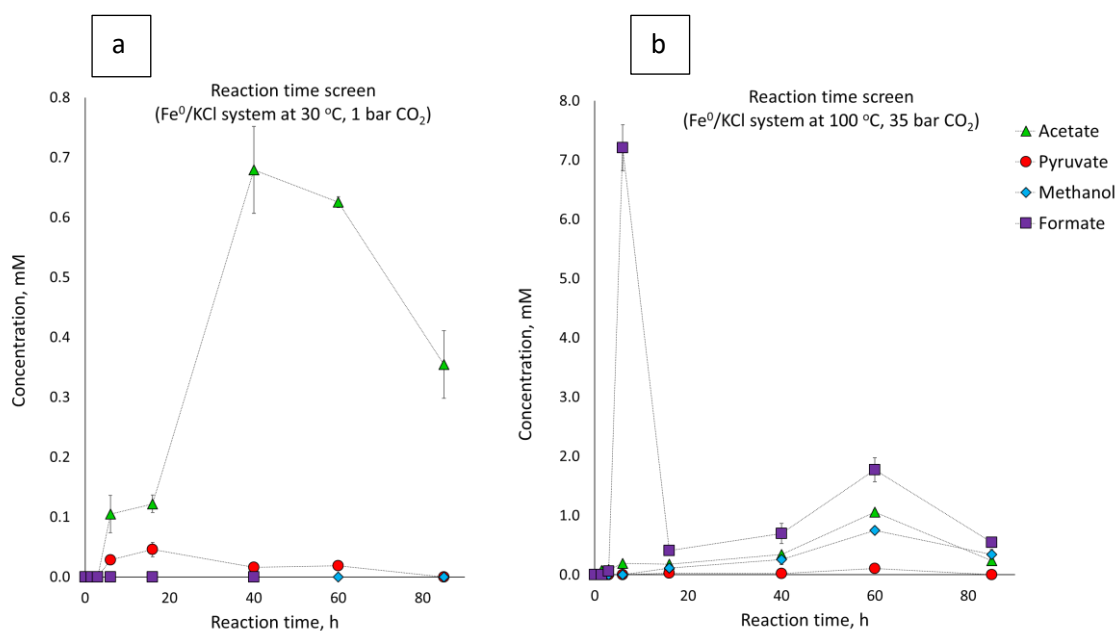


Figure 28 Reaction progress (a) 30 °C, 1 bar CO₂ and (b) 100 °C, 35 bar CO₂ for a reaction system consisting of 1 mmol Fe⁰ in 1 M aqueous KCl.

2.4.4 Mechanistic considerations

Several observations made during the present study allowed me to gain insight into the mechanism of the reaction.

1. Following an experiment using Fe⁰ at 35 bar CO₂ at 100 °C, two NMR samples were prepared in one of which KOH quenching was omitted (See Part III, Section 2.4.7.1). The resultant NMR spectrum of the sample where omission of the KOH work-up prior to the analysis leads to no C₁-C₃ products being observed (Figure 29).

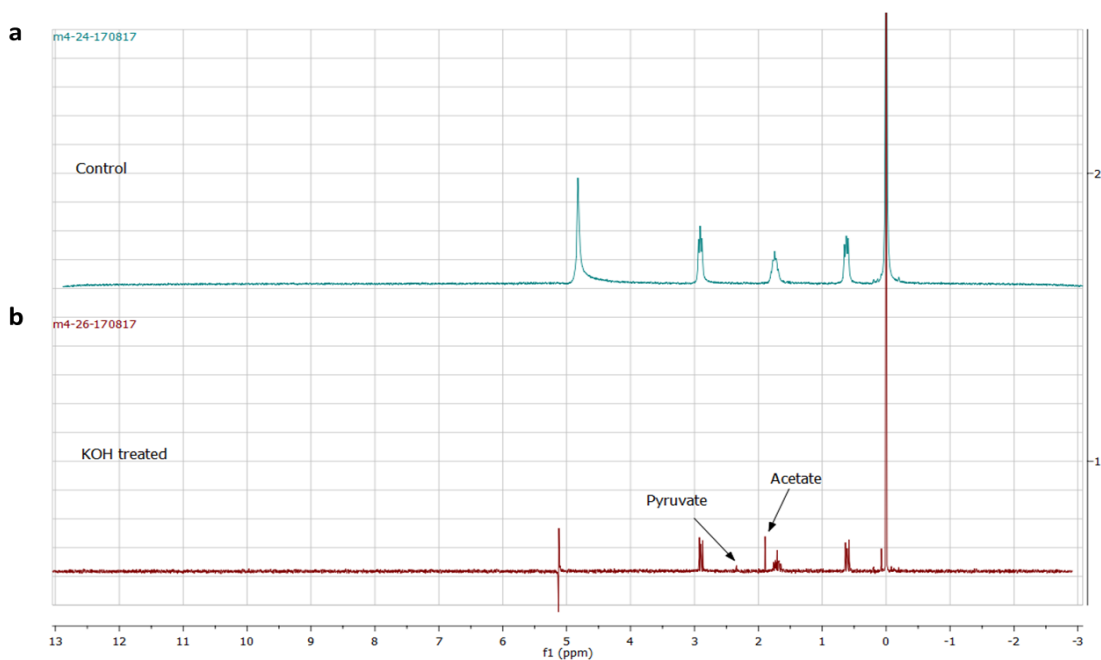


Figure 29 ¹H NMR of the reaction mixture (a) not treated with KOH during sample preparation and (b) treated with KOH during sample preparation (6 : 1 H₂O : D₂O with DSS-Na as standard).

- Introducing formate, methanol or acetate to the reaction did not result in their conversion to higher CO₂ fixation products. Therefore, free formate, methanol or acetate cannot take part in the chemistry observed in CO₂ fixation. Reactions (A)-(D) (Figure 30) were carried with 1 mmol of Fe powder and 1 mmol of KCl in 1 mL H₂O, except to each reaction vial additional CO₂-fixation products were added as starting materials: (A) sodium formate, (B) sodium methoxide, (C) potassium acetate, and (D) sodium pyruvate. The reactions were stirred at 100 °C under 35 bar CO₂ over 16 h.

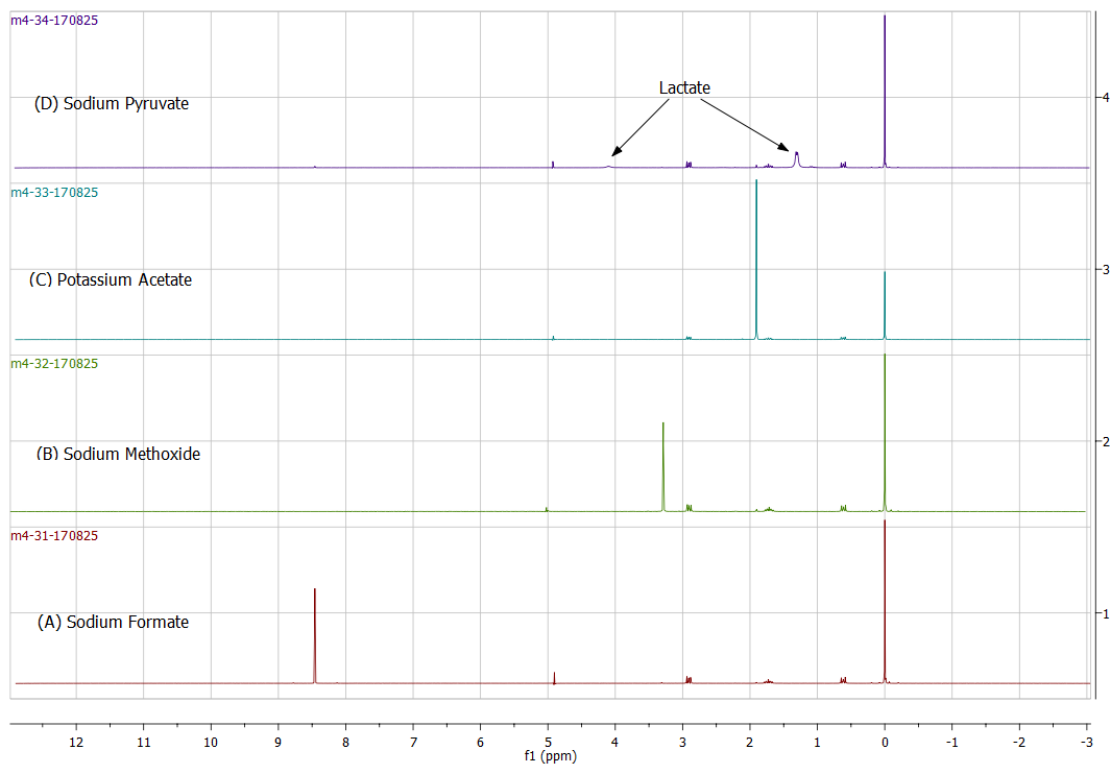


Figure 30 ^1H NMR spectra showing the result of iron-promoted CO_2 -fixation reactions in the presence of each of its products the starting material (6 : 1 H_2O : D_2O with DSS-Na as standard).

The fact that reaction (D), with pyruvate present as the starting material, yielded only its reduction product (lactate) under normal reaction conditions points towards the role of a surface bound chemistry during reaction.

3. Lactate, the reduction product of pyruvate, was not observed in the reaction mixture even though pyruvate is readily converted to lactate upon treating with native metallic iron (See the previous discussion, 2).
4. The same carbon fixation reaction using Fe^0 carried out under CO instead of CO_2 afforded only small quantities of acetate and no detectable quantity of pyruvate (Figure 31).

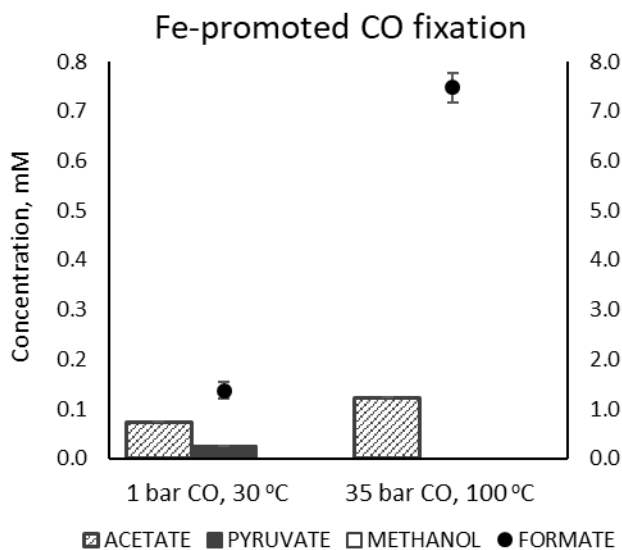


Figure 31 CO fixation reactions using the Fe⁰ (1 mmol)/KCl (1 M aqueous) system at 30 °C under 1 bar CO and at 100 °C under 35 bar CO.

These observations allowed me to arrive at the conclusion that the CO₂ fixation occurs on the surface of the metal with the intermediates and end-products remaining bound to the surface during the reaction. In accordance with these observations I would like to propose a plausible yet largely hypothetical mechanism for the phenomenon observed (Figure 32). The reaction is initiated by the reduction of CO₂ to form surface-bound formyl and carbonyl species. The formyl species is subsequently reduced to a methyl group via the expulsion of water. Next, a migratory insertion of the carbonyl to the methyl group affords the acetyl species, while a subsequent migratory carbonyl insertion or a reductive carboxylation leads to the generation of pyruvyl or pyruvate, respectively. The diminished reactivity of surface-bound pyruvyl over the free pyruvate in solution might explain the absence of pyruvate reduction to lactate. The requirement for KOH may be rationalized by the cleavage of the surface-bound species, formyl, methyl, acetyl and pyruvyl. A plausible explanation for the kinetic profile observed (Figure 28, b) could be through the initial saturation of the metal surface by the formyl species, which subsequently undergo reduction and migratory insertion to generate acetyl and pyruvyl species. Additional mechanistic studies are required to distinguish whether a surface-bound metal carboxylate or surface metal acyl species is involved.

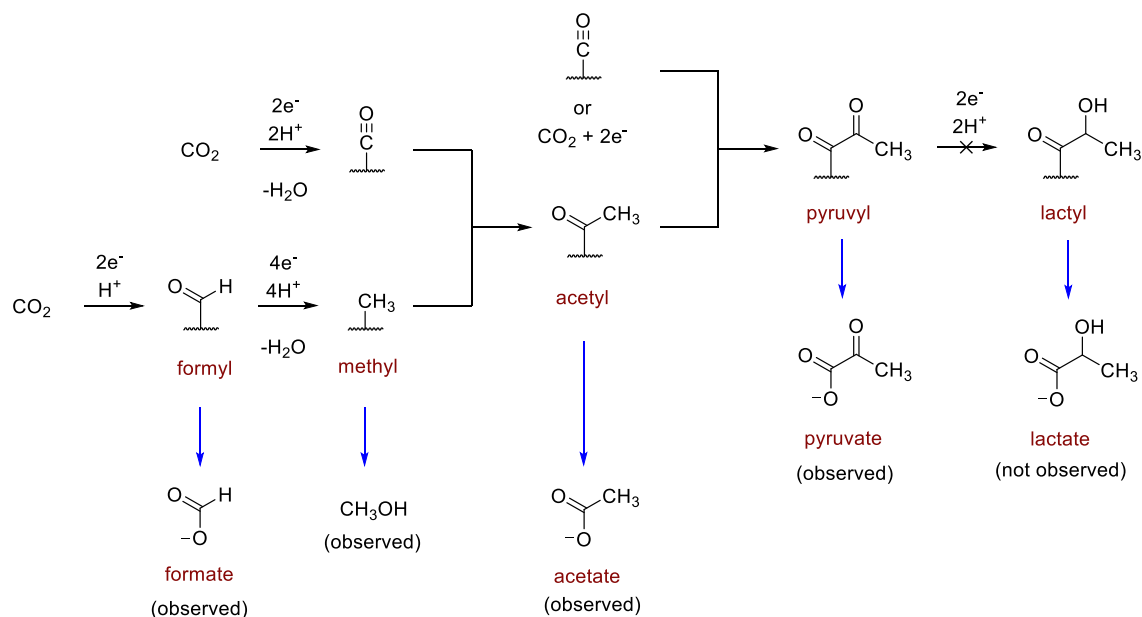


Figure 32 Proposed mechanism of CO₂ fixation reaction

2.4.5 Link to other metabolic pathways

As discussed earlier in Part I Chapter 1, the W-L pathway in tandem with the rTCA cycle is proposed to have been the earliest form of carbon fixation in biochemistry. In Part II, Section 1, I demonstrated that a combination of Fe⁰, Zn²⁺ and Cr³⁺ under strongly acidic (1 M HCl aqueous) conditions promote 6 out of 11 sequences of the rTCA cycle abiotically. Since both the W-L pathway and the rTCA cycle share a common step A (Figure 33), it has been proposed that a combination of both has been in operation in an early and possibly ancestral carbon fixation network^{20, 85}. **Erreur ! Signet non défini.** Considering these facts and the reliance of both chemistries on native metallic iron, I wanted to verify whether the chemistries of both W-L pathway and rTCA cycle are mutually compatible. Upon exposing oxaloacetate to Fe⁰, Zn²⁺ and Cr³⁺ at 35 bar CO₂ for 16 h at 140 °C, an appreciable quantity of succinate was observed, which was confirmed by NMR and GC-MS (See Part III, Section 2.4.8). A similar experiment using in situ generated oxalosuccinate (due to high instability and difficult storage oxalosuccinate was obtained by in situ hydrolysis of triethyl oxalosuccinate under the reaction conditions, see Part III, Section 2.4.8) afforded citrate (confirmed by GC-MS). Even though both reaction sequences are less efficient compared to the case in which 1 M HCl was used, these observations nonetheless suggest the mutual compatibility of both carbon fixation pathways, and the showcase the robustness of the W-L pathway and the rTCA cycle reactions.

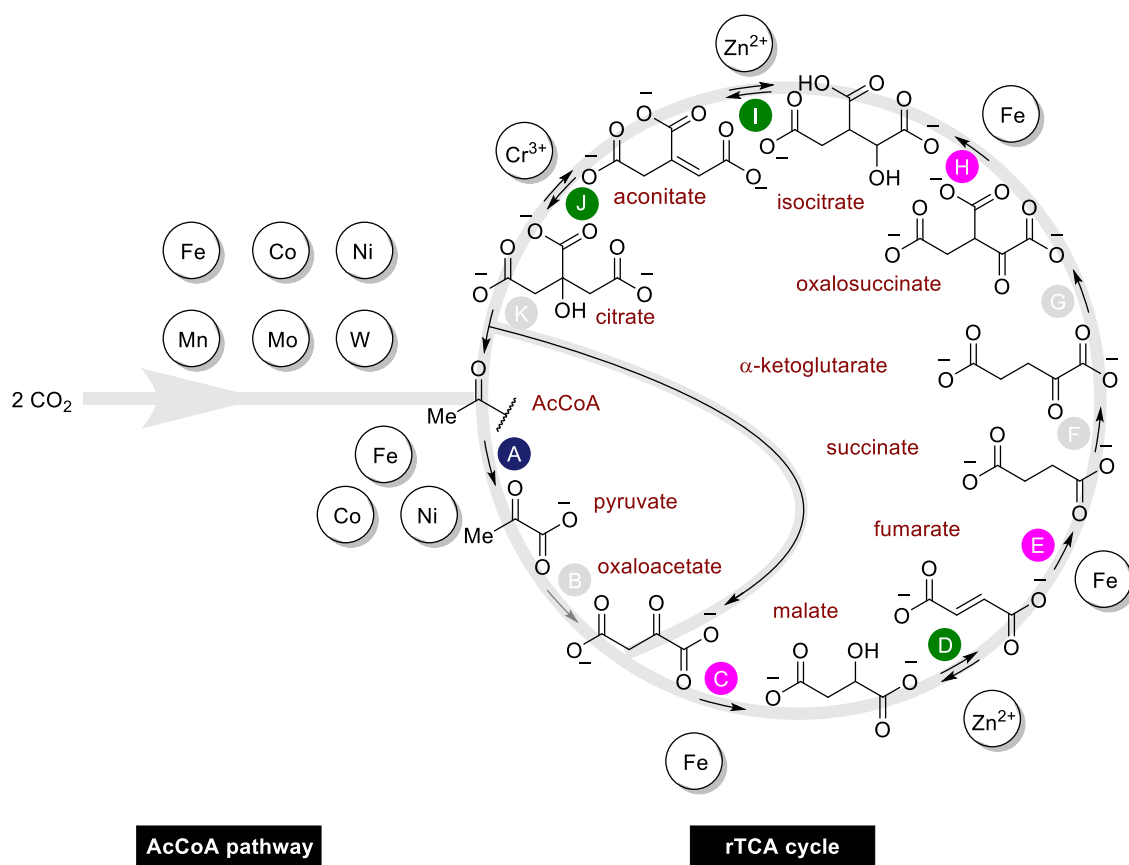


Figure 33 Combined CO₂ fixation pathways- AcCoA pathway and rTCA cycle

2.5 Conclusions

The generation of C₂ and C₃ products acetate and pyruvate by metals (Fe, Co and Ni) indicate the feasibility of CO₂ reduction and C-C bond formation in water which would have been critical to protometabolism. The remarkable selectivity of Fe⁰ at 30 °C and 1 bar of CO₂ to produce acetate and pyruvate over a myriad of other possible compounds containing C, H and O indicates that this chemistry offers kinetically a pathway of least resistance for reduction of CO₂. Although native metallic iron is not frequently encountered in the modern Earth's crust, it has been observed that during serpentinization it is produced in the form of Fe-Ni minerals.^{93,94,95} It is also formed transiently in the Earth's mantle and is believed to constitute the bulk of the Earth's core.⁹⁶ In terms of a broad geological setting, the chemistry described above might have been a consequence of constant production and consumption of Fe⁰ or other reduced metals, relieving the buildup redox gradient between a relatively reduced metal rich Earth's interior and an oxidized exterior containing CO₂ rich atmosphere and ocean- popularly termed as geobiotrophy.^{97,98,99} The observed phenomenon

draws a parallel between a pure geochemical processes and primitive CO₂-fixation pathways, reminiscent of Wächtershäuser's theory of surface metabolism.²²

3 Reductive amination⁵

Amino acid abiogenesis is one of the thoroughly explored areas of prebiotic chemistry owing to the central role of amino acids in life.¹⁰⁰ In line with the biochemistry discussed above, we limit our scope to those syntheses that employ reductive amination to introduce the amino group. Meanwhile, a more exhaustive list of references that employ chemistries such as the Strecker reaction¹⁰¹ or the Bücherer–Bergs synthesis,¹⁰² etc. is described elsewhere.¹⁰³

3.1 Reported abiotic scenarios for reductive amination

A prebiotically plausible amino acid synthesis via reductive amination was first described by Nakajima and co-workers for the amino acid alanine. They were able to synthesize the α -keto acid precursor pyruvate using Schrauzer's complex (see section 0), in situ which was subsequently aminated to produce alanine albeit in low yields.⁷⁶ A similar approach was used by Huber and Wächtershäuser using freshly prepared FeS to furnish alanine, glutamate, phenylalanine and tyrosine in yields up to 30%.¹⁰⁴ Ohno and coworkers reported a synthesis that is more in agreement with biological nitrogen assimilation, with the corresponding amino acid product formed in 52% yields.¹⁰⁵ An improved substrate scope with addition of aromatic amino acids was shown by Shinkai and coworkers with yields up to 52 % for phenylalanine, 22 % for glycine and 34 % for alanine.¹⁰⁶ However, it was not until recently that the mechanistic aspects were investigated in more details to reveal the pH dependence of this chemistry. The effects of pH on the product distribution between reductive amination product and the parallel reduction product α -hydroxy acids, was studied using an iridium catalyst system (although not a biologically relevant metal).¹⁰⁷ Building on prior work using ZnS photocatalysis to enable reactions of the rTCA cycle,⁸⁰ Su and coworkers showed that the same system could enable reductive amination.¹⁰⁸ Although low yields were obtained for the amino acids (up to 7 %), these findings complement attempts to use photochemistry to drive primordial metabolic cycles. However, all these reports describe experiments that occur in a basic environment (to ensure the nucleophilicity of the nitrogen atom) and often employ a large excess of ammonia, amine or ammonium salt as a source for nitrogen. This presents a potential problem for amino acid synthesis in the context of metabolic origins theories requiring acidic aqueous environments where the ammonia is protonated rendering it non-nucleophilic.

⁵ For detailed experimental description, please see: Part III, section 3

3.2 Aim of this chapter

In line with my findings discussed previously on metabolic reactions under acidic environments, I would like to present my findings of viable abiotic reductive amination strategies to generate amino acids that are synthesized from ketoacids that intermediates of the rTCA cycle (Figure 34, blue arrows).

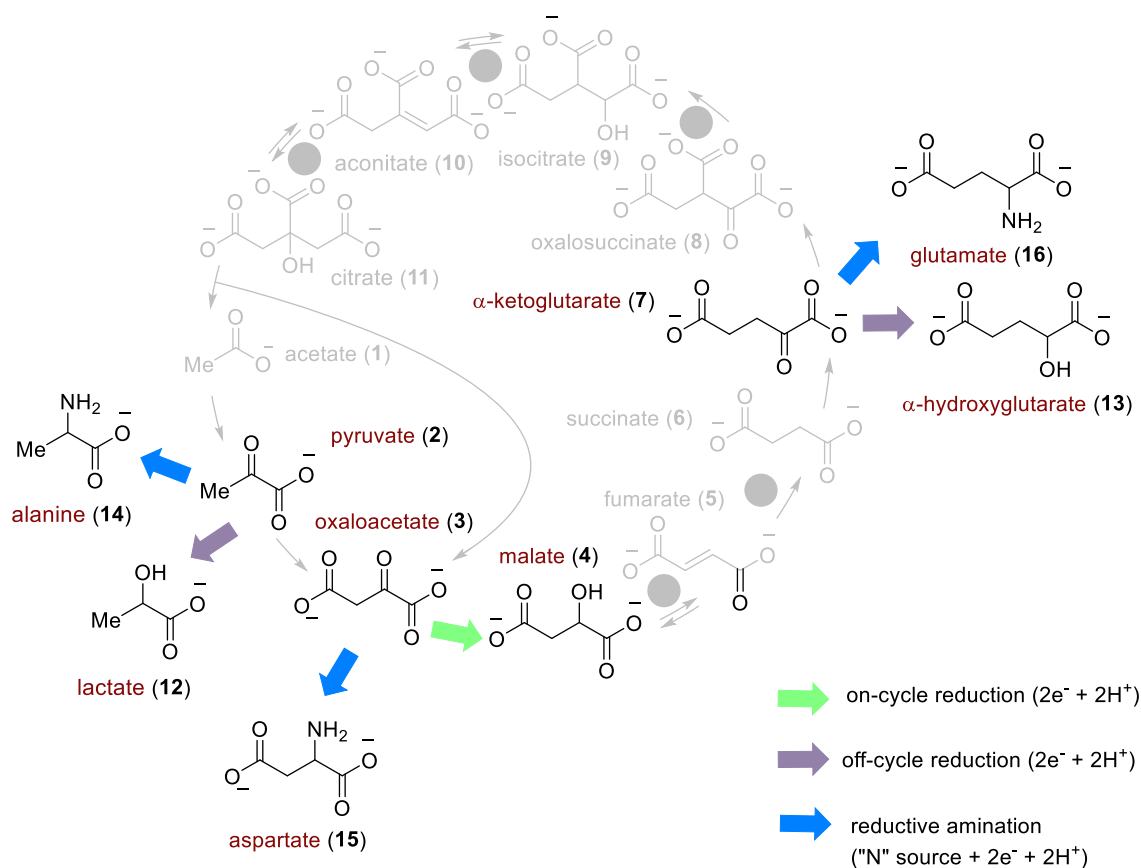


Figure 34 Reduction products of ketoacids in the rTCA cycle

3.3 Reductive amination under acidic medium

The pKa of ammonium ion in water is 9.24. Therefore, to have a free unprotonated ammonia molecule in aqueous solution, the pH must be still higher. However, this presents a major

observed in the case of oxaloacetic acid and α -ketoglutaric acid. The reason was identified (by GC-MS) to be the formation of 5- and 6-membered cyclic hydrazides (not shown) in case of oxaloacetic acid and α -ketoglutaric acid, respectively, that resisted further reduction under different conditions explored. Subjecting the reaction mixtures to different temperature values (entries 2, 5 and 6), we observed the optimal temperature to be 80 °C. To examine the limiting quantity of hydrazine required to observe the maximum yields of alanine, I varied the amount of hydrazine added (1-8 equiv.) to the reaction mixture. It was observed that just 2 equivalents of hydrazine were sufficient to give a selectivity >90% for alanine over lactate (entries 1-4). Glyoxylic acid under similar conditions afforded a 92% yield for glycine (entry 7).

Table 10 Reductive amination of ketoacids using hydrazine

Entry ^a	Ketoacid	Equivalents of Hydrazine	Temperature (°C)	Reduction products (% of mixture)			
				12	14	18	19
1		1	80	13	87	-	-
2		2	80	3	97	-	-
3	2	4	80	1	99	-	-
4		8	80	0	100	-	-
5		2	140	17	83	-	-
6		2	25	6	94	-	-
7	17	2	80	-	-	8	92

^aAll reactions were carried out in 0.1 mmol of the corresponding ketoacids with 10 mmol of Fe⁰ in 1 M HCl.

3.3.2 Hydroxylamine (H₂N-OH)

Another molecule that could be a possible candidate for prebiotic nitrogen source is hydroxylamine. This oxygen analogue of hydrazine could be generated through reduction of nitrous or nitric acids under suitable reducing environments.^{110,111} Some of these could be imagined as occurring also under a prebiotic setting. Anticipating a chemistry like that was observed in the case of hydrazine, I exposed different keto acids to an acidic solution (1 M HCl) of hydroxylamine at 100 °C. Gratifyingly, various ketoacids, including glyoxylate, yielded the corresponding amino acids, although their competing reduction products to α -hydroxy acids were also observed (Figure 34, mauve and green arrows). Varying the equivalents of hydroxylamine added in the case of alanine showed that like hydrazine just 2 equivalents of hydroxylamine were sufficient to obtain a >90 % selectivity of the amino acid product over the α -hydroxy acid (Table 11, entries 2-4). Analysis of the reaction temperature showed that at

temperatures above 100 °C, no amino acid was observed, possibly due to the thermal decomposition of hydroxylamine before it could react (entries 5, 6). At 25 °C, the amino acid was the sole product with only traces of lactic acid (entry 7).

Table 11 Reductive amination using hydroxylamine

Entry ^a	Ketoacid	Equivalents of Hydroxylamine	Temperature (°C)	Reduction products (% of mixture)							
				12	14	18	19	4	15	13	16
1		1	80	17	83	-	-	-	-	-	-
2		2	80	9	91	-	-	-	-	-	-
3	2	4	80	3	97	-	-	-	-	-	-
4		8	80	2	98	-	-	-	-	-	-
5		1	100	19	81	-	-	-	-	-	-
6		2	140	100	-	-	-	-	-	-	-
7		2	25	-	100						
8	17	1	100	-	-	29	71	-	-	-	-
9	3	1	100	-	-	-	-	46	54	-	-
10	7	1	100	-	-	-	-	-	-	61	38
11	2+3+7+ 17	1	100	-	1	37	40	12	-	10	-

^aAll reactions were carried out in 0.1 mmol of the corresponding ketoacids with 10 mmol of Fe⁰ in 1 M HCl.

Under the arbitrarily chosen reaction conditions, reductive amination of other ketoacids were also explored. Glyoxylate provided 71% of glycine with 29% glycolate as the competitive reduction product (Table 11, entry 8). Similarly, oxaloacetate gave 54% aspartate and 46% malate (entry 9); α -ketoglutarate gave 38% of glutamate and 61% α -hydroxyglutarate (entry 10). Under similar conditions, subjecting an equimolar mixture of all 4 ketoacids resulted in glycine as the sole amino acid in the mixture while other keto acids were reduced to their respective α -hydroxy acids (entry 11). Such an observation could be indicative of the highly reactive aldehydic functionality of glyoxylate over other ketoacids.

3.4 Conclusions

Reductive amination has been demonstrated under acidic medium using the intermediates of reduction of dinitrogen and nitrogen oxides. The chemistry described requires only near stoichiometric quantities of nitrogen source for the generation of the corresponding amino acids. This strategy is an improvement over other reductive amination strategies reported that requires >100 equivalents of nitrogen source (NH₃).^{106,108}

4 General conclusions and outlooks

A prebiotic metabolism that could operate under a set of abiotic geochemical conditions is critical for the understanding of metabolic origins of life. We have shown that a network formed by 6 out of 11 reactions of the rTCA cycle and the reductive amination to amino acids could be carried out under a hot acidic mixture of Fe^0 , Zn^{2+} , Cr^{3+} . The study reveals that metal ions such as Zn^{2+} and Cr^{3+} could perform the functions of FeS clusters, a hallmark of living systems. The chemistry portrayed in Section II. 1 propose a notion that the reactions of the core metabolism could have been a relic of some ancient geochemical setting which evolution exploited to link different metabolisms such as carbon, nitrogen, energy etc. together. Although such settings are hard to come by in the present day, a few scenarios have been identified:

- Hydrothermal fields offer a plausible scenario where a continuous flux of energy and matter, released from the Earth interiors, provide the necessary driving force for the chemistry.
- Although reduced metal may not be commonly encountered, the highly reducing electrical potentials associated with these geological formations, may generate the enough quantities of metallic Fe or Ni in a transient manner. This, together with the physical conditions of high temperatures and pressures, would offer a chemical setting favourable for a protometabolism.

The focus was shifted in the Section II. 2 towards adapting the reaction conditions to accommodate the chemistry of the Wood-Ljungdahl pathway. While almost every native metal used in the study could produce acetate from carbon dioxide, certain metals like Fe, Ni and Co could take the chemistry further to the next step, pyruvate. Exploring the reaction parameters revealed that even at ambient pressures and temperatures the generation of acetate and pyruvate was feasible. A geologically more appealing source of acidity was thus identified, CO_2 , which could also now promote the reaction sequences of the rTCA cycle described earlier. On a larger scale, this chemistry could be imagined as a process on early Earth where the metabolic reactions arose to dissipate the redox stress between a reduced metallic core and a relatively oxidized crust rich in CO_2 and water (Figure 1).

In the Section II. 3, I explore other anabolic pathways that could emerge from the W-L/rTCA reaction network. Under the conditions developed in Section II.1, intermediates of dinitrogen/nitrate reductions could react with the keto acids from the rTCA cycle to produce the corresponding α -amino acids, in a way resembling the biological amino acid synthesis. This allows branching into other productive off-cycle products of anabolism.

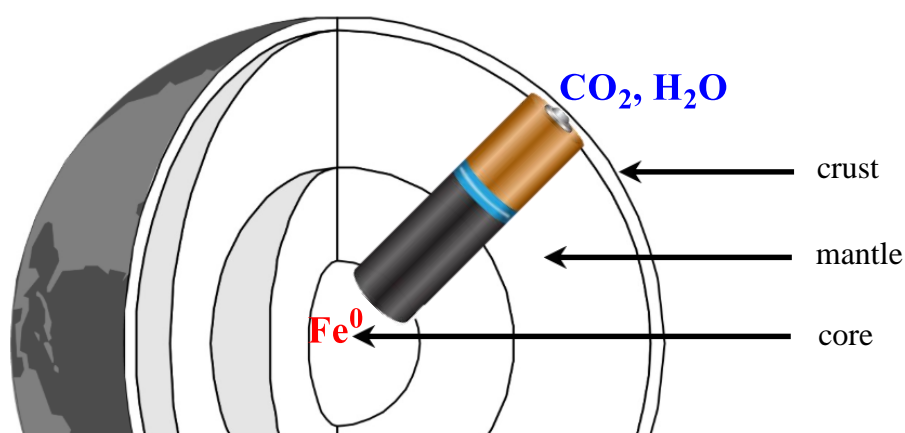


Figure 35 The redox disequilibria between the Earth's core and crust could be imagined to be analogous to that of a battery.

So far, we have identified abiotic alternatives for majority of the reactions of the metabolic network. Coincidentally, the transformations of the cycle that still elude us (Figure 2, marked by red arrows) are also those that require an activating agent such as ATP seen in contemporary biochemistry. This warrants further investigations into identifying prebiotically plausible activating agents, for example, in the form of thio-esters and phosphor-esters. They could then serve as control handles to steer the chemical flux into other metabolic pathways that are associated with the TCA cycle like the fatty acid synthesis and sugar-synthesis.

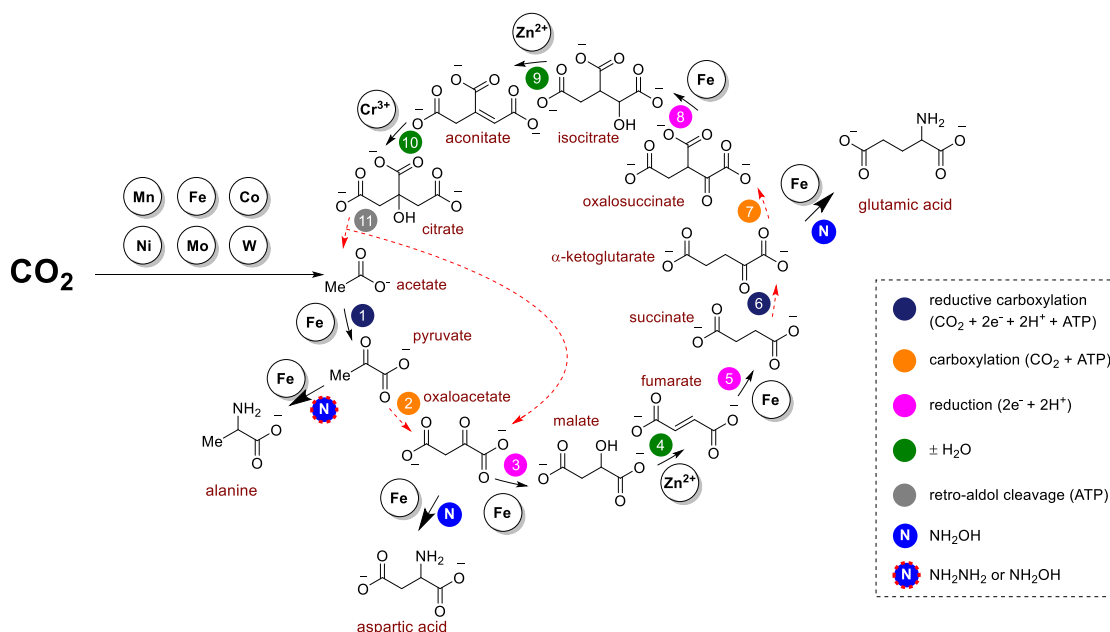


Figure 36 Abiotic agents that promote sequences of the W-L pathway and rTCA cycle. Red-dashed arrows show the transformations that were not achieved in the present study.

PART III

1 The reverse Tricarboxylic acid cycle

1.1 General information

All reactions were carried out in 10 mL Pyrex glass culture tubes under inert atmosphere unless otherwise noted.

GCMS analysis was performed on a GC System 7820A (G4320) connected to a MSD block 5977E (G7036A), using Agilent High Resolution Gas Chromatography Column: PN 19091S – 433UI, HP – 5MS UI, 28 m×0.250 mm, 0.25 Micron, SN USD 489634H. All samples were prepared in ethyl acetate (200 μ L sample volume). The analysis was carried out on a splitless 1 μ L injection volume with an injection port temperature 250 °C. Column oven temperature program was as follows: 60 °C for 1 min, ramped at 30 °C min⁻¹ to 310 °C with 3 min hold, with a total running time of 12.33 min. The mass spectrometer was turned on after 2 min and was operated at the electron ionization mode with quadrupole temperature of 150 °C. Data acquisition was performed in the full-scan mode (50-500). Hydrogen (99.999 % purity) was used as carrier gas at a constant flow rate of 1.5 mL min⁻¹.

¹H NMR spectra of starting material in CDCl₃ were recorded on a Bruker Avance400 (400 MHz) spectrometer at ambient temperature and are reported in ppm using residual CHCl₃ as the internal reference (7.26 ppm), unless otherwise noted. Coupling constants *J* are reported in Hz, as determined using the software (*MestReNova v6.0.2*). ¹³C NMR spectra were recorded on a Bruker Avance400 (100 MHz) spectrometer and are reported in ppm using the residual solvent resonance as the internal standard (CDCl₃ at 77.0 ppm). ¹H NMR spectra of authentic TCA standards and crude reaction mixtures were recorded in water on a Bruker Avance300 (300 MHz) spectrometer at ambient temperature and are reported in ppm using sodium 3-(trimethylsilyl)-1-propanesulfonate (TMSPSA) as the internal reference (CH₃ resonance at 0 ppm). Solvent suppression of water in the ¹H NMR was achieved using the Bruker ZGESGP 1D sequence for water suppression using excitation sculpting with gradient.

1.2 Materials

Unless otherwise noted, all reagents and solvents were purchased from commercial suppliers and used without further purification. Fe⁰ used was a \geq 99% reduced fine powder. ZnCl₂ was used as an anhydrous powder (reagent grade). Cr₂(SO₄)₃ was used as a dodecahydrate (reagent grade). *Cis*-aconitic acid and triethyl oxalosuccinate were prepared using literature procedures,^{112,113} as described in the Synthetic Procedures section.

1.3 Analytical methods

1.3.1 Derivatization procedure

Derivatization of carboxylic acids to esters was performed using a modified literature procedure.¹¹⁴ For optimal gas chromatography resolution, the carboxylic acids were converted to ethyl esters using a mixture of ethanol/ethyl chloroformate (EtOH/ECF) or to methyl esters using a mixture of methanol/methyl chloroformate (MeOH/MCF).

A *ca.* 0.5-0.7 mL aliquot of the reaction mixture was basified using solid KOH (in order to minimize volume change due to the usage of aqueous solution) and centrifuged (6000 rpm, 3 min). To 100 μ L of the supernatant was added 1 M NaOH solution (150 μ L), EtOH or MeOH (240 μ L) and pyridine (30 μ L), followed by ethyl chloroformate (ECF, 35 μ L) or methyl chloroformate (MCF, 35 μ L). This was vortexed for 30 s. A second 35 μ L portion of ECF (or MCF) was added and the mixture was vortexed again for 30 s. Next, CHCl₃ (200 μ L) was added, followed by vortexing (10 s). Finally, NaHCO₃ (400 μ L) was added and the mixture was vortexed again for 10 s. The CHCl₃ layer was separated and dried over anhydrous Na₂SO₄. 50 μ L of the dry CHCl₃ layer was used with 150 μ L of ethyl acetate for the GC-MS analysis.

1.3.2 Product identification

Reaction products derivatized to methyl or ethyl esters of carboxylic acids were identified by comparing the mass spectra and retention times against analogously derivatized authentic samples (Appendix I, Fig. S1 – S15). ECF derivatization was preferred for small molecule substrates (pyruvate, lactate, malate, fumarate, succinate, α -ketoglutarate and α -hydroxyglutarate, alanine), while MCF derivatization gave clearer results (less elimination by-products and better resolution) for *cis*-aconitate, tricarballylate, isocitrate and citrate.

1.4 Experimental data

Table S 1 Non-enzymatic reactions of the rTCA cycle (Fe⁰ as reductant). **Table S 1** continues the following page.

Entry	Substrate (0.1 mmol each)	Conditions ^a				Species present in the mixture post-reaction (%)											
		Fe ⁰ (equiv.)	Zn ²⁺ (equiv.)	Cr ³⁺ (equiv.)	Micelles	On-cycle						Off-cycle					
						2	4	5	6	7	9	10	11	12	13	14	15
<i>Reduction</i>																	
1	3	10	-	-	-	90±2	10±2										
2 ^b	5	10	-	-	-	15±5	20±2	65±7									
3 ^b	8	10	-	-	-			12±5		83±4	5±1						
<i>Hydration/Dehydration</i>																	
4 ^c	4	-	10	-	-	86±1	14±1										
5 ^c	4	10	10	-	-	94±1	4±1	2±1									
6 ^c	4	10	10	-	yes	84±1	6±1	10±2									
7 ^d	4	10	10	-	yes	82±1	7±2	11±3									
8 ^{c,e}	9	-	1	-	-					51±12	49±12						
9 ^e	9	-	1	-	-					93±1	7±1						
10 ^{c,e}	10	-	1	-	-					12±9	88±9						
11 ^c	10	-	1	-	-					8±0	92±0						
12 ^f	10	-		6	-						67±0	33±0					
13 ^f	11	-		6	-						23±5	77±5					
<i>Three-step sequences</i>																	
14 ^{c,g}	3	20	-	-	-	90±2	8±1	2±1									
15 ^{c,h}	3	10	15	4	-	83±1	6±3	4±1						7±3			
16	3	10	15	4	yes	55±7	4±0	23±6						19±5			
17 ^d	3	10	15	4	-	98±0	2±0										
18 ^d	3	10	15	4	yes	52±2	3±3	41±3						4±2			
19 ^{c,g,i}	8	10	-	1	-			13±7		64±11	20±4	3±1					
20 ^j	8	5	10	-	-			16±2	4±2	76±3	4±1						
21 ^j	8	-	10	6	-	<i>Mixture of oxalosuccinate decomposition products, incl. succinate</i>											
22 ^j	8	5	10	6	-					65±7	30±4	2±1		3±4			
23 ^j	8	5	10	6	yes			5±4		72±5	21±0	2±1					

Continued from the previous page

Table S 1 Non-enzymatic reactions of the rTCA cycle (Fe⁰ as reductant)

Entry	Substrate (0.1 mmol each)	Conditions ^a				Species present in the mixture post-reaction (%)										
		Fe ⁰ (equiv.)	Zn ²⁺ (equiv.)	Cr ³⁺ (equiv.)	Micelles	<i>On-cycle</i>						<i>Off-cycle</i>				
						2	4	5	6	7	9	10	11	12	13	14
<i>Competitive reduction</i>																
24 ^k	2+3+5+7+10	10	15	6	yes	20±0	6 ^l ±2	18 ^l ±2	4±2	20±3		28±4		2±0	2±1	<1±0
<i>Micelle control experiment</i>																
25 ^m	-	10	15	6	yes		99±0	1±0								

^a Unless otherwise specified: 1 M HCl in H₂O, 16 h, 140 °C. ^b 3 h, 140 °C. ^c 48 h, 140 °C. ^d 20 °C, 24 h. ^e 1 M H₂SO₄ in H₂O, 16 h, 140 °C. ^f 1 h at 20 °C, 24 h at 140 °C. ^g pH adjusted with conc. HCl to <1 after 24 h. ^h Fe⁰ and/or Zn²⁺ added in two portions. ⁱ Cr³⁺ added after 24 h. ^j Thermal cycling: 16 h at 140 °C, 10 h at 20 °C, 16 h 140 °C. ^k 3 h, 40 °C. ^l Malate-fumarate equilibrium. ^m 0.1 mmol malic acid (**4**) added post-reaction and immediately derivatized (see Synthetic procedures for details). Reported yields are average values of at least two runs. Errors correspond to ±mean absolute deviation.

Table S 2 Metal-promoted malate dehydration screen.^a

Entry	Metal salt (10 equiv.)	Malate (4) (% of mixture)	Fumarate (5) (% of mixture)	Succinate (6) (% of mixture)
1	Ni(acac) ₂	95	5	0
2	NiCl ₂ 5H ₂ O	88	12	<1
3	FeSO ₄ 7H ₂ O	94	6	0
4	CuSO ₄ 5H ₂ O	96	4	0
5	MnSO ₄ H ₂ O	94	6	0
6	CoCl ₂ 6H ₂ O	96	4	0
7	VCl ₂	92	8	<1
8	CrCl ₂	95	5	0
9	Cr ₂ (SO ₄) ₃ 12H ₂ O	98	2	<1
10	ZnCl ₂	94±1	4±1	2±1

^a Unless otherwise specified: 0.08 mmol malic acid, Fe⁰ powder (10 equiv.), 3 mL 1 M HCl in H₂O, 16 h, 140 °C. Where applicable, errors correspond to ±mean absolute deviation.

Table S 3 Metal-promoted isocitrate dehydration screen.^a

Entry	Metal salt (1 equiv.)	Temp. (°C)	Micelles	Isocitrate (9) (% of mixture)	Aconitate (10) (% of mixture)
1	Ni(acac) ₂	140 °C	-	91	9
2	FeSO ₄ 7H ₂ O	140 °C	-	95	5
3	CuSO ₄ 5H ₂ O	140 °C	-	94	6
4	MnSO ₄ H ₂ O	140 °C	-	94	6
5	CoCl ₂ 6H ₂ O	140 °C	-	94	6
6	Cd(OAc) ₂ 2H ₂ O	140 °C	-	95	5
7	VCl ₂	140 °C	-	95	5
8	Fe ₂ O ₃	140 °C	-	95	5
9	Mn ₂ O ₃	140 °C	-	97	3
10	Cr ₂ O ₃	140 °C	-	95	5
11	As ₂ O ₃	140 °C	-	49	51
12	RuCl ₃	140 °C	-	58	42
13	IrCl ₃	140 °C	-	51	49
14	RhCl ₃	140 °C	-	54	46
15	TiCl ₃	140 °C	-	100	0
16	CrCl ₃	160 °C	-	100	0

17	Pd(acac) ₂	140 °C	-	47	53
18^b	CrCl ₂	140 °C	-	62	38
19	ZnCl ₂	140 °C	-	51±12	49±12
20^c	ZnCl ₂	140 °C	-	93±1	7±1
21^c	ZnCl ₂	140 °C	1% w/w	88±2	12±2
22^c	ZnCl ₂	25 °C	-	97	3
23^c	ZnCl ₂	25 °C	1% w/w	97	3
24^c	-	140 °C	-	97	3
25^c	-	140 °C	1% w/w	98	2
26^c	-	25 °C	-	97	3

^a Unless otherwise specified: 0.08 mmol isocitrate (as trisodium isocitrate hydrate), 3 mL 1 M H₂SO₄ in H₂O, 48 h, 140 °C. ^b TiCl₃ as 20% w/w solution in 2N HCl ^c 1 M HCl in H₂O, 48 h. Where applicable, errors correspond to ±mean absolute deviation.

Table S 4 Metal-promoted aconitate hydration screen.^{a,‡}

Entry	Metal salt (1 equiv.)	Species present in the mixture post-reaction (%)			
		Isocitrate (9)	Aconitate (10)	Citrate (11)	Tricarballoylate (14)
1	FeCl ₃	-	99	1	-
2	Cr ₂ (SO ₄) ₃ 12H ₂ O	-	67	33	-
3	TiCl ₃ ^b	-	82	10	9
4	IrCl ₃	-	67	2	31
5	RuCl ₃	-	97	3	-
6	Co(OAc) ₂	-	98	2	-
7	BiBr ₃	-	>99	<1	-
8	TbCl ₃ 6H ₂ O	8	92	<1	-
9	-	-	100	-	-

^a Unless otherwise specified: 0.08 mmol aconitate, 3 mL 1 M H₂SO₄ in H₂O, 1 h at 20 °C, then 16 h at 140 °C. ^b TiCl₃ as 20% w/w solution in 2N HCl

[‡] In the aconitate hydration screen the following salts/oxides did not yield any citrate: CuI, ZnSO₄, CuSO₄ 5H₂O, NiSO₄ 7H₂O, CoSO₄ 7H₂O, FeSO₄ 7H₂O, MnSO₄ H₂O, CrCl₂, Cd(OAc)₂ 2H₂O, HgCl₂, Co(NH₃)₆Cl₃, Mn(OAc)₃ 2H₂O, MoO₂, MoO₃, WO₂, WO₃

Table S 5 Reduction selectivity screen on five rTCA intermediates.^a

Entry	Substrates	Reductant	Species present in the mixture post-reaction (%)								
			<i>On-cycle</i>					<i>Off-cycle</i>			
			2	4^b	5^b	6	7	10	12	13	14
1		Fe	13	13	3	19	1	25	1	23	1
2		Ni	32	3	5	11	25	22	0	1	1
3		Zn	0	20	30	4	0	1	2	35	8
4	2+3+5+7+10	Mn	19	7	14	4	11	25	1	14	4
5		Na ₂ S ₂ O ₄	35	0	14	3	14	33	0	0	1
6		Mo	<i>No reaction (only starting materials present)</i>								
7		MoO ₂	<i>No reaction (only starting materials present)</i>								
8		TPGS-750-M ^c	<i>No reaction (only starting materials present)</i>								

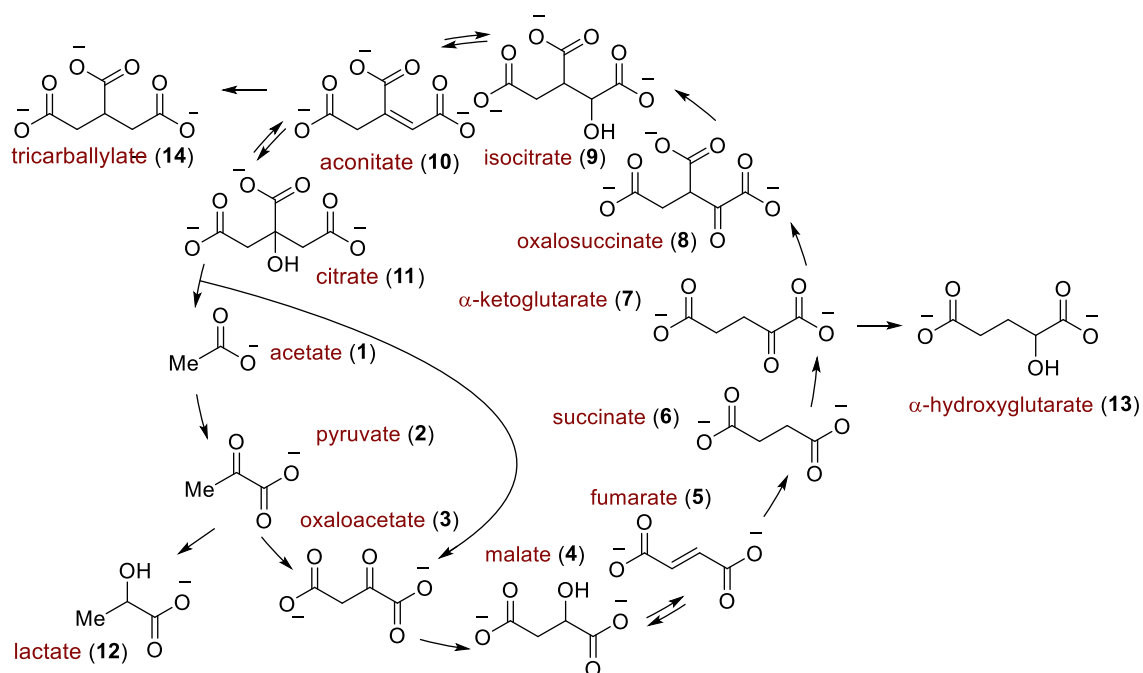
^a Reaction conditions: 0.1 mmol of each: sodium pyruvate, oxaloacetic acid, fumaric acid, α -ketoglutaric acid, *cis*-aconitic acid; 10 equiv. of reductant, 3 mL 1M HCl in H₂O, 3 h, 40°C. ^b Malate-fumarate equilibrium. ^c Control experiment to exclude reducing properties of micelles (1% w/w TPGS-750-M in 1M HCl in H₂O).

Table S 6 Non-enzymatic reactions of the rTCA cycle (Ni⁰ as reductant).

Entry	Substrate (0.1 mmol each)	Conditions ^a				Species present in the mixture post-reaction (%)											
		Ni ⁰ (equiv.)	Zn ²⁺ (equiv.)	Cr ³⁺ (equiv.)	Micelles	<i>On-cycle</i>						<i>Off-cycle</i>					
						2	4	5	6	7	9	10	11	12	13	14	15
<i>Reduction</i>																	
1 ^b	3	10	-	-	-		92±2	8±2									
2 ^b	5	10	-	-	-			19±5	81±5								
3 ^b	8	10	-	-	-				52±6		47±7	1±1					
<i>Hydration/Dehydration</i>																	
4	4	10	10	-	-		91±2	9±2	1±0								
5	4	10	10	-	yes		<i>No reaction (only starting material present)</i>										
<i>Three-step sequences</i>																	
6 ^c	3	20	-	-	-		84±0	15±0	1±0								
7 ^c	3	10	15	4	-		73±2	6±1						21±1			
8	3	10	15	4	-		66±2	9±1	2±0					24±1			
9	8	10	-	1	-				19±1		59±1	21±1	1±0				
10 ^d	8	5	10	6	-				4±0		52±1	37±2	7±1				
11	8	5	10	6	yes		<i>Mixture of oxalosuccinate decomposition products, incl. succinate</i>										
<i>Competitive reduction</i>																	
12 ^b	2+3+5+7+10	10	15	6	-		28±4	3 ^e ±0	5 ^e ±0	15±5	22±3		25±3		1±0	1±0	

^a Unless otherwise specified: 1 M HCl in H₂O, 16 h, 140 °C. ^b 3 h, 40 °C. ^c 16 h, 80 °C. ^d 48 h, 140 °C. ^e Malate-fumarate equilibrium. ^f Reaction with hydrazine hydrate (2 equiv.) Reported yields are average values of at least two runs Errors correspond to ±mean absolute deviation.

1.5 Gas chromatography traces



Sample chromatograms corresponding to entries 1 – 25 in Table S 1 can be found below (Fig. S 1 – 25).

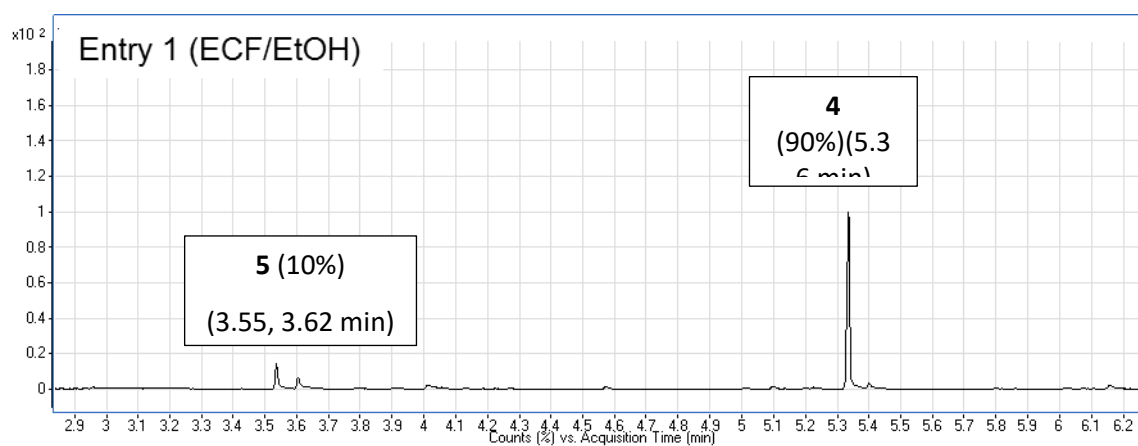


Figure S 1 Chromatogram of the reaction mixture corresponding to entry 1 (Table S 1).

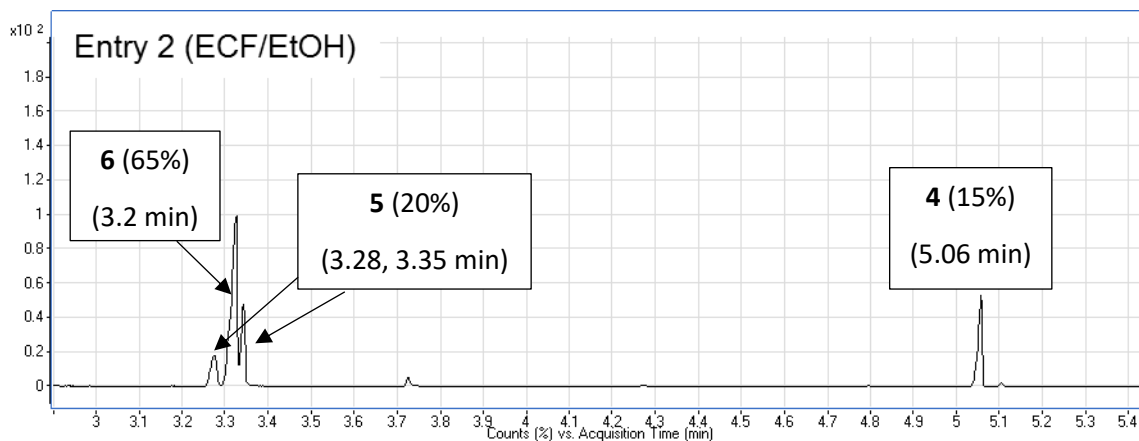


Figure S 2 Chromatogram of the reaction mixture corresponding to entry 2 (Table S 1).

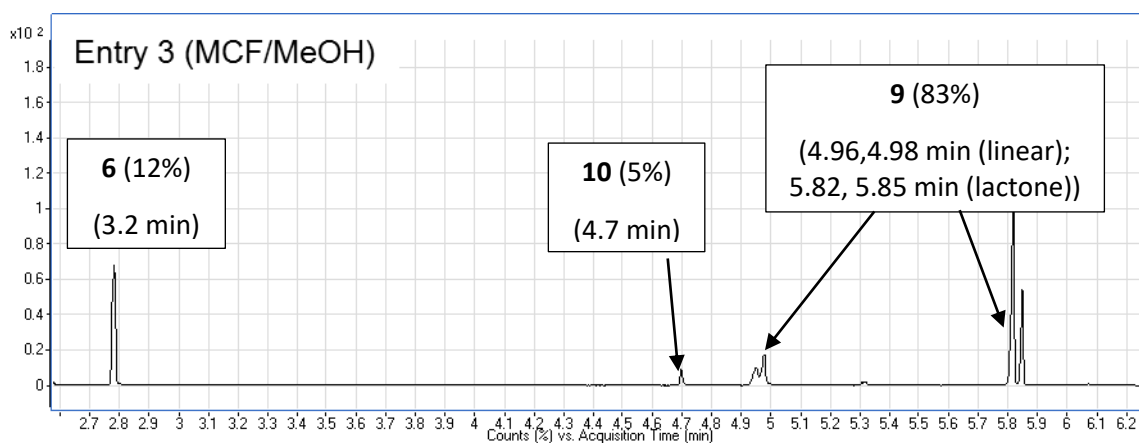


Figure S 3 Chromatogram of the reaction mixture corresponding to entry 3 (Table S 1).

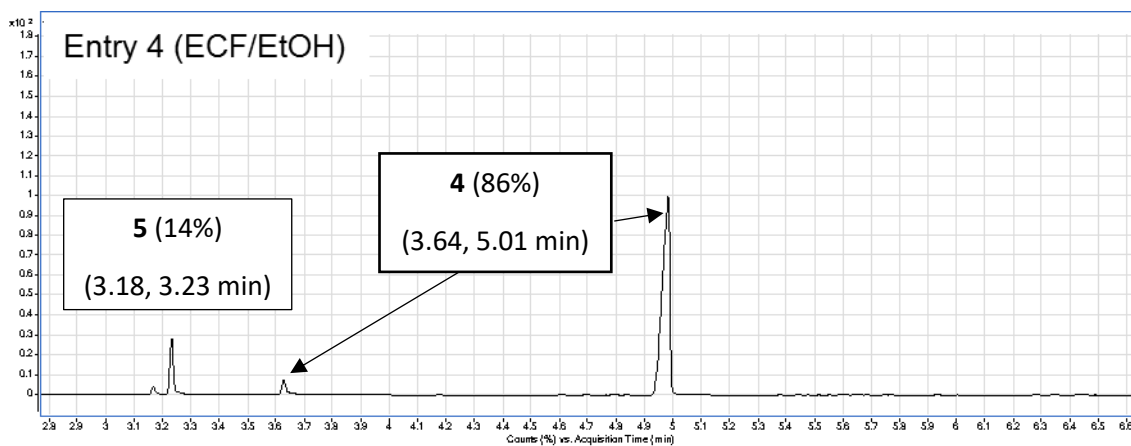


Figure S 4 Chromatogram of the reaction mixture corresponding to entry 4 (Table S 1).

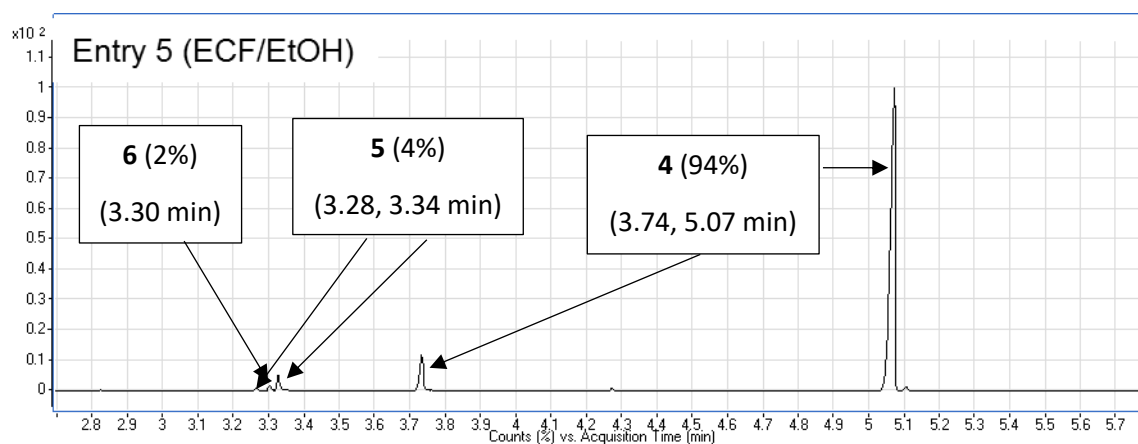


Figure S 5 Chromatogram of the reaction mixture corresponding to entry 5 (Table S 1).

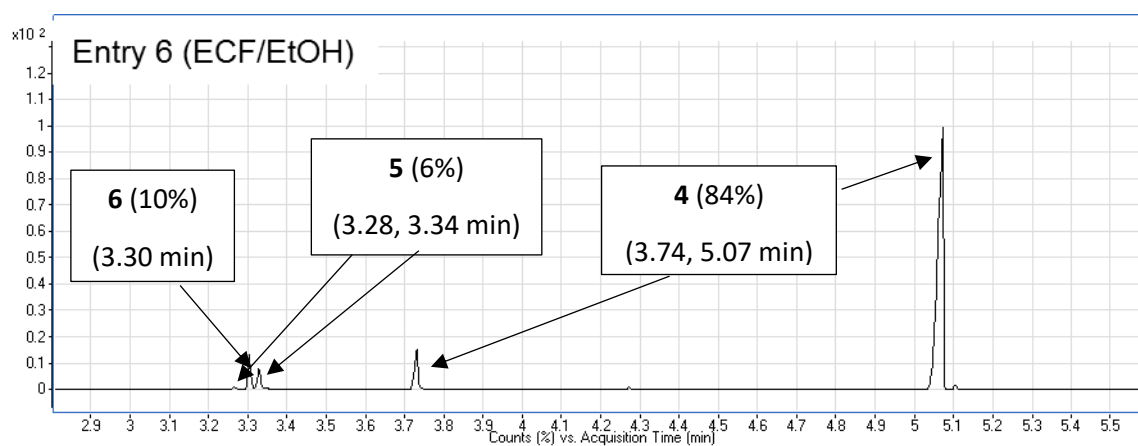


Figure S 6 Chromatogram of the reaction mixture corresponding to entry 6 (Table S 1).

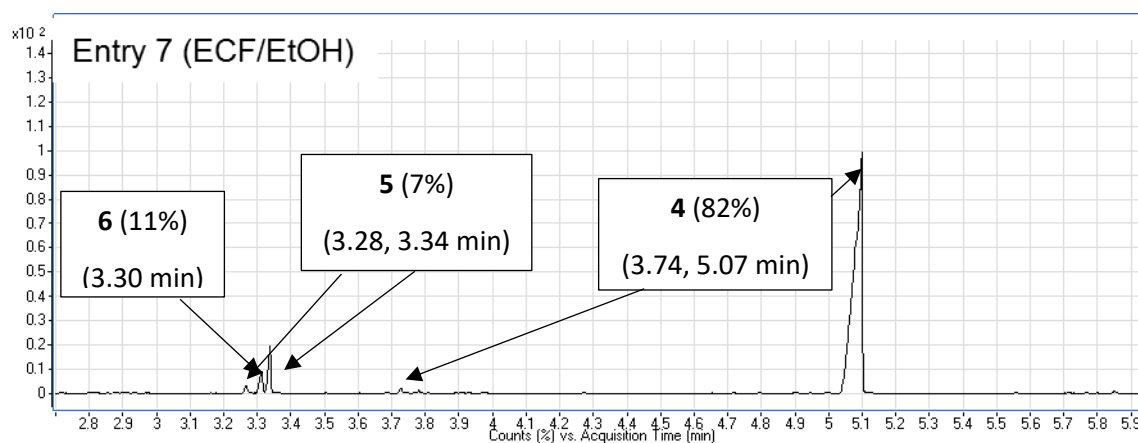


Figure S 7 Chromatogram of the reaction mixture corresponding to entry 7 (Table S 1).

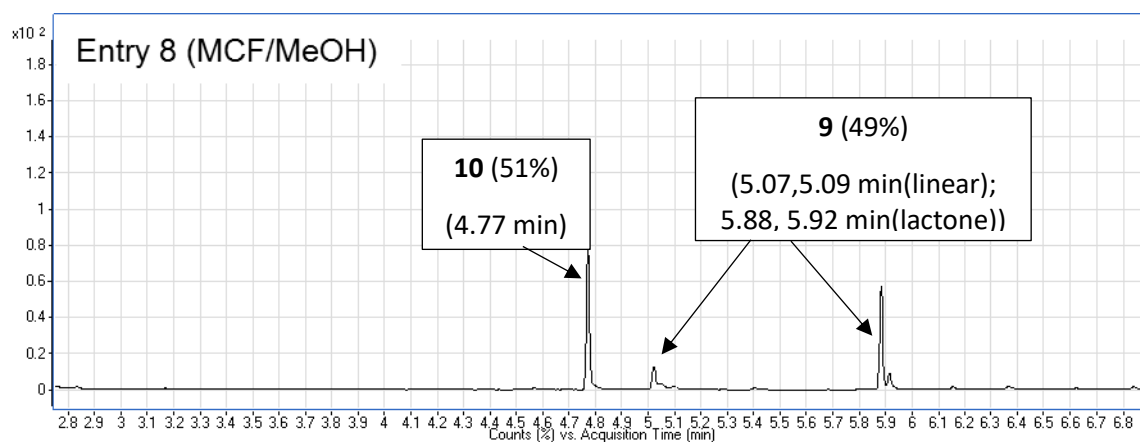


Figure S 8 Chromatogram of the reaction mixture corresponding to entry 8 (Table S 1).

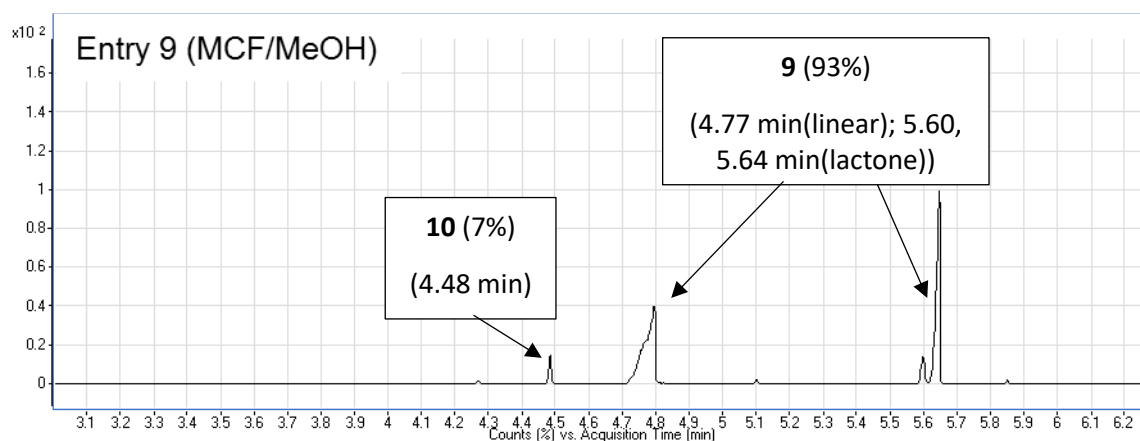


Figure S 9 Chromatogram of the reaction mixture corresponding to entry 9 (Table S 1).

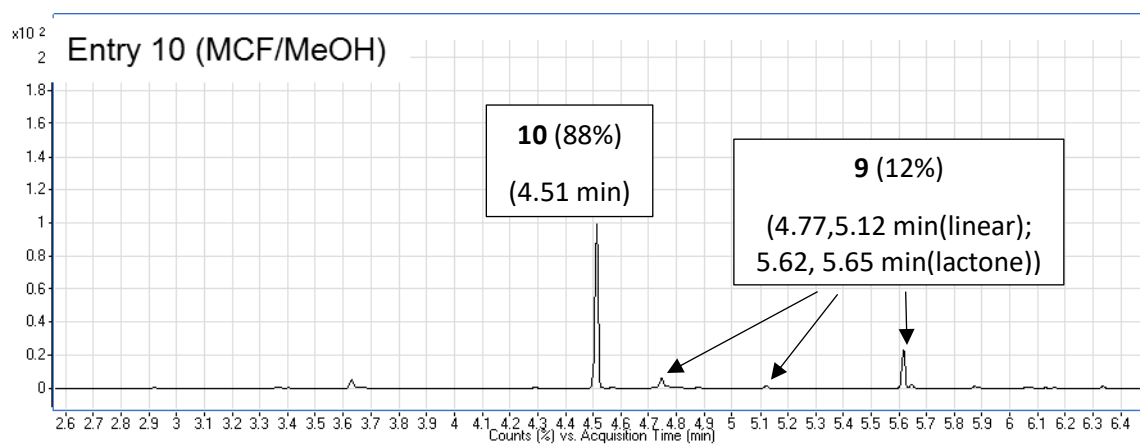


Figure S 10 Chromatogram of the reaction mixture corresponding to entry 10 (Table S 1).

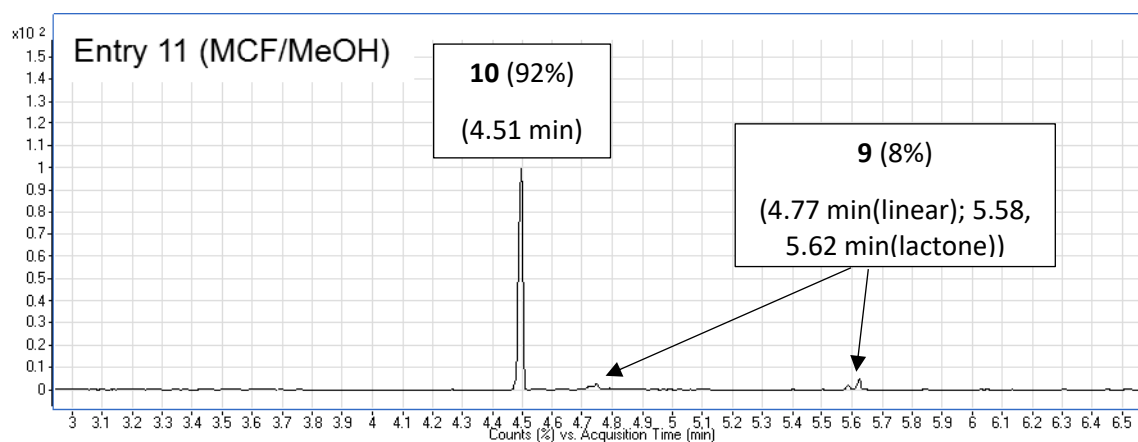


Figure S 11 Chromatogram of the reaction mixture corresponding to entry 11 (Table S 1).

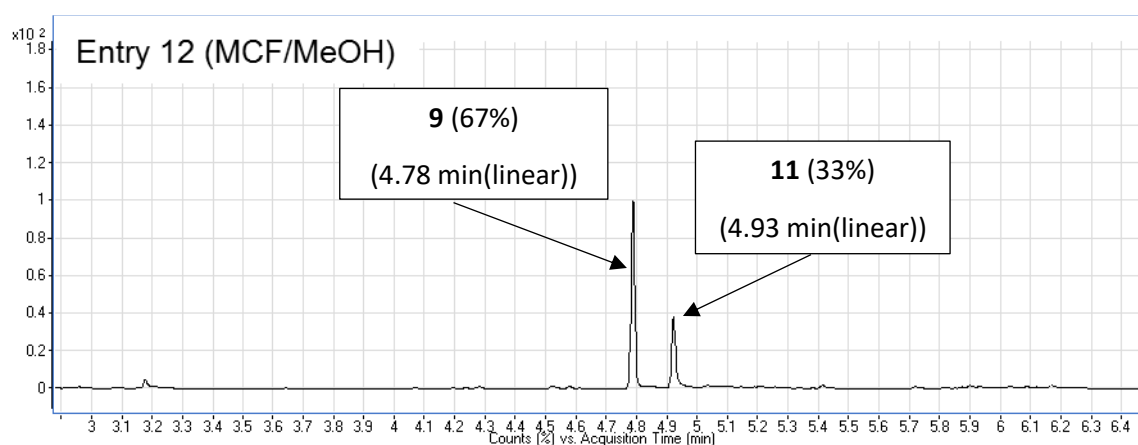


Figure S 12 Chromatogram of the reaction mixture corresponding to entry 12 (Table S 1).

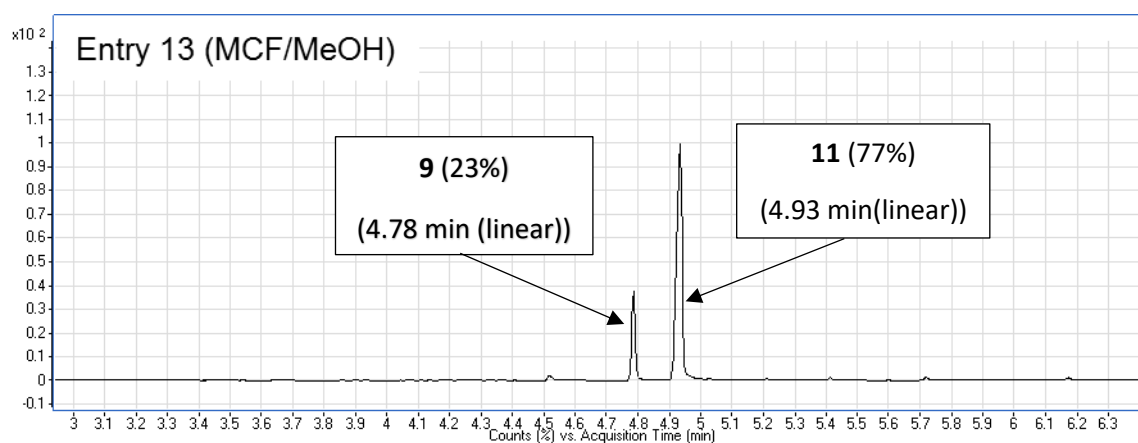


Figure S 13 Chromatogram of the reaction mixture corresponding to entry 13 (Table S 1).

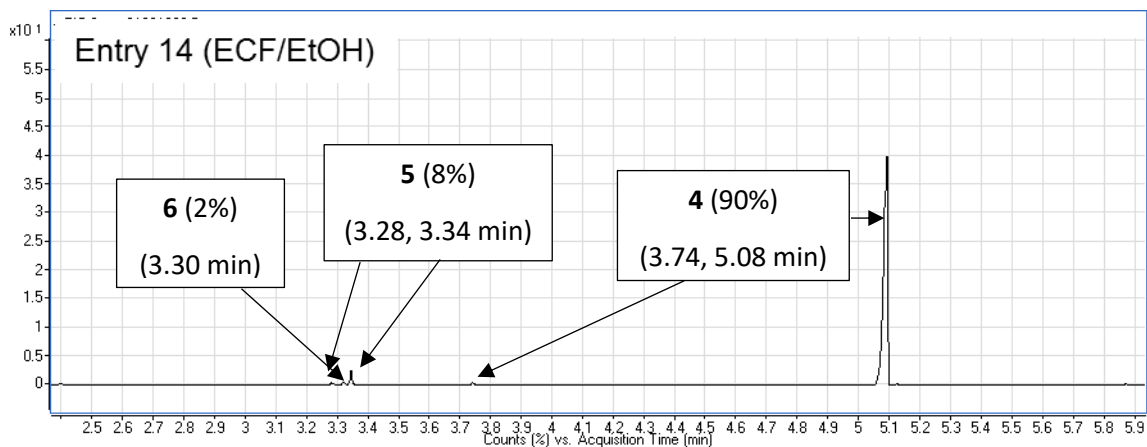


Figure S 14 Chromatogram of the reaction mixture corresponding to entry 14 (Table S 1).

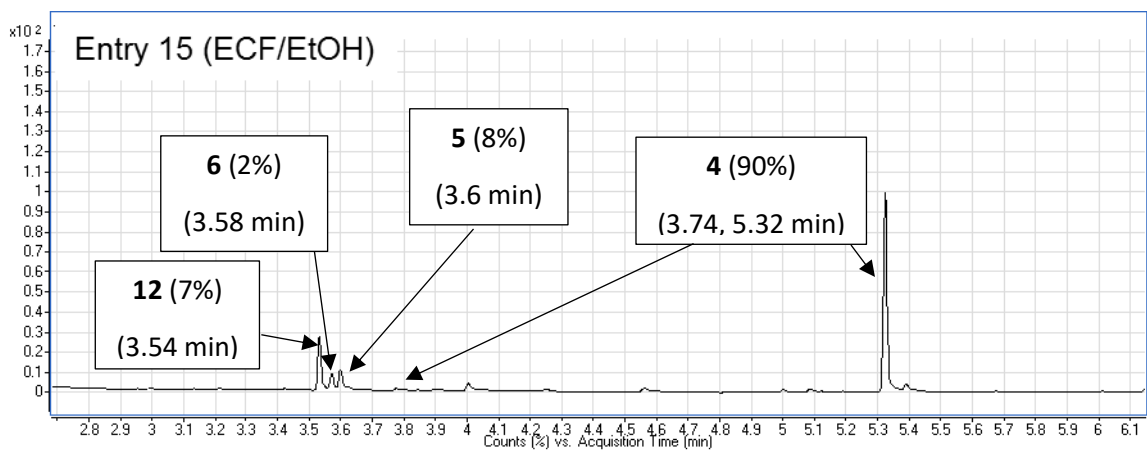


Figure S 15 Chromatogram of the reaction mixture corresponding to entry 15 (Table S 1).

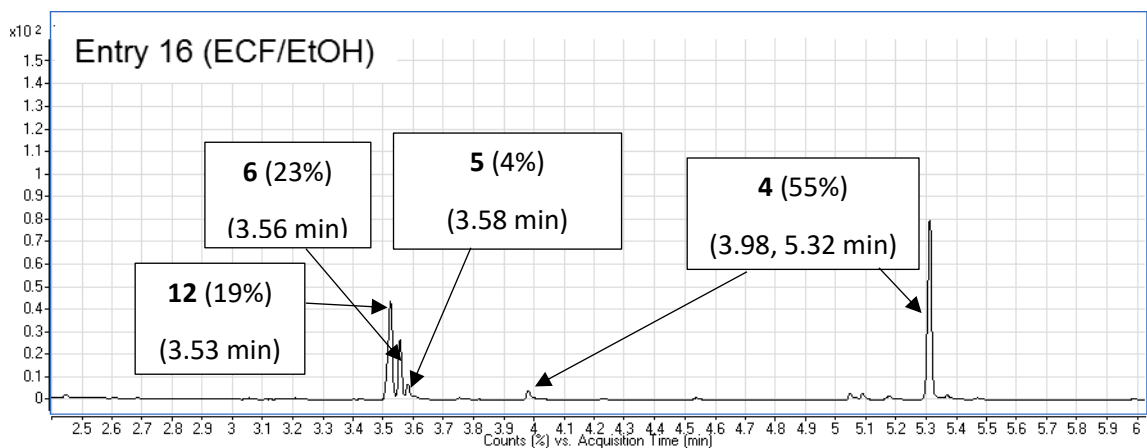


Figure S 16 Chromatogram of the reaction mixture corresponding to entry 16 (Table S 1).

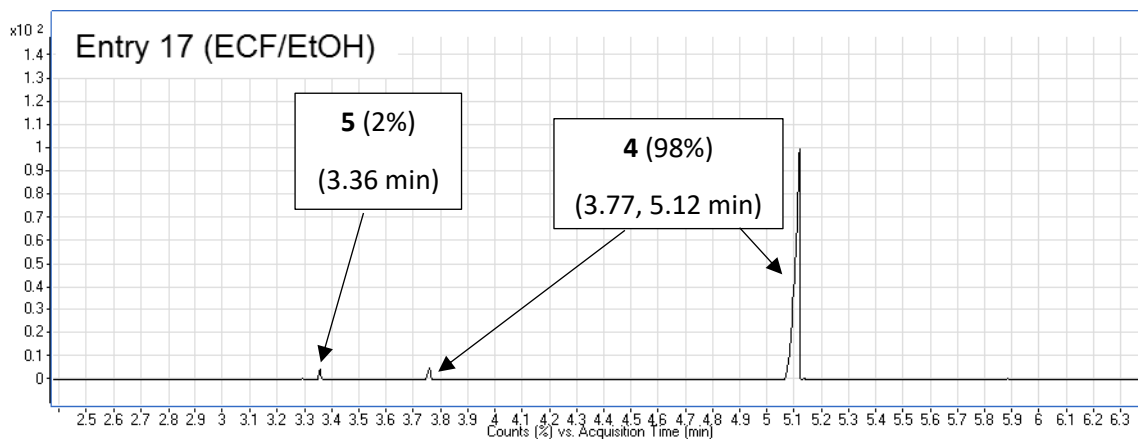


Figure S 17 Chromatogram of the reaction mixture corresponding to entry 17 (Table S 1).

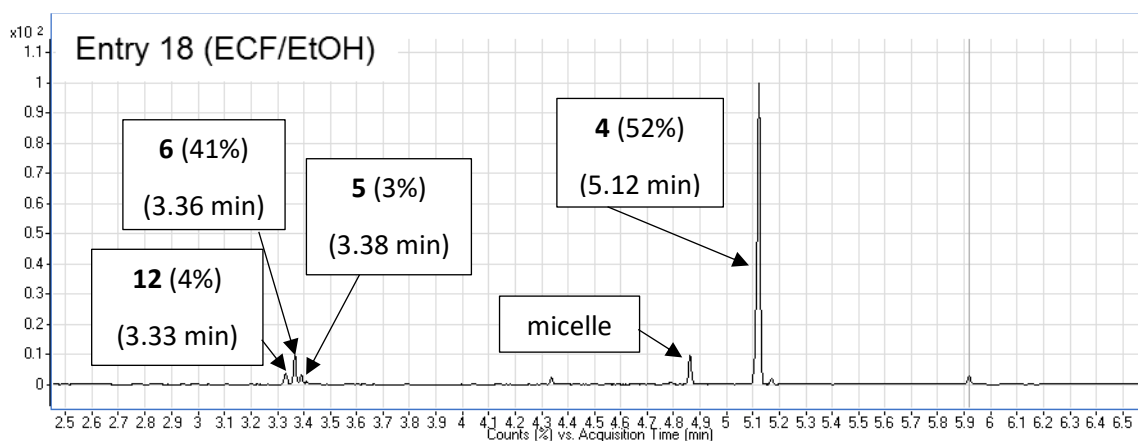


Figure S 18 Chromatogram of the reaction mixture corresponding to entry 18 (Table S 1).

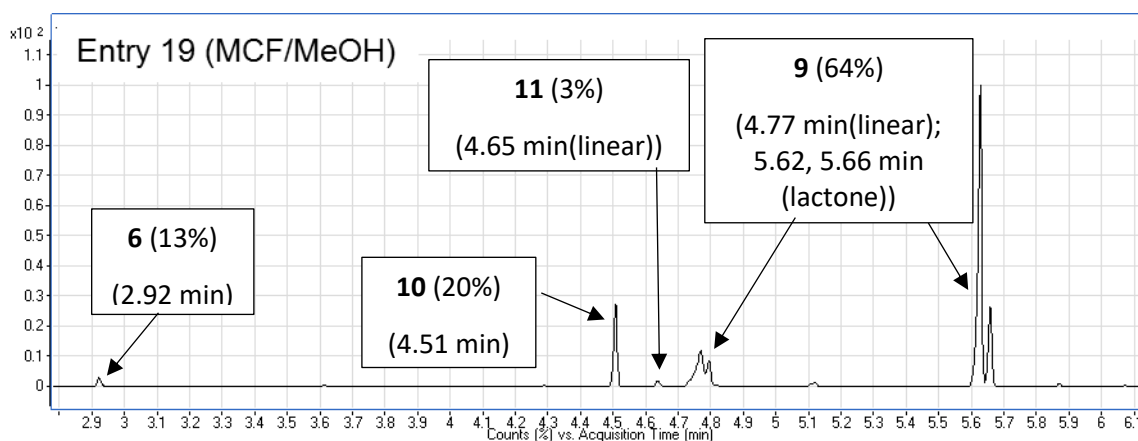


Figure S 19 Chromatogram of the reaction mixture corresponding to entry 19 (Table S 1).

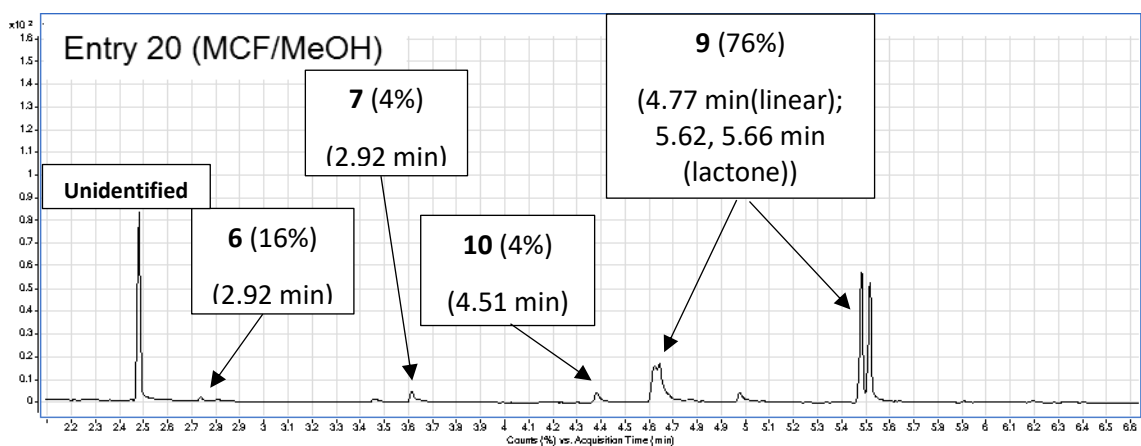


Figure S 20 Chromatogram of the reaction mixture corresponding to entry 20 (Table S 1).

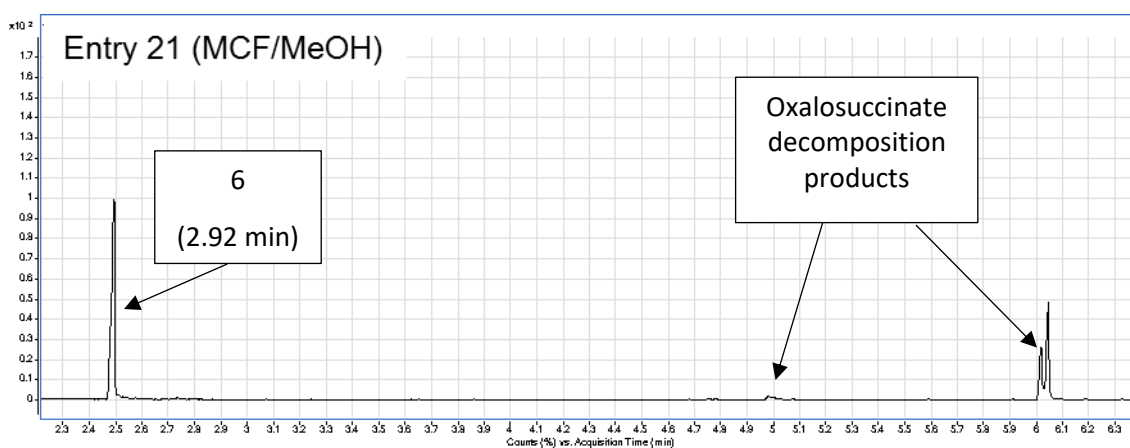


Figure S 21 Chromatogram of the reaction mixture corresponding to entry 21 (Table S 1).

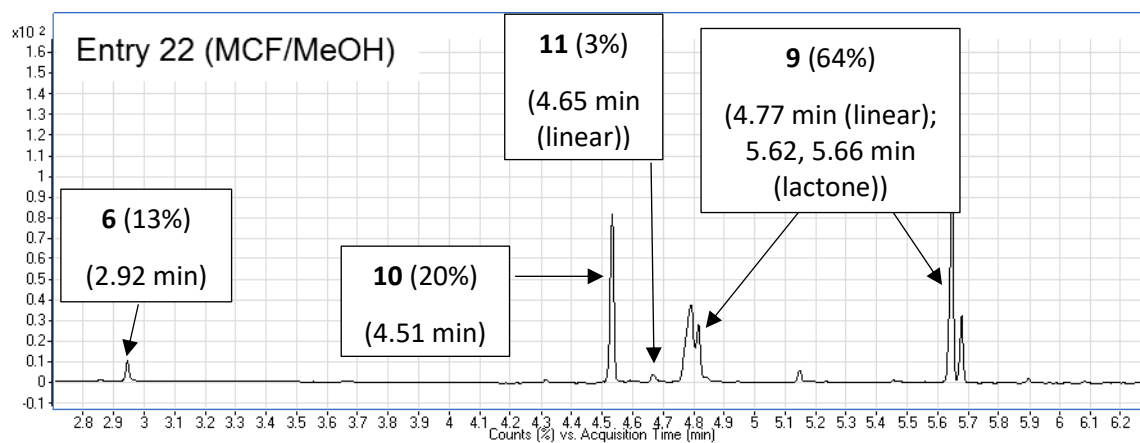


Figure S 22 Chromatogram of the reaction mixture corresponding to entry 22 (Table S 1).

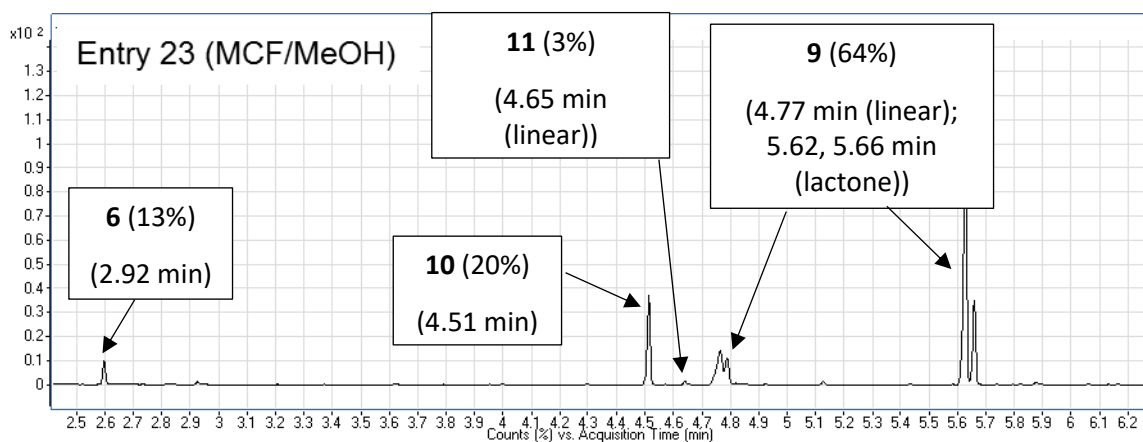


Figure S 23 Chromatogram of the reaction mixture corresponding to entry 23 (Table S 1).

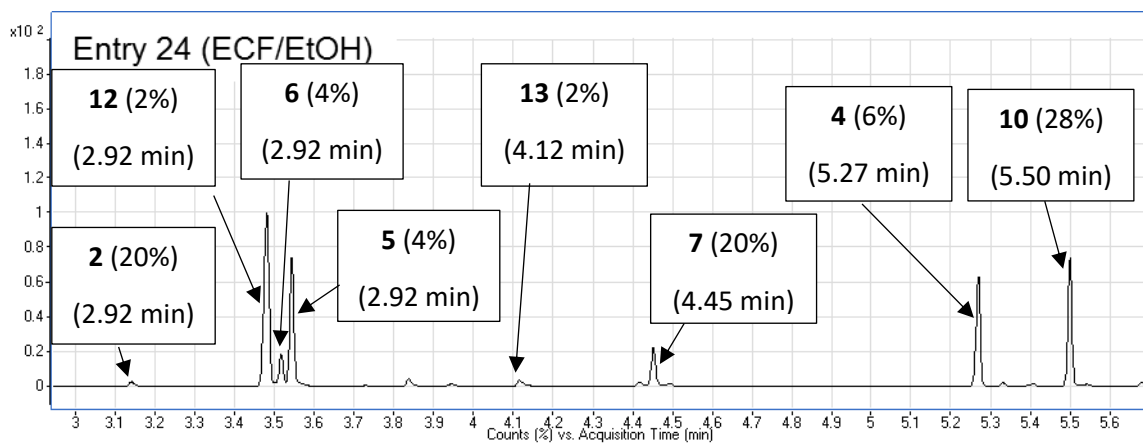


Figure S 24 Chromatogram of the reaction mixture corresponding to entry 24 (Table S 1).

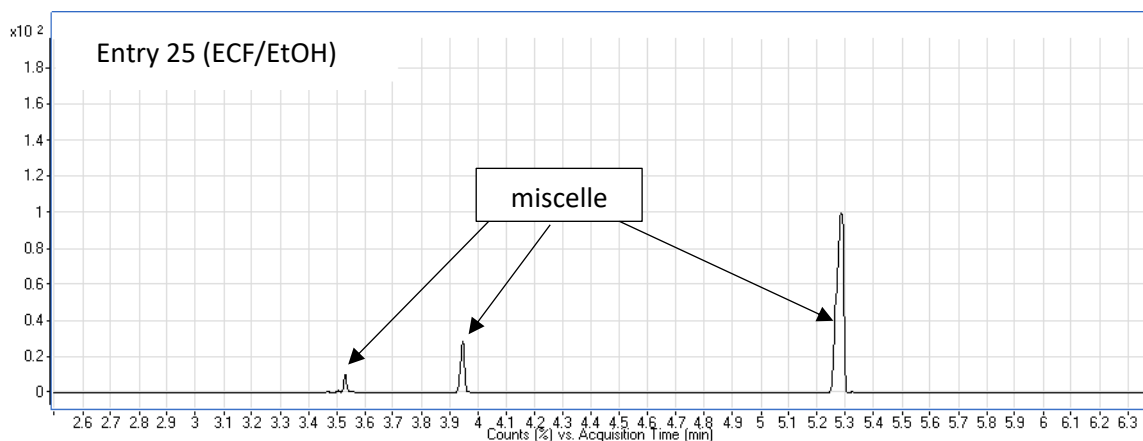


Figure S 25 Chromatogram of the reaction mixture corresponding to entry 25 (Table S 1).

Sample chromatograms corresponding to entries 1 – 13 in Table S 6 can be found below (Fig. S 26 – 38).

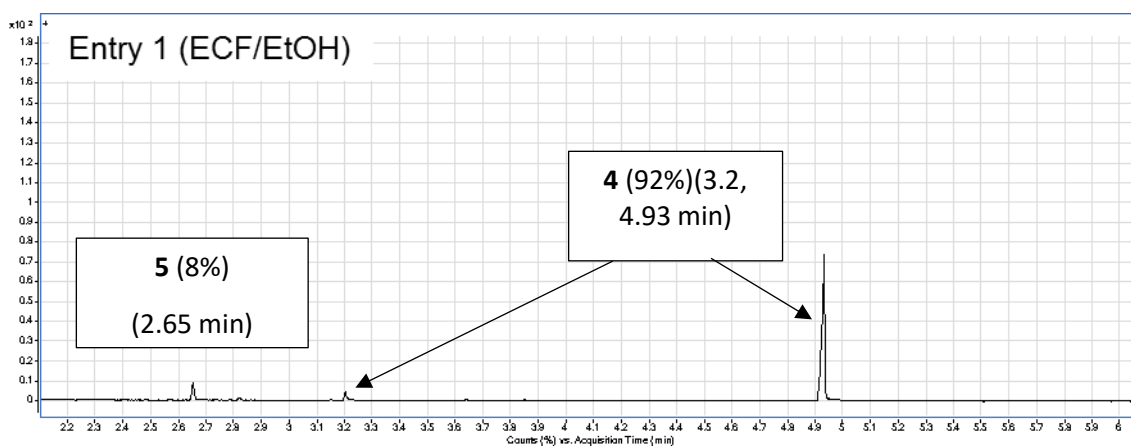


Figure S 26 Chromatogram of the reaction mixture corresponding to entry 1 (Table S 6).

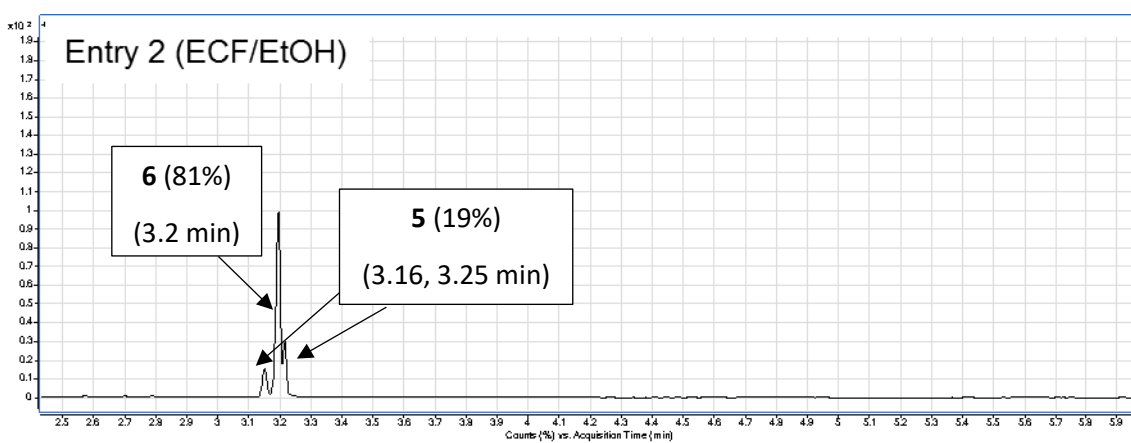


Figure S 27 Chromatogram of the reaction mixture corresponding to entry 2 (Table S 6).

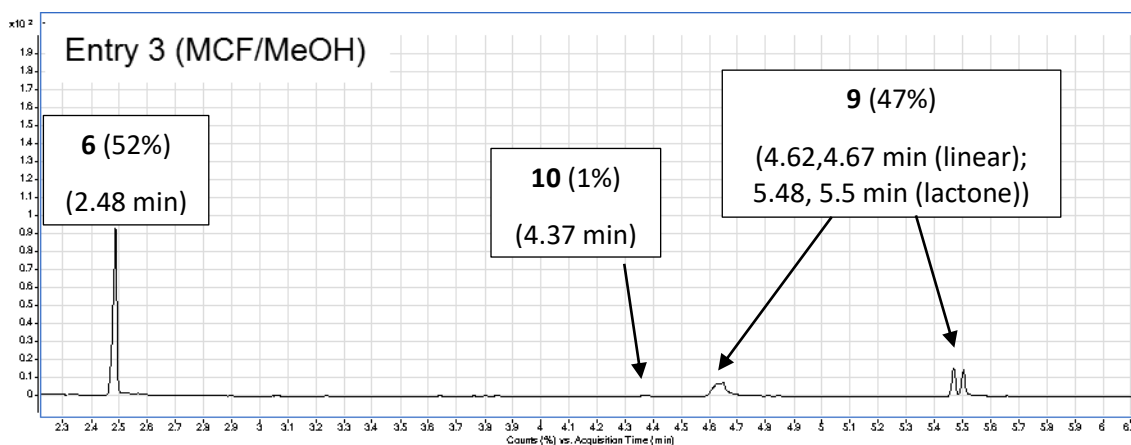


Figure S 28 Chromatogram of the reaction mixture corresponding to entry 3 (Table S 6).

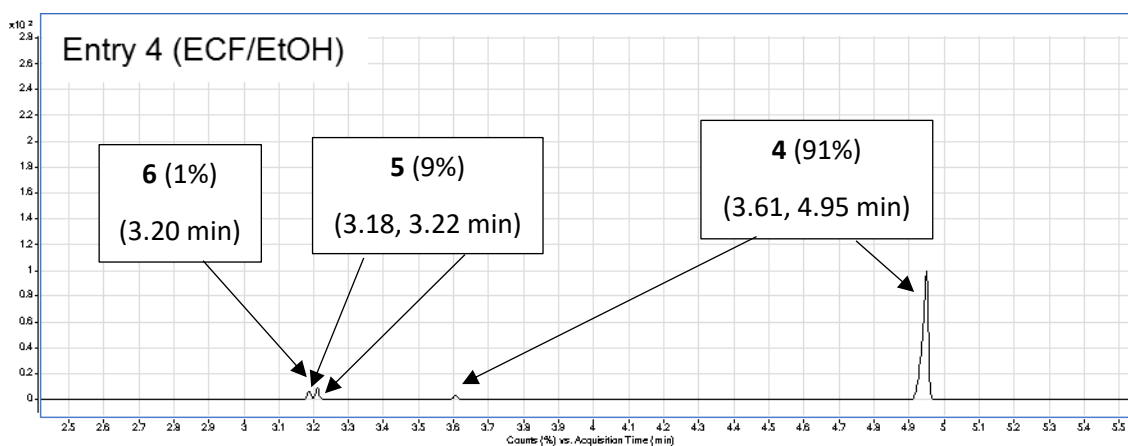


Figure S 29 Chromatogram of the reaction mixture corresponding to entry 4 (Table S 6).

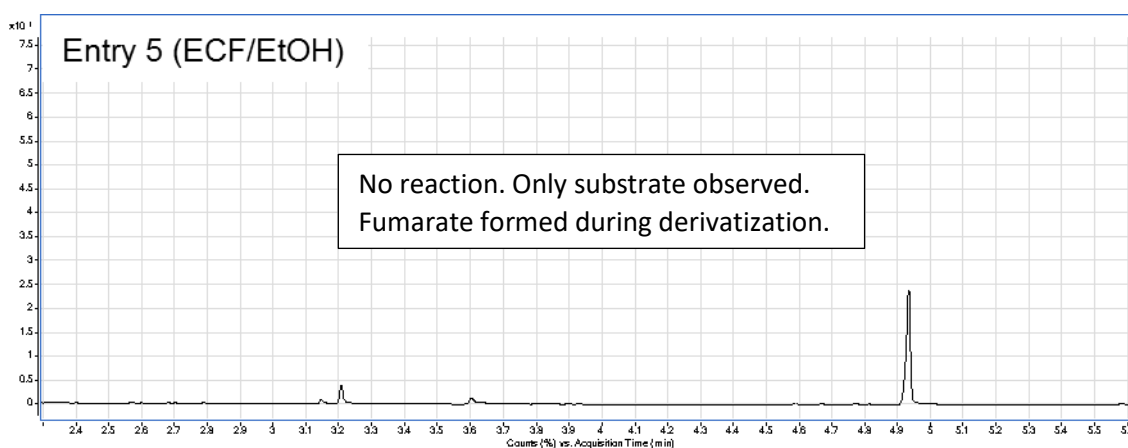


Figure S 30 Chromatogram of the reaction mixture corresponding to entry 5 (Table S 6).

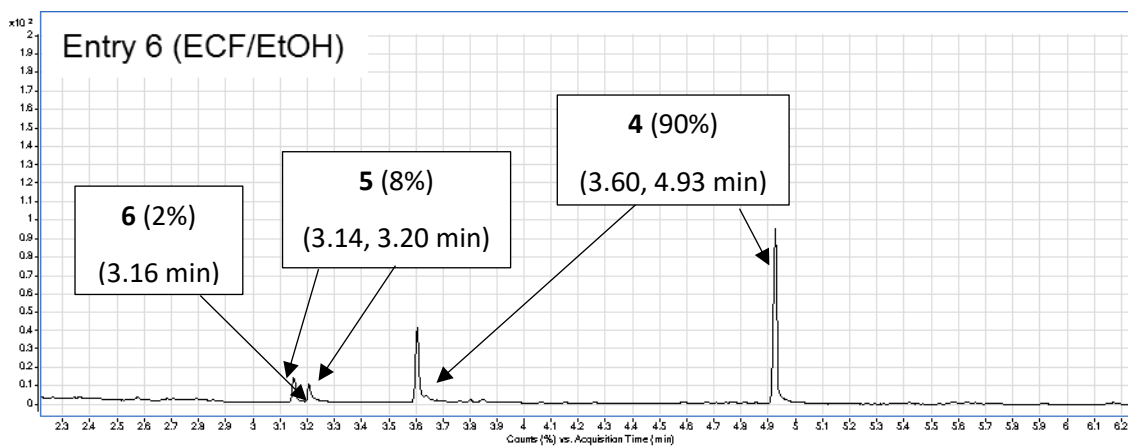


Figure S 31 Chromatogram of the reaction mixture corresponding to entry 6 (Table S 6).

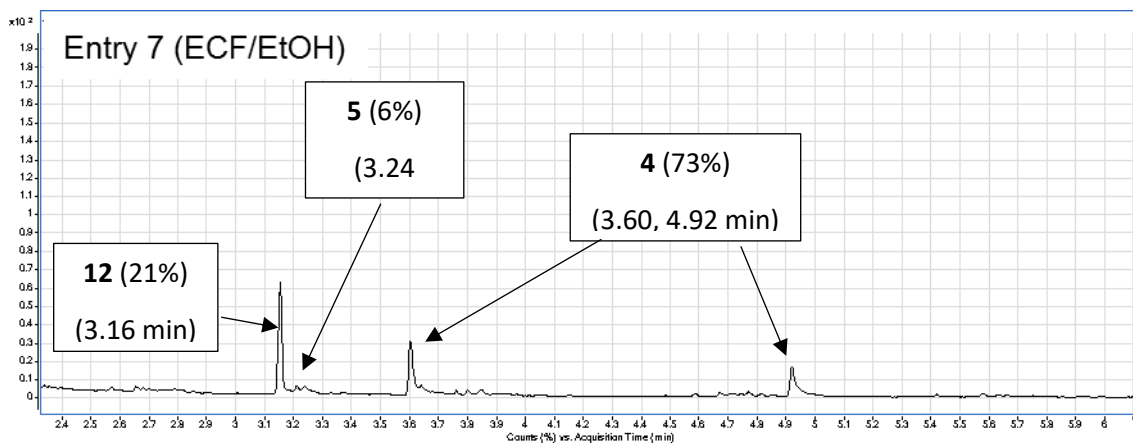


Figure S 32 Chromatogram of the reaction mixture corresponding to entry 7 (Table S 6).

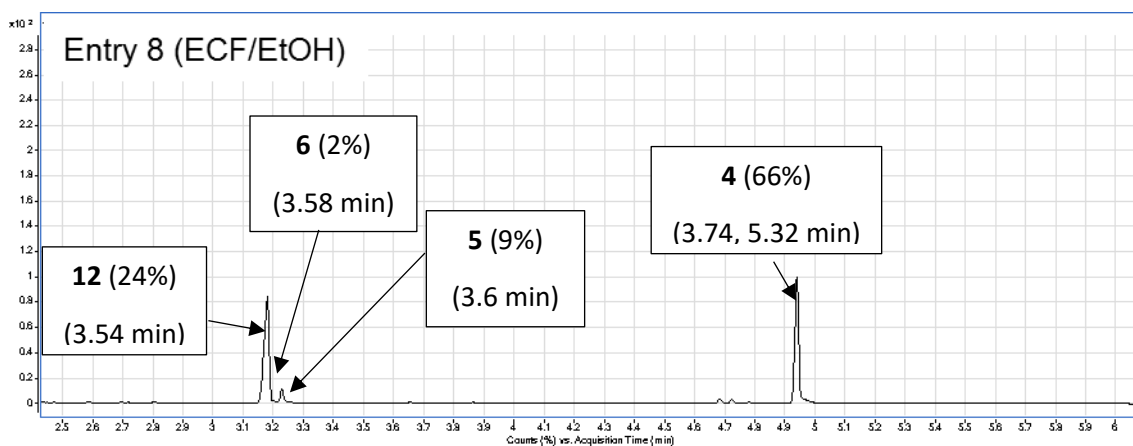


Figure S 33 Chromatogram of the reaction mixture corresponding to entry 8 (Table S 6).

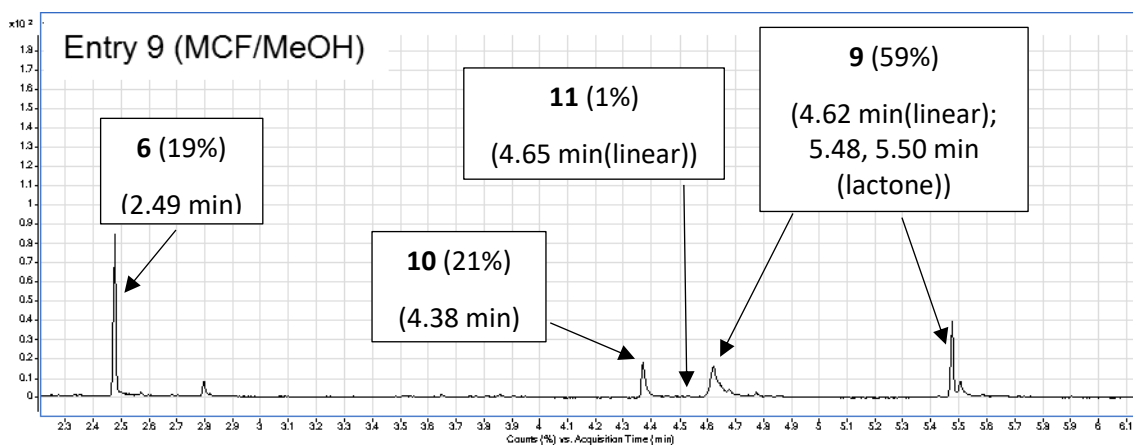


Figure S 34 Chromatogram of the reaction mixture corresponding to entry 9 (Table S 6).

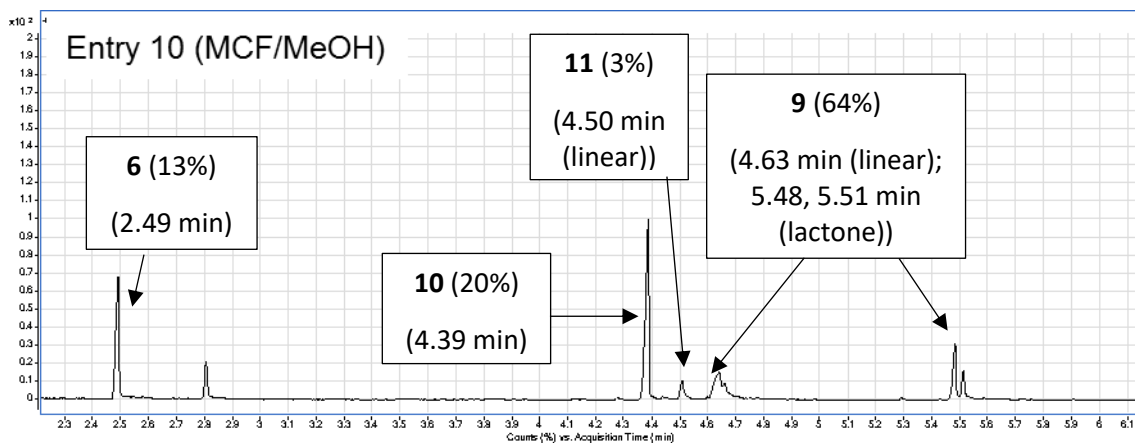


Figure S 35 Chromatogram of the reaction mixture corresponding to entry 10 (Table S 6).

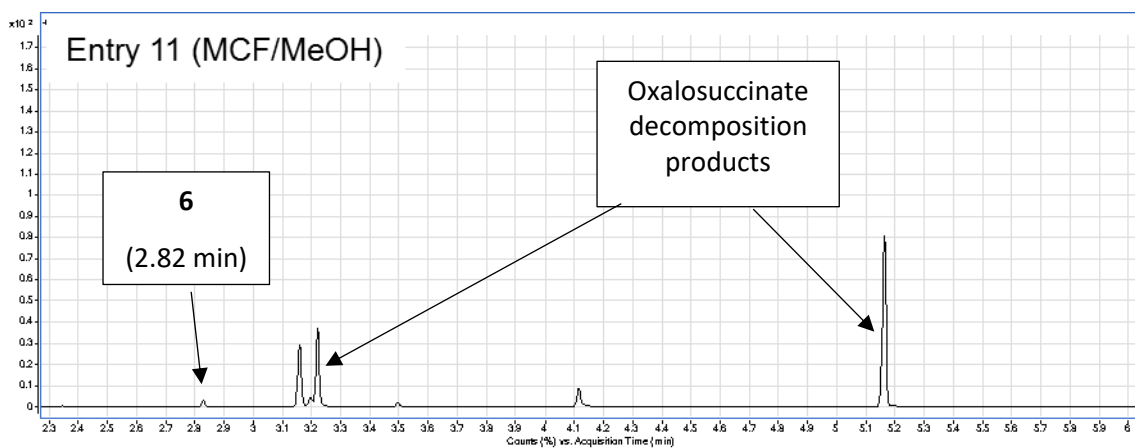


Figure S 36 Chromatogram of the reaction mixture corresponding to entry 11 (Table S 6).

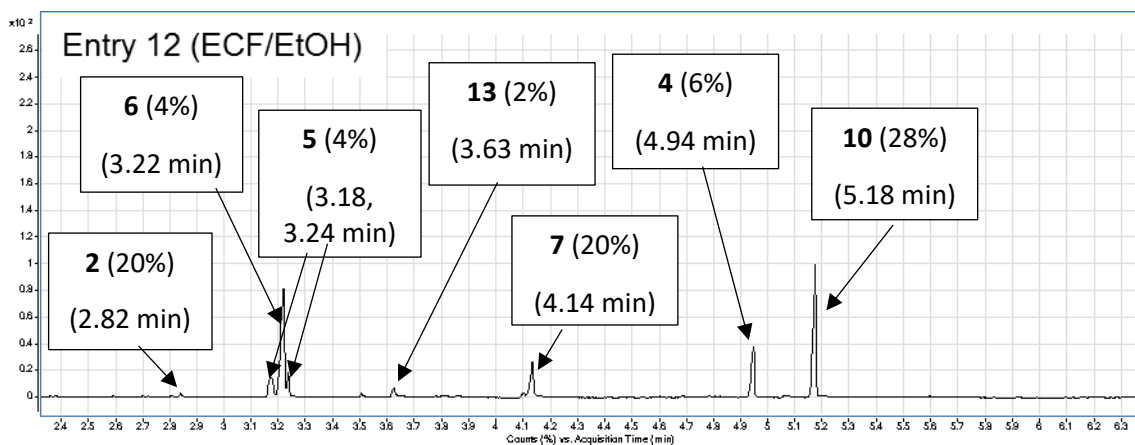


Figure S 37 Chromatogram of the reaction mixture corresponding to entry 12 (Table S 6).

1.6 Synthetic procedures

1.6.1 General procedure: Fe⁰ / Zn²⁺ / Cr³⁺ and Ni⁰/Zn²⁺/Cr³⁺ –catalyzed reactions

For Table S 1 and Table S 6.

To a 10 mL Pyrex pressure tube containing a Teflon-coated magnetic stir bar was added (unless otherwise specified) carboxylic acid substrate(s) (1 equiv, 0.100 mmol of each acid), Fe⁰ or Ni⁰ powder (10 equiv, 1.0 mmol, 56 mg Fe⁰ or 59 mg Ni⁰), and/or ZnCl₂ (15 equiv, 1.50 mmol, 204 mg), and/or Cr₂(SO₄)₃·12H₂O (3 equiv, 0.300 mmol, 183 mg). This was followed by the addition of 3 mL of solvent (unless otherwise specified: 1 M HCl in H₂O). The contents of the tube were flushed for ≈ 30 s with Ar. The tube was then quickly sealed, and the reaction mixture magnetically agitated for 16 h in a 12-tube metal heating block that was maintained at an internal temperature of 140 °C using an electronic thermocouple. The reaction tube was subsequently removed from the heating block and allowed to cool to room temperature before derivatization and GC-MS analysis.

1.6.2 Metal screens⁶

Malate dehydration – inorganic salts of the following metals were used in the malate dehydration reaction screen: Zn²⁺, Cu²⁺, Ni²⁺, Co²⁺, Fe²⁺, Mn²⁺, Cr²⁺, V²⁺. Zn²⁺ gave the best yields when used together with Fe⁰ (2-step reaction) (Table S 2).

Isocitrate dehydration – inorganic salts of the following metals were used in the isocitrate dehydration reaction screen: Zn²⁺, Cu²⁺, Ni²⁺, Co²⁺, Fe²⁺, Mn²⁺, Cr²⁺, V²⁺, Pd²⁺, Cd²⁺, Fe³⁺, Mn³⁺, Cr³⁺, As³⁺, Ru³⁺, Ir³⁺, Rh³⁺, Ti³⁺. Zn²⁺ was chosen for further experiments due to high yields and geochemical accessibility, although considerable reactivity was also seen for Cr²⁺, Pd²⁺, Fe³⁺, Mn³⁺, As³⁺, Ru³⁺, Ir³⁺ and Rh³⁺ (Table S 3).

Aconitate hydration – inorganic salts of the following metals were used in the aconitate hydration reaction screen: Cu⁺, Zn²⁺, Cu²⁺, Ni²⁺, Co²⁺, Fe²⁺, Mn²⁺, Cr²⁺, Cd²⁺, Hg²⁺, Fe³⁺, Co³⁺, Mn³⁺, Cr³⁺, Ti³⁺, Ru³⁺, Mo⁴⁺, W⁴⁺, Mo⁶⁺, W⁶⁺. Only Cr³⁺ yielded a significant positive result (Table S 4).

⁶ The metals/metal ions described are thought to be present in hydrothermal fluids. See Seyfried, W. E.Jr., J. S. Seewald, M. E. Berndt, K. Ding, and D. I. Foustoukos (2003), Chemistry of hydrothermal vent fluids from the Main Endeavour Field, northern Juan de Fuca Ridge: Geochemical controls in the aftermath of June 1999 seismic events, *J. Geophys. Res.*, 108, 2429, doi: 10.1029/2002JB001957, B9.

Reductions – Metals Zn, Fe, Ni, Mo were used in powder form. These results were compared against MoO₂ and sodium dithionite. Through a control experiment, the reducing properties of TPGS-750-M were excluded (Table S 5).

1.6.3 Reactions in micellar solutions.

For reactions carried out in micelles, 3 mL of a TPGS-750-M solution (DL- α -tocopherol methoxypolyethylene glycol succinate, 1% w/w) in 1 M HCl was used as the solvent. Stirring was maintained at 1000 rpm. In order to control for the contribution of the surfactant molecule towards succinate detected in the chromatograms, a control reaction was carried out (Reaction 26 in Table S1). A mixture of Fe⁰ powder (10 equiv., 1.0 mmol, 56 mg), ZnCl₂ (15 equiv. 1.5 mmol, 204 mg), Cr₂(SO₄)₃·12H₂O (3 equiv., 0.3 mmol, 183 mg) in TPGS-750-M (3 mL, 1% w/w in 1 M HCl in H₂O) was heated at 140 °C for 16 h. After cooling, a 0.1 mmol portion of malic acid was dissolved in the mixture, a 100 μ L aliquot of which was immediately derivatised. It was found (two runs) that succinate originating from TPGS-750-M (DL- α -tocopherol methoxypolyethylene glycol succinate) contributes to not more than 1% of the control reaction composition (Table S 1). Micelles may play various roles in the oxaloacetate-malate-fumarate-succinate sequence, e.g. bias the malate-fumarate equilibrium towards fumarate by increasing solubilities of fumarate and succinate or increase the stability of carboxylic acids and thus minimise the mass loss as carbon dioxide.

1.6.4 Portion-wise reagent addition.

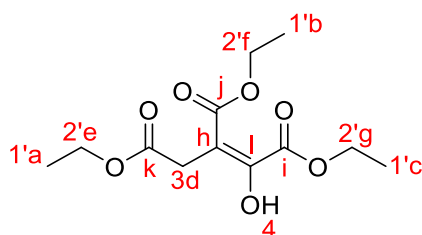
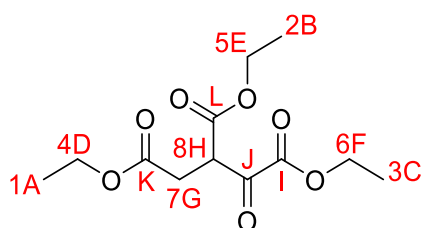
For reactions where portion-wise addition of reagents was performed (Reactions 1 and 15 in Table S 1): the first half of reagents was added at the beginning of the reaction; the second portion was added after 24 h to a cooled reaction mixture, after which the reaction vessel was re-sealed and heating resumed.

1.6.5 Reactions with oxalosuccinic acid

For Table S 1: entries 3 and 19 – 23; Table S 6: entries 3 and 9 – 11.

Due to its high instability, rapid decarboxylation and storage difficulties,¹¹⁵ oxalosuccinic acid was prepared on demand by *in situ* hydrolysis of triethyl oxalosuccinate ester under typical acidic reaction conditions (1 M HCl).

1.6.6 Triethyl oxalosuccinate



Prepared following the literature procedure¹¹² from diethyl succinate (5 mmol) and diethyl oxalate (5 mmol), with commercial available potassium ethoxide instead of potassium metal. Triethyl oxalosuccinate was obtained as a light-yellow liquid (1.2 g, 89%).

¹H NMR (400 MHz, CDCl₃) δ 12.77 (s, enol **4'**), 4.64 (dd, $J = 8.9, 5.2$ Hz, 1H, **8**), 4.34 (q, $J = 7.1$ Hz, 2H, **6**), 4.28 (dd, $J = 12.1, 7.2$ Hz, enol **2'**), 4.17 (dd, $J = 14.8, 7.7$ Hz, 2H, **5**), 4.11 (dd, $J = 14.3, 7.1$ Hz, 2H, **4**), 3.61 (s, enol **3'**), 3.00 (dd, $J = 17.3, 8.9$ Hz, 1H, **7**), 2.88 (dd, $J = 17.4, 5.1$ Hz, 1H, **7**), 1.36 (t, $J = 7.1$ Hz, 3H, **3**), 1.29 (dd, $J = 13.1, 6.0$ Hz, enol **1'**), 1.22 (t, $J = 7.1$ Hz, 3H, **2**), 1.21 (t, $J = 7.1$ Hz, 3H, **1**).

¹³C NMR (101 MHz, CDCl₃) δ 188.30 (**L**), 172.55 (enol **I**), 171.05 (enol **k**), 170.60 (**K**), 167.70 (**J**), 162.32 (enol **j**), 160.21 (**I**), 158.40 (enol **i**), 102.57 (enol **h**), 62.84 (**F**), 62.17 (enol **g**), 62.06 (**E**), 61.99 (enol **f**), 61.21 (**D**), 60.74 (enol **e**), 49.25 (**H**), 31.94 (**G**), 31.27 (enol **d**), 14.15 (enol **c**), 14.00 (**C**), 13.91 (GSD-resolved, enol **a, b**) 13.88 (**B**), 13.83 (**A**).

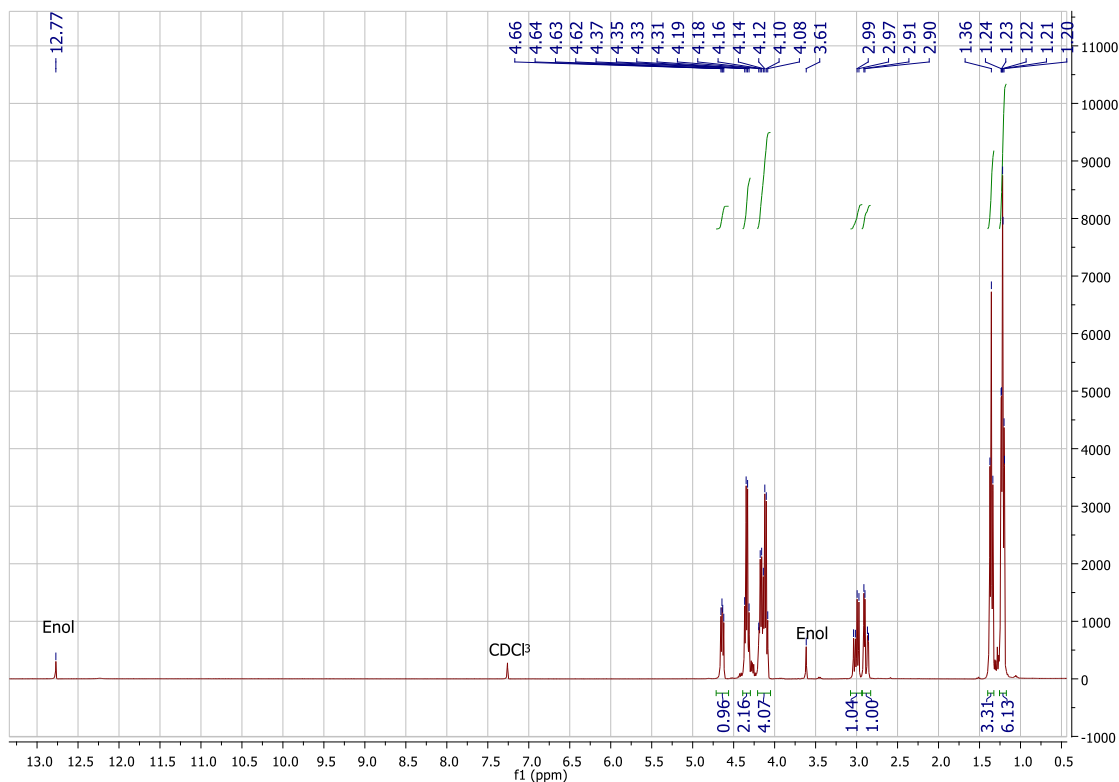


Figure S 38 ¹H NMR of triethyl oxalosuccinate in CDCl₃ at 25 °C

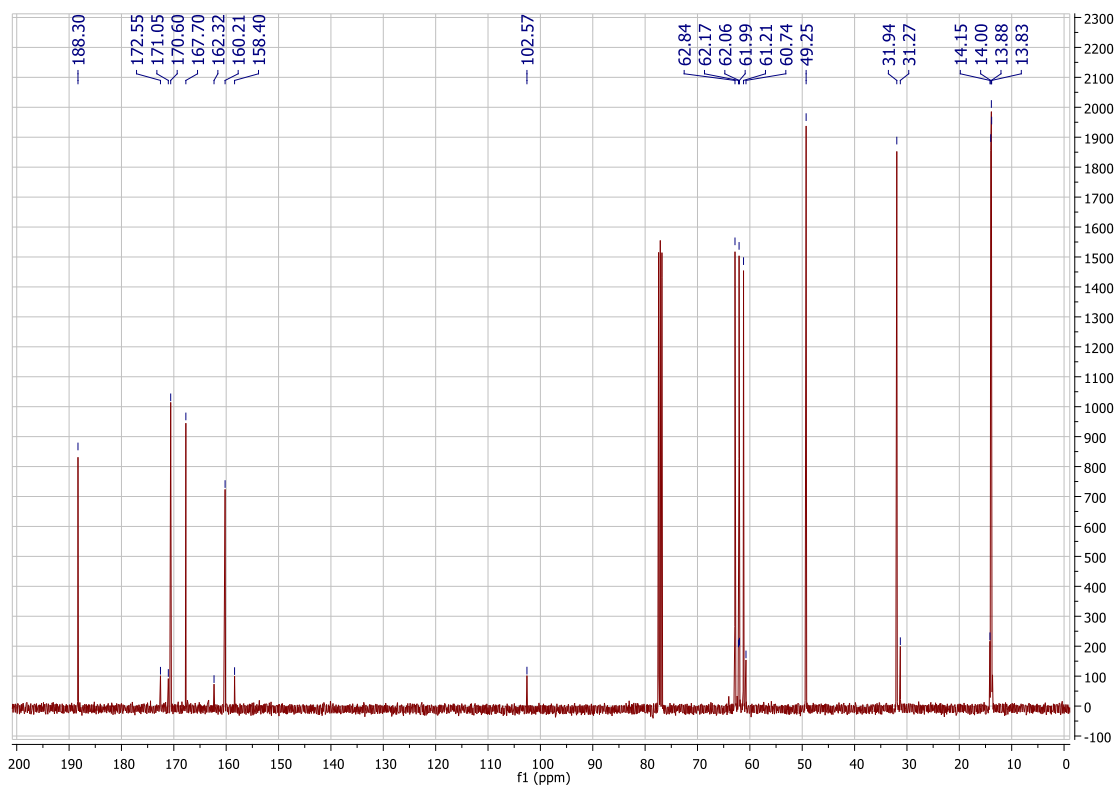


Figure S 39 ¹³C NMR of triethyl oxalosuccinate in CDCl₃ at 25 °C

1.6.7 *Cis*-aconitic acid

Cis-aconitic acid used in this study was prepared on a gram scale (19.7 g, 45%) from citric acid (48 g, 0.25 mol) using a literature procedure.¹¹³ The identity of the product was confirmed using existing literature data,¹¹⁶ as well as by comparison of the GC-MS data (chromatogram and MS fragmentation pattern) with an authentic sample.

¹H NMR (400 MHz, D₂O) δ 6.91 (s, 1H), 3.74 (s, 2H). ¹³C NMR (101 MHz, D₂O) δ 174.64, 169.32, 168.54, 139.09, 130.48.

2 The Wood-Ljungdahl pathway

2.1 General information

All reactions were carried out in stainless-steel Parr pressure reactors in 1.5 mL vials with pierced PTFE-lined caps under CO₂ atmosphere, unless otherwise noted.

¹H NMR spectra were recorded on a Bruker Avance300 (300 MHz) spectrometer at ambient temperature in a H₂O:D₂O mixture (6:1) as solvent, with sodium 3-(trimethylsilyl)-1-propanesulfonate (DSS-Na) as the internal standard (CH₃ peak at 0 ppm). Solvent suppression was achieved through excitation sculpting, using the Bruker ZGESGP pulse program adjusted for the water resonance. 32 scans were acquired for each sample. Relaxation delay D1 was set to 87 s, with time domain size TD = 32768 and sweep width SWH = 4789.27 Hz (11.963 ppm), to allow for quantitative measurements. Integration was performed using *MestReNova v6.0.2* software.

GC-MS analysis was performed on a GC System 7820A (G4320) using an Agilent High Resolution Gas Chromatography Column (PN 19091S – 433UI, HP – 5MS UI, 28 m×0.250 mm, 0.25 Micron, SN USD 489634H). The system was connected to an MSD block 5977E (G7036A). Hydrogen (99.999 % purity) was used as carrier gas at a constant flow rate of 1.5 mL min⁻¹. The analysis was carried out in a splitless mode with 1 μL injection volume, at the injection port temperature of 250 °C. The column was maintained at 60 °C for 1 min, then ramped at 30 °C min⁻¹ to 310 °C with 3 min hold, and the total running time was 12.33 min. The mass spectrometer was turned on after a 2-min solvent delay and was operated at the electron ionization (EI) mode with quadrupole temperature of 150 °C. Data was acquired in the full-scan mode (50-500 amu).

2.1.1 Materials

All reagents were purchased from commercial suppliers and were of a grade presented below in Table S 7.

Table S 7 Specifications of materials used

No.	Reagent	CAS	Supplier
1	Mn powder, 325 mesh, ≥99% trace	7439-96-5	Sigma Aldrich
2	Fe powder (fine), ≥ 99%, reduced	7439-89-6	Sigma Aldrich

3	Co powder, 2 μm particle size, 99.8% trace metal basis	7440-48-4	Sigma Aldrich
4	Ni powder, <150 μm , 99.99% trace metal basis	7440-02-0	Sigma Aldrich
5	Mo powder, 1-5 μm , $\geq 99.9\%$ trace metal basis	7439-98-7	Sigma Aldrich
6	W powder, 12 μm , 99.9% trace metal basis	7440-33-7	Sigma Aldrich

All reagents were tested for the presence of trace acetate and/or formate impurities prior to use – see the “Analytical methods: 2.2.2. Starting material control experiments” section below. Water was obtained from a Milli-Q purification system (18 M Ωcm).

2.2 Analytical methods

2.2.1 Product identification

All compounds detected in this study were analysed using the Bruker ZGESGP 1D pulse sequence with water suppression, as described in the General information section above. Sodium 3-(trimethylsilyl)-1-propanesulfonate (DSS-Na) was used as the internal standard (Figure S 40). Acetate, pyruvate, methanol, formate and lactate were identified based on their chemical shifts compared to authentic samples (Figure S 41).

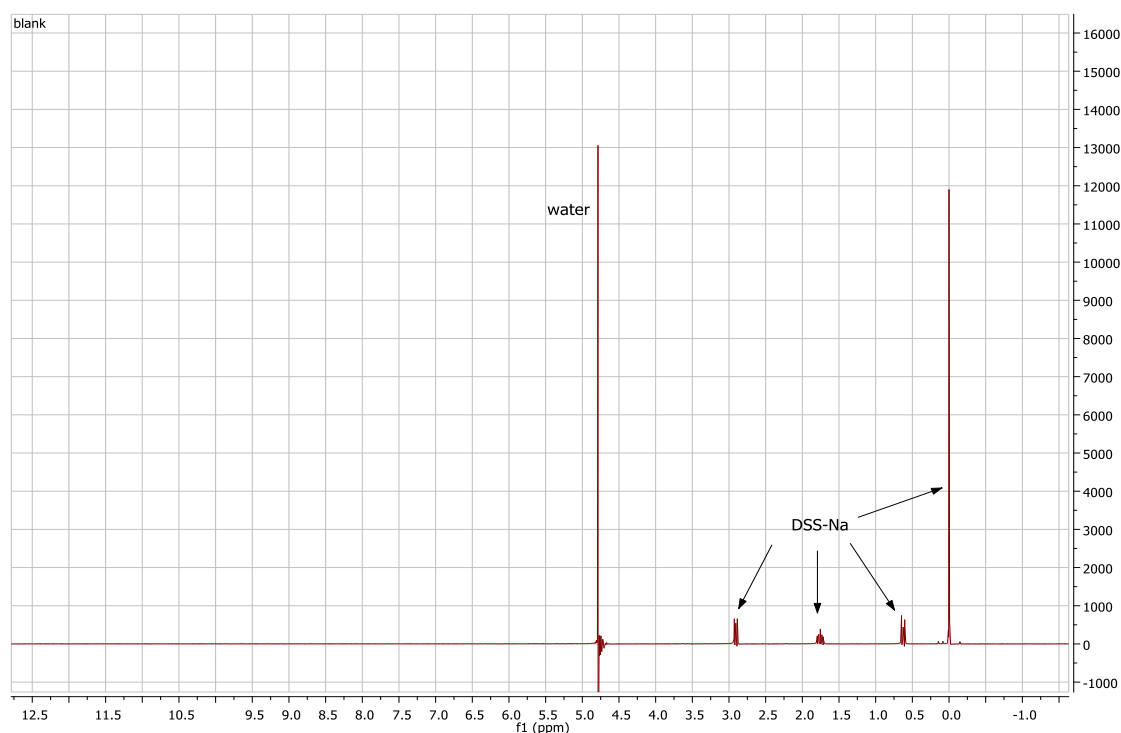


Figure S 40 ^1H NMR spectrum of sodium 3-(trimethylsilyl)-1-propanesulfonate (DSS-Na) in $\text{H}_2\text{O} : \text{D}_2\text{O}$ (6 : 1).

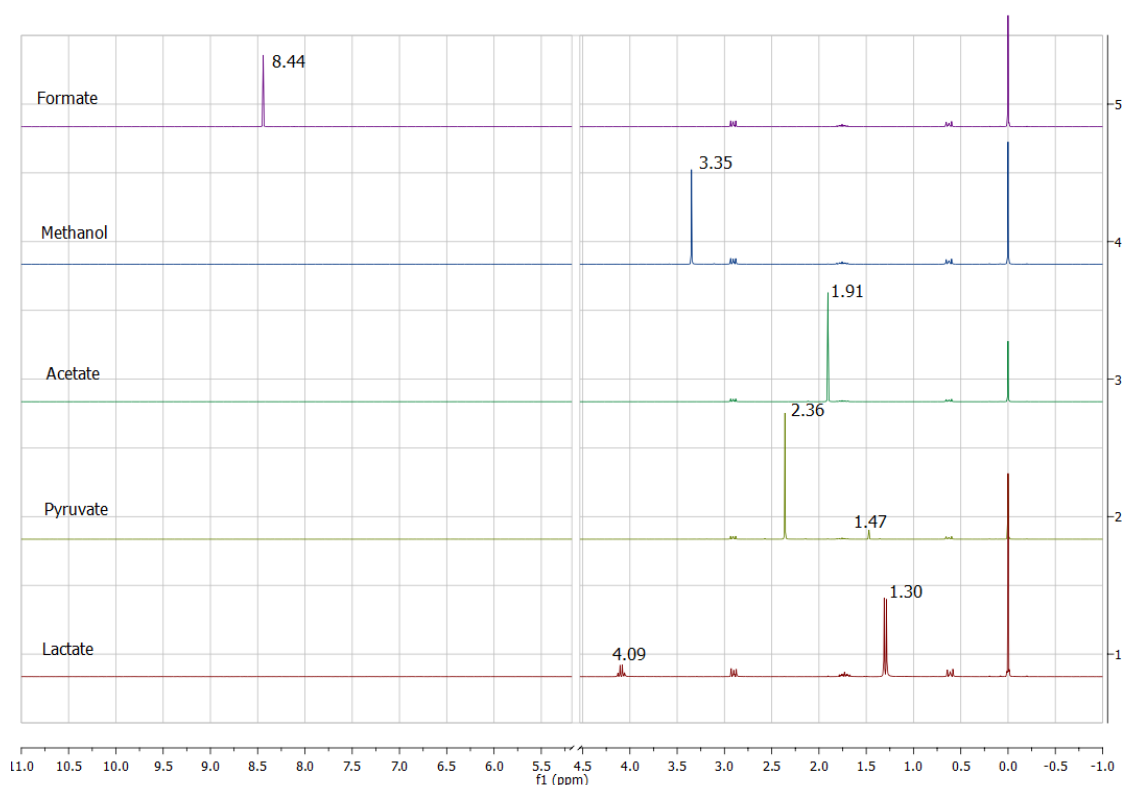


Figure S 41 ¹H NMR spectra of products detected in this study – formate, methanol, acetate, pyruvate and lactate – with DSS-Na standard in H₂O:D₂O (6:1). The residual suppressed water peak was omitted for clarity.

2.2.2 Starting material control experiments

Control experiments were carried out to test for possible trace contamination of organics in the inorganic starting materials and to exclude false positive results.

An aliquot of 1 mmol of the reagent in question (metal powders: 55 mg Mn, or 56 mg Fe, or 59 mg Ni, or 59 mg Co, or 96 mg Mo, or 184 mg W; salts: 59 mg NaCl, 75 mg KCl, 95 mg MgCl₂, 111 mg CaCl₂) was suspended in 1 mL Milli-Q H₂O, basified using ca. 300 mg sodium hydroxide, vortexed for 1 min, and then centrifuged. 0.6 mL of the supernatant was added to an NMR tube with 0.1 mL D₂O, containing 0.05 M of the internal standard (DSS-Na). This was subjected to NMR spectroscopy. A stack of the control spectra is shown below (Figure S 42).

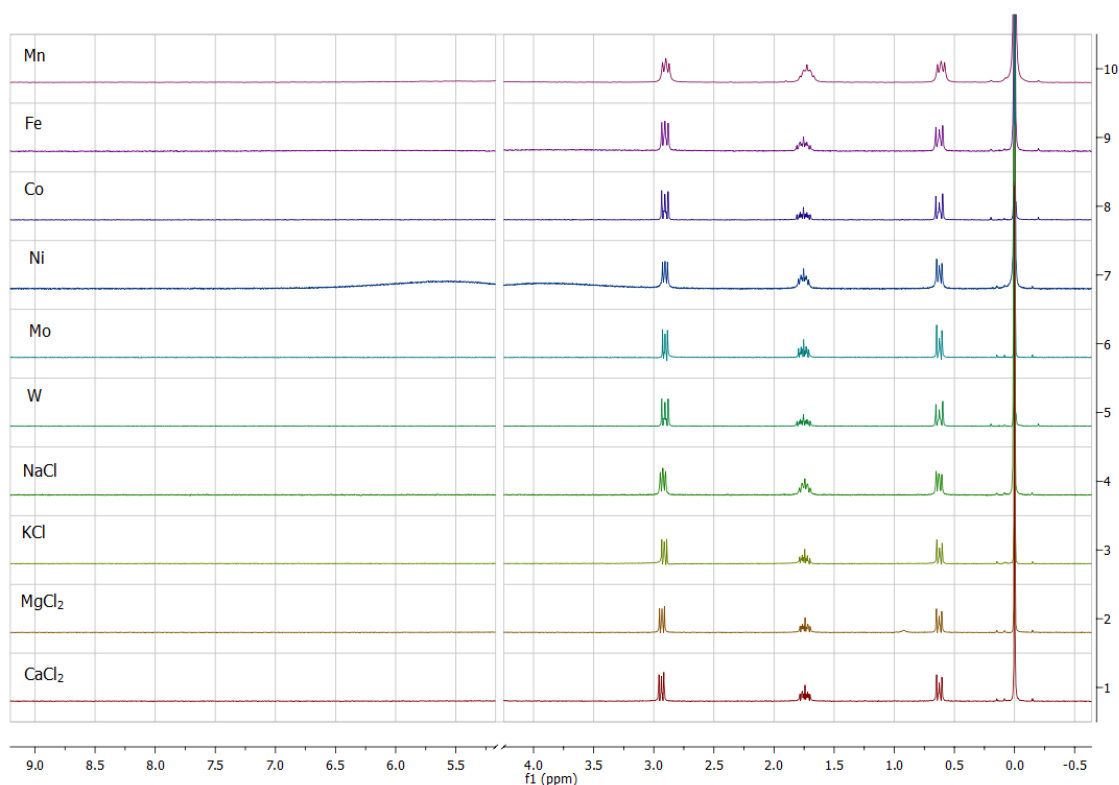


Figure S 42 ^1H NMR spectra obtained from control experiments with starting materials used in this study: metal powders: Mn, Fe, Ni, Co, Mo, W; salts: NaCl, KCl, MgCl_2 , CaCl_2 . DSS-Na was used as standard in $\text{H}_2\text{O} : \text{D}_2\text{O}$ (6 : 1). The residual suppressed water peak was deleted for clarity.

2.2.3 NMR sample preparation

To the reaction mixture was added ~ 300 mg of solid KOH ($\text{NaHS}\cdot x\text{H}_2\text{O}$ in the case of Mo-promoted reactions, due to the solubility of molybdenum oxides/hydroxides) in order to precipitate out any metal ions as their hydroxides (or sulfides in the case of Mo). This was mixed thoroughly. The resulting thick suspension was transferred to a 1.5 mL plastic microtube and centrifuged at 10 000 rpm for 20 minutes. To 600 μL of the supernatant was added 100 μL of 0.05 M solution of internal standard (DSS-Na in D_2O). The resulting solution was analysed by NMR using the Bruker ZGESGP pulse program, as described in the General Information section.

2.2.4 Confirmation of formate, acetate and pyruvate by GC-MS

The identities of formate, acetate and pyruvate detected in the reaction mixtures in this study were also confirmed by GC-MS. Formate and acetate were detected as their amides of *N*-methylphenylethylamine. To facilitate detection, pyruvate was reduced to lactate, since lactate esters have a much better response than pyruvate esters on our GC-MS system.¹ Methanol cannot be detected using either GC-MS method.

a. *Confirmation of formate and acetate in the reaction mixture by GC-MS*

To a 100 μL aliquot of a reaction mixture were added sequentially: 50 μL of 0.12 M solution of 1-hydroxybenzotriazole in H_2O , 75 μL of 0.08 M 1-ethyl-3-(3-dimethyl-aminopropyl)carbodiimide solution (EDC) in acetonitrile/ H_2O (1:1) and 75 μL of 0.06 M *N*-methylphenylethylamine (MPEA) acetonitrile. The resulting mixture was vortexed for 30 s and incubated at 60 $^\circ\text{C}$ for 45 min. Subsequently, 200 μL of CHCl_3 was added to the reaction mixture and vortexed for 30 s. The CHCl_3 layer was then removed, dried over anhydrous MgSO_4 and from this 50 μL was added to 150 μL of EtOAc and analysed by the GC-MS (Figure S 43, Figure S 44 and Figure S 45).

b. *Confirmation of pyruvate in the reaction mixture by GC-MS*

Four individual 1 mL reactions of pyruvate-containing reaction mixture ($\text{Fe}/\text{KCl}/\text{H}_2\text{O}$, 100 $^\circ\text{C}$, 16 h; see Synthetic procedures below) were combined in a centrifugation tube, basified with KOH (see Analytical methods: C. NMR sample preparation), vortexed for 1 min and centrifuged at 10 000 rpm for 20 minutes. The supernatant was transferred to another centrifugation tube, which was then immersed in liquid nitrogen for 15 min. Water was then removed by lyophilization over 12 hrs. The white residue was dissolved in 400 μL of Milli-Q water and to this excess NaBH_4 (*ca.* 20 mg) was added. The mixture was vortexed for 1 min and left to react for \sim 1 h at ambient temperature. After this time, the mixture was derivatized with ethyl chloroformate and ethanol, following the procedure we previously reported.¹ GC-MS detected the presence of ethyl esters of several lactate adducts (Figure S 46), whose retention times and mass spectra agreed with those obtained for an authentic sodium pyruvate solution in Milli-Q water, reduced and derivatized analogously (Figure S 47).

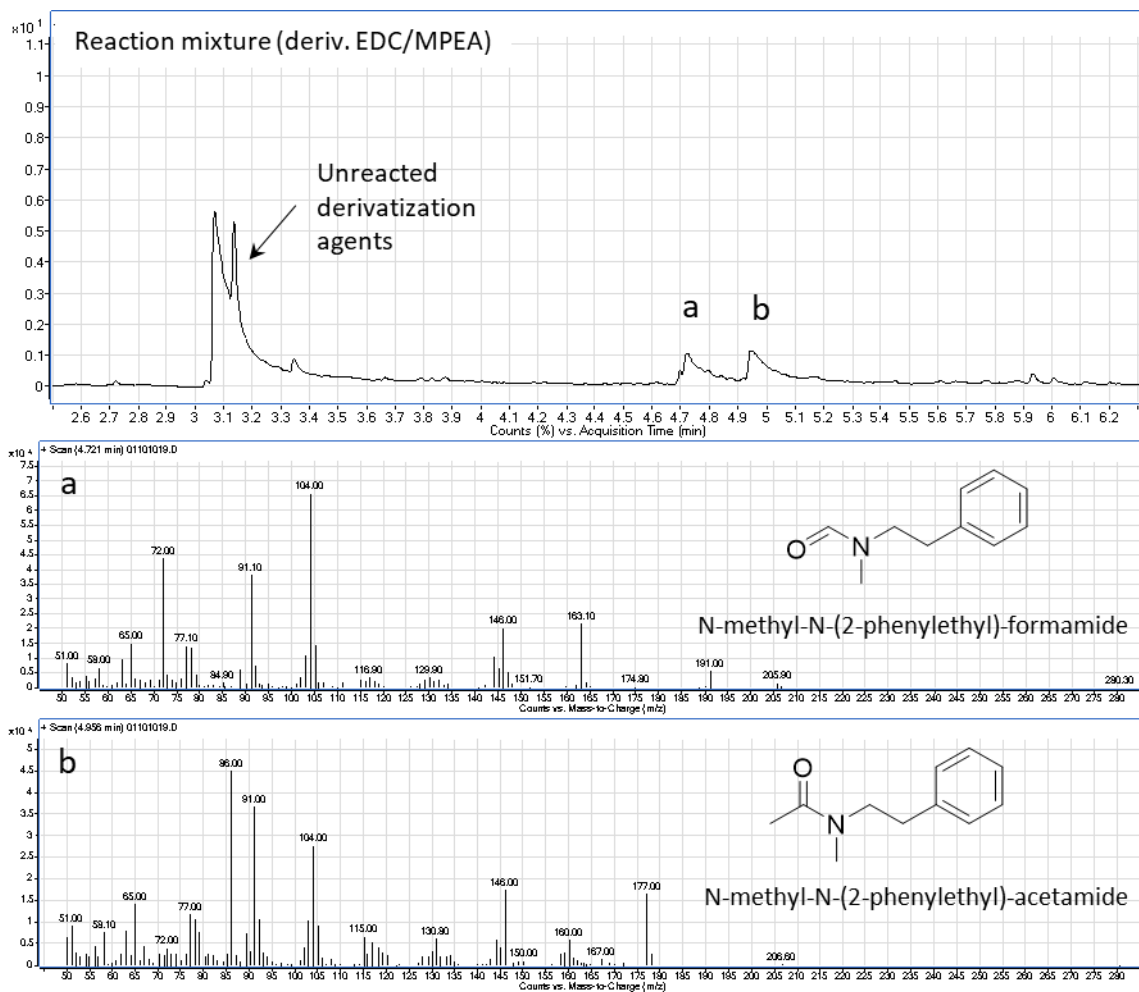


Figure S 43 GC trace and mass spectra confirming the presence of formate and acetate, detected as their respective amides, after derivatization of a typical reaction mixture with EDC/MPEA.

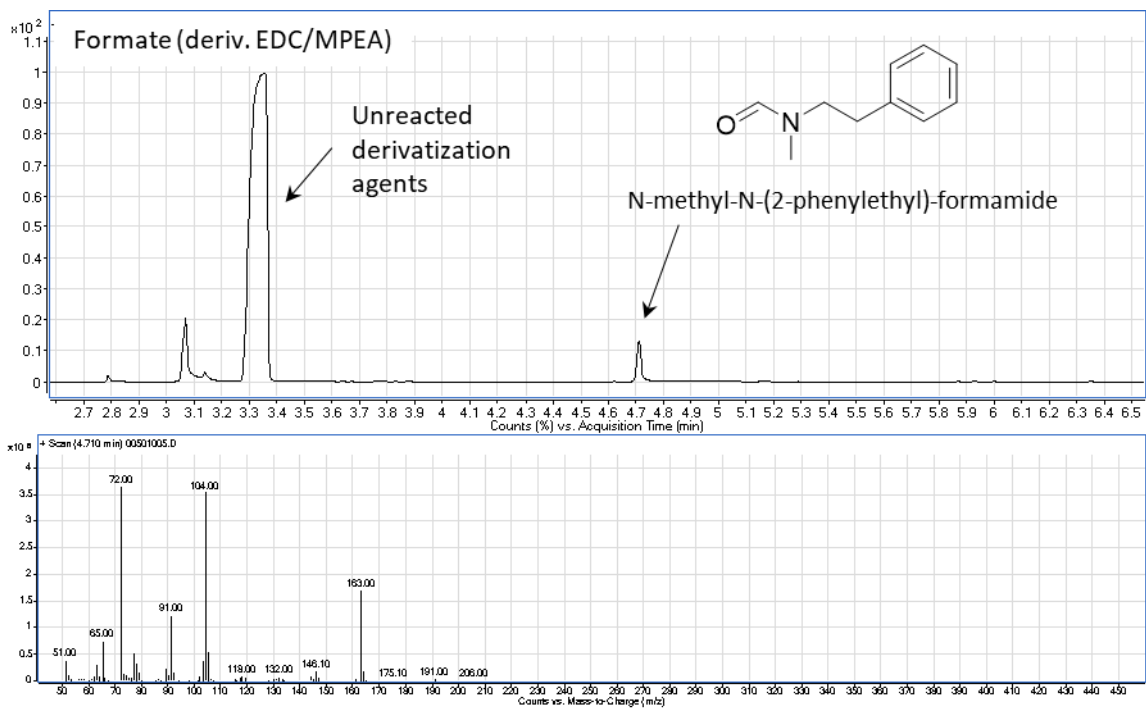


Figure S 44 GC trace and mass spectra of authentic formate derivatized with EDC/MPEA.

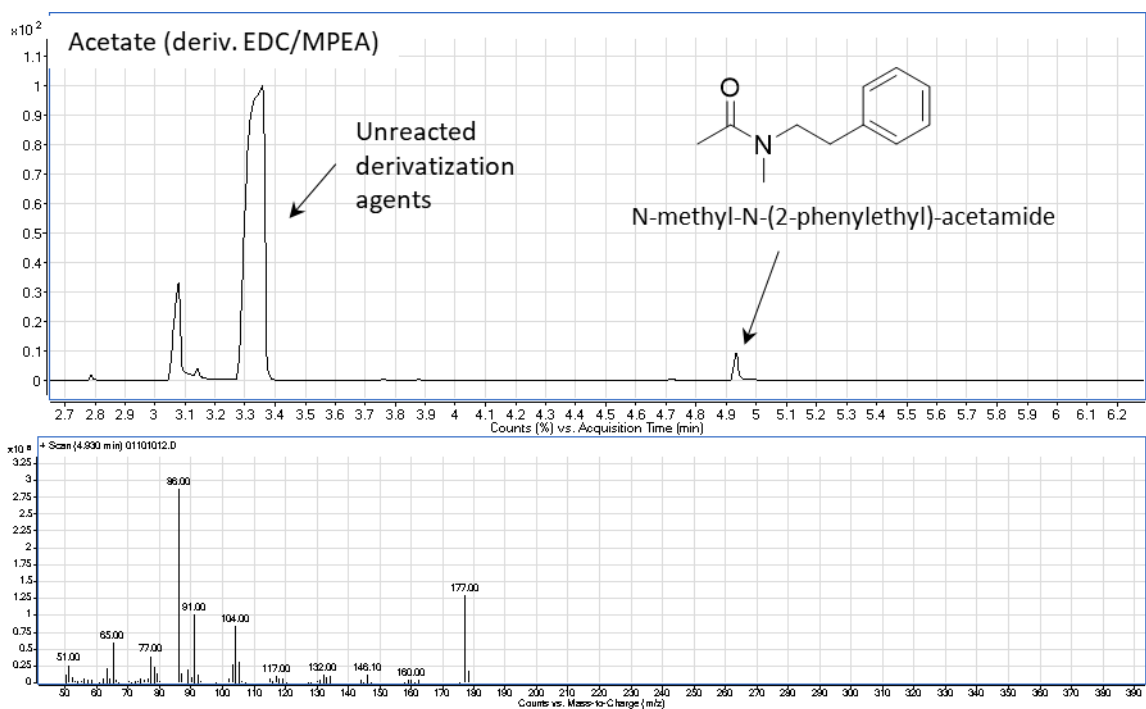
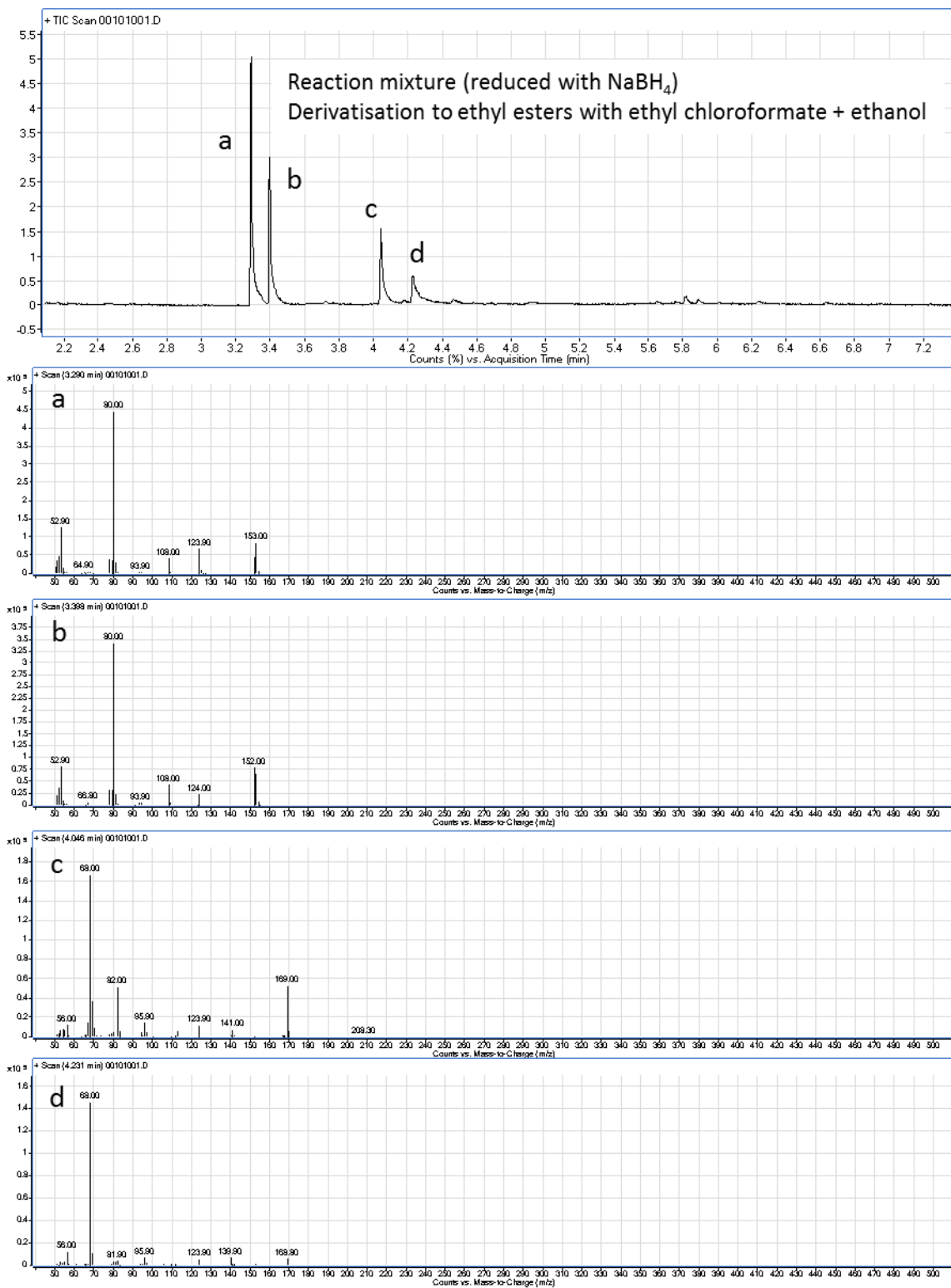


Figure S 45 GC trace and mass spectra of authentic acetate derivatized with EDC/MPEA.



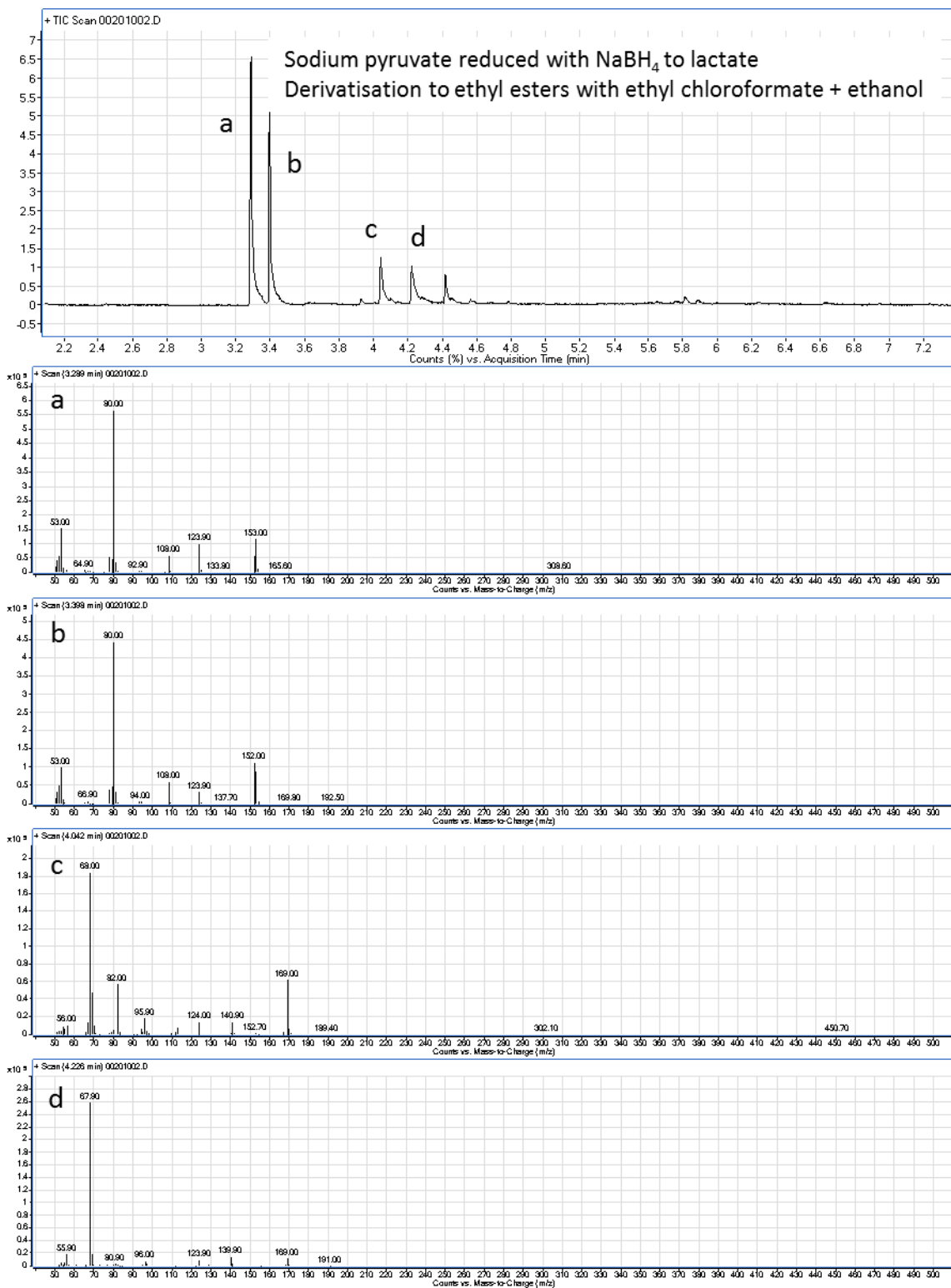


Figure S 47 GC trace and mass spectra of authentic pyruvate reduced to lactate with NaBH_4 and subsequently derivatized to lactate ethyl esters with ethyl chloroformate and ethanol.

2.3 Synthetic procedures

2.3.1 General procedure A

For metal-promoted CO₂ fixing reactions

To a 1.5 mL glass vial with a PTFE-coated stir-bar was added 1 mmol of each tested reagent (56 mg Fe, or 58 mg Co, or 58 mg Ni, or 55 mg Mn, or 96 mg Mo, or 184 mg W, and/or 58 mg NaCl, and/or 75 mg KCl, and/or 95 mg MgCl₂, and/or 111 mg CaCl₂) and 1 mL of Milli-Q water. The initial pH was adjusted to the desired value with HCl or NaOH (pH screens). To prevent cross-contamination, the vials were closed with caps with punctured PTFE septa. After placing the vials in a stainless-steel Parr pressure reactor, it was flushed with *ca.* 5 bar CO₂, pressurized to a final value of 35 bar CO₂ (unless noted otherwise), and stirred at the desired temperature (an external heating mantle was used where needed) for 16 h.

2.3.2 General procedure B

For rTCA cycle reaction sequence compatibility with metal-promoted CO₂ fixation

To a 1.5 mL glass vial with a PTFE-coated stir-bar were added carboxylic acid substrate (oxaloacetic acid (0.03 mmol, 4 mg) or triethyl oxalosuccinate⁷ (0.03 mmol, ~8 μL)), Fe⁰ powder (1.0 mmol, 56 mg), KCl (1.0 mmol, 75 mg) and Cr₂(SO₄)₃·12H₂O (1 equiv., 0.03 mmol, 18 mg). This was followed by the addition of 1 mL of 0.24 M HCl in H₂O (2 μL conc. HCl in 1 mL MilliQ H₂O), which corresponds to an initial pH = ~ 0.6. To prevent cross-contamination, the vial was closed with a cap with a punctured PTFE septum. After placing the vial in a stainless-steel Parr pressure reactor, it was flushed with *ca.* 5 bar CO₂, pressurized to a final value 35 bar CO₂, and stirred at 140 °C (an external heating mantle was used) for 16 h.

2.4 Experimental data

2.4.1 Control reactions

Two control reactions were carried out according to general procedure A, in the absence of metals:

- a) 1 mL 1 M KCl solution in H₂O at 100 °C under 35 bar CO₂ over 16 h
- b) 1 mL H₂O at 100 °C under 35 bar CO₂ over 16 h

⁷ As previously reported,^{Erreur ! Signet non défini.}¹¹⁷ due to high instability and difficult storage oxalosuccinate was obtained by in situ hydrolysis of triethyl oxalosuccinate under the reaction conditions.

Next, NMR samples were prepared using the method described in section 2.2.3. NMR sample preparation. Results showing that carbon fixation products are not produced in the absence of metals are presented in the ^1H NMR spectra stack below (Figure S 48).

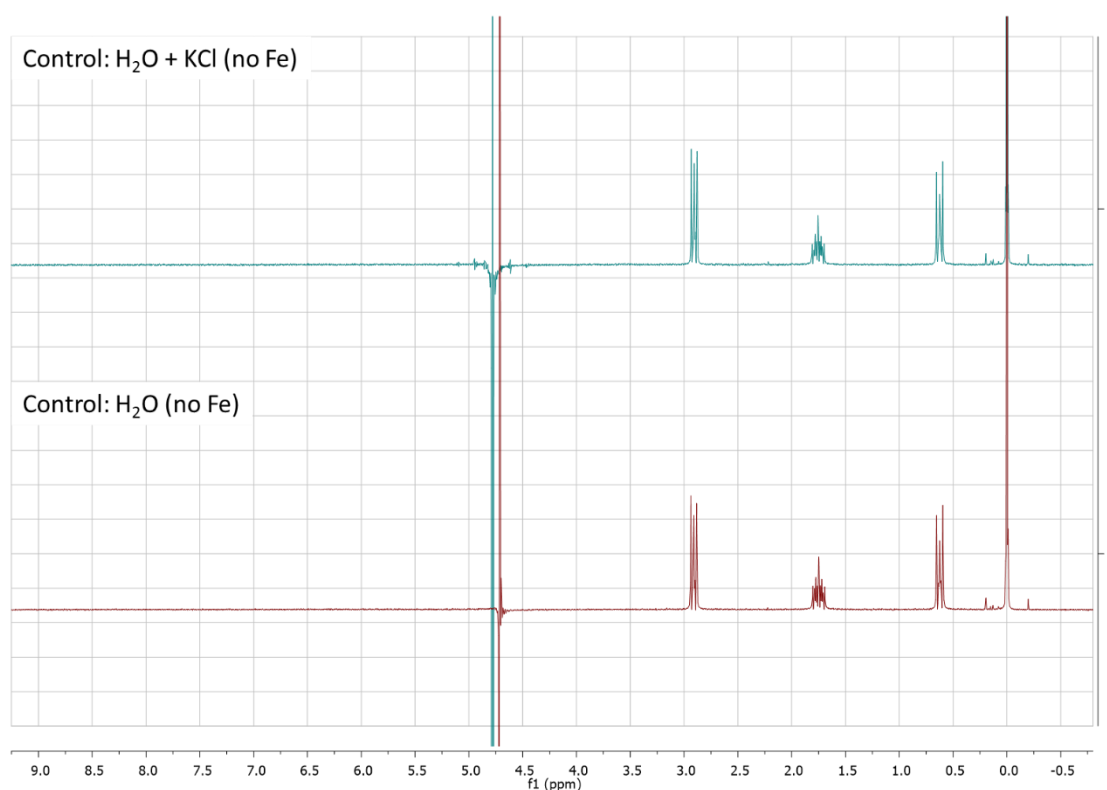


Figure S 48 ^1H NMR spectra showing the result of control reactions in the absence of metals (6 : 1 H_2O : D_2O with DSS-Na as standard).

Another control reaction was carried out according to general procedure A, in the absence of CO_2 : 1 mL 1 M KCl solution in H_2O at 100 °C under 1 bar or argon, over 16 h.

Next, an NMR sample was prepared using the method described in section 2.2.3. NMR sample preparation. Results proving no carbon fixation products in the absence of CO_2 are presented in the ^1H NMR spectrum below (Figure S 49).

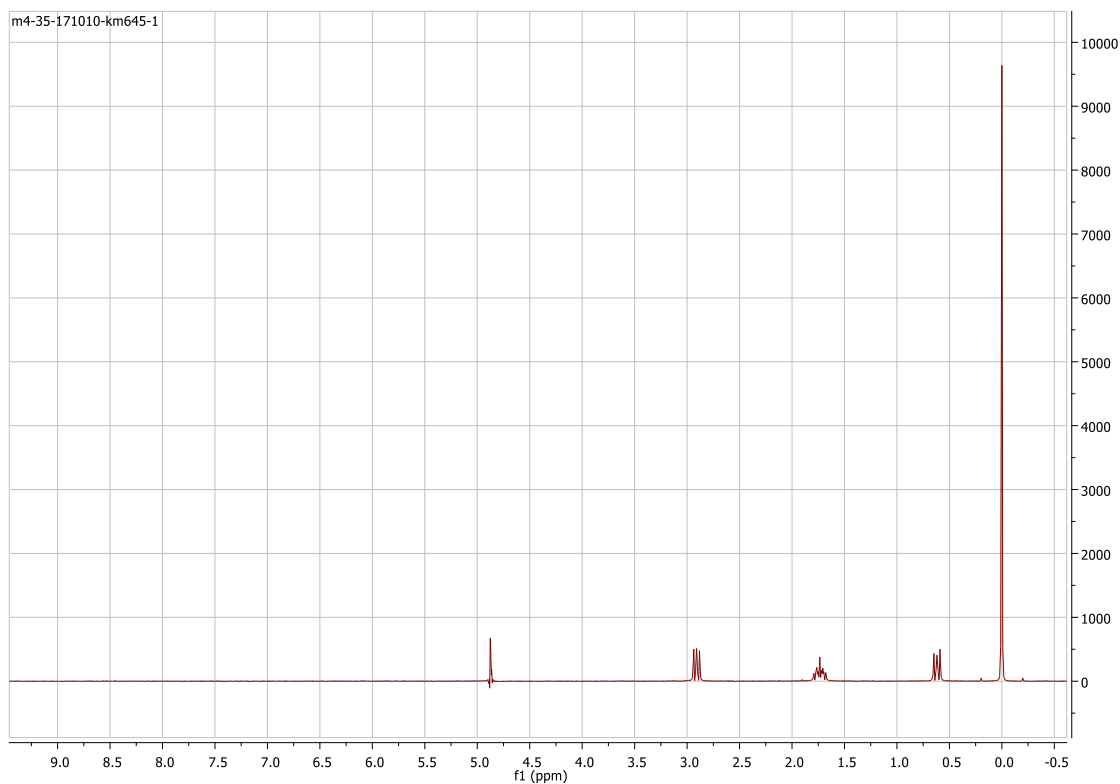


Figure S 49 ¹H NMR spectra showing the result of control reactions in the absence of CO₂ (6 : 1 H₂O : D₂O with DSS-Na as standard).

2.4.2 Reaction parameter screens.

Reaction parameters such as temperature, CO₂ pressure and reaction time were probed to study their effect on metal-promoted CO₂ fixation reaction yields.

2.4.2.1 Temperature screen

Reactions were carried out according to general procedure A with 1 mmol (56 mg) of Fe powder and 1 mmol (75 mg) of KCl in 1 mL H₂O at various temperature values (30 °C, 50 °C, 100 °C and 140 °C), under 35 bar CO₂ over 16 h.

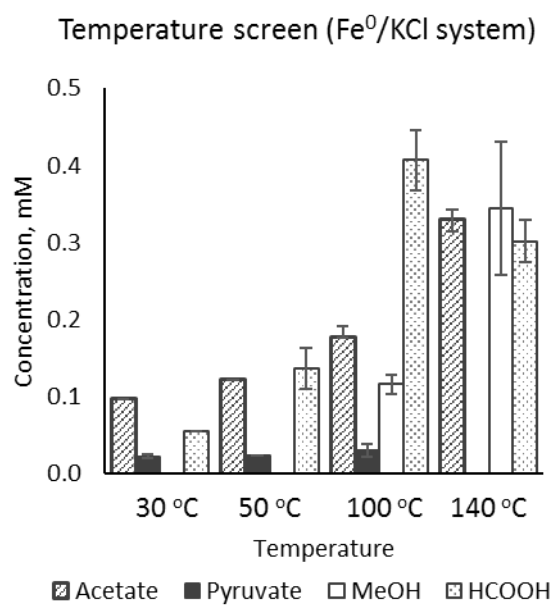


Figure S 50 Temperature screen for the Fe⁰/KCl system under 35 bar CO₂

Table S 8 Temperature screen for the Fe⁰/KCl system under 35 bar CO₂

Temperature, °C		30	50	100	140
Products, mM	Acetate	0.10 ± 0.00	0.12 ± 0.00	0.18 ± 0.01	0.33 ± 0.01
	Pyruvate	0.02 ± 0.00	0.02 ± 0.00	0.03 ± 0.01	0.00 ± 0.00
	Methanol	0.00 ± 0.00	0.00 ± 0.00	0.12 ± 0.01	0.34 ± 0.09
	Formate	0.06 ± 0.00	0.14 ± 0.03	0.41 ± 0.04	0.30 ± 0.03

2.4.2.2 Pressure screen

Reactions were carried out according to general procedure A with 1 mmol (56 mg) of Fe powder and 1 mmol (75 mg) of KCl in 1 mL H₂O under final reaction pressures 1, 10, 20, 30 and 40 bar at 30 °C, over 16 h.

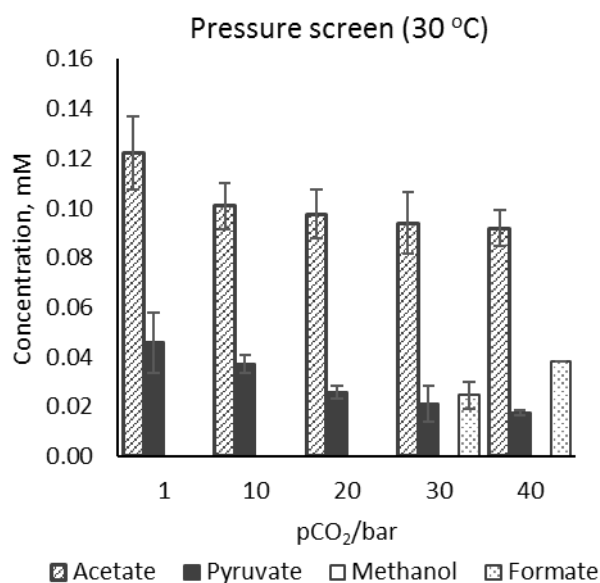


Figure S 51 Pressure screen for the Fe⁰/KCl system at 30 °C

Table S 9 Pressure screen for Fe/KCl system at 30 °C

Pressure, bar		1	1 ⁸	10	20	30	40
Products, mM	Acetate	0.12 ± 0.01	0.07 ± 0.00	0.10 ± 0.01	0.10 ± 0.01	0.09 ± 0.01	0.09 ± 0.01
	Pyruvate	0.05 ± 0.01	0.00 ± 0.00	0.04 ± 0.00	0.03 ± 0.00	0.02 ± 0.01	0.02 ± 0.00
	Methanol	0.00 ± 0.00	0.00 ± 0.00	0.00 ± 0.00	0.00 ± 0.00	0.00 ± 0.00	0.00 ± 0.00
	Formate	0.00 ± 0.00	0.00 ± 0.00	0.00 ± 0.00	0.00 ± 0.00	0.02 ± 0.00	0.04 ± 0.00

⁸ Reaction in pure H₂O without KCl added

2.4.2.3 The effect of time on the yield of CO₂ fixation products.

Reactions were carried out according to general procedure A with 1 mmol (56 mg) of Fe powder and 1 mmol (75 mg) of KCl in 1 mL H₂O at 100 °C under 35 bar CO₂ over 1.5 h, 3 h, 6 h, 16 h, 60 h and 85 h.

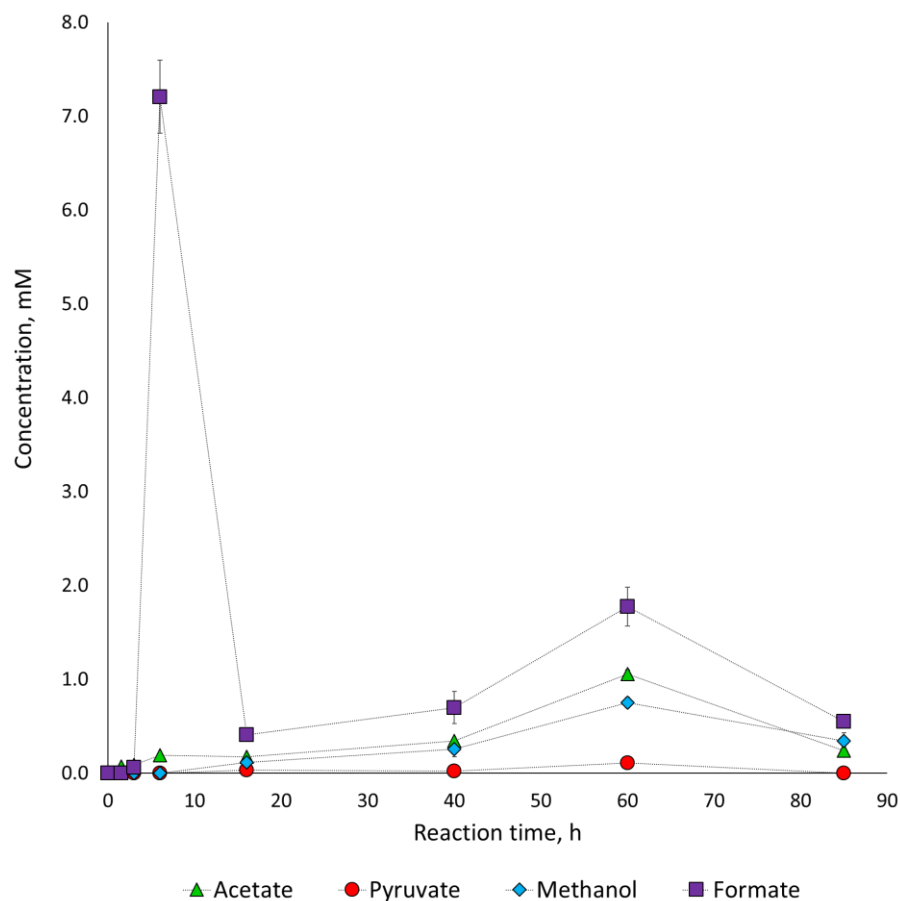


Figure S 52 Reaction time screen for the Fe⁰/KCl system at 100 °C under 35 bar CO₂

Table S 10 Reaction time screen for the Fe⁰/KCl system at 100 °C under 35 bar CO₂

Reaction time, h		1.5	3	6	16	60	85
Products, mM	Acetate	0.07 ± 0.00	0.08 ± 0.01	0.19 ± 0.002	0.18 ± 0.01	1.06 ± 0.04	0.24 ± 0.02
	Pyruvate	0.00 ± 0.00	0.00 ± 0.00	0.00 ± 0.00	0.03 ± 0.01	0.11 ± 0.01	0.00 ± 0.00
	Methanol	0.00 ± 0.00	0.00 ± 0.00	0.00 ± 0.00	0.12 ± 0.01	0.75 ± 0.05	0.34 ± 0.09
	Formate	0.00 ± 0.00	0.06 ± 0.01	7.21 ± 0.39	0.41 ± 0.04	1.77 ± 0.21	0.55 ± 0.04

2.4.3 Distribution of electrons among detected CO₂ fixation products

In order to estimate the contribution of electrons available from iron (1 mmol in 1 mL H₂O) towards the formation of CO₂ fixation products (formate - 2e⁻ product, eq. I; methanol - 6e⁻ product, eq. II; acetate - 8e⁻ product, eq. III; pyruvate - 10e⁻ product, eq. IV), the yields of each species (concentration in mM) detected after 16 h reaction time were multiplied by the number of electrons the product required to form from CO₂. These numbers were divided by 2000, with the assumption that each Fe⁰ atom would furnish a maximum of 2 electrons upon oxidation to Fe²⁺ (therefore the maximum available electron “concentration” would equal 2000 mM in each reaction mixture). The distribution of these electrons between carbon fixation products, expressed as percentage of all Fe⁰-sourced electrons available for reaction, is shown below (Erreur ! Source du renvoi introuvable.).



Table S 11 Percentage contribution of electrons available from iron towards detected CO₂ fixation products.

Entry	Conditions				Formate (2e ⁻ product), %	Methanol (6e ⁻ product), %	Acetate (8e ⁻ product), %	Pyruvate (10e ⁻ product), %
	Fe (1 mmol)	KCl (1 mmol)	Temperature, °C	Pressure, bar				
1	yes	yes	30	1 (CO ₂)	-	-	0.048 ± 0.006	0.023 ± 0.006
2	yes	yes	30	35 (CO ₂)	0.006 ± 0.000	-	0.039 ± 0.000	0.012 ± 0.002
3	yes	no	30	35 (CO ₂)	0.012 ± 0.000	-	0.075 ± 0.014	-
4	yes	no	30	1 (CO ₂)	-	-	0.029 ± 0.000	-
5	yes	no	100	35 (CO ₂)	0.014 ± 0.003	0.026 ± 0.000	0.054 ± 0.005	0.012 ± 0.000
6	yes	yes	100	35 (CO ₂)	0.041 ± 0.005	0.035 ± 0.005	0.071 ± 0.006	0.015 ± 0.005
7 ^a	yes	yes	100	35 (CO ₂)	0.177 ± 0.021	0.225 ± 0.016	0.422 ± 0.017	0.053 ± 0.007
8	yes	yes	100	1 (Ar)	-	-	-	-
9	no	yes	100	35 (CO ₂)	-	-	-	-

^a Reaction time 60 h.

2.4.4 Detection of ethanol in the reaction mixture after 85 h

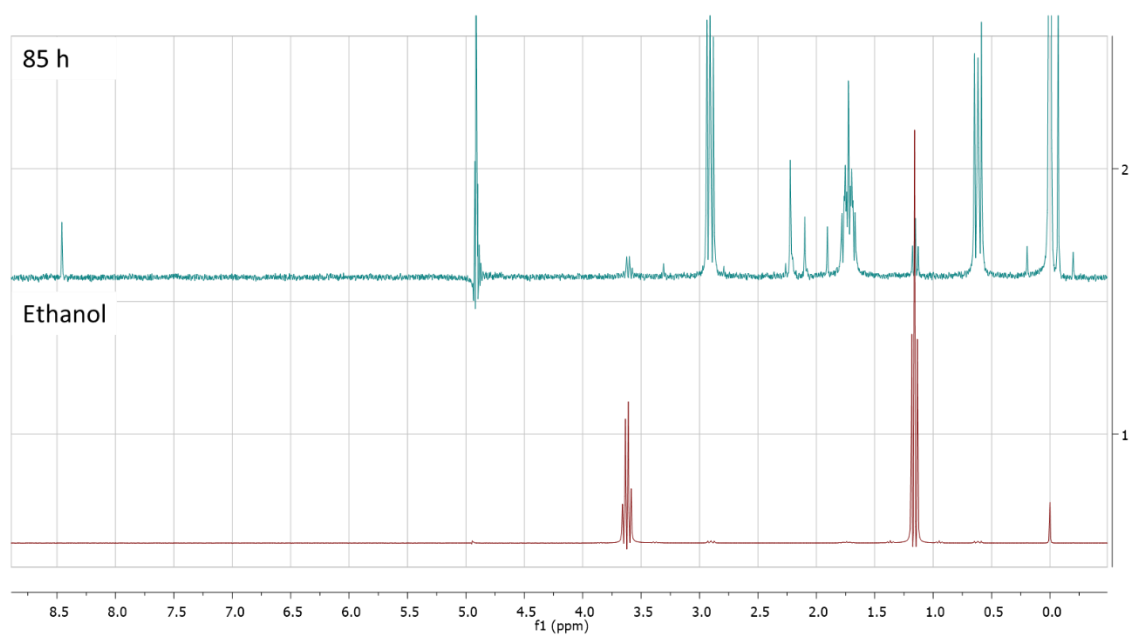


Figure S 53 ¹H NMR spectrum of the crude reaction mixture, stacked with a spectrum of an authentic sample of ethanol (6 : 1 H₂O : D₂O with DSS-Na as standard), confirming the presence of ethanol after 85 hrs reaction time. Conditions: Fe, KCl, 35 bar CO₂, 100 °C.

2.4.5 Metal screens in CO₂ fixation reactions

2.4.5.1 Manganese

a. pH screen at 100 °C and 30 °C

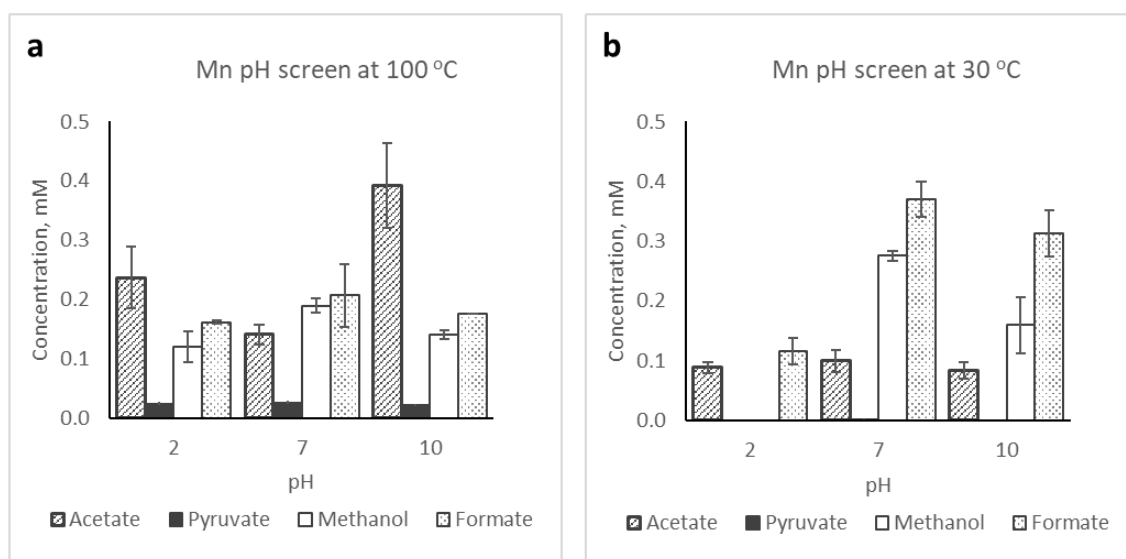


Figure S 54 pH screen for manganese at (a) 100 °C and (b) 30 °C

Table S 12 pH screen for manganese at 100 °C and 30 °C

Temperature		100 °C			30 °C		
pH		2	7	10	2	7	10
Products, mM	Acetate	0.24 ± 0.05	0.14 ± 0.02	0.39 ± 0.07	0.09 ± 0.01	0.10 ± 0.02	0.08 ± 0.01
	Pyruvate	0.02 ± 0.00	0.03 ± 0.00	0.02 ± 0.00	0.00 ± 0.00	0.01 ± 0.00	0.00 ± 0.00
	Methanol	0.12 ± 0.03	0.19 ± 0.01	0.14 ± 0.01	0.00 ± 0.00	0.28 ± 0.01	0.16 ± 0.05
	Formate	0.16 ± 0.00	0.21 ± 0.05	0.18 ± 0.00	0.12 ± 0.02	0.37 ± 0.03	0.31 ± 0.04

b. Salt screen at 100 °C and 30 °C

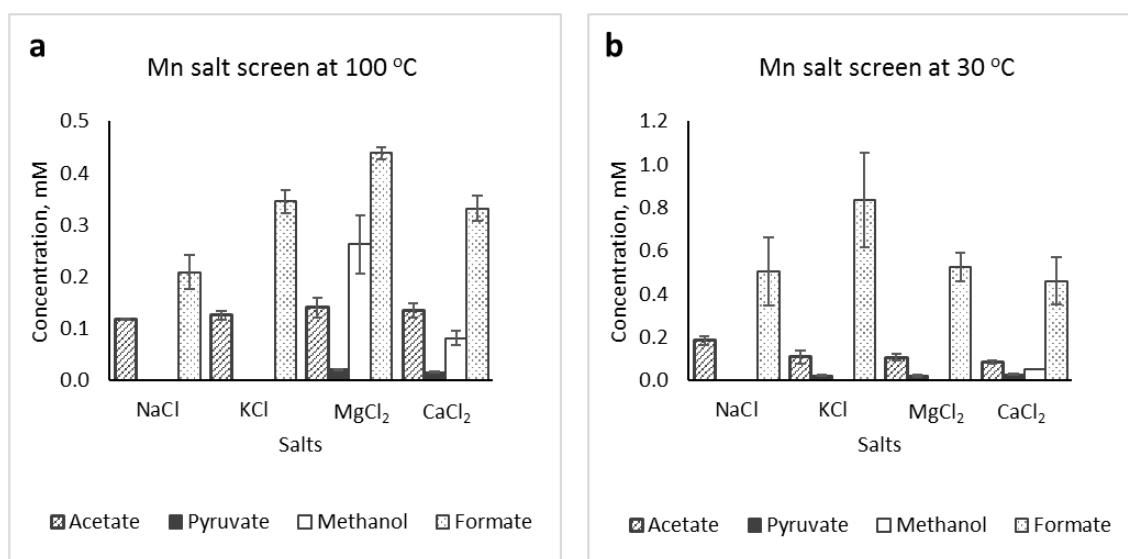


Figure S 55 Salt screen for manganese at (a) 100 °C and (b) 30 °C

Table S 13 Salt screen for manganese at 100 °C and 30 °C

Temperature		100 °C				30 °C			
Salts		NaCl	KCl	MgCl ₂	CaCl ₂	NaCl	KCl	MgCl ₂	CaCl ₂
Products, mM	Acetate	0.12 ± 0.00	0.12 ± 0.01	0.14 ± 0.02	0.14 ± 0.01	0.18 ± 0.02	0.11 ± 0.03	0.11 ± 0.01	0.09 ± 0.01
	Pyruvate	0.00 ± 0.00	0.00 ± 0.00	0.02 ± 0.00	0.02 ± 0.00	0.00 ± 0.00	0.02 ± 0.00	0.02 ± 0.00	0.03 ± 0.00
	Methanol	0.00 ± 0.00	0.00 ± 0.00	0.26 ± 0.06	0.08 ± 0.01	0.00 ± 0.00	0.00 ± 0.00	0.00 ± 0.00	0.05 ± 0.00
	Formate	0.21 ± 0.03	0.34 ± 0.02	0.44 ± 0.01	0.33 ± 0.02	0.50 ± 0.16	0.84 ± 0.22	0.53 ± 0.07	0.46 ± 0.11

2.4.5.2 Iron

a. pH screen at 100 °C and 30 °C

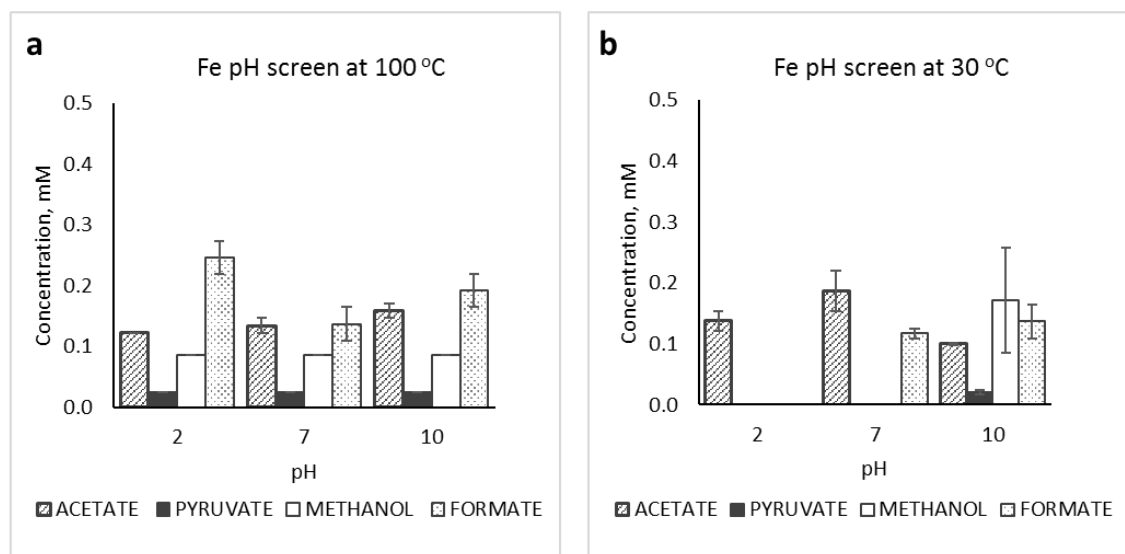


Figure S 56 pH screen for iron at (a) 100 °C and (b) 30 °C

Table S 14 pH screen for iron at 100 °C and 30 °C

Temperature		100 °C			30 °C		
pH		2	7	10	2	7	10
Products, mM	Acetate	0.12 ± 0.00	0.13 ± 0.01	0.16 ± 0.01	0.14 ± 0.02	0.19 ± 0.03	0.10 ± 0.00
	Pyruvate	0.02 ± 0.00	0.02 ± 0.00	0.02 ± 0.00	0.00 ± 0.00	0.00 ± 0.00	0.02 ± 0.00
	Methanol	0.09 ± 0.00	0.09 ± 0.00	0.09 ± 0.000	0.00 ± 0.00	0.00 ± 0.00	0.17 ± 0.09
	Formate	0.25 ± 0.03	0.14 ± 0.03	0.19 ± 0.03	0.00 ± 0.00	0.12 ± 0.01	0.14 ± 0.03

b. Salt screen at 100 °C and 30 °C

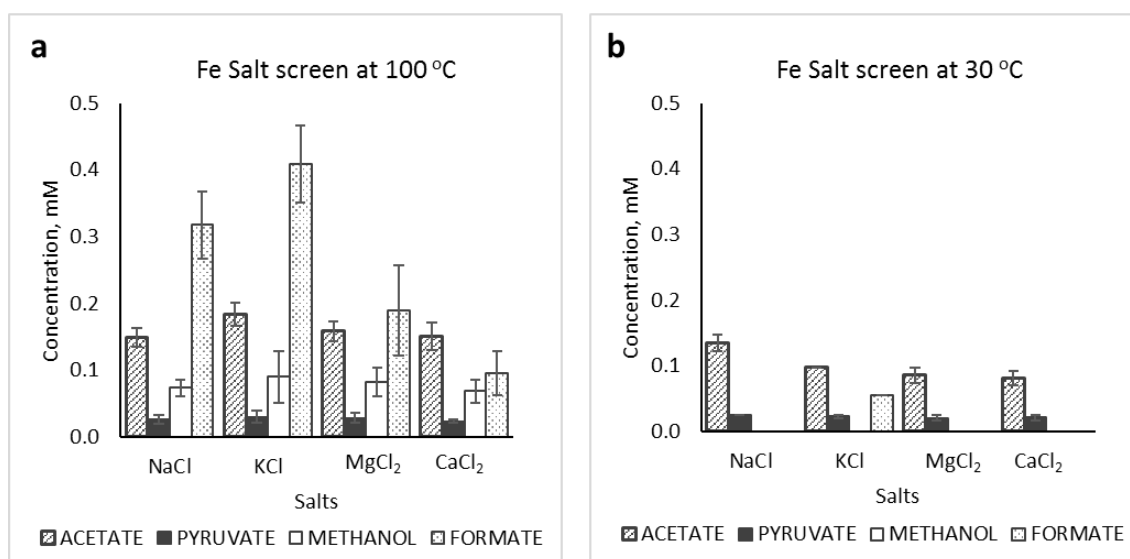


Figure S 57 Salt screen for iron at (a) 100 °C and (b) 30 °C

Table S 15 Salt screen for iron at 100 °C and 30 °C

Temperature		100 °C				30 °C			
Salts		NaCl	KCl	MgCl ₂	CaCl ₂	NaCl	KCl	MgCl ₂	CaCl ₂
Products, mM	Acetate	0.15 ± 0.02	0.18 ± 0.01	0.16 ± 0.01	0.15 ± 0.02	0.13 ± 0.01	0.10 ± 0.00	0.08 ± 0.01	0.08 ± 0.01
	Pyruvate	0.03 ± 0.01	0.03 ± 0.01	0.03 ± 0.01	0.02 ± 0.00	0.02 ± 0.00	0.02 ± 0.00	0.02 ± 0.00	0.02 ± 0.00
	Methanol	0.07 ± 0.01	0.12 ± 0.01	0.08 ± 0.02	0.07 ± 0.02	0.00 ± 0.00	0.00 ± 0.00	0.00 ± 0.00	0.00 ± 0.00
	Formate	0.32 ± 0.05	0.41 ± 0.04	0.16 ± 0.03	0.10 ± 0.03	0.00 ± 0.00	0.06 ± 0.00	0.00 ± 0.00	0.00 ± 0.00

2.4.5.3 Cobalt

a. pH screen at 100 °C and 30 °C

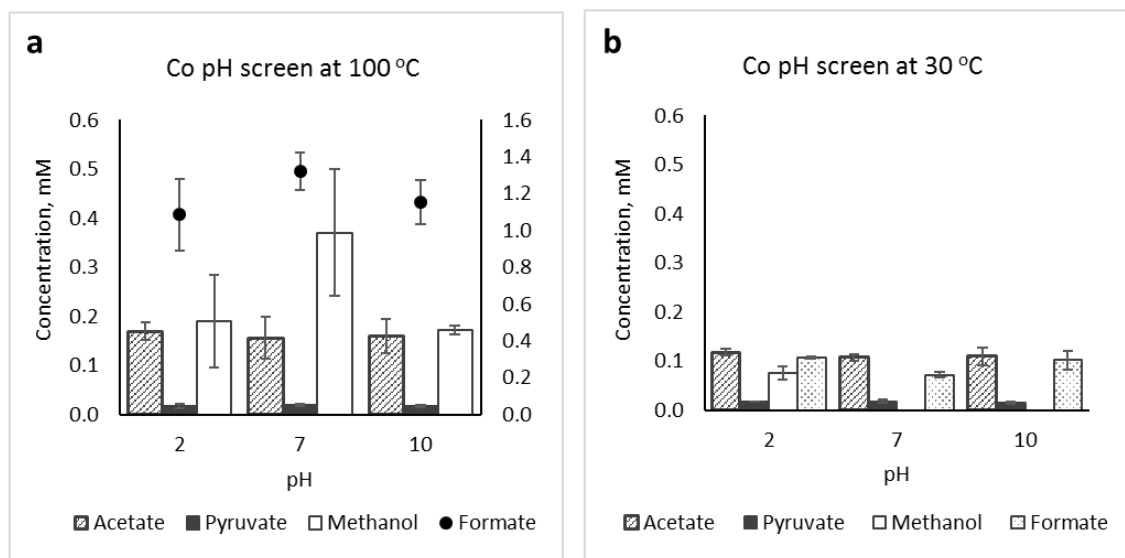


Figure S 58 pH screen for cobalt at (a) 100 °C and (b) 30 °C

Table S 16 pH screen for cobalt at 100 °C and 30 °C

Temperature		100 °C			30 °C		
pH		2	7	10	2	7	10
Products, mM	Acetate	0.17 ± 0.02	0.16 ± 0.04	0.16 ± 0.04	0.12 ± 0.01	0.12 ± 0.01	0.11 ± 0.02
	Pyruvate	0.02 ± 0.00	0.02 ± 0.00	0.02 ± 0.00	0.02 ± 0.00	0.02 ± 0.00	0.02 ± 0.00
	Methanol	0.19 ± 0.10	0.37 ± 0.13	0.17 ± 0.01	0.08 ± 0.01	0.00 ± 0.00	0.00 ± 0.00
	Formate	1.09 ± 0.19	1.32 ± 0.10	1.16 ± 0.12	0.11 ± 0.00	0.07 ± 0.00	0.10 ± 0.02

b. Salt screen at 100 °C and 30 °C

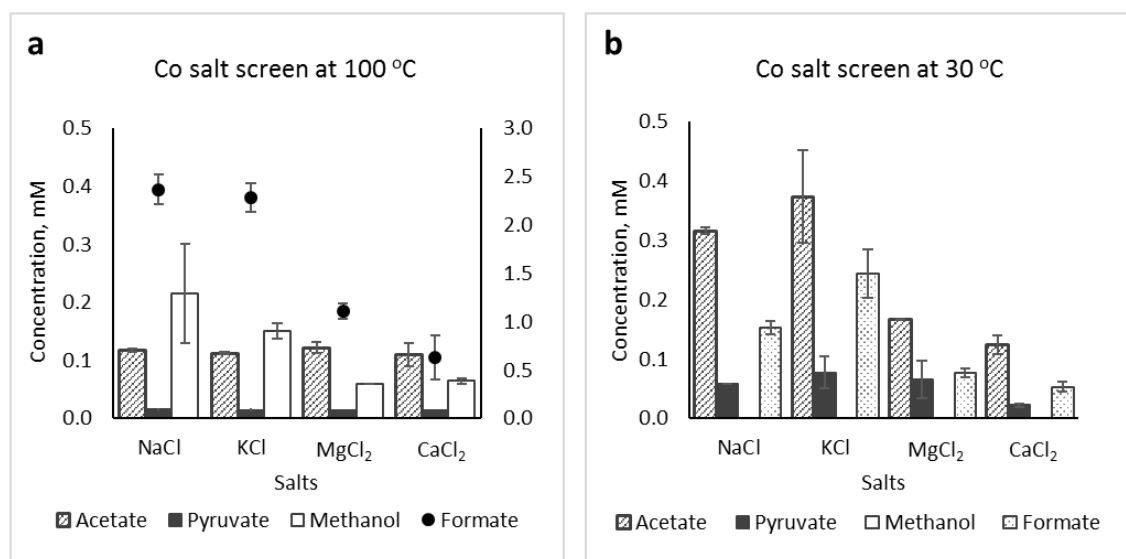


Figure S 59 Salt screen for cobalt at (a) 100 °C and (b) 30 °C

Table S 17 Salt screen for cobalt at 100 °C and 30 °C

Temperature		100 °C				30 °C			
Salts		NaCl	KCl	MgCl ₂	CaCl ₂	NaCl	KCl	MgCl ₂	CaCl ₂
Products, mM	Acetate	0.12 ± 0.00	0.11 ± 0.00	0.12 ± 0.01	0.11 ± 0.02	0.32 ± 0.01	0.37 ± 0.08	0.17 ± 0.00	0.12 ± 0.02
	Pyruvate	0.02 ± 0.00	0.01 ± 0.00	0.01 ± 0.00	0.01 ± 0.00	0.06 ± 0.00	0.08 ± 0.03	0.07 ± 0.03	0.02 ± 0.00
	Methanol	0.22 ± 0.09	0.15 ± 0.01	0.06 ± 0.00	0.06 ± 0.00	0.00 ± 0.00	0.00 ± 0.00	0.00 ± 0.00	0.00 ± 0.00
	Formate	2.37 ± 0.16	2.28 ± 0.15	1.11 ± 0.08	0.63 ± 0.23	0.15 ± 0.01	0.24 ± 0.04	0.08 ± 0.01	0.05 ± 0.01

2.4.5.4 Nickel

a. pH screen at 100 °C and 30 °C

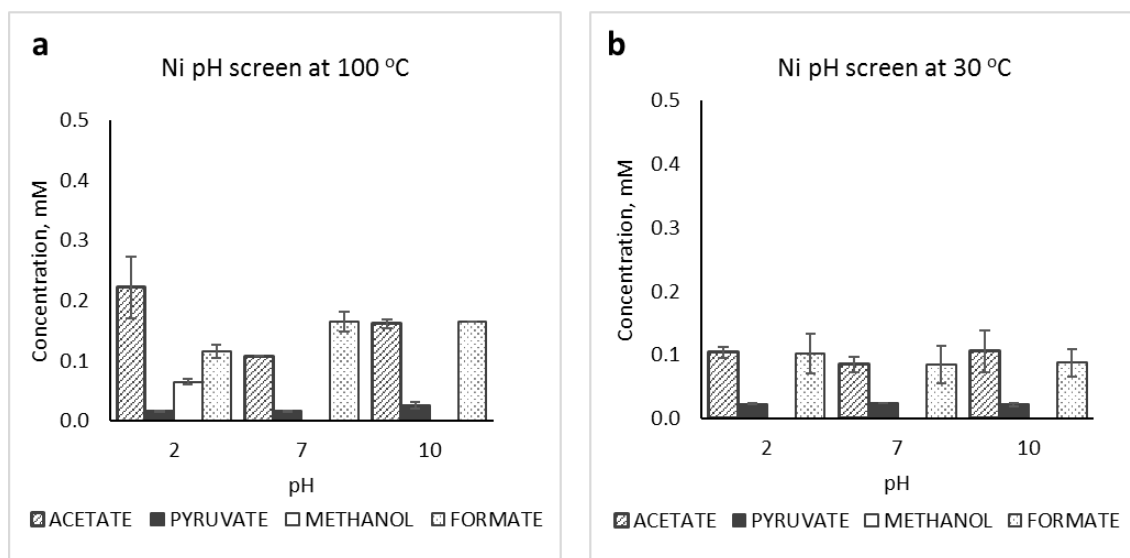


Figure S 60 pH screen for nickel at (a) 100 °C and (b) 30 °C

Table S 18 pH screen for nickel at 100 °C and 30 °C

Temperature		100 °C			30 °C		
pH		2	7	10	2	7	10
Products, mM	Acetate	0.22 ± 0.05	0.11 ± 0.00	0.16 ± 0.01	0.10 ± 0.01	0.09 ± 0.01	0.11 ± 0.03
	Pyruvate	0.02 ± 0.00	0.02 ± 0.00	0.02 ± 0.01	0.02 ± 0.00	0.02 ± 0.00	0.02 ± 0.00
	Methanol	0.06 ± 0.00	0.00 ± 0.00	0.00 ± 0.00	0.00 ± 0.00	0.00 ± 0.00	0.00 ± 0.00
	Formate	0.12 ± 0.01	0.16 ± 0.02	0.16 ± 0.00	0.10 ± 0.03	0.08 ± 0.03	0.09 ± 0.02

b. Salt screen at 100 °C and 30 °C

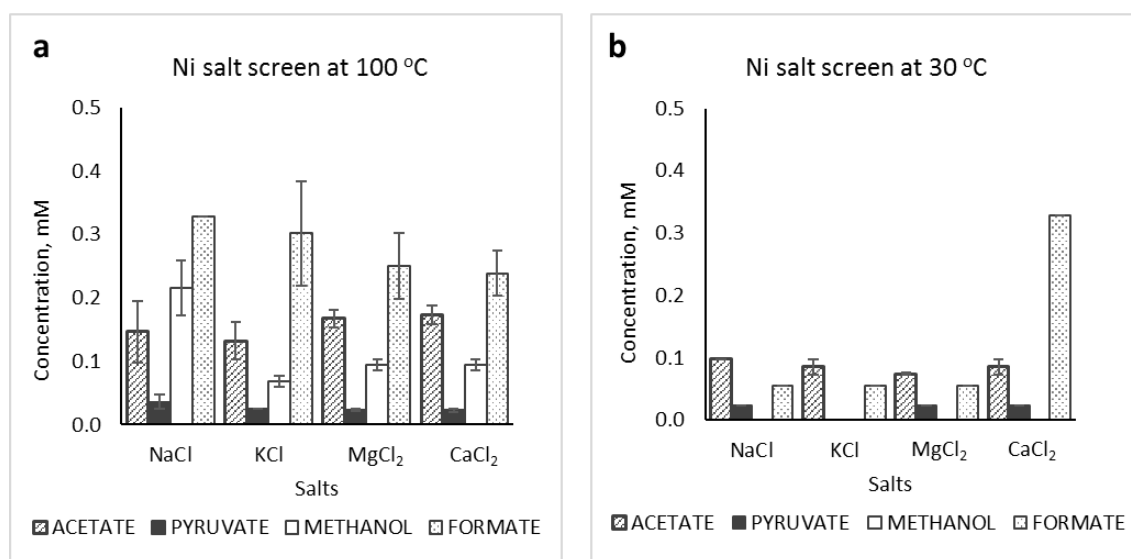


Figure S 61 Salt screen for nickel at (a) 100 °C and (b) 30 °C

Table S 19 Salt screen for nickel at 100 °C and 30 °C

Temperature		100 °C				30 °C			
Salts		NaCl	KCl	MgCl ₂	CaCl ₂	NaCl	KCl	MgCl ₂	CaCl ₂
Products, mM	Acetate	0.15 ± 0.05	0.13 ± 0.03	0.17 ± 0.01	0.17 ± 0.02	0.10 ± 0.00	0.08 ± 0.01	0.07 ± 0.00	0.08 ± 0.01
	Pyruvate	0.04 ± 0.01	0.02 ± 0.00	0.02 ± 0.00	0.02 ± 0.00	0.02 ± 0.00	0.00 ± 0.00	0.02 ± 0.00	0.02 ± 0.00
	Methanol	0.22 ± 0.64	0.07 ± 0.01	0.10 ± 0.01	0.10 ± 0.01	0.00 ± 0.00	0.00 ± 0.00	0.00 ± 0.00	0.00 ± 0.00
	Formate	0.33 ± 0.04	0.30 ± 0.08	0.25 ± 0.05	0.24 ± 0.04	0.06 ± 0.00	0.06 ± 0.00	0.06 ± 0.00	0.33 ± 0.00

2.4.5.5 Molybdenum

a. pH screen at 100 °C and 30 °C

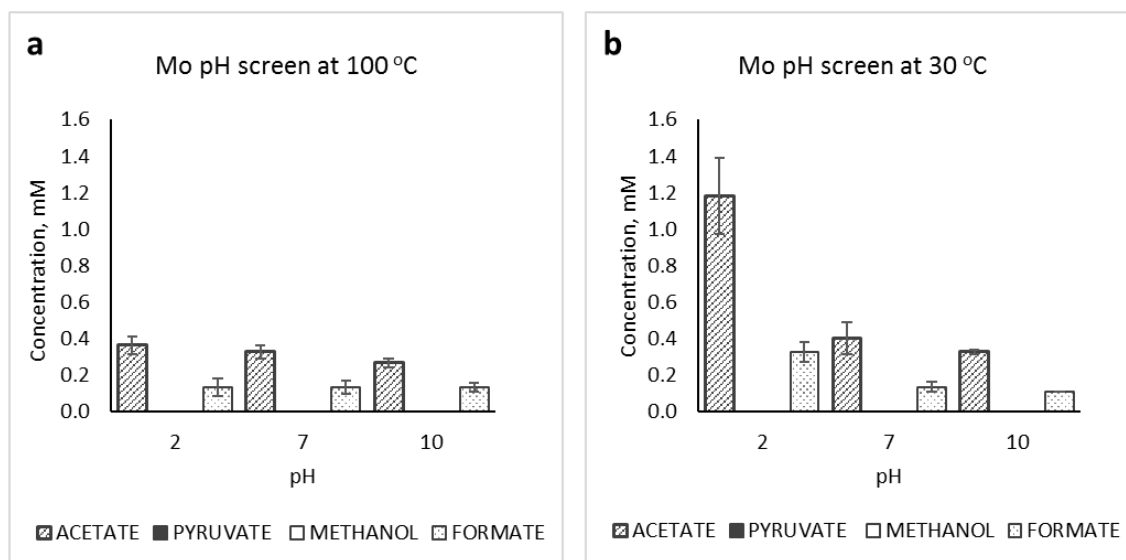


Figure S 62 pH screen for molybdenum at (a) 100 °C and (b) 30 °C

Table S 20 pH screen for molybdenum at 100 °C and 30 °C

Temperature		100 °C			30 °C		
pH		2	7	10	2	7	10
Products, mM	Acetate	0.37 ± 0.05	0.33 ± 0.04	0.27 ± 0.02	1.18 ± 0.21	0.40 ± 0.08	0.33 ± 0.01
	Pyruvate	0.00 ± 0.00	0.00 ± 0.00	0.00 ± 0.00	0.00 ± 0.00	0.00 ± 0.00	0.00 ± 0.00
	Methanol	0.00 ± 0.00	0.00 ± 0.00	0.00 ± 0.00	0.00 ± 0.00	0.00 ± 0.00	0.00 ± 0.00
	Formate	0.14 ± 0.03	0.14 ± 0.03	0.14 ± 0.03	0.33 ± 0.06	0.14 ± 0.03	0.11 ± 0.00

b. Salt screen at 100 °C and 30 °C

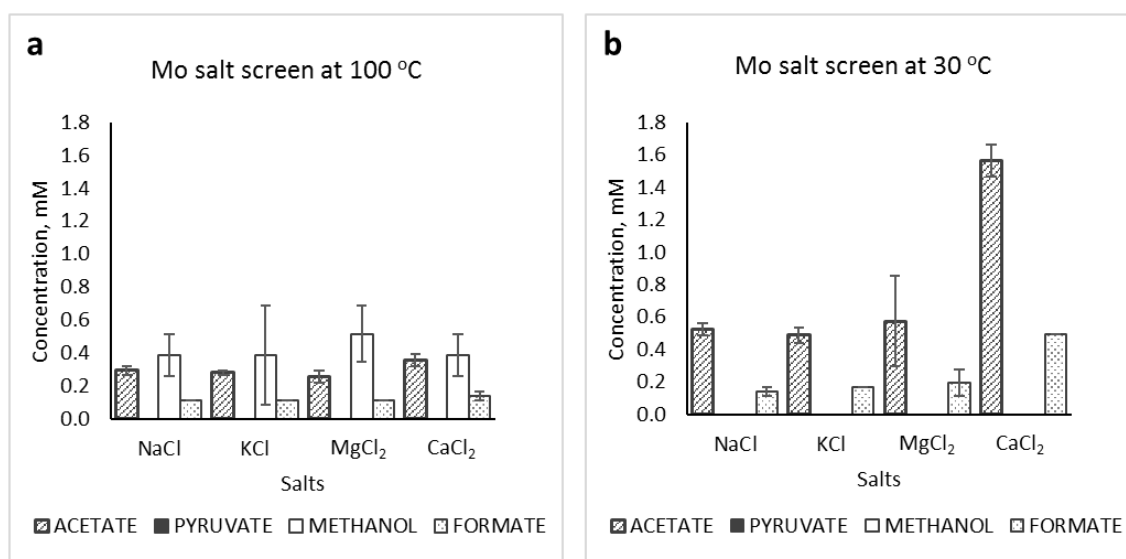


Figure S 63 Salt screen for molybdenum at (a) 100 °C and (b) 30 °C

Table S 21 Salt screen for molybdenum at 100 °C and 30 °C

Temperature		100 °C				30 °C			
Salts		NaCl	KCl	MgCl ₂	CaCl ₂	NaCl	KCl	MgCl ₂	CaCl ₂
Products, mM	Acetate	0.29 ± 0.02	0.28 ± 0.01	0.26 ± 0.04	0.35 ± 0.04	0.53 ± 0.04	0.49 ± 0.05	0.57 ± 0.28	1.56 ± 0.10
	Pyruvate	0.00 ± 0.00	0.00 ± 0.00	0.00 ± 0.00	0.00 ± 0.00	0.00 ± 0.00	0.00 ± 0.00	0.00 ± 0.00	0.00 ± 0.00
	Methanol	0.39 ± 0.13	0.39 ± 0.30	0.52 ± 0.17	0.39 ± 0.13	0.00 ± 0.00	0.00 ± 0.00	0.00 ± 0.00	0.00 ± 0.00
	Formate	0.10 ± 0.00	0.11 ± 0.00	0.11 ± 0.00	0.14 ± 0.03	0.14 ± 0.02	0.16 ± 0.00	0.19 ± 0.08	0.49 ± 0.00

2.4.5.6 Tungsten

a. pH screen at 100 °C and 30 °C

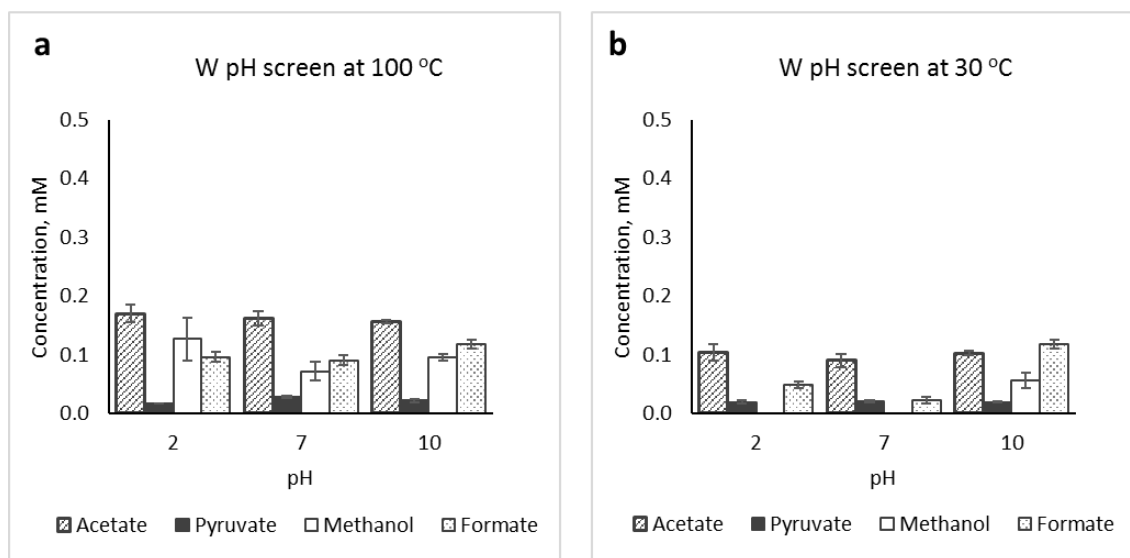


Figure S 64 pH screen for tungsten at (a) 100 °C and (b) 30 °C

Table S 22 pH screen for tungsten at 100 °C and 30 °C

Temperature		100 °C			30 °C		
pH		2	7	10	2	7	10
Products, mM	Acetate	0.17 ± 0.02	0.16 ± 0.01	0.16 ± 0.00	0.10 ± 0.01	0.09 ± 0.01	0.10 ± 0.00
	Pyruvate	0.02 ± 0.00	0.03 ± 0.00	0.02 ± 0.00	0.02 ± 0.00	0.02 ± 0.00	0.02 ± 0.00
	Methanol	0.13 ± 0.04	0.07 ± 0.02	0.10 ± 0.01	0.00 ± 0.00	0.00 ± 0.00	0.06 ± 0.01
	Formate	0.10 ± 0.01	0.09 ± 0.01	0.12 ± 0.01	0.05 ± 0.00	0.02 ± 0.00	0.12 ± 0.01

b. Salt screen at 100 °C and 30 °C

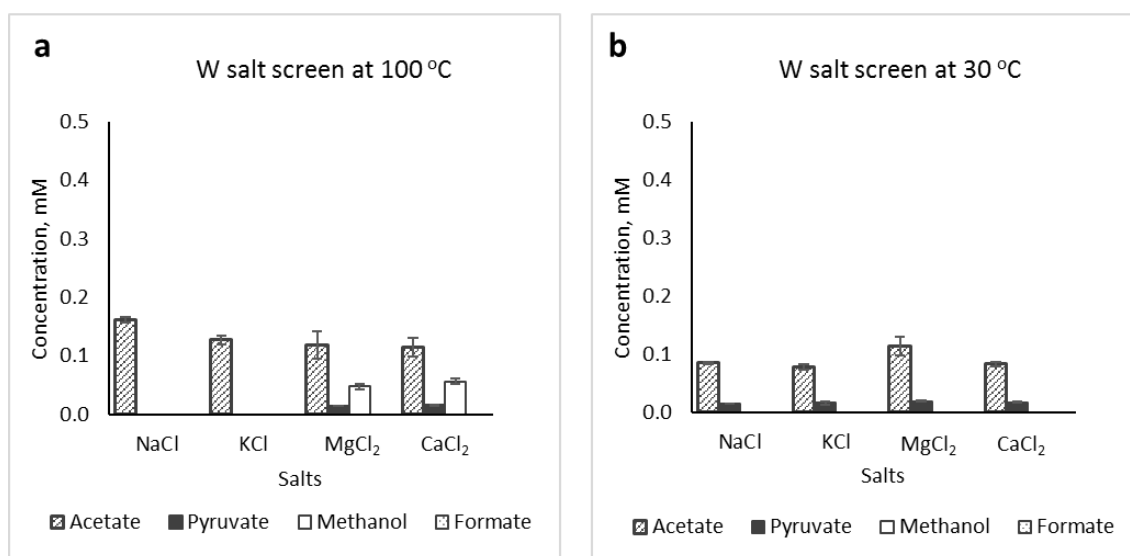


Figure S 65 Salt screen for tungsten at (a) 100 °C and (b) 30 °C

Table S 23 Salt screen for tungsten at 100 °C and 30 °C

Temperature		100 °C				30 °C			
Salts		NaCl	KCl	MgCl ₂	CaCl ₂	NaCl	KCl	MgCl ₂	CaCl ₂
Products, mM	Acetate	0.16 ± 0.00	0.13 ± 0.01	0.12 ± 0.02	0.11 ± 0.02	0.08 ± 0.00	0.08 ± 0.00	0.11 ± 0.02	0.08 ± 0.00
	Pyruvate	0.00 ± 0.00	0.00 ± 0.00	0.01 ± 0.00	0.02 ± 0.00	0.01 ± 0.00	0.02 ± 0.00	0.02 ± 0.00	0.02 ± 0.00
	Methanol	0.00 ± 0.00	0.00 ± 0.00	0.05 ± 0.00	0.06 ± 0.00	0.00 ± 0.00	0.00 ± 0.00	0.00 ± 0.00	0.00 ± 0.00
	Formate	0.00 ± 0.00	0.00 ± 0.00	0.00 ± 0.00	0.00 ± 0.00	0.00 ± 0.00	0.00 ± 0.00	0.00 ± 0.00	0.00 ± 0.00

2.4.6 The effect of salt concentration on reaction yields

Reactions were carried out according to general procedure A with 1 mmol of Fe powder and with varying quantity of KCl in 1 mL H₂O (0.1, 0.5, 1.0 and 2.0 mmol), at 100 °C over 16 h.

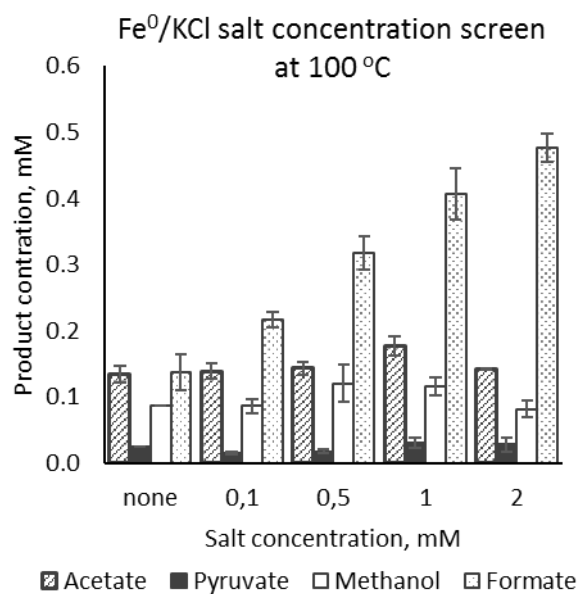


Figure S 66 KCl concentration screen for the Fe⁰ system at 100 °C

Table S 24 KCl concentration screen for the Fe⁰ system at 100 °C

KCl. mM		0.1	0.5	1.0	2.0
Products, mM	Acetate	0.14 ± 0.01	0.14 ± 0.01	0.18 ± 0.01	0.14 ± 0.00
	Pyruvate	0.02 ± 0.00	0.02 ± 0.00	0.03 ± 0.01	0.03 ± 0.01
	Methanol	0.09 ± 0.01	0.12 ± 0.03	0.12 ± 0.01	0.08 ± 0.01
	Formate	0.22 ± 0.01	0.32 ± 0.03	0.41 ± 0.04	0.48 ± 0.02

2.4.7 Miscellaneous experiments

2.4.7.1 The effect of KOH workup

Two reactions were carried out in parallel according to general procedure A with 1 mmol of Fe powder in 1 mL H₂O at 100 °C under 35 bar CO₂ over 16 h. Next, NMR samples were prepared using the method described in section 2.2.3. NMR sample preparation, except in one of the cases where the KOH quenching step was omitted. Compared results are presented in the ¹H NMR spectra stack below (Figure S 67).

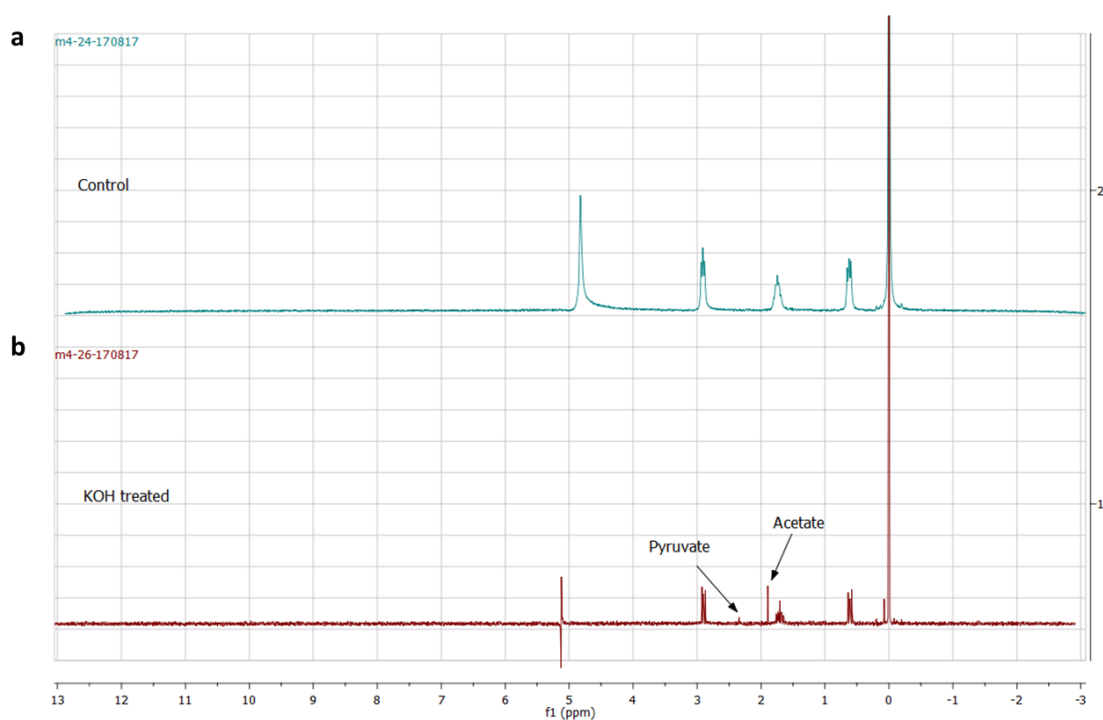


Figure S 67 ¹H NMR of the reaction mixture (a) not treated with KOH during sample preparation and (b) treated with KOH during sample preparation (6 : 1 H₂O : D₂O with DSS-Na as standard).

The addition of KOH during the NMR sample preparation allows for the separation of all analysed products otherwise bound to the metal species present in solution, thus permitting us to acquire quantitative ¹H NMR spectra.

2.4.7.2 *Iron-promoted CO₂-fixation in the presence of each of its products as the starting material.*

Reactions (A)-(D) (Figure S 68) were carried out according to general procedure A with 1 mmol of Fe powder and 1 mmol of KCl in 1 mL H₂O, except to each reaction vial additional CO₂-fixation products were added as starting materials: (A) sodium formate, (B) sodium methoxide, (C) potassium acetate, and (D) sodium pyruvate. The reactions were stirred at 100 °C under 35 bar CO₂ over 16 h.

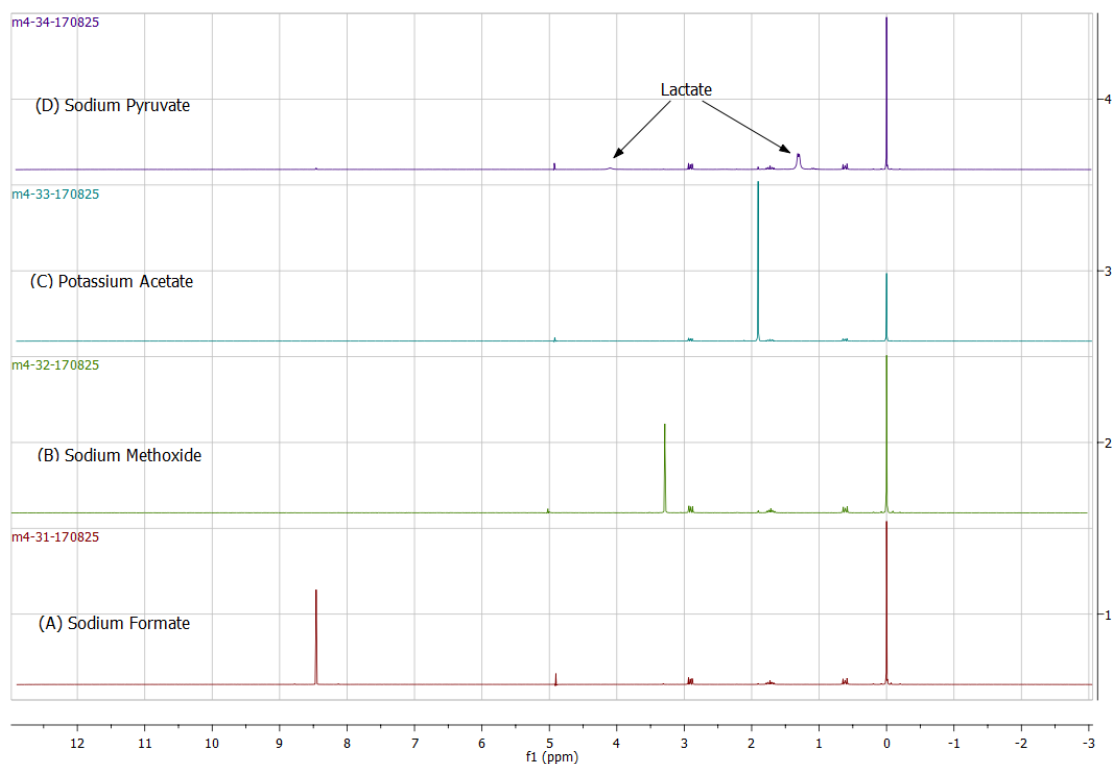


Figure S 68 ¹H NMR spectra showing the result of iron-promoted CO₂-fixation reactions in the presence of each of its products the starting material (6 : 1 H₂O : D₂O with DSS-Na as standard).

The fact that reaction (D), with pyruvate present as the starting material, yielded only its reduction product (lactate) under normal reaction conditions points towards the role of a surface bound chemistry during the course of reaction (see Part II, Section 2.4.4).

2.4.7.3 Iron-promoted CO fixation

Two reactions were carried out according to general procedure A with 1 mmol of Fe powder and 1 mmol of KCl in 1 mL H₂O:

- at 30 °C under 1 bar CO over 16 h
- at 100 °C under 35 bar CO over 16 h

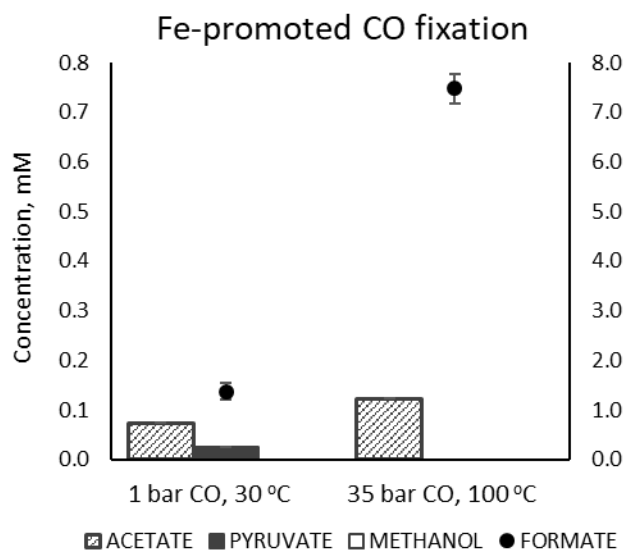


Figure S 69 CO fixation reactions using the Fe⁰/KCl system at 30 °C under 1 bar CO and at 100 °C under 35 bar CO.

Table S 25 CO fixation reactions using the Fe⁰/KCl system at 30 °C under 1 bar CO and at 100 °C under 35 bar CO.

Conditions		1 bar CO 30 °C	35 bar CO 100 °C
Products	Acetate	0.07 ± 0.00	0.12 ± 0.00
	Pyruvate	0.02 ± 0.00	0.00 ± 0.00
	Methanol	0.00 ± 0.00	0.00 ± 0.00
	Formate	1.37 ± 0.16	7.48 ± 0.30

2.4.8 Compatibility with 3-reaction sequences of the rTCA cycle

Two rTCA cycle reaction sequences were carried out in two replicas each, according to general procedure B following which the mixtures were subjected to a KOH workup. In the case of the oxaloacetate-malate-fumarate-succinate sequence, NMR spectra were acquired (as described in the Analytical methods section). NMR spectra (Figure S 70) allowed only for a qualitative detection of acetate, formate, malate, fumarate, succinate, lactate and levulinate (side product), due to high complexity and low concentration of the reaction mixture. In the case of the oxalosuccinate-isocitrate-aconitate-citrate sequence, the obtained spectrum of a crude reaction mixture was too complex to allow for unambiguous product determination. Therefore, the presence of all rTCA cycle products in both sequences was confirmed additionally by GC-MS. 200 μ L of the basified reaction mixture was derivatized with ethyl chloroformate/ethanol or methyl chloroformate/methanol to convert the carboxylic acid products to their respective ethyl (or methyl) esters, using a well-established literature procedure.¹¹⁷ The obtained ester mixtures were subjected to GC-MS measurements (Figure S 71 and Figure S 72). Note that acetate, formate and methanol cannot be detected using this method. The identity of the detected species was confirmed by the comparison with ^1H NMR spectra of authentic samples (for the oxaloacetate-malate-fumarate-succinate sequence), as well as by the obtained mass spectra (Figure S 70, Figure S 71 and Figure S 72), which agree with the data we reported previously.¹¹⁷

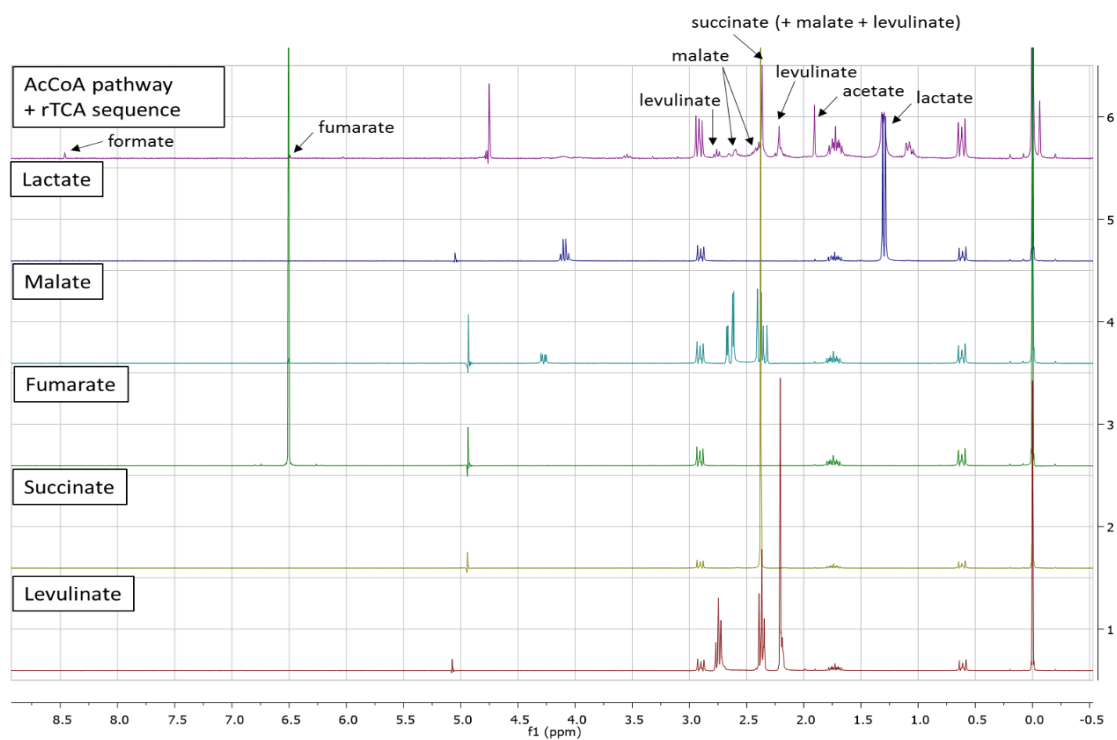


Figure S 70 ¹H NMR spectra of the rTCA cycle (3-step sequence) reaction mixture, stacked with analogous spectra of authentic samples of rTCA cycle intermediates and levulinate (6 : 1 H₂O : D₂O with DSS-Na as standard).

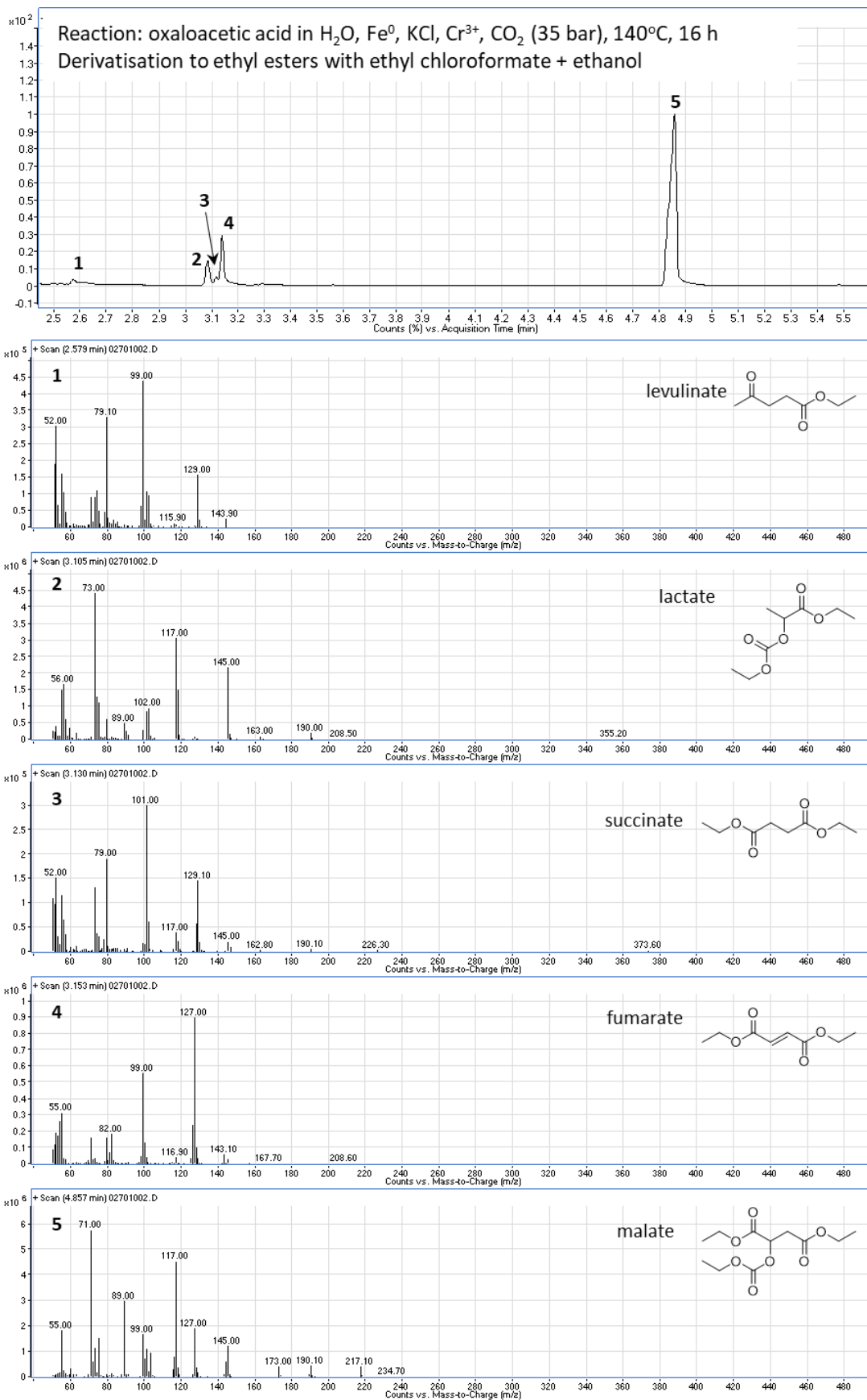
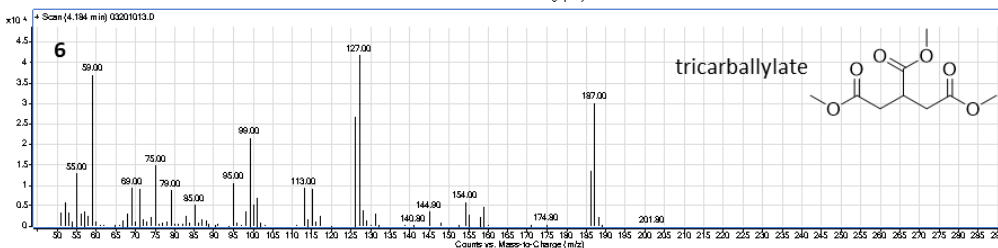
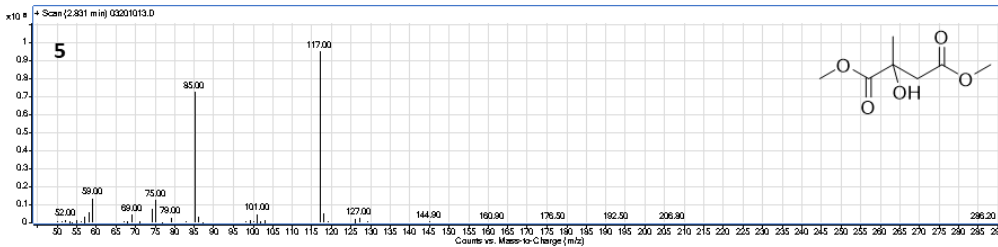
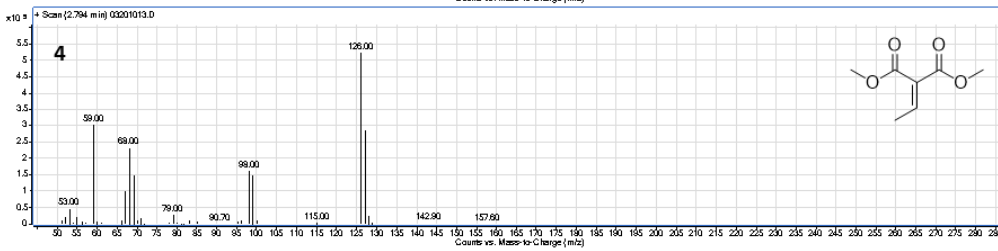
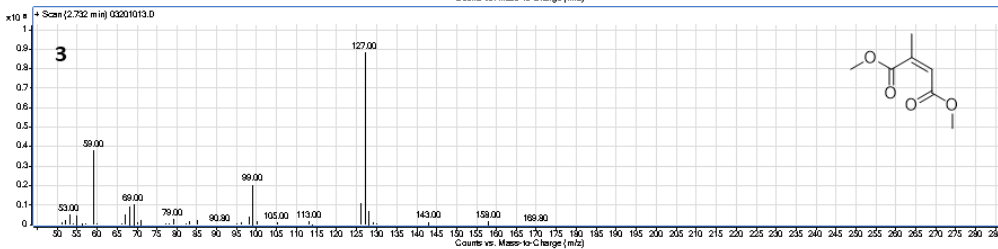
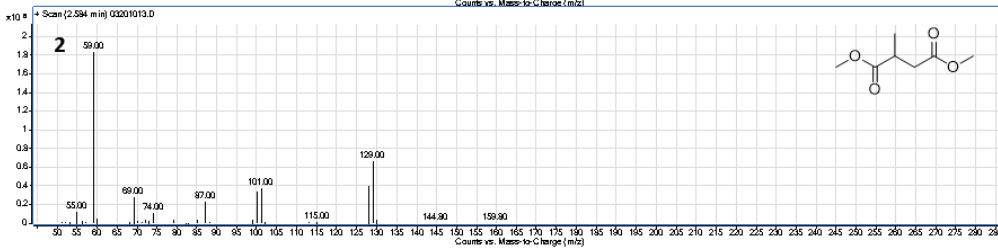
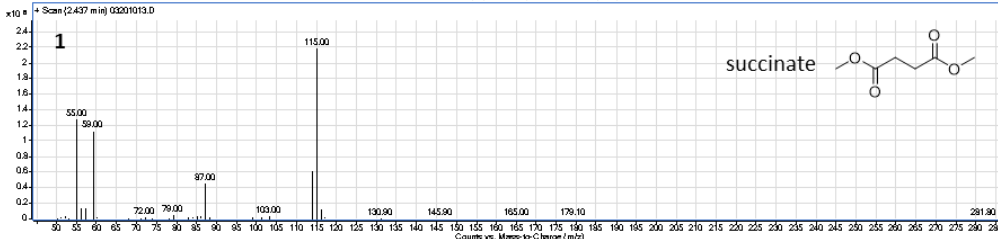
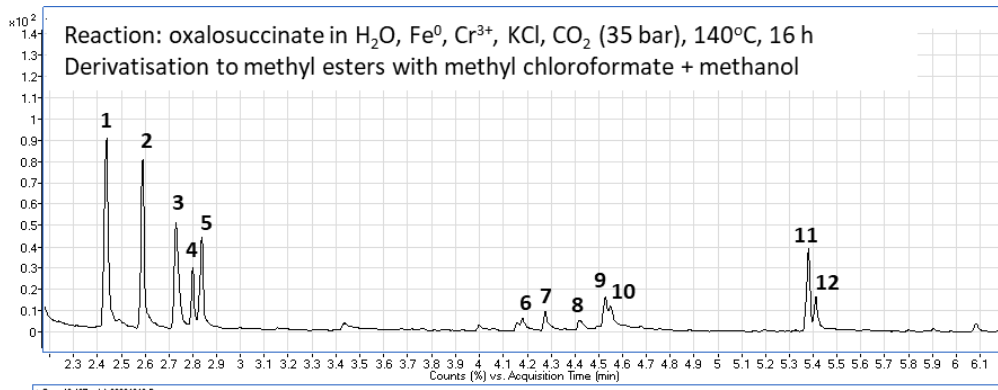


Figure S 71 GC traces and mass spectra obtained for the rTCA cycle (3-step sequence: oxaloacetate-malate-fumarate-succinate) reaction mixture, subjected to ethyl chloroformate/ethanol derivatization to ethyl esters.



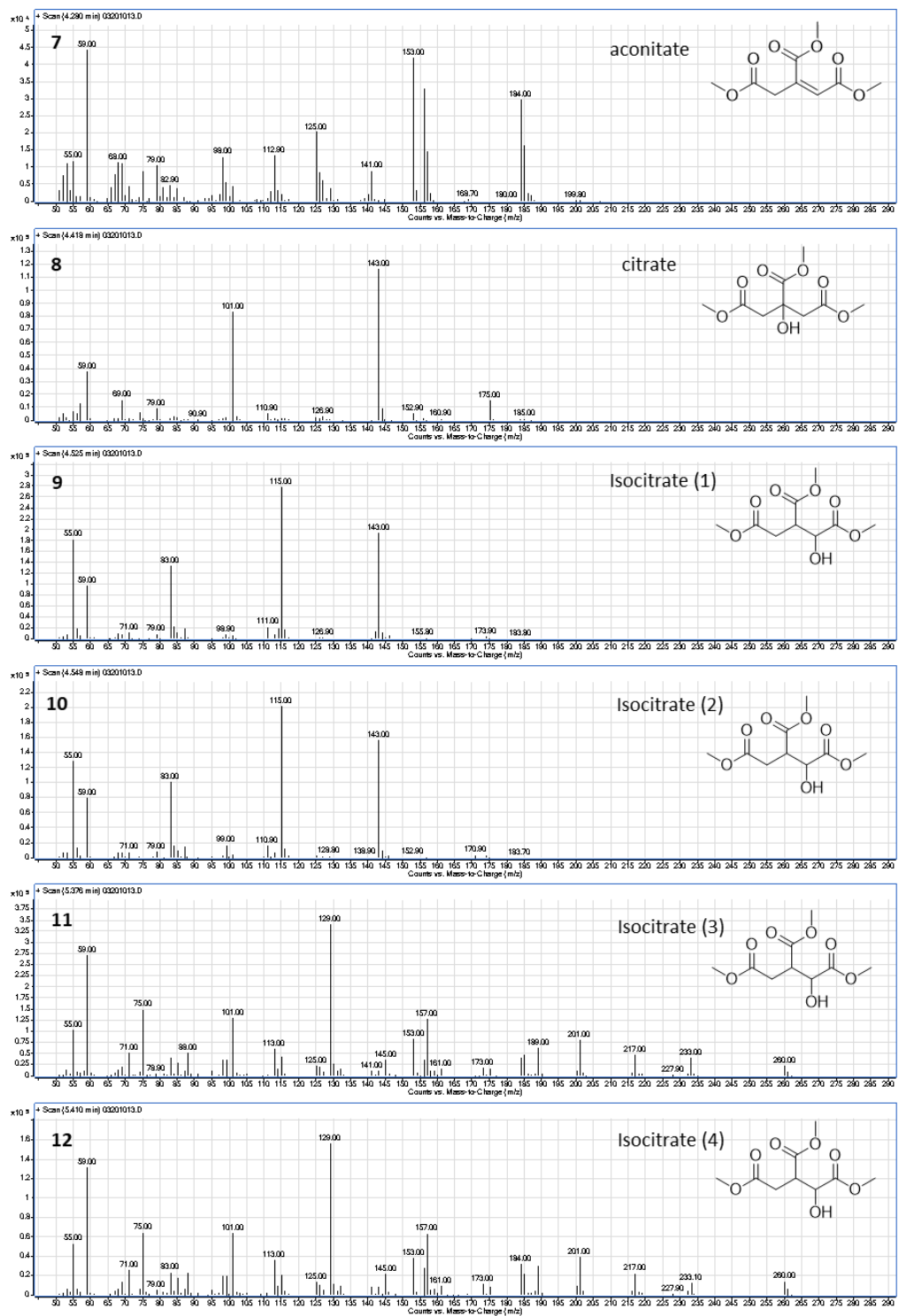


Figure S 72 GC traces and mass spectra obtained for the rTCA cycle (3-step sequence: oxalosuccinate-isocitrate-aconitate-citrate) reaction mixture, subjected to methyl chloroformate/methanol derivatization to methyl esters.

3 Reductive Amination

3.1 General information

All reactions were carried out in 10 mL Pyrex glass culture tubes under inert atmosphere unless otherwise noted.

GCMS analysis was performed on a GC System 7820A (G4320) connected to a MSD block 5977E (G7036A), using Agilent High Resolution Gas Chromatography Column: PN 19091S – 433UI, HP – 5MS UI, 28 m×0.250 mm, 0.25 Micron, SN USD 489634H. All samples were prepared in ethyl acetate (200 μ L sample volume). The analysis was carried out on a splitless 1 μ L injection volume with an injection port temperature 250 °C. Column oven temperature program was as follows: 60 °C for 1 min, ramped at 30 °C min⁻¹ to 310 °C with 3 min hold, with a total running time of 12.33 min. The mass spectrometer was turned on after 2 min and was operated at the electron ionization mode with quadrupole temperature of 150 °C. Data acquisition was performed in the full-scan mode (50-500). Hydrogen (99.999 % purity) was used as carrier gas at a constant flow rate of 1.5 mL min⁻¹.

3.1.1 Materials

Unless otherwise noted, all reagents and solvents were purchased from commercial suppliers and used without further purification. Fe(0) used was a \geq 99% reduced fine powder. ZnCl₂ was used as an anhydrous powder (reagent grade). Cr₂(SO₄)₃ was used as a dodecahydrate (reagent grade).

3.2 Analytical methods

3.2.1 Derivatization procedure

Derivatization of amino acids to esters was performed using a modified literature procedure. For optimal gas chromatography resolution, the amino acids were converted to ethyl esters using a mixture of ethanol/ethyl chloroformate (EtOH/ECF).

A *ca.* 0.5-0.7 mL aliquot of the reaction mixture was basified using solid KOH and centrifuged (6000 rpm, 3 min). To 100 μ L of the supernatant was added 1 M NaOH solution (150 μ L), EtOH (240 μ L) and pyridine (30 μ L), followed by ethyl chloroformate (ECF, 35 μ L). This was vortexed for 30 s. A second 35 μ L portion of ECF was added and the mixture was vortexed again for 30 s. Next, CHCl₃ (200 μ L) was added, followed by vortexing (10 s). Finally, NaHCO₃ (400 μ L) was added and the mixture was vortexed again for 10 s. The CHCl₃ layer was separated and dried over anhydrous Na₂SO₄. 50 μ L of the dry CHCl₃ layer was used with 150 μ L of ethyl acetate for the GC-MS analysis.

3.2.2 Product identification

Reaction products derivatized to ethyl esters of amino acids were identified by comparing the mass spectra and retention times against analogously derivatized authentic samples (Appendix, Figure S30 – S33).

3.3 Experimental data

Table S 26 Reductive amination of ketoacids (0.1 mmol) using hydrazine, Fe⁰ (1mmol), 1 M HCl, 16 h.

Entry ^a	Ketoacid	Equivalents of Hydrazine	Temperature (°C)	Reduction products (% of mixture)			
				12	14	18	19
1		1	80	13	87	-	-
2		2	80	3	97	-	-
3	2	4	80	1	99	-	-
4		8	80	0	100	-	-
5		2	140	17	83	-	-
6		2	25	6	94	-	-
7	17	2	80	-	-	8	92

^aAll reactions were carried out in 0.1 mmol of the corresponding ketoacids with 10 mmol of Fe⁰.

Table S 27 Reductive amination of ketoacids (0.1 mmol) using hydroxylamine, Fe⁰ (1mmol), 1 M HCl, 16 h.

Entry ^a	Ketoacid	Equivalents of Hydroxylamine	Temperature (°C)	Reduction products (% of mixture)							
				12	14	18	19	4	15	13	16
1		1	80	17	83	-	-	-	-	-	-
2		2	80	9	91	-	-	-	-	-	-
3	2	4	80	3	97	-	-	-	-	-	-
4		8	80	2	98	-	-	-	-	-	-
5		1	100	19	81	-	-	-	-	-	-
6		2	140	100	-	-	-	-	-	-	-
7		2	25	-	100						
8	17	1	100	-	-	29	71	-	-	-	-
9	3	1	100	-	-	-	-	46	54	-	-
10	7	1	100	-	-	-	-	-	-	61	38
11	2+3+7+17	1	100	-	1	37	40	12	-	10	-

^aAll reactions were carried out in 0.1 mmol of the corresponding ketoacids with 10 mmols of Fe⁰.

3.4 Gas chromatography traces

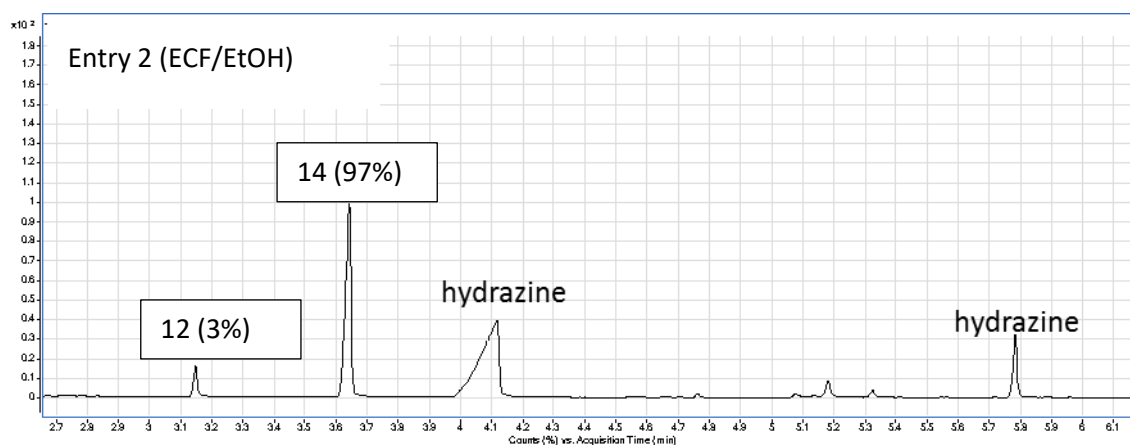


Figure S 73 Chromatogram of the reaction mixture corresponding entry 2 (Table S 26).

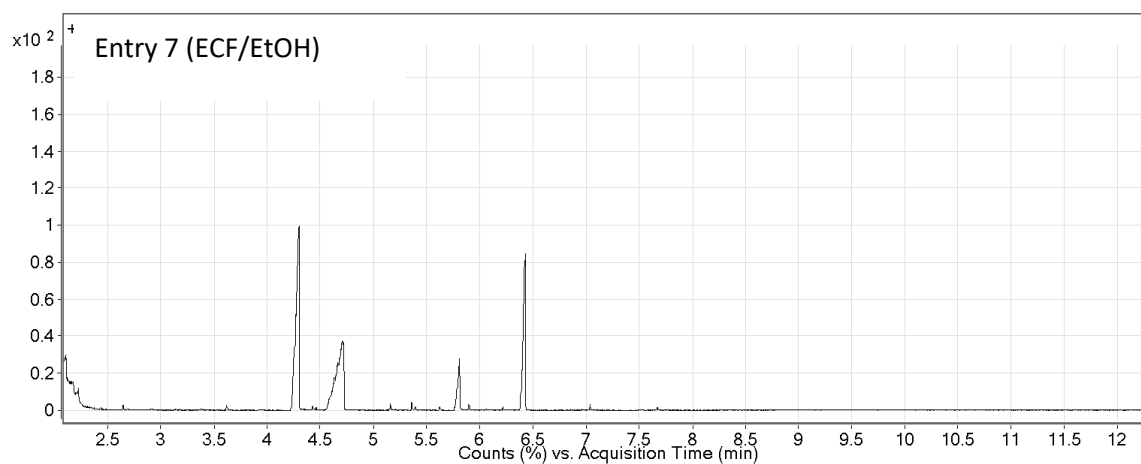


Figure S 74 Chromatogram of the reaction mixture corresponding to entry 7 (Table S 26).

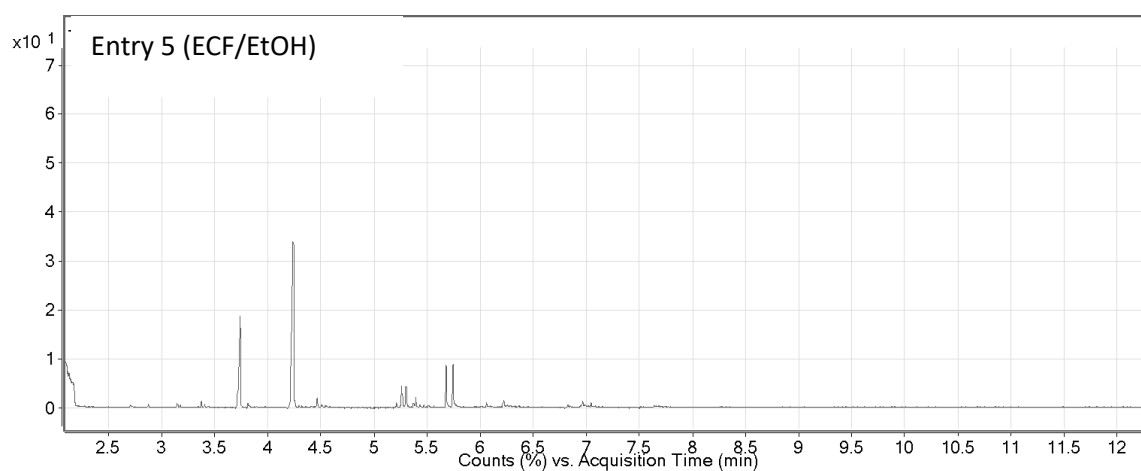


Figure S 75 Chromatogram of the reaction mixture corresponding to entry 5 (Table S 27).

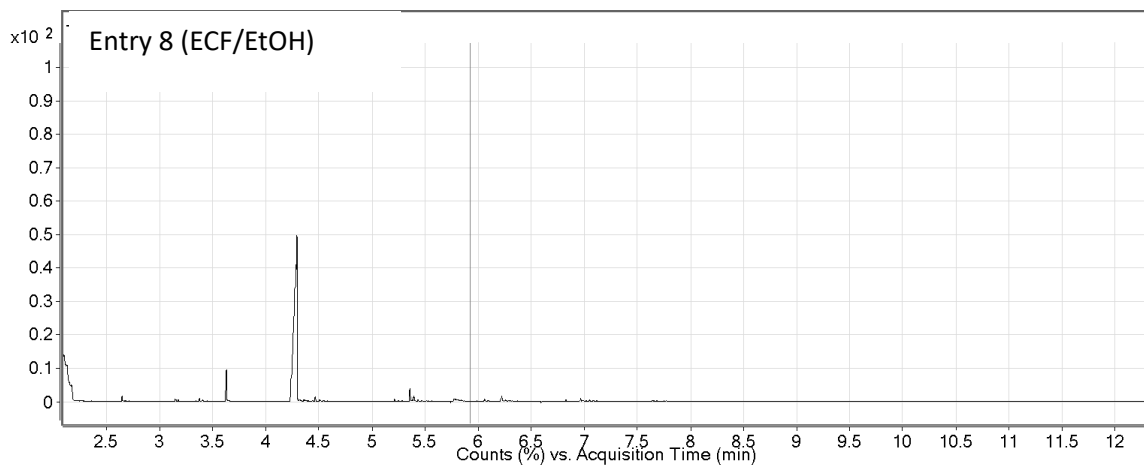


Figure S 76 Chromatogram of the reaction mixture corresponding to entry 8 (Table S 27).

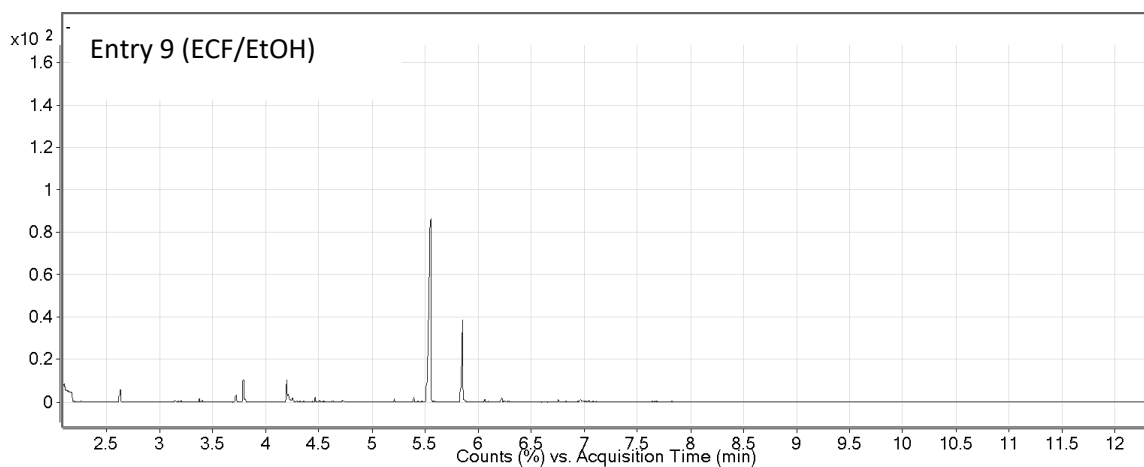


Figure S 77 Chromatogram of the reaction mixture corresponding to entry 9 (Table S 27).

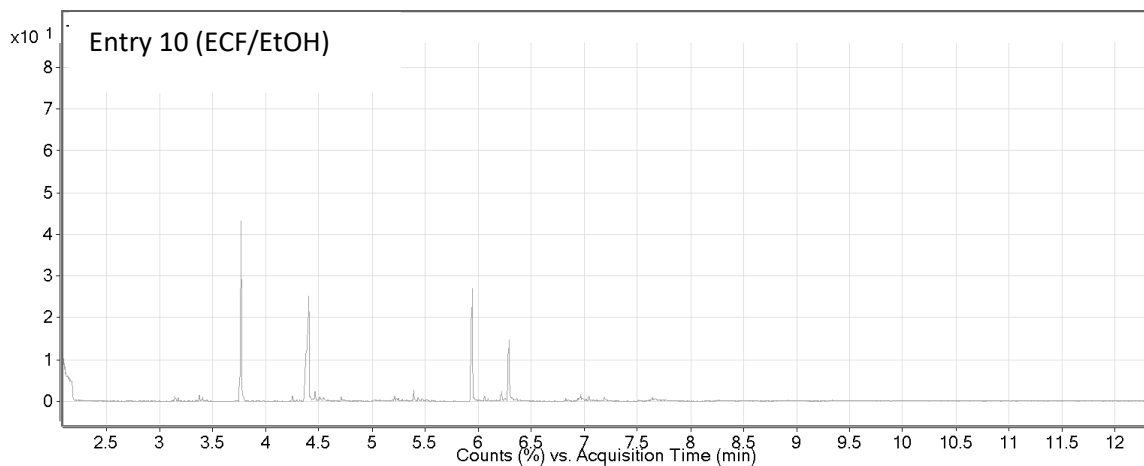


Figure S 78 Chromatogram of the reaction mixture corresponding to entry 10 (Table S 27).

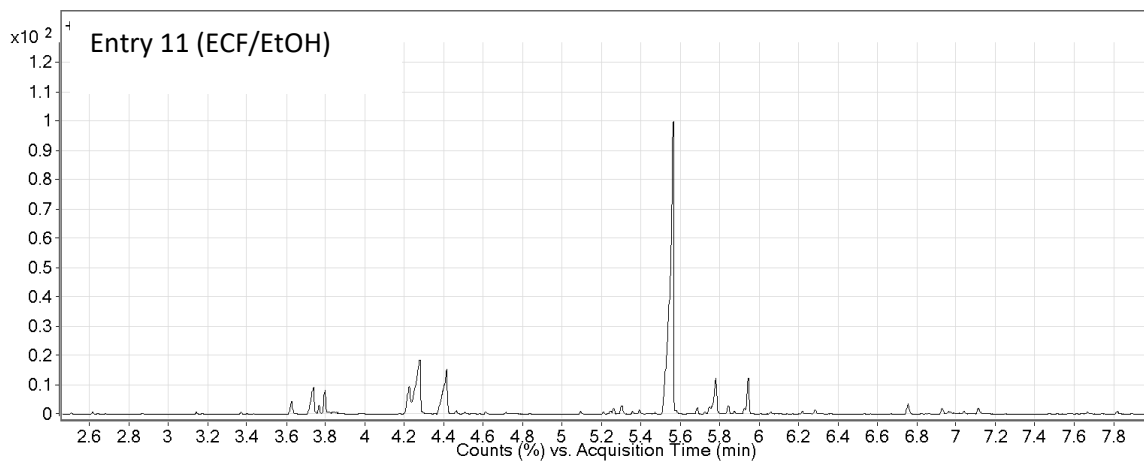


Figure S 79 Chromatogram of the reaction mixture corresponding to entry 11 (Table S 27).

APPENDIX

Appendix I

Representative chromatograms and Mass spectrum for rTCA cycle intermediates

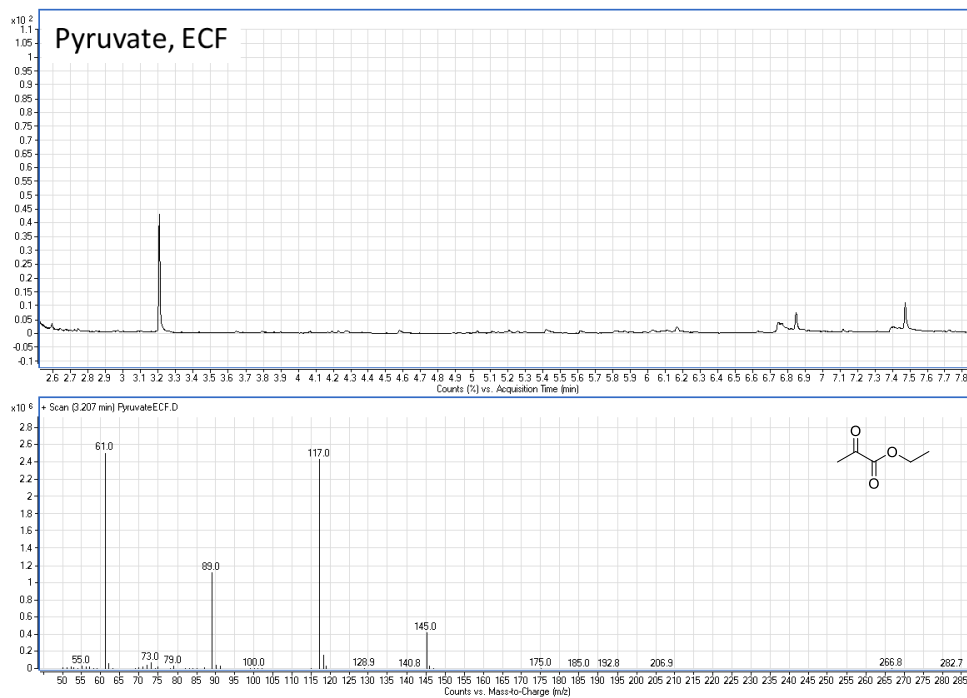


Figure S 80 GC trace and mass spectrum of pyruvate characteristic peak (ECF derivatization).

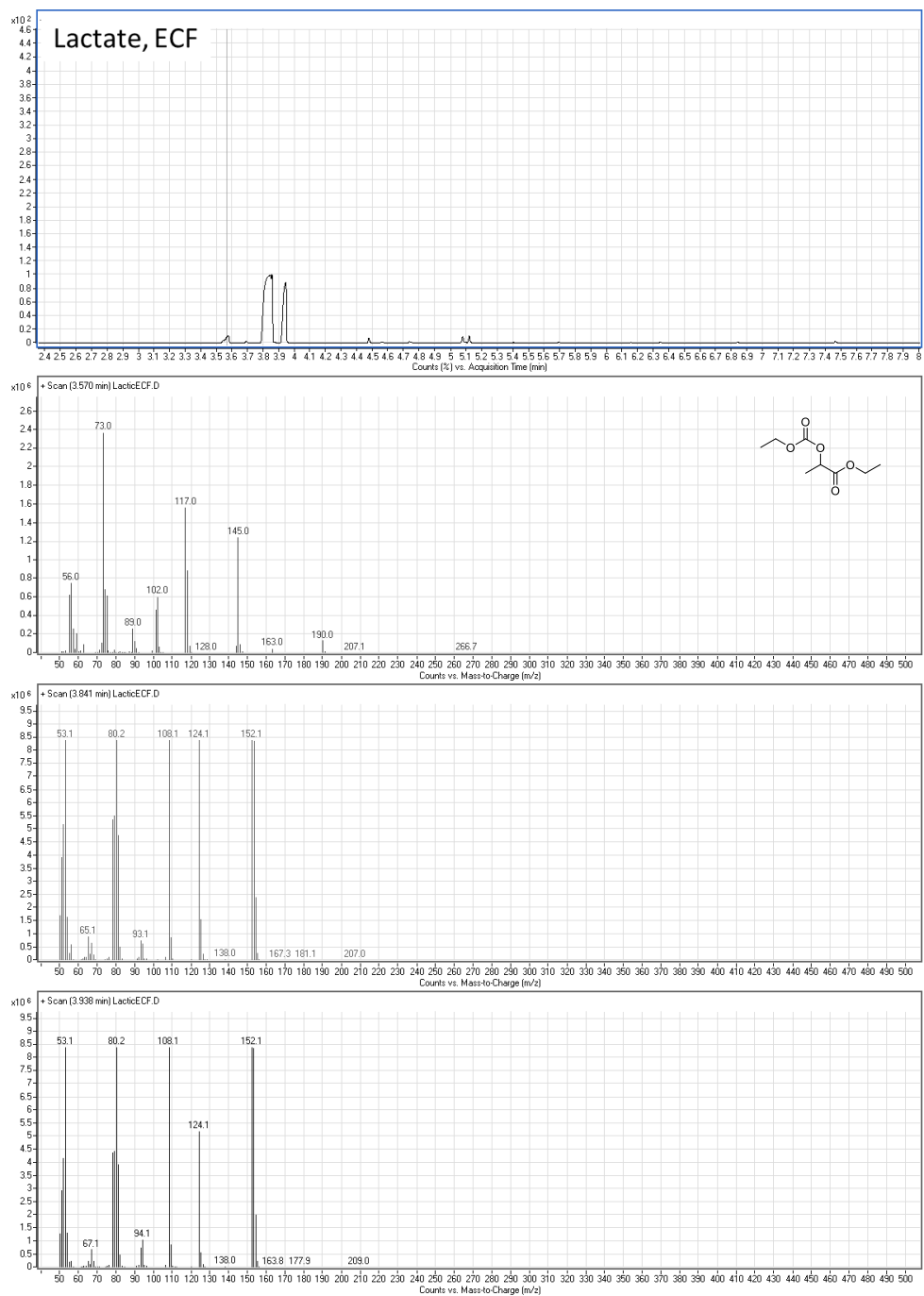


Figure S 81 GC trace and mass spectra of lactate characteristic peaks (ECF derivatization).

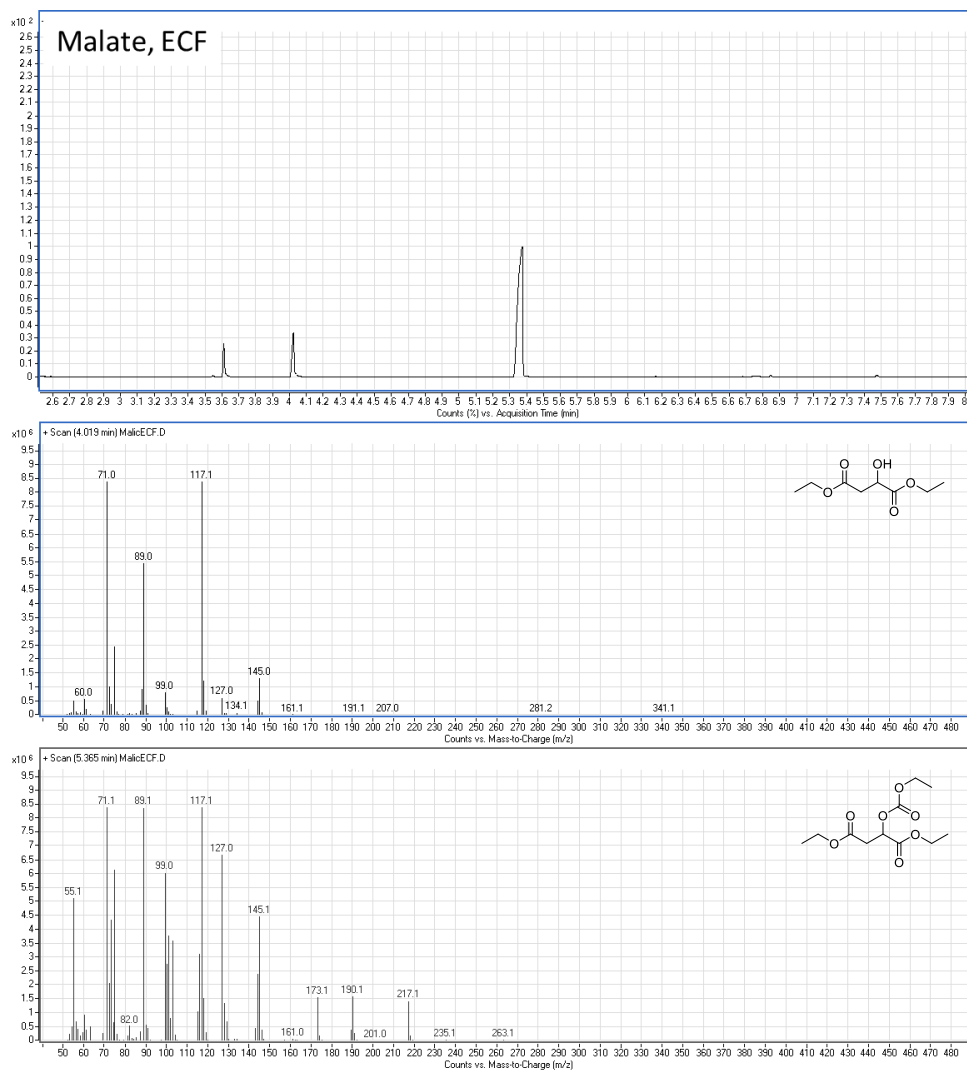


Figure S 82 GC trace and mass spectra of malate characteristic peaks (ECF derivatization). The additional peak at ~3.6 min corresponds to trace fumarate (result of O-acylation of the hydroxyl group during derivatization and subsequent elimination, well below 5 % at malate concentrations ≤ 0.04 M).

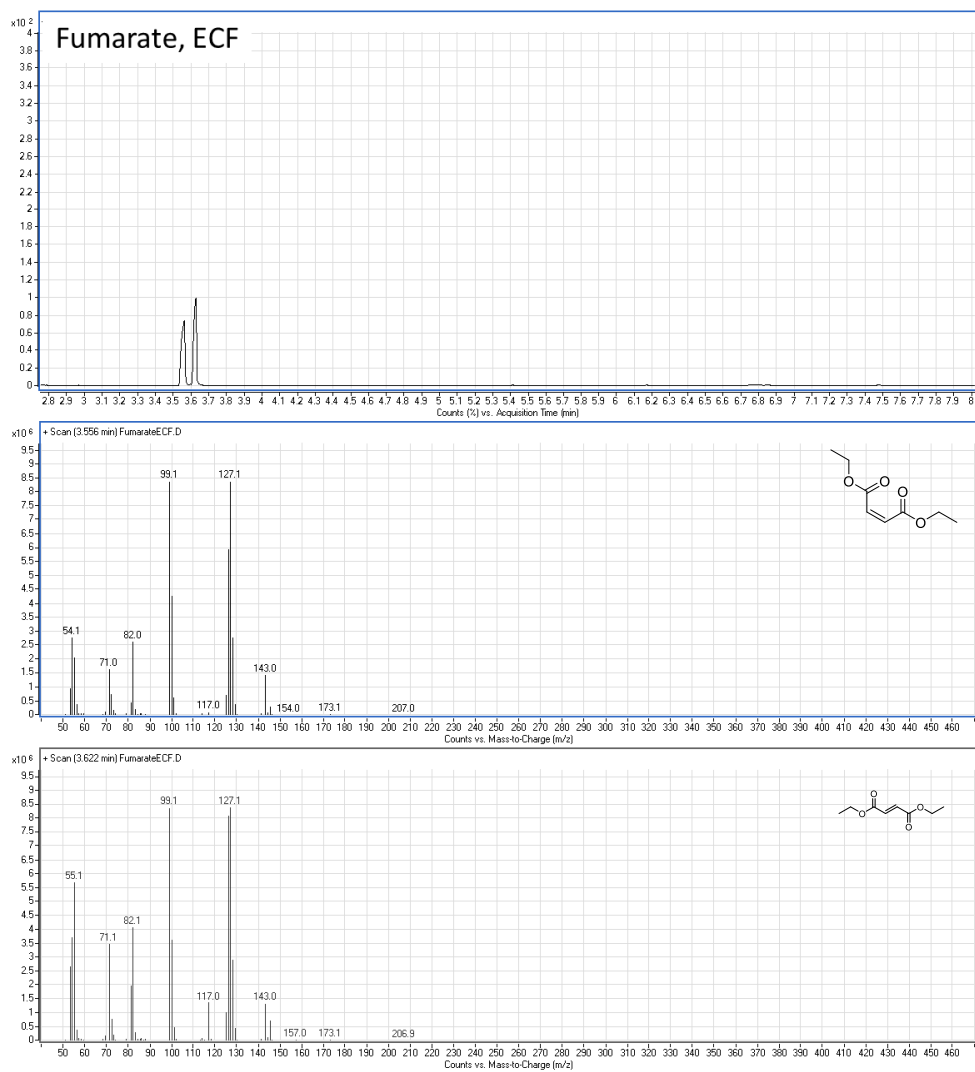


Figure S 83 GC trace and mass spectra of fumarate characteristic peaks (ECF derivatization).

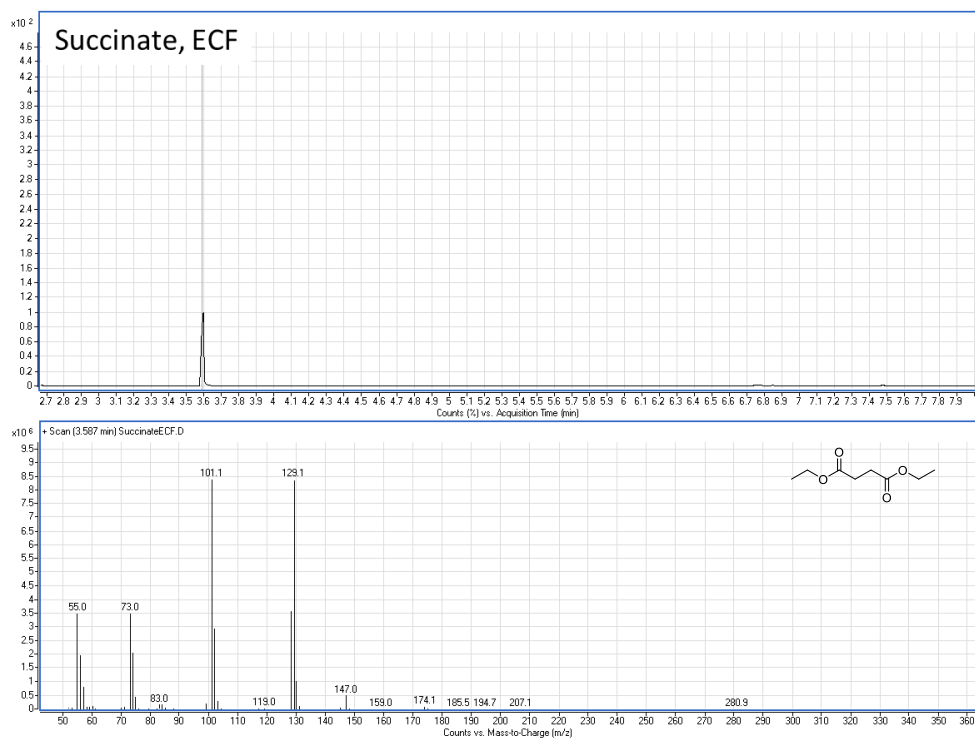


Figure S 84 GC trace and mass spectrum of succinate characteristic peak (ECF derivatization).

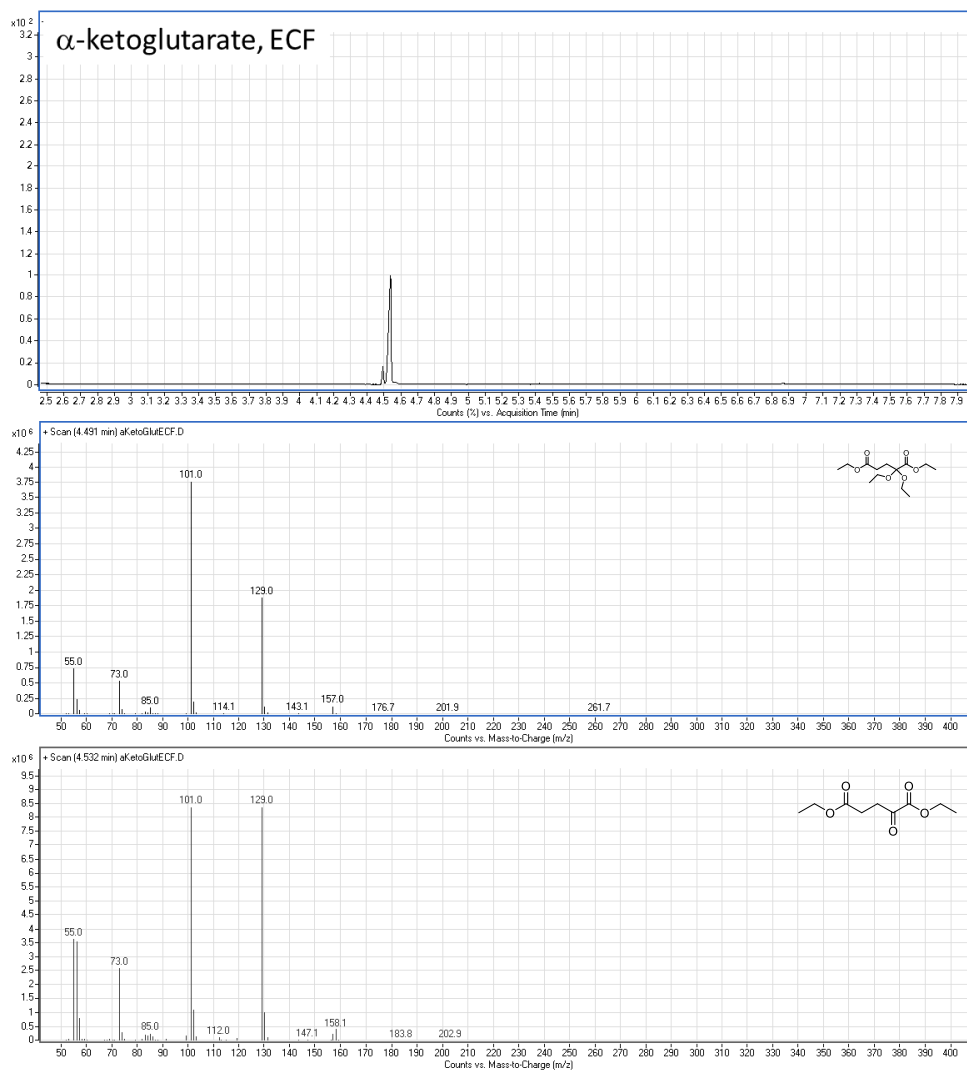


Figure S 85 GC trace and mass spectra of α -ketoglutarate characteristic peaks (ECF derivatization).

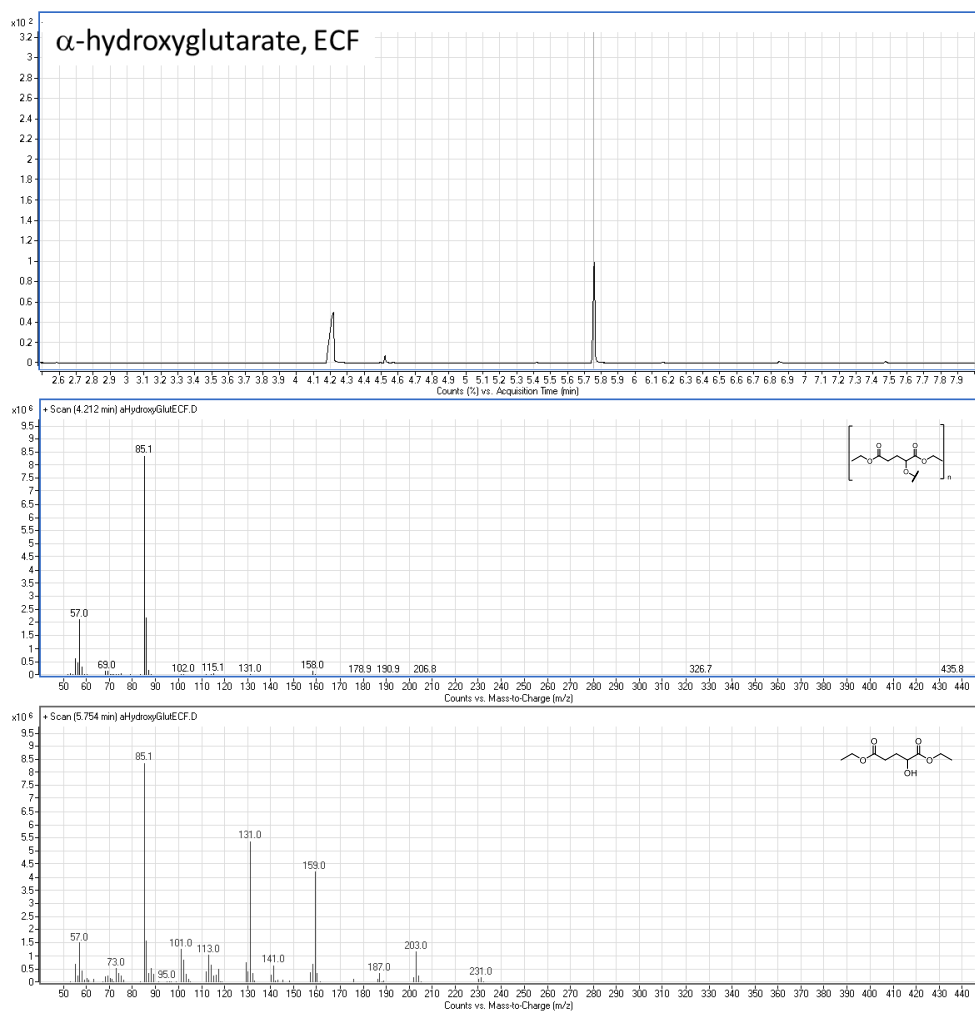


Figure S 86 GC trace and mass spectra of α -hydroxyglutarate characteristic peaks (ECF derivatization).

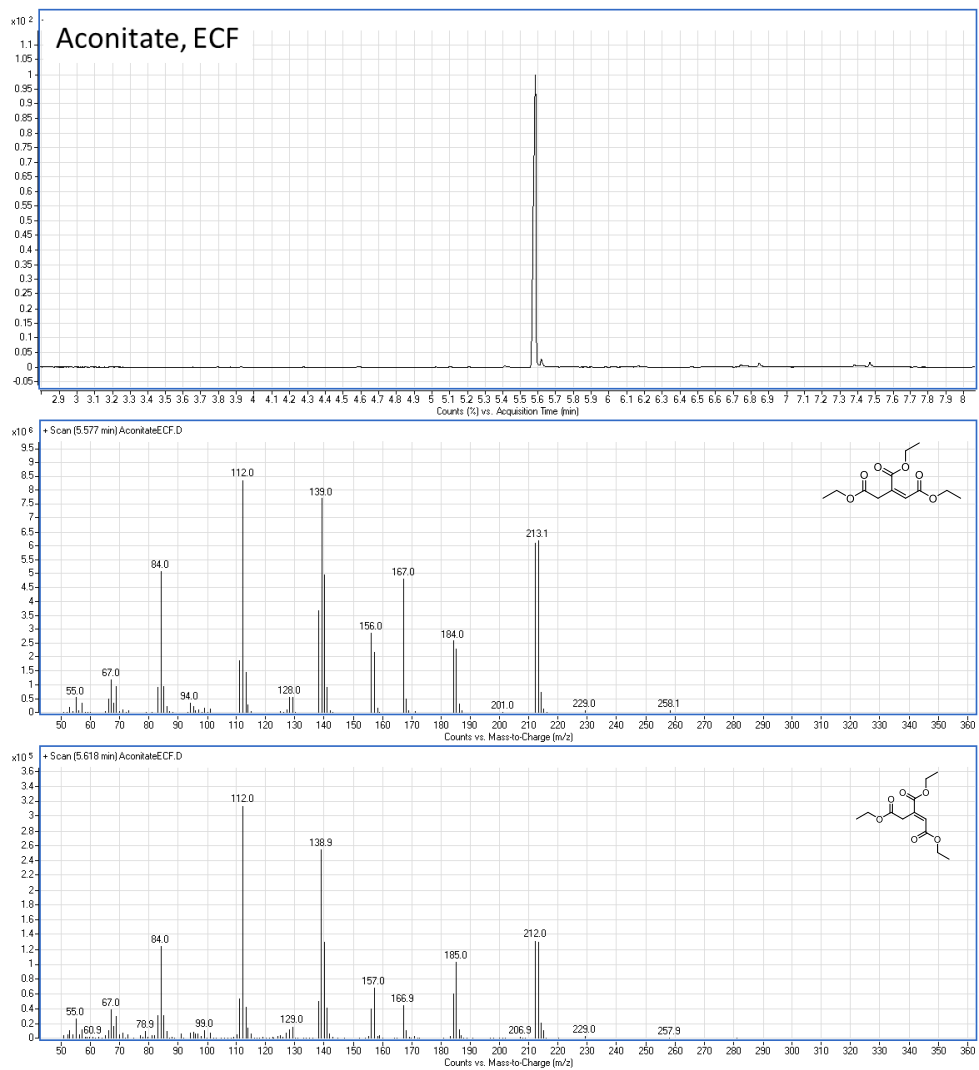


Figure S 87 GC trace and mass spectra of *cis*-aconitate characteristic peaks (ECF derivatization).

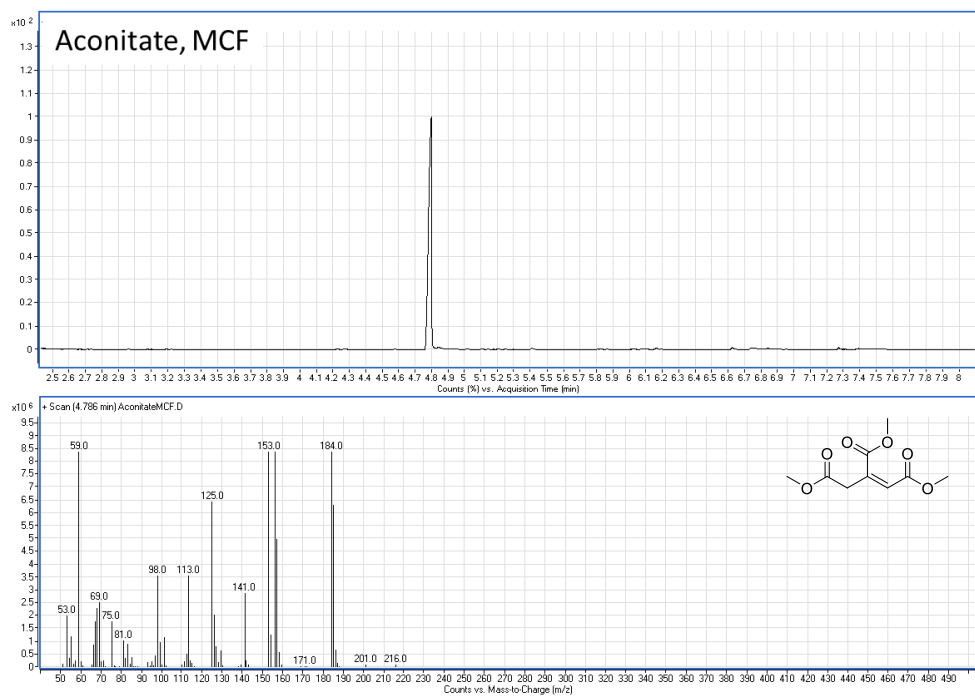


Figure S 88 GC trace and mass spectrum of *cis*-aconitate characteristic peak (MCF derivatization).

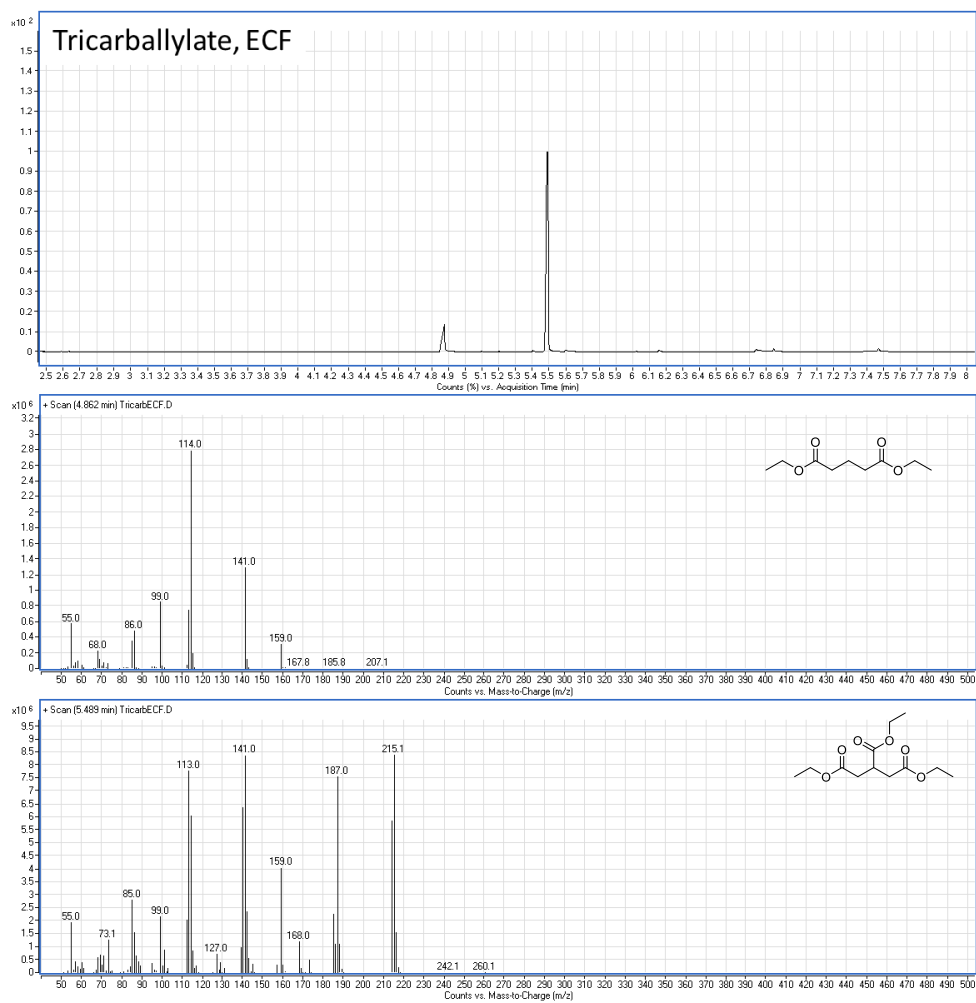


Figure S 89 GC trace and mass spectra of tricarballylate characteristic peaks (ECF derivatization).

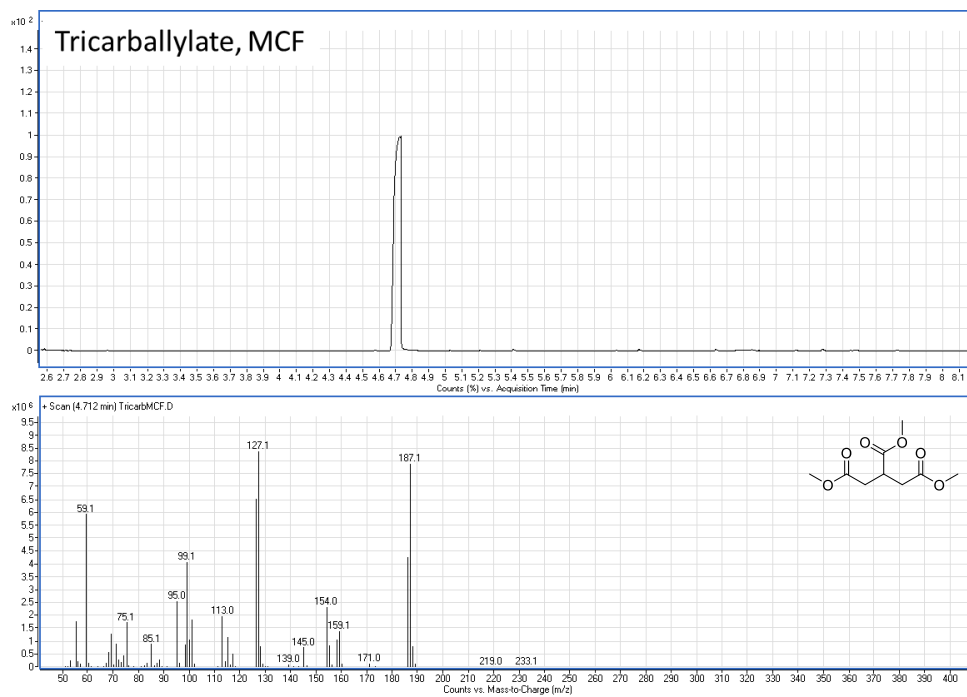


Figure S 90 GC trace and mass spectrum of tricarballylate characteristic peak (MCF derivatization).

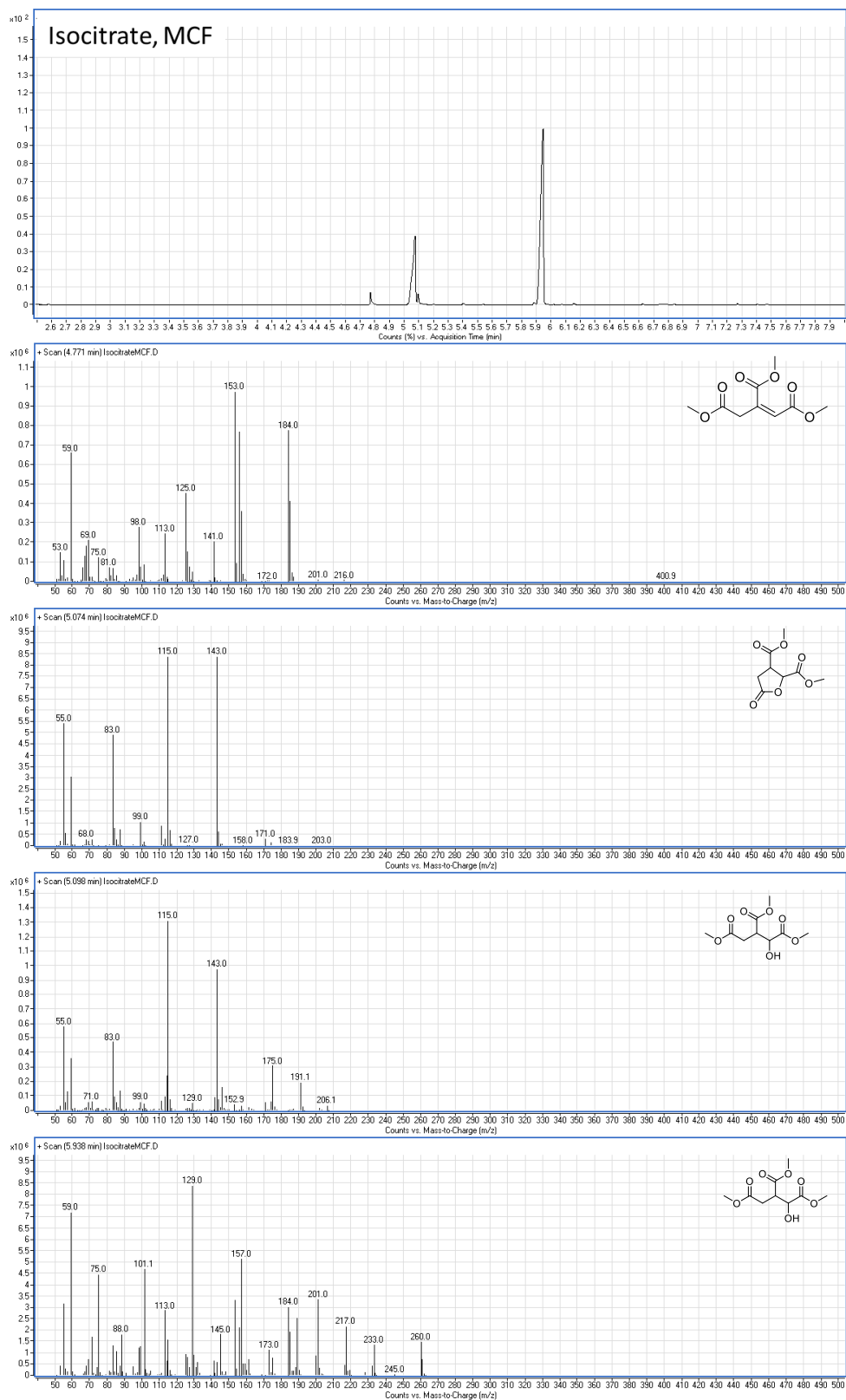


Figure S 91 GC trace and mass spectra of isocitrate characteristic peaks (MCF derivatization). The additional peak at ~4.8 min corresponds to trace aconitate (result of O-acylation of the hydroxyl group during derivatization and subsequent elimination, < 5 % at isocitrate concentrations ≤ 0.04 M).

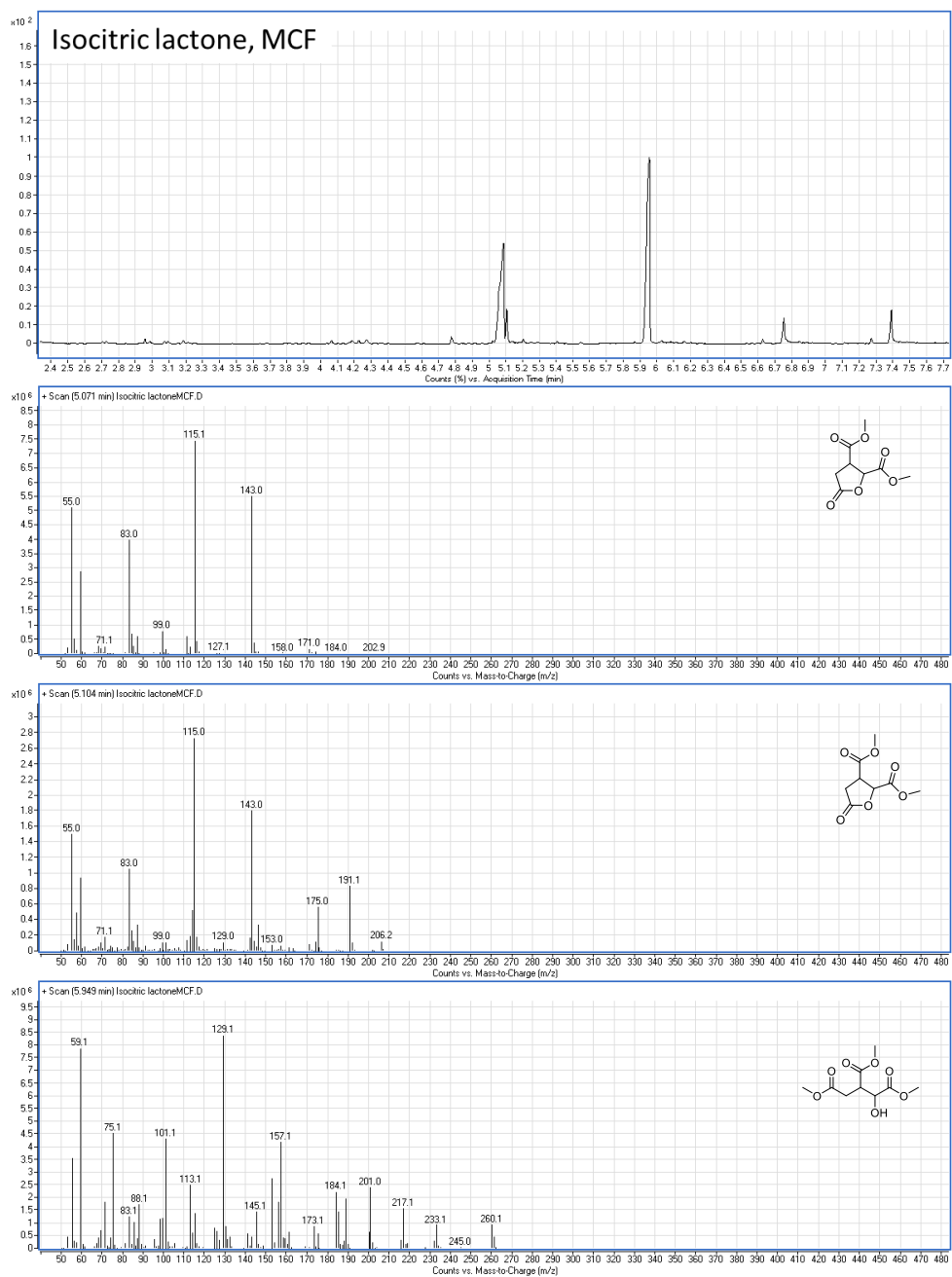


Figure S 92 GC trace and mass spectra of isocitric lactone characteristic peaks (MCF derivatization).

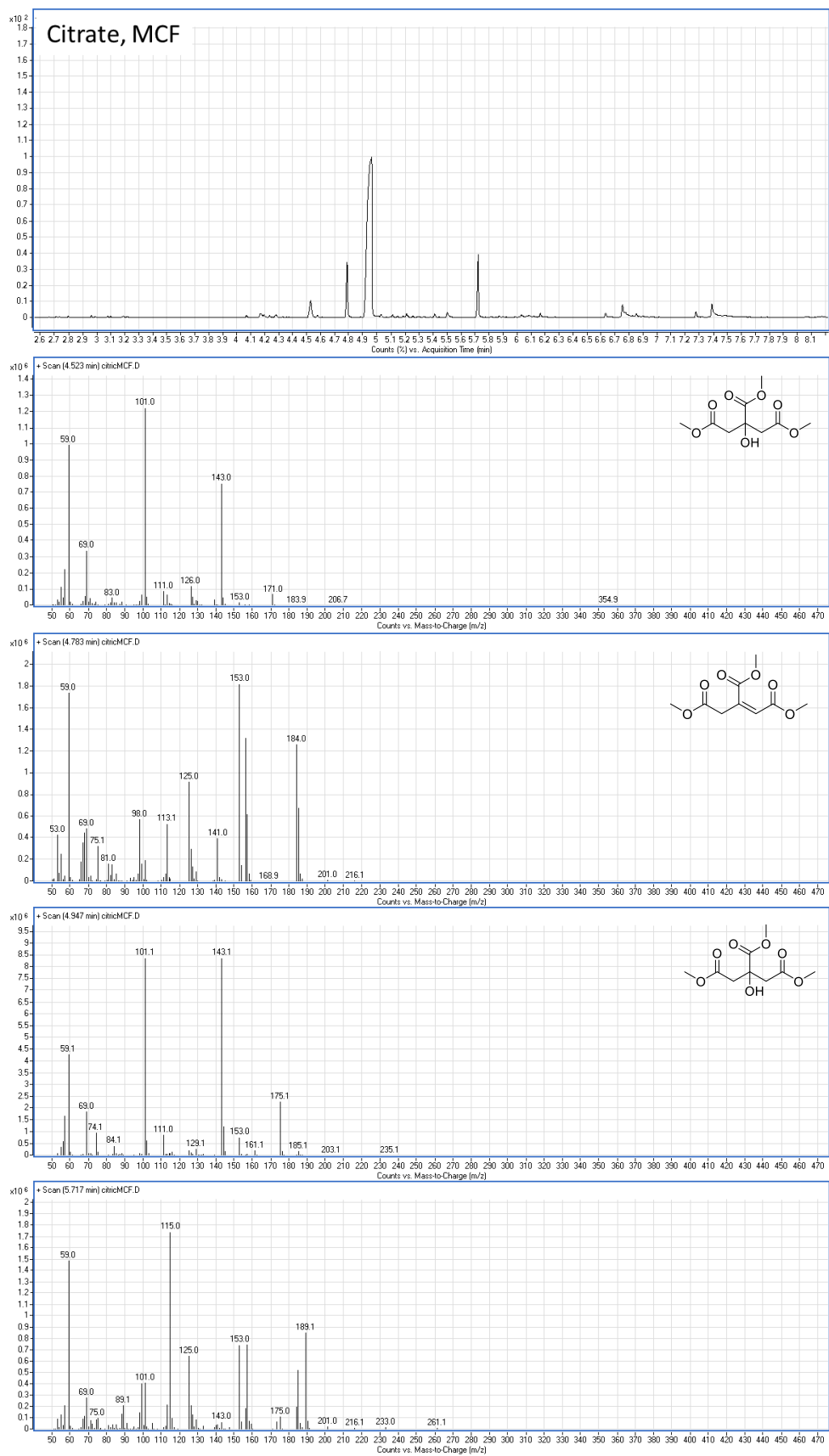


Figure S 93 GC trace and mass spectra of citrate characteristic peaks (MCF derivatization). The additional peak at ~4.8 min corresponds to trace aconitate (result of O-acylation of the hydroxyl group during derivatization and subsequent elimination, < 5 % at citrate concentrations ≤ 0.04 M).

Yield determination and error analysis

3 mL standard aqueous solutions of rTCA carboxylic acids at different concentrations (0.006 M, 0.013 M, 0.020 M, 0.027 M, 0.033 M and 0.040 M) were prepared by diluting 0.1 – 0.5 M stock solutions of these acids. 100 μ L of each standard solution was derivatized using the derivatization procedure described herein (see: Analytical procedures). For each acid, a six-point graph was plotted, correlating the sum of characteristic GC peaks (as integrated automatically by the *Agilent MassHunter Workstation v.B.06.00* software) with substrate concentration (Figure S 94 – S 105). Each data point was obtained from three independent measurements (carried out by three different researchers) and the correlation line was obtained from the least-squares fitting (intercept = 0). Error bars on graphs are shown as \pm standard deviation for each data point. Overall percentage error of the response factor corresponds to \pm standard deviation for each slope value.

The yields of products were calculated by comparing the product peak area with the calibration line. For the purpose of this study, reported are not the absolute percentage yields based on the number of moles of the starting materials, but rather percentage contributions to the total composition of the final reaction mixture. This allows to account for potential concentration changes due to solvent loss (since many reactions were carried out in sealed tubes at temperatures above the boiling point of water), as well as potentially incomplete extraction during the derivatization procedure. Each reaction was performed at least twice to ensure reproducibility, and reported percentage compositions are an average of these two runs, with an error corresponding to \pm mean absolute deviation.

Derivatization with ethyl chloroformate (ECF)

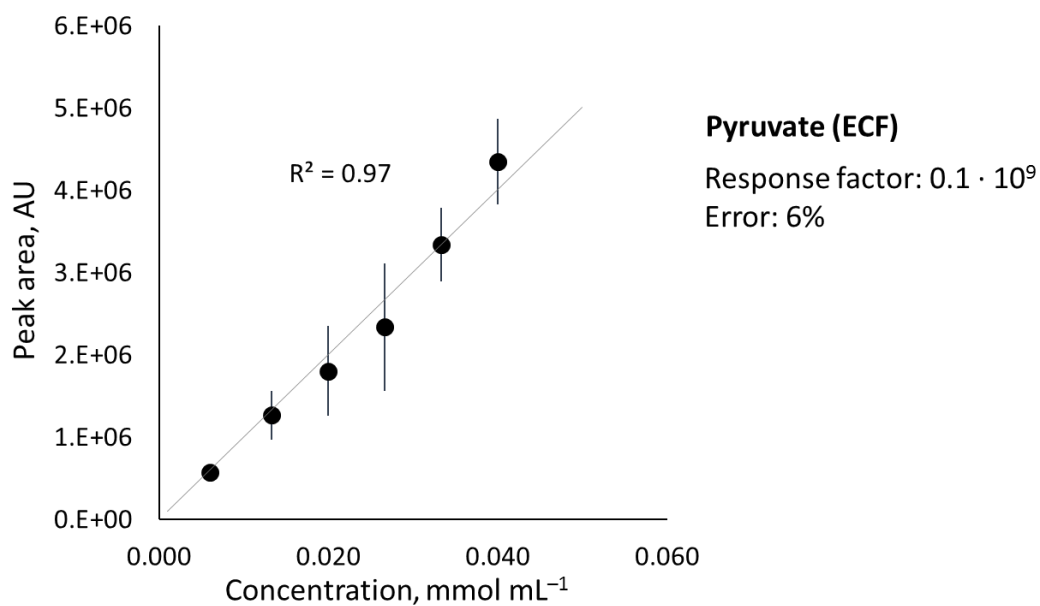


Figure S 94 Correlation between the concentration of an aqueous solution of pyruvate and the measured gas chromatography peak area.

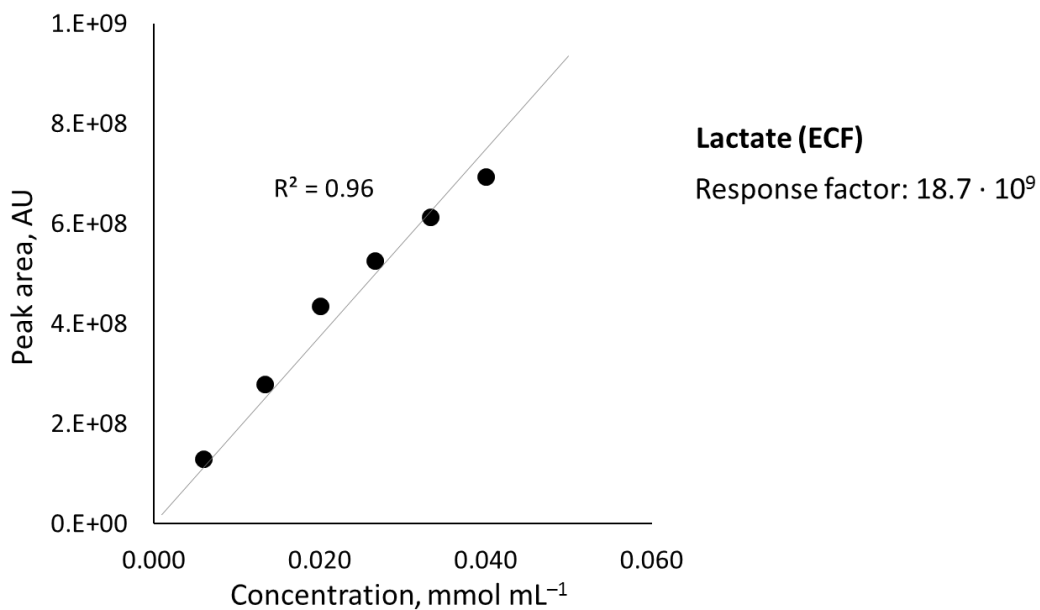


Figure S 95 Correlation between the concentration of an aqueous solution of lactate and the measured gas chromatography peak area. Lactate was obtained by a complete reduction of an aqueous solution of sodium pyruvate with NaBH₄. The correlation line shown here corresponds to a single run.

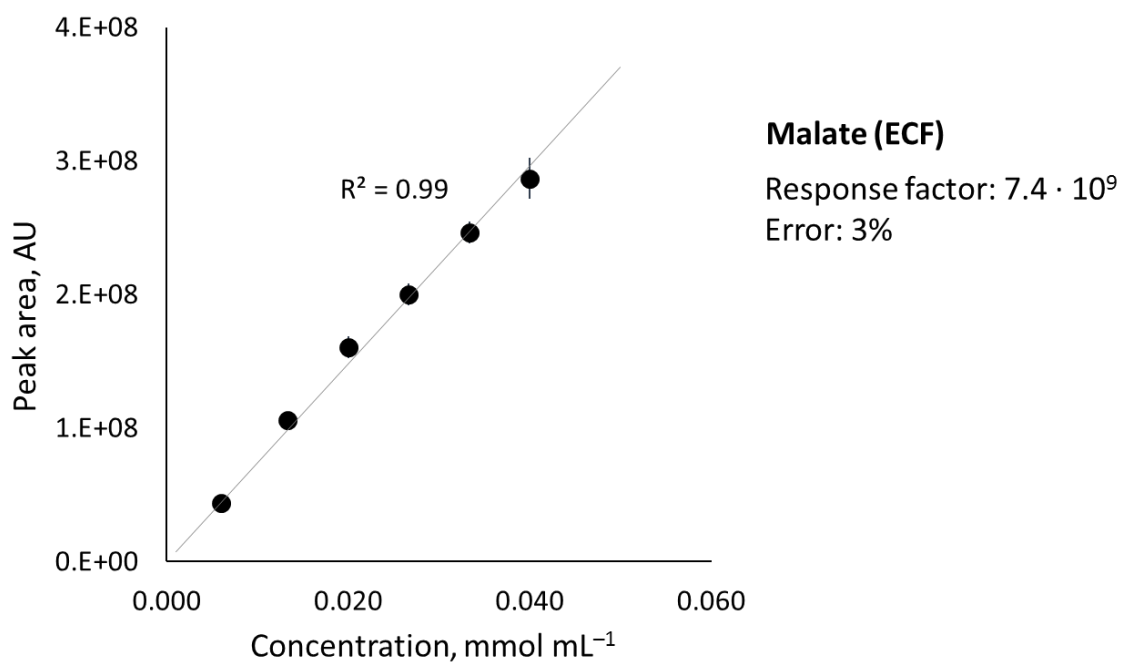


Figure S 96 Correlation between the concentration of an aqueous solution of malate and the measured gas chromatography peak area.

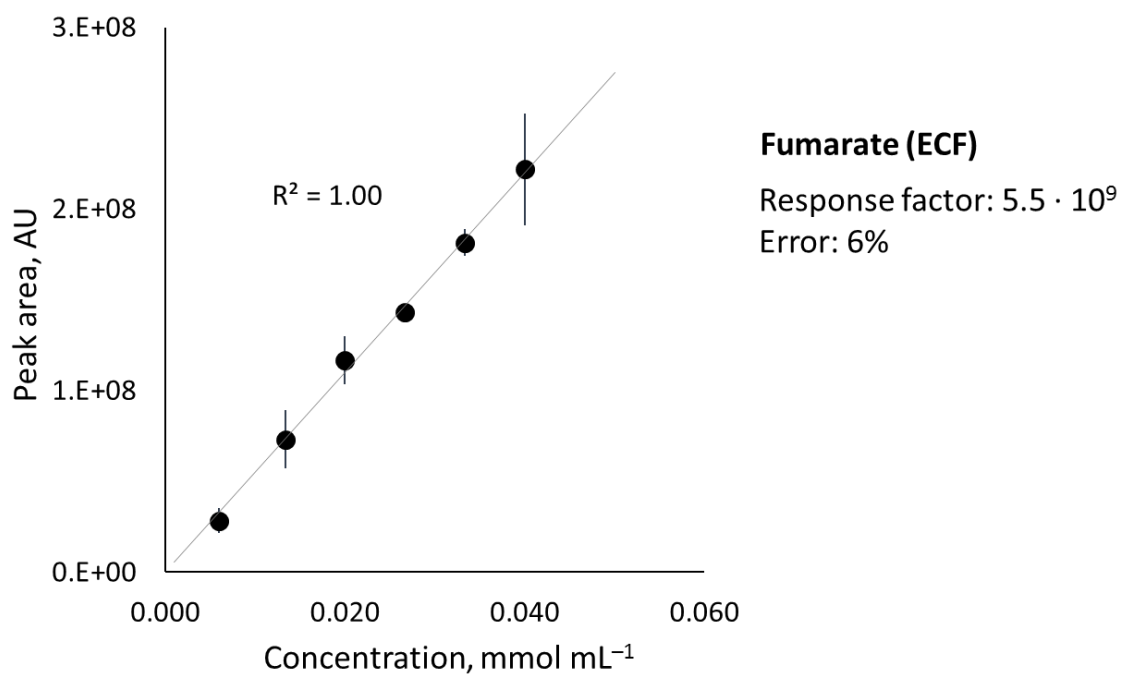


Figure S 97 Correlation between the concentration of an aqueous solution of fumarate and the measured gas chromatography peak area.

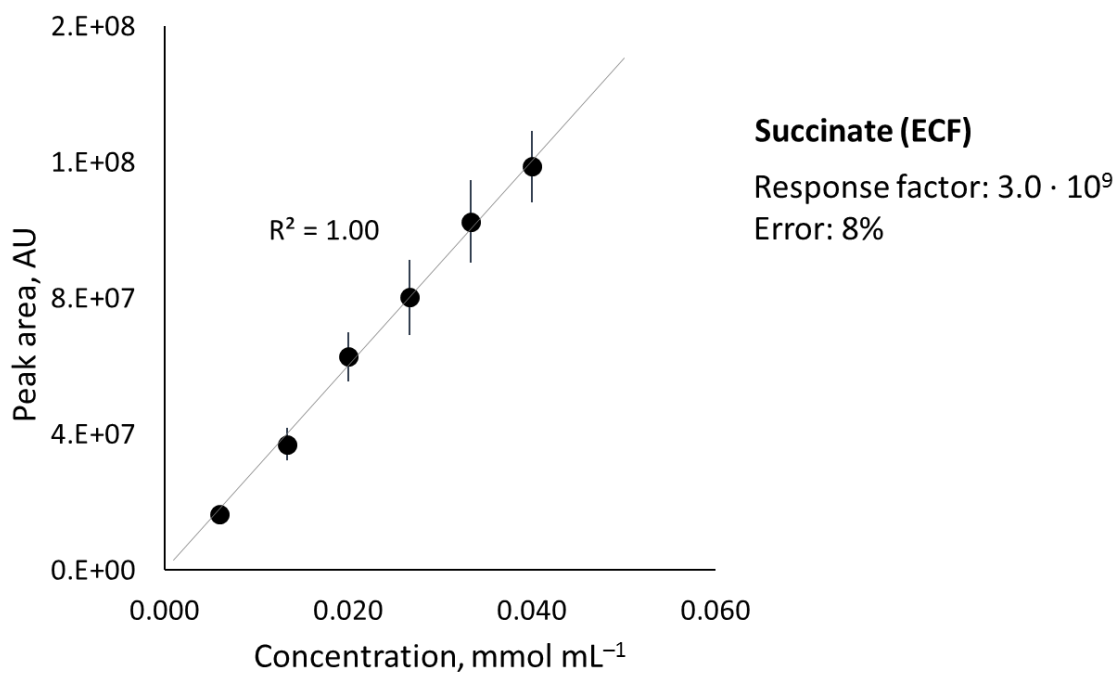


Figure S 98 Correlation between the concentration of an aqueous solution of succinate and the measured gas chromatography peak area.

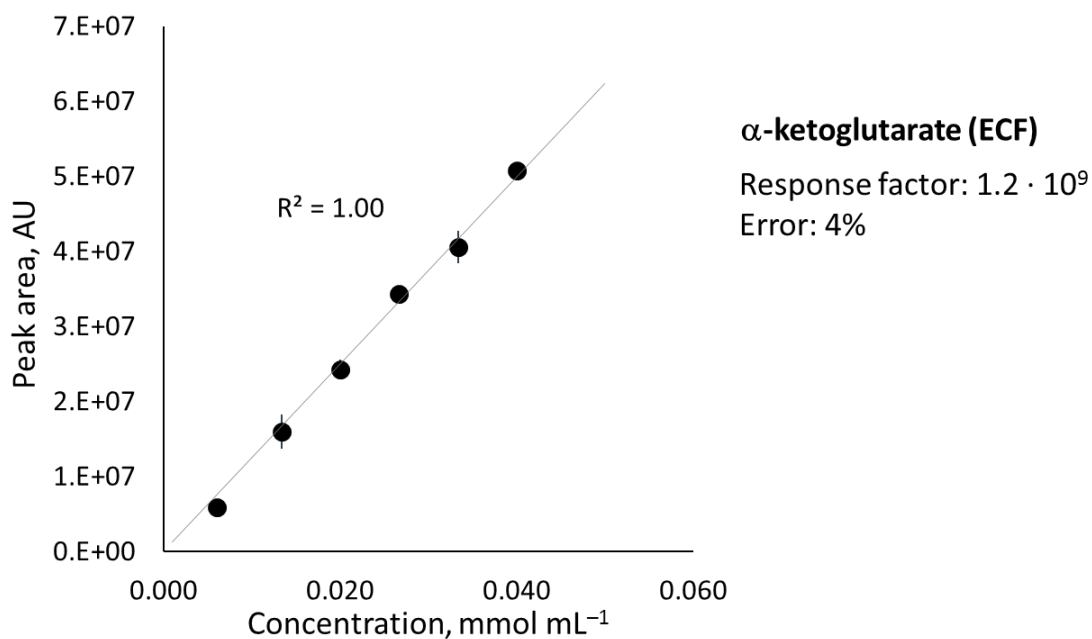


Figure S 99 Correlation between the concentration of an aqueous solution of α -ketoglutarate and the measured gas chromatography peak area.

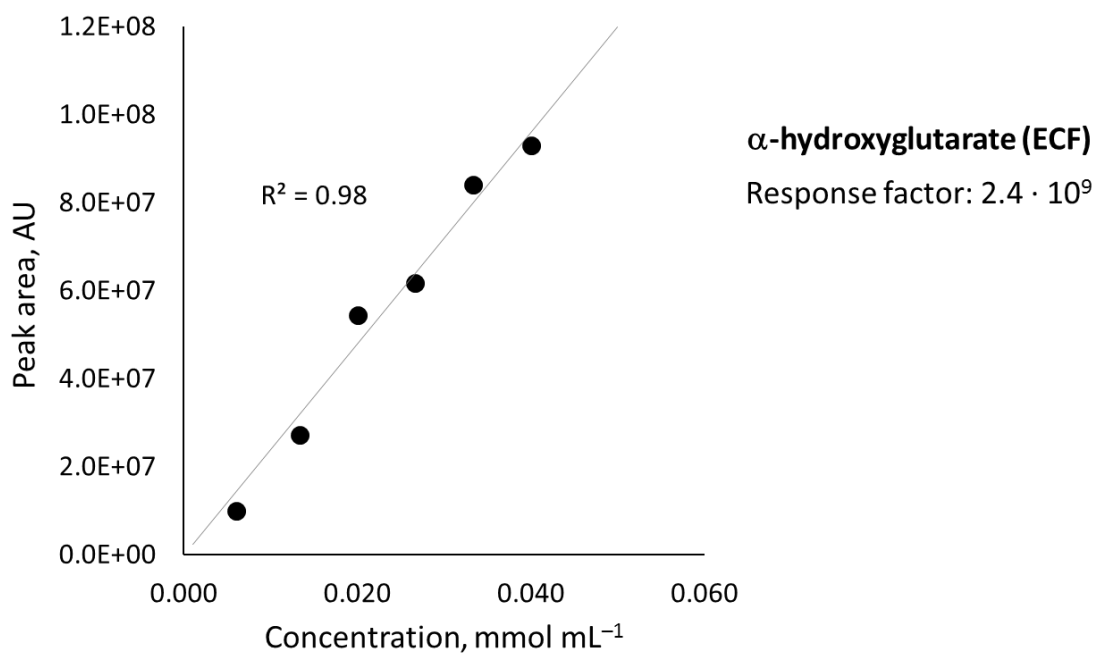


Figure S 100 Correlation between the concentration of an aqueous solution of α -hydroxyglutarate and the measured gas chromatography peak area. α -Hydroxyglutarate was obtained by a complete reduction of an aqueous solution of α -ketoglutarate with NaBH_4 . The correlation line shown here corresponds to a single run.

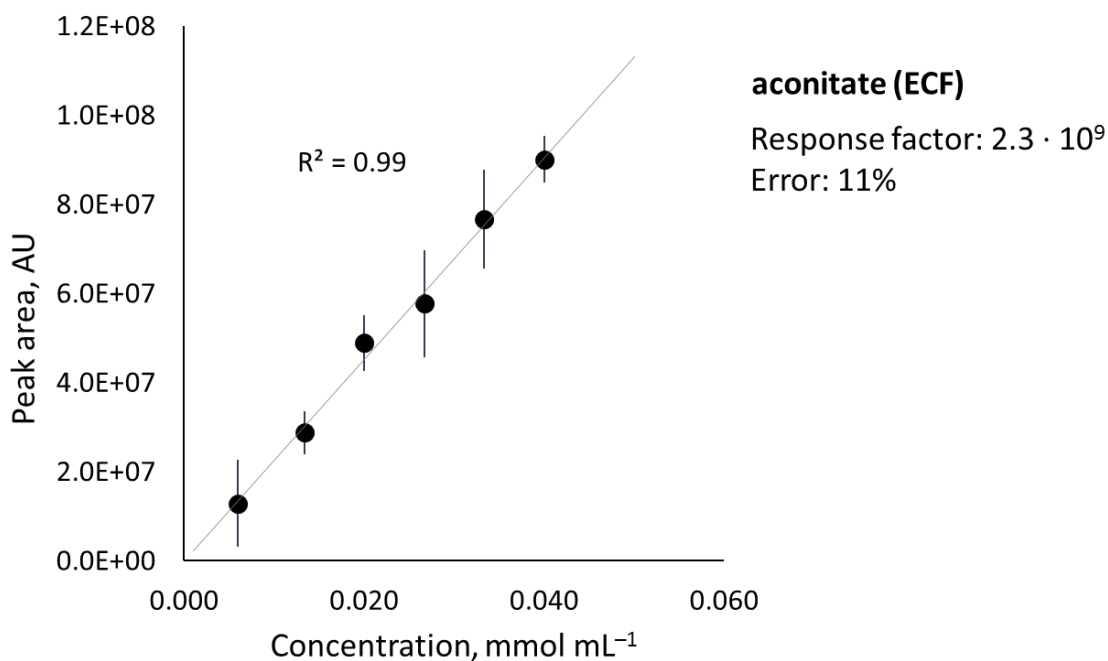


Figure S 101 Correlation between the concentration of an aqueous solution of cis-aconitate and the measured gas chromatography peak area.

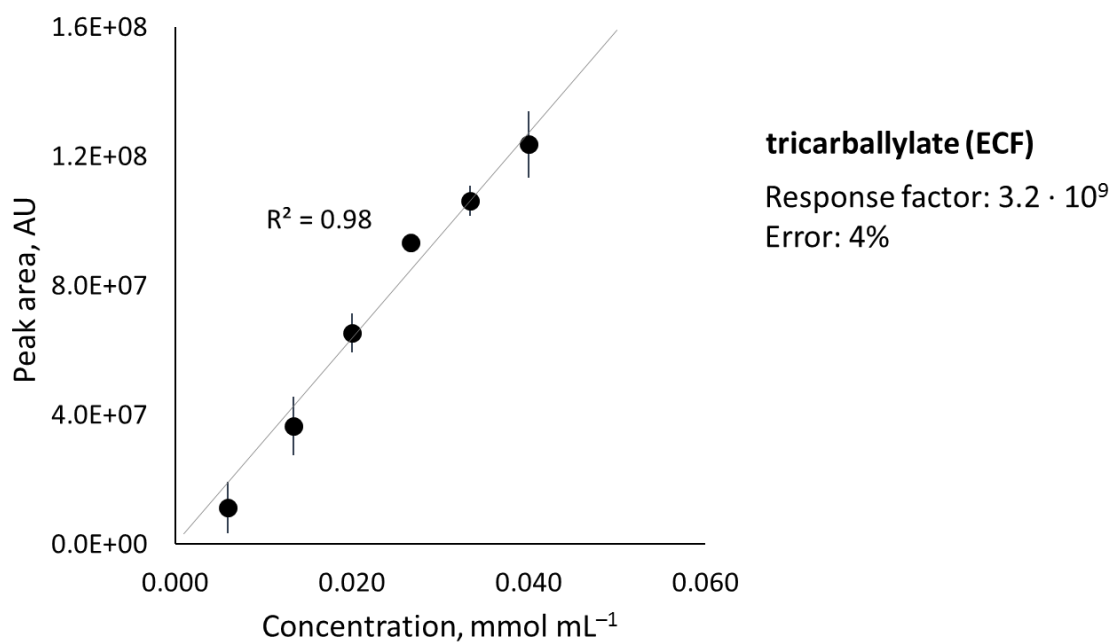


Figure S 102 Correlation between the concentration of an aqueous solution of tricarballylate and the measured gas chromatography peak area.

Derivatization with methyl chloroformate (MCF)

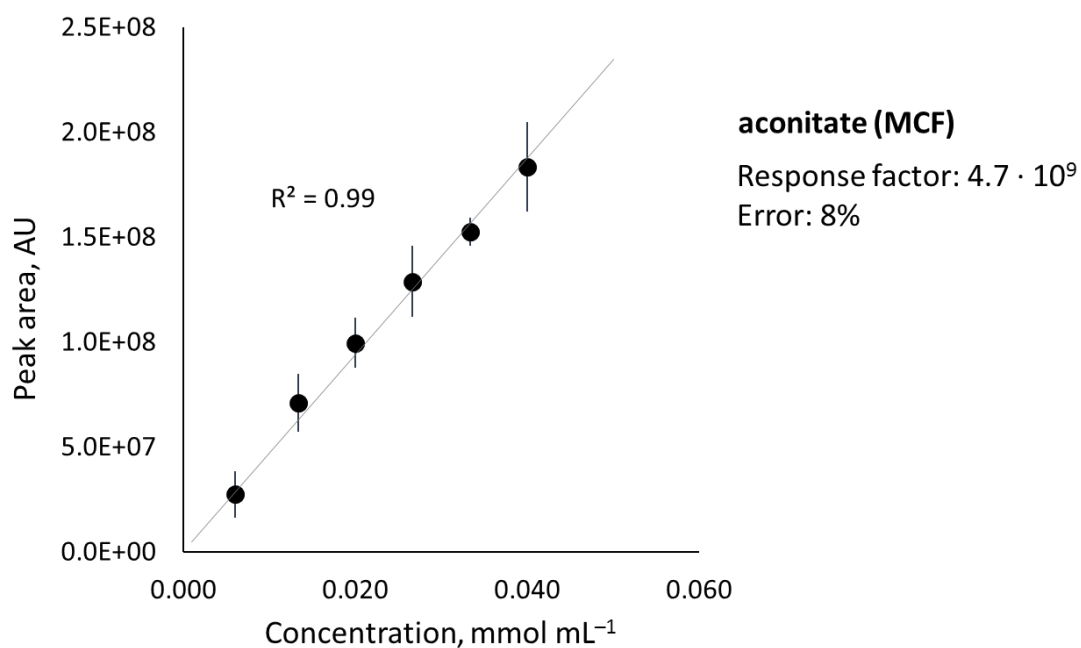


Figure S 103 Correlation between the concentration of an aqueous solution of cis-aconitate and the measured gas chromatography peak area.

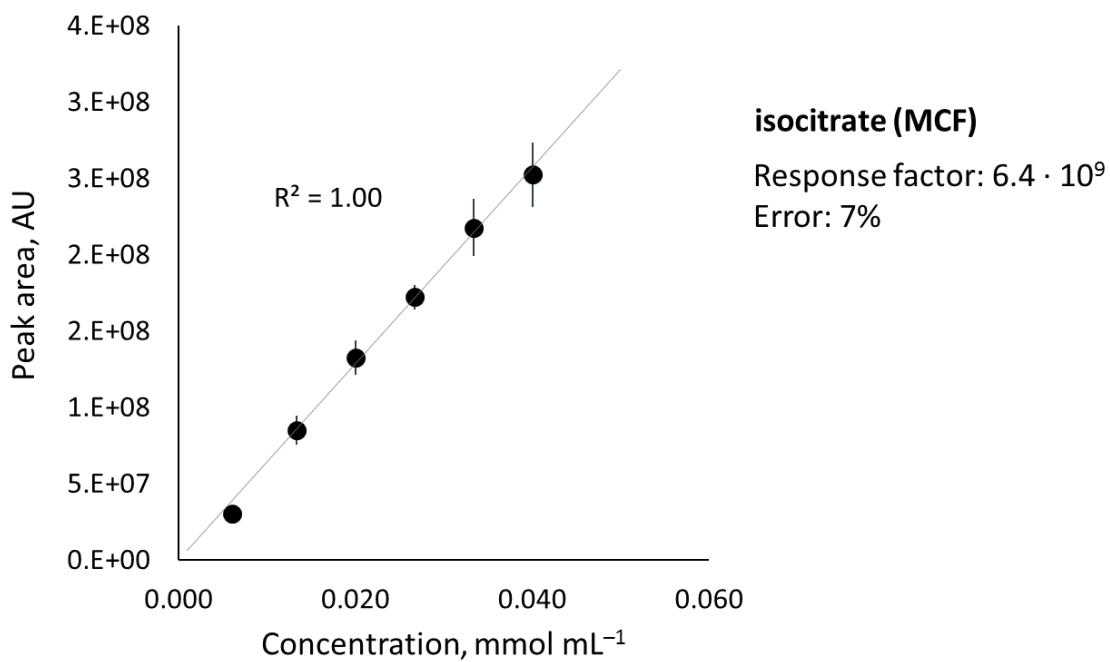


Figure S 104 Correlation between the concentration of an aqueous solution of isocitrate and the measured gas chromatography peak area.

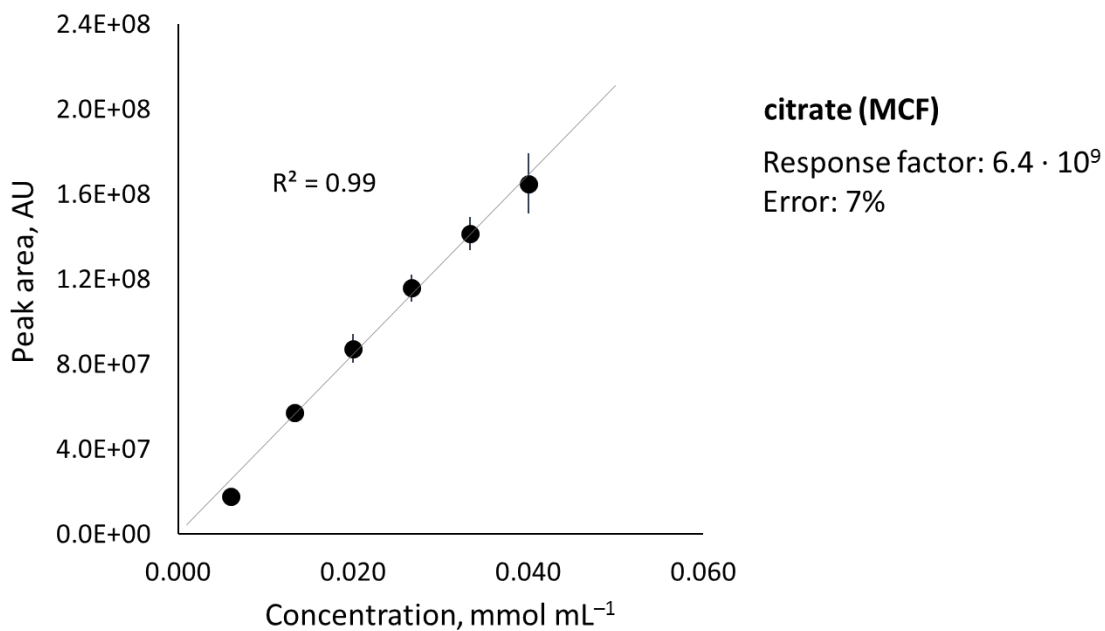


Figure S 105 Correlation between the concentration of an aqueous solution of citrate and the measured gas chromatography peak area.

Qualitative corroboration of GC-MS data by ^1H NMR

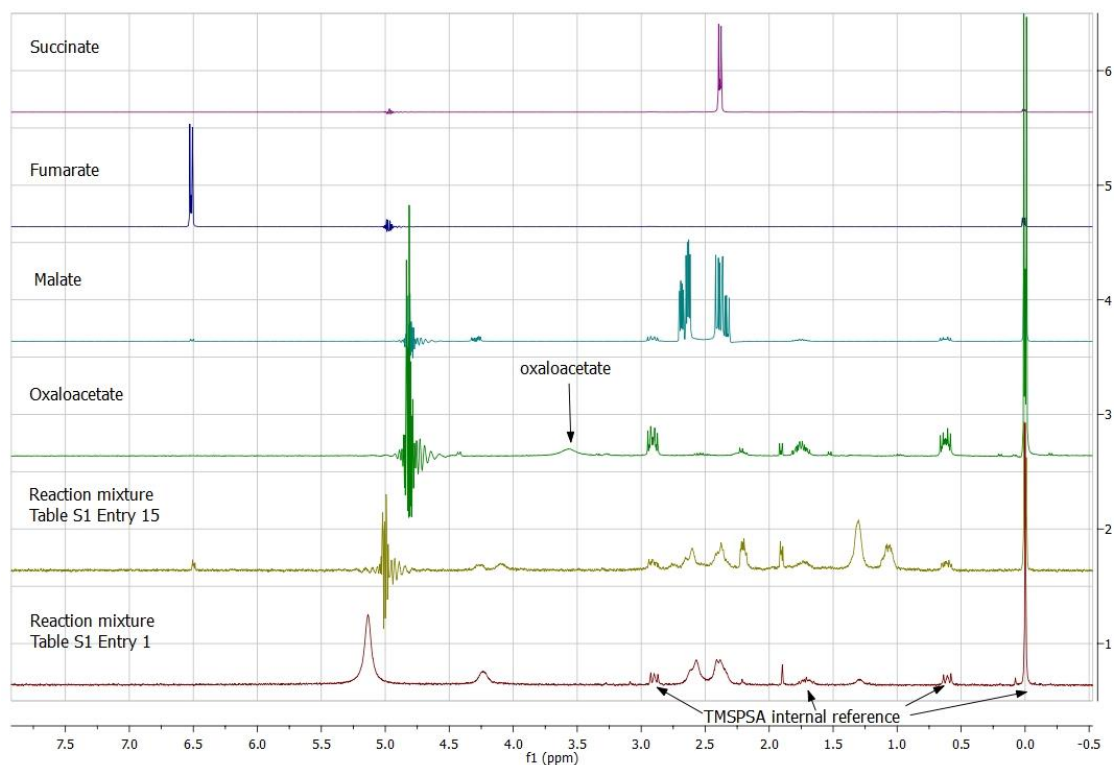


Figure S 106 Verification of Table S 1, entries 1 and 15 by ^1H NMR.

In an attempt to cross-validate the GC-MS analytical method under real reaction conditions, reactions run under conditions corresponding to Part III, Table S 1, entries 1 and 15 were basified, doped with an internal standard and analysed by ^1H NMR. The reaction mixture was basified with solid KOH (pH \sim 14) to precipitate metal cations. Subsequently, the mixture was centrifuged, and 600 μL of the supernatant was combined in an NMR tube with 75 μL of D_2O and 25 μL of 0.05 M sodium 3-(trimethylsilyl)-1-propanesulfonate (TMSPSA) as the internal reference (CH_3 peak at 0 ppm). Solvent suppression of water in the ^1H NMR was achieved using the Bruker ZGESGP 1D sequence for water suppression using excitation sculpting with gradient. Sixteen scans were acquired for each sample. Spectra of the reaction mixtures were compared against authentic substrate samples prepared using the same procedure. In both cases, resonances corresponding to oxaloacetate had disappeared and the same products detected by GC-MS were indeed confirmed to be present. While ^1H NMR under ZGESGP water suppression qualitatively validates the GC-MS data, we hesitate to use it as a quantitative technique for these reactions since (1) the chemical shifts of different di-acids are unresolved (e.g. malate and succinate), and a qualitative deconvolution of the peaks using ^1H - ^{13}C 2D NMR experiments is not practical at such low concentrations; (2) the water suppression technique affects the magnitude of resonances in proximity to the suppressed water resonance (e.g. the

peak of oxaloacetate at 3.5 ppm is not quantifiable); (3) any non-precipitated metal cations might bind the TCA acids, changing the chemical shifts of their typical resonances.

Appendix II

Yield determination and error analysis for CO₂ fixation reactions

700 μL aqueous solutions of potassium acetate, sodium methoxide, sodium pyruvate and sodium formate at different concentrations (0.71, 1.78, 3.57, 5.35, 7.14, 8.92 and 10.71 mM) were prepared by diluting their respective stock solutions (50 mM in Milli-Q water) with Milli-Q water to 600 μL and adding to each an aliquot of 100 μL of 50 mM solution of the standard compound (DSS-Na) in D₂O. Each of the samples was prepared in two replicas by two researchers and subjected to NMR spectroscopy (1H, ZGESGP water suppression, as described in the General information section). For each of these, three 32-scan spectra were acquired, to account for the instrumental errors. The data from these six measurements for every concentration allowed us to obtain seven-point calibration plots for formate, methanol, acetate and pyruvate, correlating the substrate-to-standard ratios of peaks (8.45 ppm for formate, 3.34 ppm for methanol, 2.36 for pyruvate or 2.08 ppm for acetate, 0 ppm for the methyl peak of the standard DSS-Na) with the product concentration (Figure S 107).

The data points were subjected to least-squares fitting (intercept = 0), from which the calibration line equation was obtained. Detection thresholds were estimated for each analyzed compound by integrating across the baseline in these regions of NMR spectra where no peaks were present, and were thus established to be 0.007 mM for acetate and pyruvate, 0.0016 mM for formate and 0.0026 mM for methanol. We note these values are much below the concentrations of acetate, pyruvate, methanol and formate detected in this study (Table S 8-Table S 25).

Error bars on the calibration graphs correspond to \pm standard deviation for each data point. The yields of the CO₂ fixation experiments were calculated using the calibration coefficient corresponding to the slope of each calibration line. All yields of the CO₂ fixation experiments reported in this study are an average of at least two independent runs, with an error corresponding to \pm mean absolute deviation.

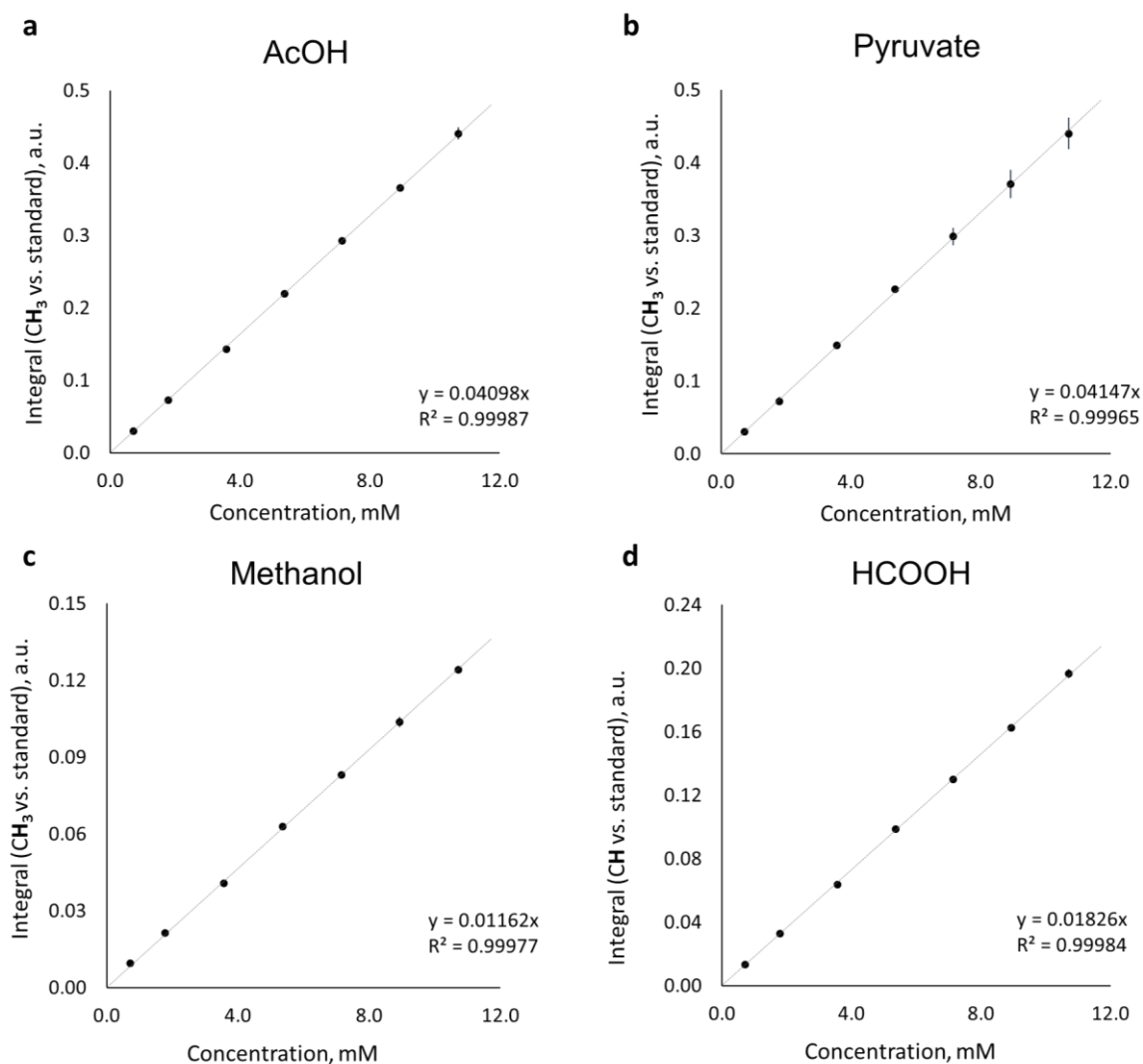


Figure S 107 Correlation between the concentration of an aqueous solution of (a) acetate and the ratio of the methyl peak (1.91 ppm), (b) pyruvate and the ratio of the methyl peak (2.36 ppm), (c) methanol and the ratio of the methyl peak (3.35 ppm), and (d) formate and the ratio of the formyl hydrogen peak (8.45 ppm), to the methyl peak of the standard (DSS-Na, 0 ppm). In the cases where error bars are not visible, the error is small enough to be contained within the data point marker.

Appendix III

Representative chromatograms and Mass spectrum for Glycine, Alanine, Aspartic acid and Glutamic acid

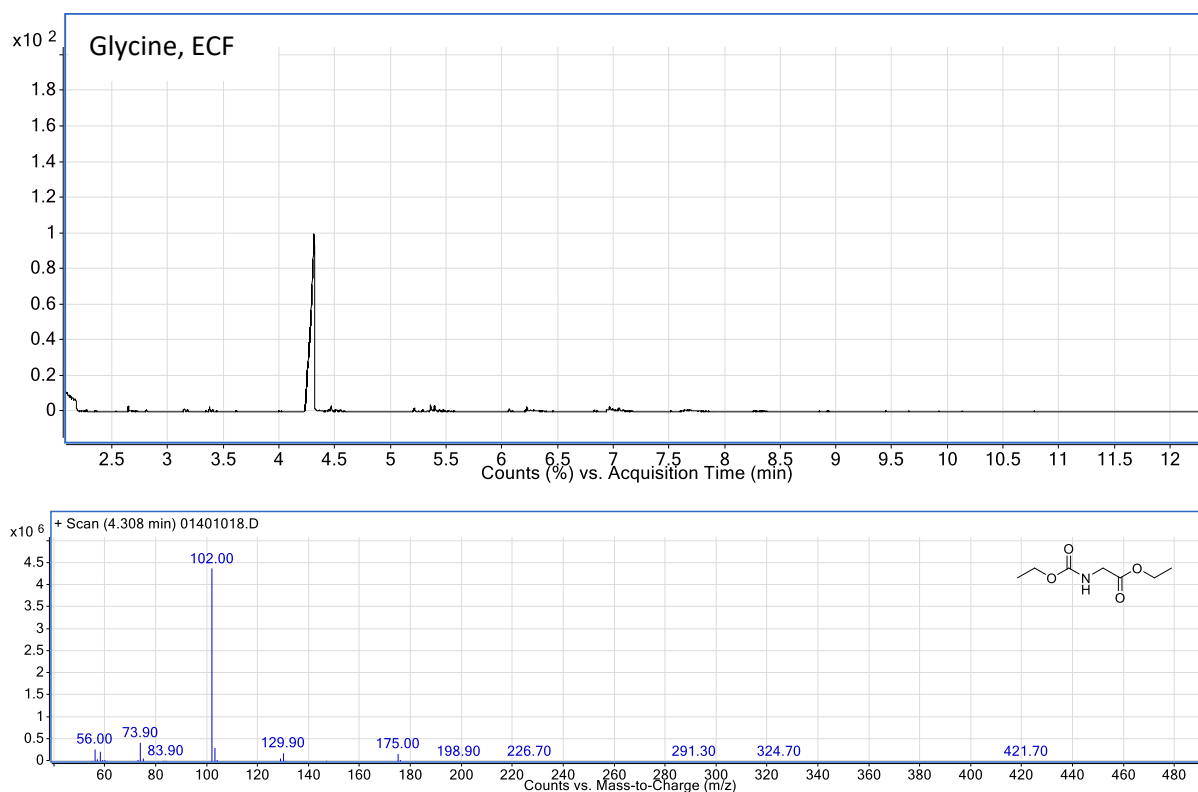


Figure S 108 GC trace and mass spectra of glycine characteristic peaks (ECF derivatization).

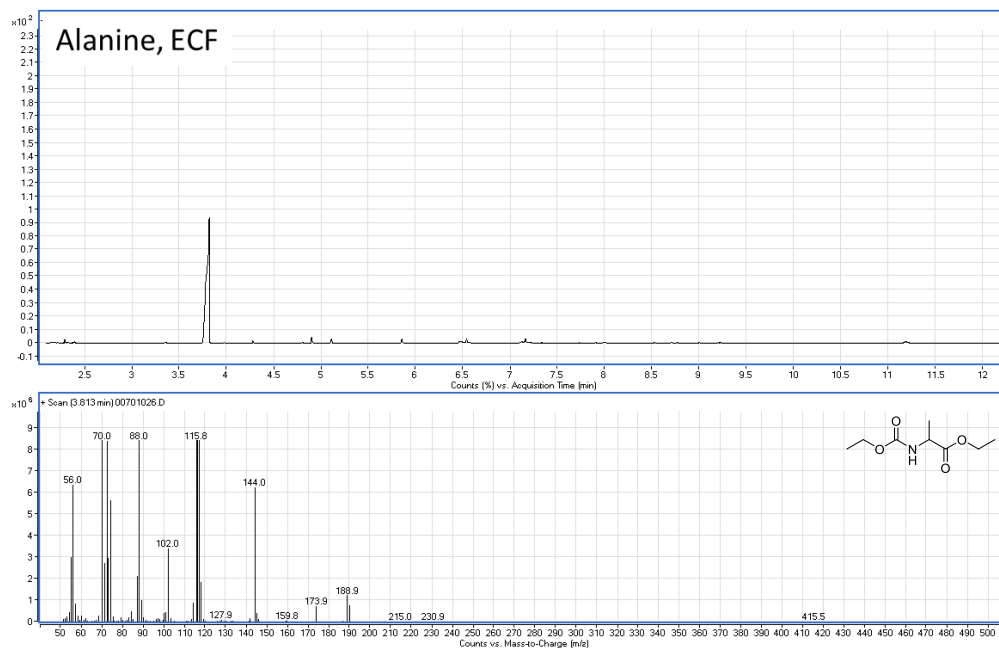


Figure S 109 GC trace and mass spectra of alanine characteristic peaks (ECF derivatization).

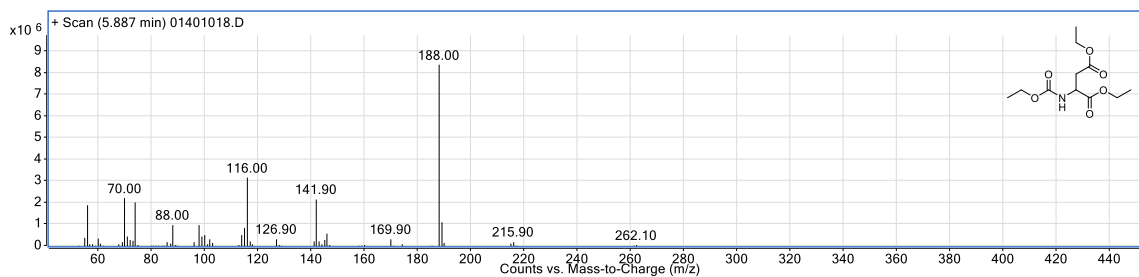
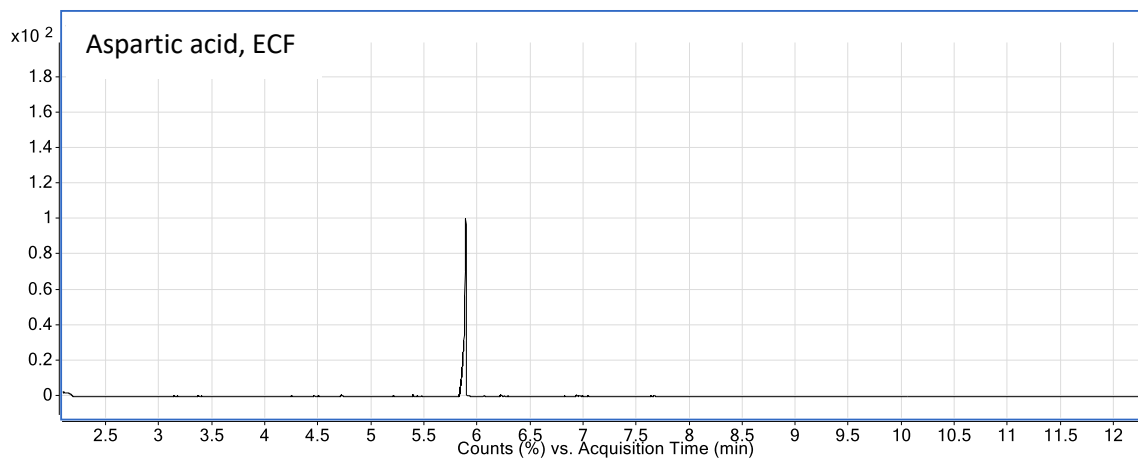
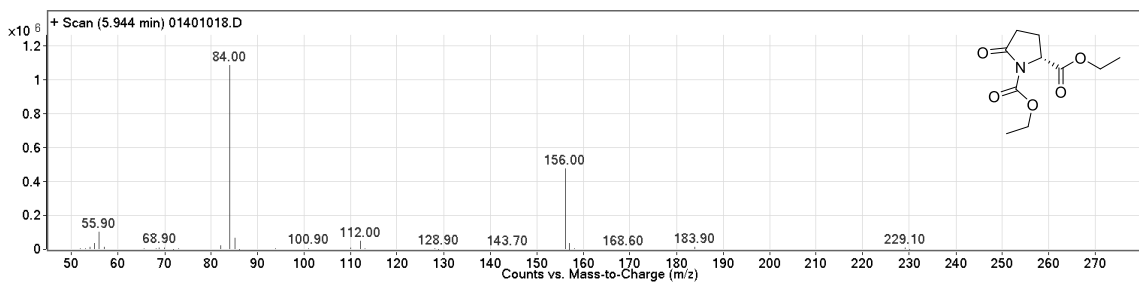
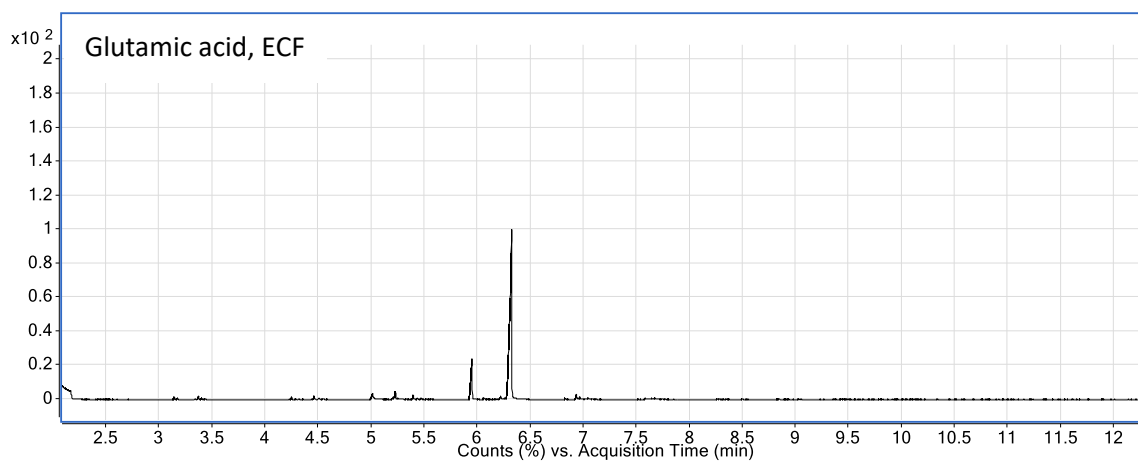


Figure S 110 GC trace and mass spectra of aspartic acid characteristic peaks (ECF derivatization).



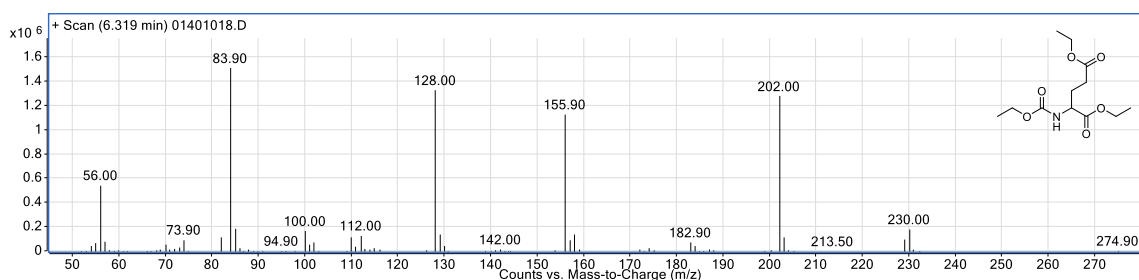


Figure S 111 GC trace and mass spectra of aspartic acid characteristic peaks (ECF derivatization).

Yield determination and error analysis

3 mL standard aqueous solutions of amino acids at different concentrations (0.006 M, 0.010 M, 0.013 M, 0.017 M, 0.020 M and 0.023 M) were prepared by diluting 0.1 – 0.5 M stock solutions of these amino acids. 200 μ L of each standard solution was derivatized using the derivatization procedure described herein (see: Part III, Chapter 3, Analytical procedures). For each acid, a six-point graph was plotted, correlating the sum of characteristic GC peaks (as integrated automatically by the *Agilent MassHunter Workstation v.B.06.00* software) with substrate concentration (Fig. S112-S115). Each data point was obtained from three independent measurements and the correlation line was obtained from the least-squares fitting (intercept = 0). Error bars on graphs are shown as \pm standard deviation for each data point. Overall percentage error of the response factor corresponds to \pm standard deviation for each slope value.

The yields of products were calculated by comparing the product peak area with the calibration line. For the purpose of this study, reported are not the absolute percentage yields based on the number of moles of the starting materials, but rather percentage contributions to the total composition of the final reaction mixture. This allows to account for potential concentration changes due to solvent loss (since many reactions were carried out in sealed tubes at temperatures above the boiling point of water), as well as potentially incomplete extraction during the derivatization procedure. Each reaction was performed at least twice to ensure reproducibility, and reported percentage compositions are an average of these two runs, with an error corresponding to \pm mean absolute deviation.

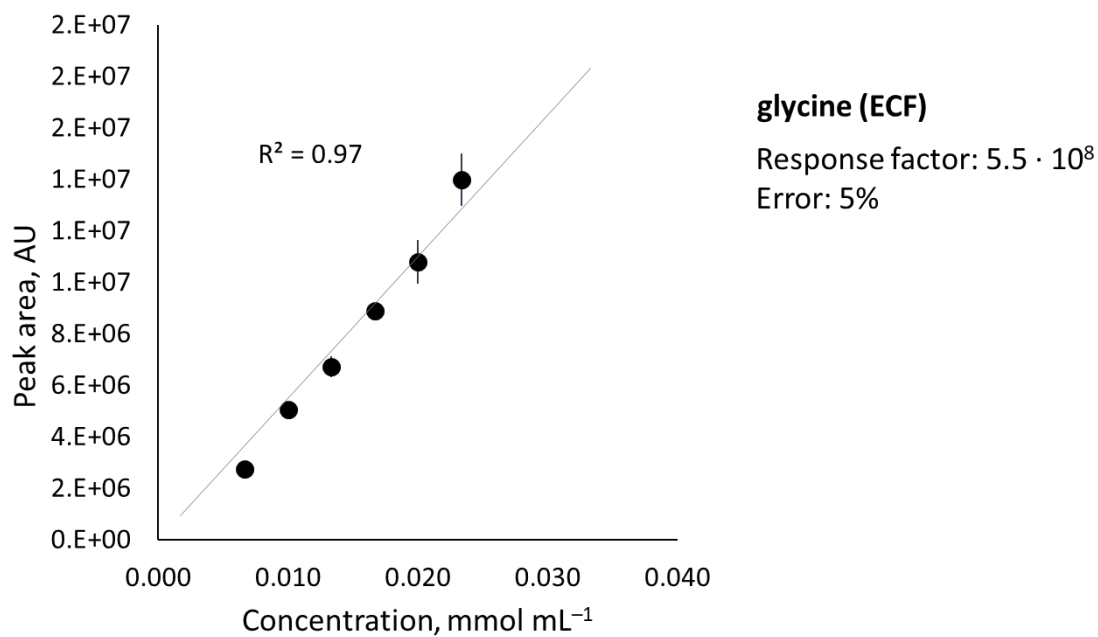


Figure S 112 Correlation between the concentration of an aqueous solution of glycine and the measured gas chromatography peak area.

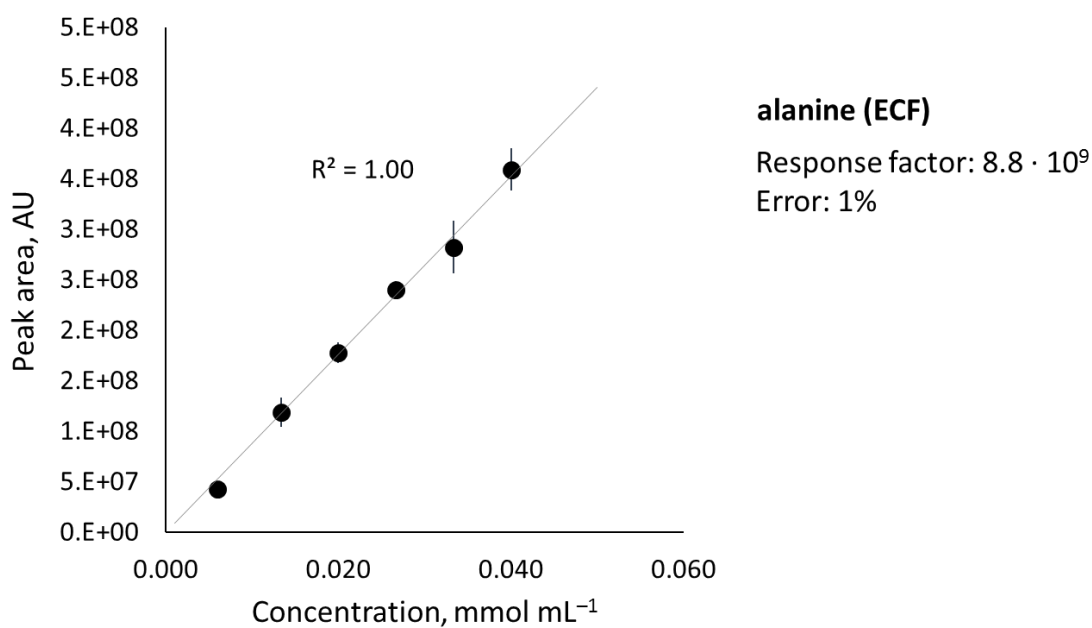


Figure S 113 Correlation between the concentration of an aqueous solution of alanine and the measured gas chromatography peak area.

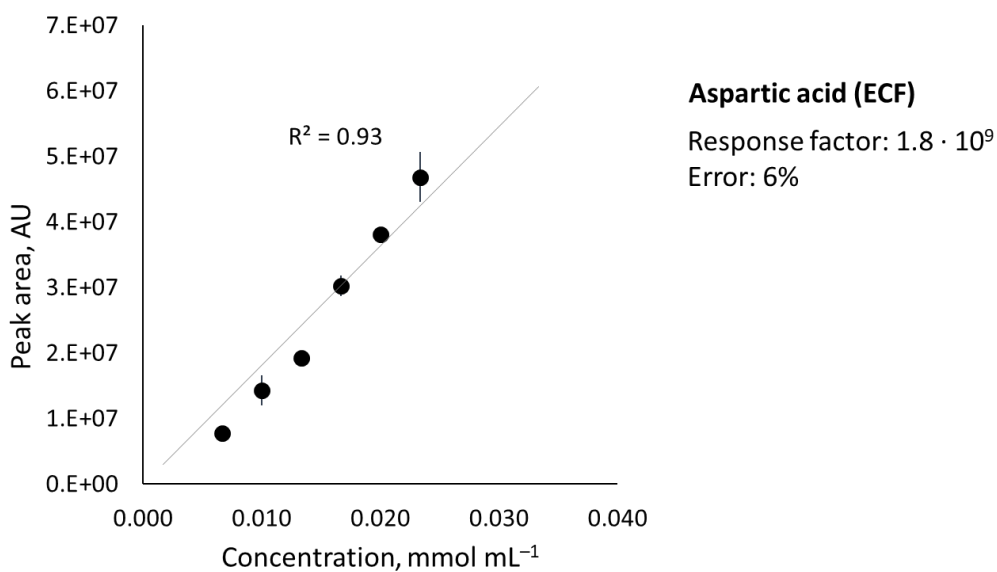


Figure S 114 Correlation between the concentration of an aqueous solution of aspartic acid and the measured gas chromatography peak area.

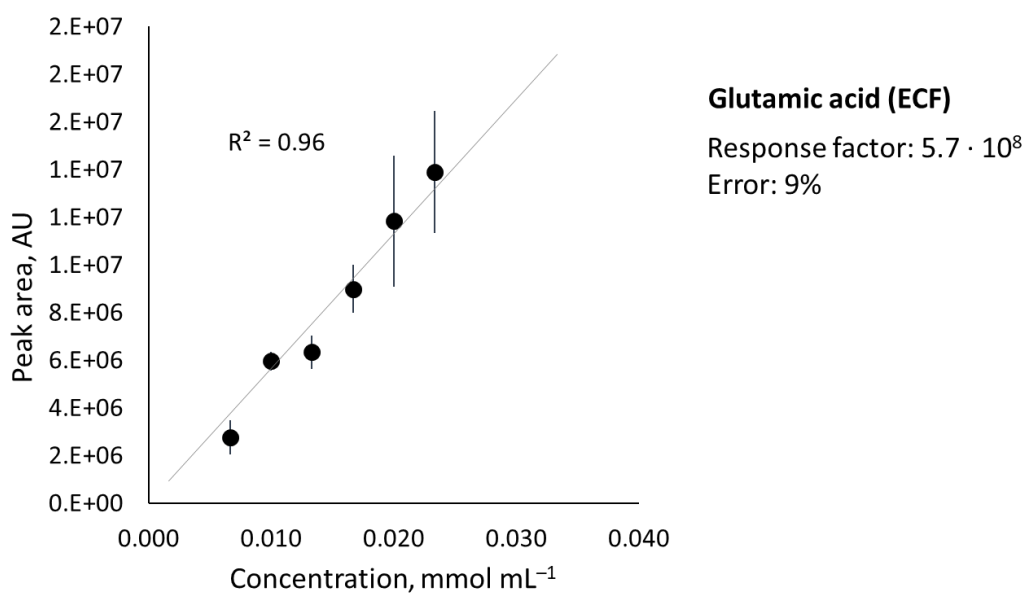


Figure S 115 Correlation between the concentration of an aqueous solution of glutamic acid and the measured gas chromatography peak area.

References

- ¹ Tirard, S. (2014). Abiogenesis. In *Encyclopedia of Astrobiology* (Berlin, Heidelberg: Springer Berlin Heidelberg), pp. 1–1.
- ² Wöhler, F. (1828). Ueber künstliche Bildung des Harnstoffs. *Ann. der Phys. und Chemie* 88, 253–256.
- ³ Pasteur, L. (1857). Mémoire sur la fermentation appelée lactique. *Compt. Rend.* 45, 913–916.
- ⁴ Peretó, J., Bada, J.L., and Lazcano, A. (2009). Charles Darwin and the Origin of Life. 395–406.
- ⁵ Fox, S.W. (2018). Aleksandr Oparin. *Encycl. Br. inc.* Available at: <https://www.britannica.com/biography/Aleksandr-Oparin> [Accessed July 16, 2018]
- ⁶ Schrödinger, E. (1992). *What is life? : the physical aspect of the living cell with Mind and matter & Autobiographical sketches*, Cambridge University Press (Cambridge, New York).)
- ⁷ Miller, S.L. (1953). A Production of Amino Acids Under Possible Primitive Earth Conditions. *Science* 117, 528–529.
- ⁸ Harada, K., and Fox, S.W. (1958). The Thermal Condensation of Glutamic Acid and Glycine to Linear Peptides. *J. Am. Chem. Soc.* 80, 2694–2697.
- ⁹ Oró, J. (1960). Synthesis of adenine from ammonium cyanide. *Biochem. Biophys. Res. Commun.* 2, 407–412.
- ¹⁰ Fox, S.W., and Matsuno, K. (1983). Genetic takeover and the mineral origins of life. *Trends Biochem. Sci.* 8, 341–342.
- ¹¹ Kruger, K., Grabowski, P.J., Zaug, A.J., Sands, J., Gottschling, D.E., and Cech, T.R. (1982). Self-splicing RNA: Autoexcision and autocyclization of the ribosomal RNA intervening sequence of tetrahymena. *Cell* 31, 147–157.
- ¹² Orgel, L.E. (1968). Evolution of the genetic apparatus. *J. Mol. Biol.* 38, 381–393.
- ¹³ Gilbert, W. (1986). Origin of life: The RNA world. *Nature* 319, 618–618.
- ¹⁴ Ferris, J.P., Huang, C.-H., and Hagan, W.J. (1988). Montmorillonite: A multifunctional mineral catalyst for the prebiological formation of phosphate esters. *Orig. Life Evol. Biosph.* 18, 121–133.
- ¹⁵ Eschenmoser, A., and Dobler, M. (1992). Warum Pentose- und nicht Hexose-Nucleinsäuren? Teil I. Einleitung und Problemstellung, Konformationsanalyse für Oligonucleotid-Ketten aus 2,3-Dideoxyglucopyranosyl-Bausteinen sowie Betrachtungen zur Konformation von A- und B-DNS. *Helv. Chim. Acta* 75, 218–259.
- ¹⁶ Nielsen, P.E., Egholm, M., Berg, R.H., and Buchardt, O. (1991). Sequence-selective recognition of DNA by strand displacement with a thymine-substituted polyamide. *Science* 254, 1497–1500.
- ¹⁷ Haase, R. (1972). P. Glansdorff and I. Prigogine: Thermodynamic Theory of Structure, Stability and Fluctuations, *Berichte der Bunsengesellschaft für Phys. Chemie* 76, 466–466.
- ¹⁸ Woese, C.R., and Fox, G.E. (1977). Phylogenetic structure of the prokaryotic domain: the primary kingdoms. *Proc. Natl. Acad. Sci. U. S. A.* 74, 5088–5090.
- ¹⁹ Russell, M. J., Hall, A. J. and Turner, D. (1989), *In vitro* growth of iron sulphide chimneys: possible culture chambers for origin-of-life experiments. *Terra Nova*, 1: 238-241.
- ²⁰ Martin, W., and Russell, M.J. (2007). On the origin of biochemistry at an alkaline hydrothermal vent. *Philos. Trans. R. Soc. B Biol. Sci.* 362, 1887–1926.
- ²¹ de Duve, C. (1998). Clues from present-day biology: the thioester world. In *The Molecular Origins of Life: Assembling Pieces of the Puzzle*, Cambridge, Cambridge University Press, 219–236.
- ²² Wächtershäuser, G. (1988). Before enzymes and templates: theory of surface metabolism. *Microbiol. Rev.* 52, 452–484.
- ²³ Wächtershäuser, G. (1990). Evolution of the first metabolic cycles. *Proc. Natl. Acad. Sci.* 87, 200–204.
- ²⁴ Blöchl, E., Keller, M., Wächtershäuser, G., and Stetter, K.O. (1992). Reactions depending on iron sulfide and linking geochemistry with biochemistry. *Proc. Natl. Acad. Sci. U. S. A.* 89, 8117–8120.
- ²⁵ Cleaves, H. (2013). Prebiotic Chemistry: Geochemical Context and Reaction Screening. *Life* 3, 331–345.
- ²⁶ Powner, M.W., Gerland, B., and Sutherland, J.D. (2009). Synthesis of activated pyrimidine ribonucleotides in prebiotically plausible conditions. *Nature* 459, 239–242.
- ²⁷ Shapiro, R. (2007) A Simpler Origin for Life: *Scientific American*. *Sci. Am.*, 296 (6), 46–53.
- ²⁸ Patel, B. H.; Percivalle, C.; Ritson, D. J.; Duffy, C. D.; Sutherland, J. D. (2015) Common Origins of RNA, Protein and Lipid Precursors in a Cyanosulfidic Protometabolism. *Nat. Chem.*, 7 (4), 301–307.
- ²⁹ Kun, Á., Papp, B., and Szathmáry, E. (2008). Computational identification of obligatorily autocatalytic replicators embedded in metabolic networks. *Genome Biol.* 9, R51.
- ³⁰ Orgel, L.E. (2008). The implausibility of metabolic cycles on the prebiotic earth. *PLoS Biol.* 6, 0005-0013.
- ³¹ Smith, E.; Morowitz, H. J. (2016) *The Origin and Nature of Life on Earth: The Emergence of the Fourth Geosphere*; Cambridge University Press.
- ³² Zahnle, K., Schaefer, L., and Fegley, B. (2010). Earth’s earliest atmospheres. *Cold Spring Harb. Perspect. Biol.* 2, 1–17.
- ³³ Evans, M.C., Buchanan, B.B., and Arnon, D.I. (1966). A new ferredoxin-dependent carbon reduction cycle in a photosynthetic bacterium. *Proc. Natl. Acad. Sci. U. S. A.* 55, 928–934.

- ³⁴ Smith, E., and Morowitz, H.J. (2004). Universality in intermediary metabolism. *Proc. Natl. Acad. Sci. U. S. A.* *101*, 13168–13173.
- ³⁵ Weiss, M.C., Sousa, F.L., Mrnjavac, N., Neukirchen, S., Roettger, M., Nelson-Sathi, S., and Martin, W.F. (2016). The physiology and habitat of the last universal common ancestor. *Nat. Microbiol.* *1*, 1–8.
- ³⁶ Nitschke, W., and Russell, M.J. (2013). Beating the acetyl coenzyme A-pathway to the origin of life. *Philos. Trans. R. Soc. B Biol. Sci.* *368*, 20120258–20120258.
- ³⁷ Sousa, F.L., and Martin, W.F. (2014). Biochemical fossils of the ancient transition from geoenergetics to bioenergetics in prokaryotic one carbon compound metabolism. *Biochim. Biophys. Acta - Bioenerg.* *1837*, 964–981.
- ³⁸ Krebs, H.A., and Johnson, W.A. (1937). Metabolism of ketonic acids in animal tissues. *Biochem. J.* *31*, 645.
- ³⁹ Evans, M.C., Buchanan, B.B., and Arnon, D.I. (1966). A new ferredoxin-dependent carbon reduction cycle in a photosynthetic bacterium. *Proc. Natl. Acad. Sci. U. S. A.* *55*, 928–934.
- ⁴⁰ Braakman, R., and Smith, E. (2012). The emergence and early evolution of biological carbon-fixation. *PLoS Comput. Biol.* *8*, e1002455.
- ⁴¹ Ragsdale, S.W. (2008). Enzymology of the Wood-Ljungdahl pathway of acetogenesis. *Ann. N. Y. Acad. Sci.* *1125*, 129–136.
- ⁴² Buckel, W., and Thauer, R.K. (2013). Energy conservation via electron bifurcating ferredoxin reduction and proton/Na⁺ translocating ferredoxin oxidation. *Biochim. Biophys. Acta - Bioenerg.* *1827*, 94–113.
- ⁴³ Poehlein, A., Schmidt, S., Kaster, A.K., Goenrich, M., Vollmers, J., Thürmer, A., Bertsch, J., Schuchmann, K., Voigt, B., Hecker, M., *et al.* (2012). An ancient pathway combining carbon dioxide fixation with the generation and utilization of a sodium ion gradient for ATP synthesis. *PLoS One* *7*, E33439.
- ⁴⁴ Ferry, J.G. (1999). Enzymology of one-carbon metabolism in methanogenic pathways. *FEMS Microbiol. Rev.* *23*, 13–38.
- ⁴⁵ Zhu, X., and Tan, X. (2009). Metalloproteins/metalloenzymes for the synthesis of acetyl-CoA in the Wood-Ljungdahl pathway. *Sci. China, Ser. B Chem.* *52*, 2071–2082.
- ⁴⁶ Ragsdale, S.W. (2003). Pyruvate Ferredoxin Oxidoreductase and Its Radical Intermediate. *Chem. Rev.* *103*, 2333–2346.
- ⁴⁷ Yamamoto, M., Arai, H., Ishii, M., and Igarashi, Y. (2006). Role of two 2-oxoglutarate:ferredoxin oxidoreductases in *Hydrogenobacter thermophilus* under aerobic and anaerobic conditions. *FEMS Microbiol. Lett.* *263*, 189–193.
- ⁴⁸ Strain, S. (1996). 2-Oxoacid : Ferredoxin Oxidoreductase from the Thermoacidophilic. *120*, 587–599.
- ⁴⁹ Kai, Y., Matsumura, H., and Izui, K. (2003). Phosphoenolpyruvate carboxylase: Three-dimensional structure and molecular mechanisms. *Arch. Biochem. Biophys.* *414*, 170–179.
- ⁵⁰ Aoshima, M., and Igarashi, Y. (2006). A novel oxalosuccinate-forming enzyme involved in the reductive carboxylation of 2-oxoglutarate in *Hydrogenobacter thermophilus* TK-6. *Mol. Microbiol.* *62*, 748–759.
- ⁵¹ Aoshima, M., Ishii, M., and Igarashi, Y. (2004). A novel biotin protein required for reductive carboxylation of 2-oxoglutarate by isocitrate dehydrogenase in *Hydrogenobacter thermophilus* TK-6. *Mol. Microbiol.* *51*, 791–798.
- ⁵² Atkinson, D.E., Barnes, L.D., and McGuire, J.J. (1972). Yeast Diphosphopyridine Nucleotide Specific Isocitrate Dehydrogenase. Regulation of Activity and Unidirectional Catalysis. *Biochemistry* *11*, 4322–4329.
- ⁵³ Yogev, O., Naamati, A., and Pines, O. (2011). Fumarase: A paradigm of dual targeting and dual localized functions. *FEBS J.* *278*, 4230–4242.
- ⁵⁴ Neilson, N.E. (1955). The aconitase of *Aspergillus niger*. *BBA - Biochim. Biophys. Acta* *17*, 139–140.
- ⁵⁵ Broderick, J.B. (2003). 8.27 Iron–Sulfur Clusters in Enzyme Catalysis. In *Comprehensive Coordination Chemistry II* (East Lansing, Michigan, USA: Michigan State University), pp. 739–757.
- ⁵⁶ Maklashina, E., Hellwig, P., Rothery, R.A., Kotlyar, V., Sher, Y., Weiner, J.H., and Cecchini, G. (2006). Differences in protonation of ubiquinone and menaquinone in fumarate reductase from *Escherichia coli*. *J. Biol. Chem.* *281*, 26655–26664.
- ⁵⁷ Miura, A., Kameya, M., Arai, H., Ishii, M., and Igarashi, Y. (2008). A soluble NADH-dependent fumarate reductase in the reductive tricarboxylic acid cycle of *Hydrogenobacter thermophilus* TK-6. *J. Bacteriol.* *190*, 7170–7177.
- ⁵⁸ Fraser, M.E., James, M.N.G., Bridger, W.A., and Wolodko, W.T. (1999). A detailed structural description of *Escherichia coli* succinyl-CoA synthetase. *J. Mol. Biol.* *285*, 1633–1653.
- ⁵⁹ Aoshima, M., Ishii, M., and Igarashi, Y. (2004). A novel enzyme, citryl-CoA lyase, catalysing the second step of the citrate cleavage reaction in *Hydrogenobacter thermophilus* TK-6. *Mol. Microbiol.* *52*, 763–770.
- ⁶⁰ Kanao, T., Fukui, T., Atomi, H., and Imanaka, T. (2002). Kinetic and biochemical analyses on the reaction mechanism of a bacterial ATP-citrate lyase. *Eur. J. Biochem.* *269*, 3409–3416.
- ⁶¹ Schmid, M., Wild, M.R., Dahinden, P., and Dimroth, P. (2002). Subunit γ of the oxaloacetate decarboxylase Na⁺ pump: Interaction with other subunits/domains of the complex and binding site for the Zn²⁺ metal ion. *Biochemistry* *41*, 1285–1292.

-
- ⁶² Wiegand, G., and Remington, S.J. (1986). Citrate Synthase: Structure, Control, and Mechanism. *Annu. Rev. Biophys. Biophys. Chem.* 15, 97–117.
- ⁶³ Yankovskaya, V., Horsefield, R., Törnroth, S., Luna-Chavez, C., Miyoshi, H., Léger, C., Byrne, B., Cecchini, G., and Iwata, S. (2003). Architecture of succinate dehydrogenase and reactive oxygen species generation. *Science*, 299, 700–704.
- ⁶⁴ Voet, D., Voet, J.G., and Pratt, C.W. (2015). *Fundamentals of Biochemistry: Life at the Molecular Level*, pp 574-575.
- ⁶⁵ Atkinson, D.E., Barnes, L.D., and McGuire, J.J. (1972). Yeast Diphosphopyridine Nucleotide Specific Isocitrate Dehydrogenase. Regulation of Activity and Unidirectional Catalysis. *Biochemistry* 11, 4322–4329.
- ⁶⁶ Zhou, Z.H., McCarthy, D.B., O'Connor, C.M., Reed, L.J., and Stoops, J.K. (2001). The remarkable structural and functional organization of the eukaryotic pyruvate dehydrogenase complexes. *Proc National Acad Sci* 98, 14802–14807.
- ⁶⁷ McCartney, R.G., Rice, J.E., Sanderson, S.J., Bunik, V., Lindsay, H., and Lindsay, J.G. (1998). Subunit Interactions in the Mammalian α -Ketoglutarate Dehydrogenase Complex. *J. Biol. Chem.* 273, 24158–24164.
- ⁶⁸ Schulze, U. (1995) *Anaerobic Physiology of Saccharomyces Cerevisiae*; Thesis, Technical University of Denmark.
- ⁶⁹ McMurry, J. E., and Begley, T. P. (2016) *The Organic Chemistry of Biological Pathways* 2nd ed., Roberts and Company Publishers, Inc., Greenwood Village, Colorado.
- ⁷⁰ Liaw, S. -H, Kuo, I., and Eisenberg, D. (1995). Discovery of the ammonium substrate site on glutamine synthetase, A third cation binding site. *Protein Sci.* 4, 2358–2365.
- ⁷¹ Srinivasan, V., and Morowitz, H.J. (2009). Analysis of the Intermediary Metabolism of a Reductive Chemoautotroph. *Biol. Bull.* 217, 222–232.
- ⁷² Carbonell, P., Lecointres, G., and Faulon, J.L. (2011). Origins of specificity and promiscuity in metabolic networks. *J. Biol. Chem.* 286, 43994–44004.
- ⁷³ Olson, M. V, and Taube, H. (1970). Hydration and isomerization of coordinated maleate. *J. Am. Chem. Soc.* 92, 3236–3237.
- ⁷⁴ Rozelle, L.T., and Alberty, R. A. (1957). Kinetics of the acid catalysis of the hydration of fumaric acid to malic acid. *J. Phys. Chem.* 61, 1637–1640.
- ⁷⁵ Gahan, L.R., Harrowfield, J.M., Herlt, A.J., Lindoy, L.F., Whimp, P.O., and Sargeson, A.W. (1985). Metal ion promoted hydration of pendant alkenes and its possible relationship to aconitase. *J. Am. Chem. Soc.* 107, 6231–6242.
- ⁷⁶ Nakajima, T., Yabushita, Y., and Tabushi, I. (1975). Amino acid synthesis through biogenetic-type CO₂ fixation. *Nature* 256, 60.
- ⁷⁷ Cody, G.D., Boctor, N.Z., Filley, T.R., Hazen, R.M., Scott, J.H., Sharma, A., and Yoder, H.S. (2000). Primordial Carbonylated Iron-Sulfur Compounds and the Synthesis of Pyruvate. *Science* 289, 1337–1340.
- ⁷⁸ Pokhodenko, V.D., Koshechko, V.G., Titov, V.E., and Lopushanskaja, V.A. (1995). A convenient electrochemical synthesis of α -oxoacids. *Tetrahedron Lett.* 36, 3277–3278.
- ⁷⁹ Wang, W., Yang, B., Qu, Y., Liu, X., and Su, W. (2011). FeS/S/FeS₂ Redox System and Its Oxidoreductase-like Chemistry in the Iron-Sulfur World. *Astrobiology* 11, 471–476.
- ⁸⁰ Zhang, X. V., and Martin, S.T. (2006). Driving parts of Krebs cycle in reverse through mineral photochemistry. *J. Am. Chem. Soc.* 128, 16032–16033.
- ⁸¹ Keller, M.A., Kampjut, D., Harrison, S.A., and Ralser, M. (2017). Sulfate radicals enable a non-enzymatic Krebs cycle precursor. *Nat. Ecol. Evol.* 1, 83.
- ⁸² Buckel, W., and Thauer, R.K. (2013). Energy conservation via electron bifurcating ferredoxin reduction and proton/Na⁺ translocating ferredoxin oxidation. *Biochim. Biophys. Acta - Bioenerg.* 1827, 94–113.
- ⁸³ Bernát, I. (1983). The Distribution of Iron in Nature. In *Iron Metabolism* (Boston, MA: Springer US), pp. 9–13.
- ⁸⁴ Ruiz-Mirazo, K., Briones, C. & de la Escosura, A. (2014) Prebiotic systems chemistry: new perspectives for the origins of life. *Chem. Rev.* 114, 285–366.
- ⁸⁵ Camprubi, E., Jordan, S.F., Vasiliadou, R., and Lane, N. (2017). Iron catalysis at the origin of life. *IUBMB Life* 69, 373–381.
- ⁸⁶ Ragsdale, S.W., and Pierce, E. (2008). Acetogenesis and the Wood–Ljungdahl pathway of CO₂ fixation. *Biochim. Biophys. Acta - Proteins Proteomics* 1784, 1873–1898.
- ⁸⁷ Huber, C. and Wächtershäuser, G. (1997). Activated acetic acid by carbon fixation on (Fe,Ni)S under primordial conditions. *Science* 276, 245–247.
- ⁸⁸ Cody, G.D., Boctor, N.Z., Filley, T.R., Hazen, R.M., Scott, J.H., Sharma, A., and Yoder, H.S. (2000). Primordial Carbonylated Iron-Sulfur Compounds and the Synthesis of Pyruvate. *Science* (80-). 289, 1337–1340.
- ⁸⁹ Takahashi, H., Liu, L.H., Yashiro, Y., Ioku, K., Bignall, G., Yamasaki, N., and Kori, T. (2006). CO₂ reduction using hydrothermal method for the selective formation of organic compounds. *J. Mater. Sci.* 41, 1585–1589.

-
- ⁹⁰ He, C., Tian, G., Liu, Z., and Feng, S. (2010). A mild hydrothermal route to fix carbon dioxide to simple carboxylic acids. *Org. Lett.* *12*, 649–651.
- ⁹¹ Liu, Y., Chen, S., Quan, X., and Yu, H. (2015). Efficient Electrochemical Reduction of Carbon Dioxide to Acetate on Nitrogen-Doped Nanodiamond. *J. Am. Chem. Soc.* *137*, 11631–11636.
- ⁹² Roldan, A., Hollingsworth, N., Roffey, A., Islam, H.-U., Goodall, J.B.M., Catlow, C.R.A., Darr, J.A., Bras, W., Sankar, G., Holt, K.B., *et al.* (2015). Bio-inspired CO₂ conversion by iron sulfide catalysts under sustainable conditions. *Chem. Commun.* *51*, 7501–7504.
- ⁹³ Klöck, W., Palme, H. and Tobschall, H. J. (1986). Trace elements in natural metallic iron from Disko Island, Greenland. *Contrib. Mineral. Petrol.* *93*, 273–282.
- ⁹⁴ McCollom, T. M. (2016). Abiotic methane formation during experimental serpentinization of olivine. *Proc. Natl Acad. Sci. USA* *113*, 13965–13970.
- ⁹⁵ Sleep, N. H., Meibom, A., Fridriksson, T., Coleman, R. G. and Bird, D. K. (2004) H₂-rich fluids from serpentinization: geochemical and biotic implications. *Proc. Natl Acad. Sci. USA* *101*, 12818–12823.
- ⁹⁶ Frost, D. J. *et al.* (2004). Experimental evidence for the existence of iron-rich metal in the Earth's lower mantle. *Nature* *428*, 409–412.
- ⁹⁷ Russell, M. J., Hall, A. J. & Mellersh, A. R. (2003). in *Natural and Laboratory Simulated Thermal Geochemical Processes* (ed. Ikan, R.) 325–388 (Springer, Dordrecht).
- ⁹⁸ Bassez, M.-P. (2015) Water, air, earth and cosmic radiation. *Orig. Life Evol. Biosph.* *45*, 5–13.
- ⁹⁹ Bassez, M.-P. (2017) Anoxic and oxic oxidation of rocks containing Fe(II) Mg-silicates and Fe(II)-monosulfides as source of Fe(III)-minerals and hydrogen. *Geobiotropy. Orig. Life Evol. Biosph.* *47*, 453–480.
- ¹⁰⁰ Hughes, A. (2009). *Amino Acids, Peptides and Proteins in Organic Chemistry*, Wiley-VCH Verlag GmbH & Co (Weinheim, Germany)
- ¹⁰¹ Ruiz-Bermejo, M., Osuna-Esteban, S., and Zorzano, M.-P. (2013). Role of Ferrocyanides in the Prebiotic Synthesis of α -Amino Acids. *Orig. Life Evol. Biosph.* *43*, 191–206.
- ¹⁰² Taillades, J., Beuzelin, I., Garrel, L., Tabacik, V., Bied, C., and Commeyras, A. (1998). N-carbamoyl- α -amino acids rather than free α -amino acids formation in the primitive hydrosphere: A novel proposal for the emergence of prebiotic peptides. *Orig. Life Evol. Biosph.* *28*, 61–77.
- ¹⁰³ Kitadai, N., and Maruyama, S. (2018). Origins of building blocks of life: A review. *Geoscience Frontiers* *9*, 1117–1153.
- ¹⁰⁴ Huber, C., and Wächtershäuser, G. (2003). Primordial reductive amination revisited. *Tetrahedron Lett.* *44*, 1695–1697.
- ¹⁰⁵ Nakamura, K., Ohno, A., and Oka, S. (1977). Reduction by a model of NAD(P)H. XIX. Mimesis for the reaction with glutamate dehydrogenases. *Tetrahedron Lett.* *18*, 4593–4594.
- ¹⁰⁶ Shinkai, S., Hamada, H., Dohyama, A., and Manabe, O. (1980). NADH Model Reduction Biomimetic Synthesis of α -amino acids from α -keto acids. *Tetrahedron Lett.* *21*, 1661–1664.
- ¹⁰⁷ Ogo, S., Uehara, K., Abura, T., and Fukuzumi, S. (2004). pH-Dependent Chemoselective Synthesis of α -Amino Acids. Reductive Amination of α -Keto Acids with Ammonia Catalyzed by Acid-Stable Iridium Hydride Complexes in Water. *J. Am. Chem. Soc.* *126*, 3020–3021.
- ¹⁰⁸ Wang, W., Liu, X., Yang, Y., and Su, W. (2013). Reversible transformation between α -oxo acids and α -amino acids on ZnS particles: a photochemical model for tuning the prebiotic redox homeostasis. *Int. J. Astrobiol.* *12*, 69–77.
- ¹⁰⁹ Scholz, F., and Kahlert, H. (2015). The calculation of the solubility of metal hydroxides, oxide-hydroxides, and oxides, and their visualisation in logarithmic diagrams. *ChemTexts* *1*, 7.
- ¹¹⁰ Hale, A.J. (1919). *The Manufacture of Chemicals by Electrolysis* (Van Nostrand).
- ¹¹¹ Osswald, P., Geisler, W. (1941). Process of preparing hydroxylamine hydrochloride (US2242477). U.S. Patent Office.
- ¹¹² Friedman, L., Kosower, E. (1955) *Org. Synth.*, *3*, 510.
- ¹¹³ Bruce, W. F. (1937) *Org. Synth.*, *17*, 1.
- ¹¹⁴ Smart, K. F., Aggio, R. B. M., Van Houtte, J. R., Villas-Bôas, S. G. (2010) *Nat. Protoc.*, *5*, 1709-1729.
- ¹¹⁵ Wiscelinus, W. (1889) *Ber. Dtsch. Chem. Ges.*, *22*, 885.
- ¹¹⁶ Choi, K. H., Lee, H. J. *et al.* (2009) *Anal. Chem.*, *81*, 4734-4741.
- ¹¹⁷ Muchowska, K. B., *et al.* (2017) Metals promote sequences of the reverse Krebs cycle. *Nature Ecol. Evol.* *1*, 1716-1721.

Résumé

Toutes les formes de vie assemblent et désassemblent continuellement des composés chimiques via un processus de consommation d'énergie appelé métabolisme. Le métabolisme est généralement modélisé en chimie et biologie par un cycle. Ce modèle dynamique traduit la transformation de composés de base en une cascade de produits appelés métabolites. Celui-ci est comparable à un ouragan à l'échelle moléculaire. De manière analogique et imagée un cyclone est constitué de deux éléments, l'air et l'eau, et transforme l'environnement qui l'entoure par un processus endothermique (consommateur d'énergie). Traditionnellement, la recherche chimique sur les origines de la vie est concentrée principalement sur la synthèse de composés chimiques sans suffisamment apprécier leur place dans la plus grande organisation biochimique de la vie. La vie construit toutes ses molécules à partir du dioxyde de carbone, pourtant elle manque étonnamment d'innovation à cet égard. Malgré presque 4 milliards d'années d'évolution, les organismes autotrophes utilisent seulement six voies différentes pour construire leurs molécules à partir du CO₂. Parmi elles, deux voies – la voie de l'acétyl CoA (aussi appelée voie Wood-Ljungdahl) et le cycle du rTCA (également appelé le cycle de Krebs inverse) - sont considérées comme primitives, et contiennent les cinq molécules servant de précurseurs chimiques universels pour toute la biochimie. Comment et pourquoi les voies de l'acétyl CoA et du rTCA sont-elles apparues? Pour répondre à cette question, une recherche systématique a été effectuée afin de trouver des catalyseurs chimiques non-enzymatiques ou des minéraux simples, ainsi que des réactifs pouvant promouvoir les réactions d'anabolisme principal, particulièrement la voie de l'Acétyl CoA et le cycle de rTCA. A l'origine, pour créer les molécules organiques complexes comme les enzymes il a fallu que des molécules plus simples avec un moins grand nombre de carbone se forme sur terre et cela à partir du CO₂. On peut donc supposer que les premiers produits à plusieurs carbones sont issus de synthèse totalement inorganique comme celles développées dans notre laboratoire, plutôt que d'une évolution chimique et organométallique simultanée, c'est à dire une interaction efficace entre une molécule carbonée et un ou plusieurs métaux à l'instar de certains enzymes. Après avoir trouvé autant de façons possible de promouvoir individuellement chaque étape des cycles catalytiques étudiés, seules les conditions réactionnelles mutuellement compatibles (à savoir des conditions permettant de produire l'ensemble des métabolites dans le bon ordre) ont été retenues.

Mots clés : Métabolisme, la voie de l'acétyl CoA ou voie Wood-Ljungdahl, le cycle du rTCA ou le cycle de Krebs inverse

Abstract

All life forms continuously build up and break down its constituent chemical building blocks, through an energy consuming process called metabolism. Just like a hurricane's dynamic patterns and its building blocks (air and water) as being equally fundamental to its nature, so too should metabolism's dynamic chemical patterns and chemical building blocks be viewed as equally characteristic. Traditionally, much chemical research on the origins of life is overly focused on the synthesis of chemical building blocks without sufficiently appreciating their place in life's larger biochemical self-organization. Life ultimately builds all of its molecules from carbon dioxide, yet it is surprisingly lacking in innovation in this respect. Despite nearly 4 billion years of evolution, autotrophic organisms use only six pathways to build their molecules from CO₂. Two of these pathways – the acetyl CoA pathway (also known as the Wood-Ljungdahl pathway) and rTCA cycle (also known as the reverse Krebs cycle) - are thought to be ancestral, with just five molecules within them serving as the universal chemical precursors for all of biochemistry. How and why did these pathways get their start? To answer this question, a systematic search was designed to find simple, non-enzymatic chemical or mineral catalysts and reagents, that can promote the reactions of core anabolism, particularly the acetyl CoA pathway and the rTCA cycle. After finding as many ways as possible to promote each reaction, they could be narrowed down to mutually compatible conditions where many reactions can occur in sequence. The more of core anabolism that can be achieved under a single set of purely chemical conditions, the more likely it is to have constituted early prebiotic chemistry rather than a later product of chemical and biological evolution.

Key words: Metabolism, Acetyl CoA pathway or the Wood-Ljungdahl Pathway, rTCA cycle or the reverse Krebs cycle